OPTIMIZATION OF TAPERED COMPOSITE BEAMS FOR VIBRATION

F. Daniel F. Duarte

A thesis

in

the Department

of

Mechanical and Industrial Engineering

Presented in Partial Fulfillment of the Requirements

For the Degree of

Master of Applied Science (Mechanical Engineering) at

Concordia University

Montreal, Quebec, Canada

May 2019

CONCORDIA UNIVERSITY
School of Graduate Studies

This is to certify that the thesis prepared

By: F. Daniel F. Duarte

Entitled: OPTIMIZATION OF TAPERED COMPOSITE BEAMS FOR VIBRATION

and submitted in partial fulfillment of the requirements for the degree of

Master in Applied Science

complies with the regulations of the University and meets the accepted standards with respect to originality and quality.

Signed by the final examining committee:

_____ Chair

Dr. W. F. Xie

_____ Examiner

Dr. S. V. Hoa

_____ Examiner

Dr. L. Lin

_____ Thesis Supervisor(s)

Dr. R. Ganesan

_____

Approved by _____

Chair of Department or Graduate Program Director

_____

Dean,

Date May 20, 2019

ABSTRACT

Optimization of tapered composite beams for vibration

F. Daniel F. Duarte

A study on the optimization of tapered composite beams for vibration is conducted. Designers of tapered rotating structural components such as wind mill, helicopter or turbine blades are increasingly considering composite materials as an option to create lighter structures without compromising structural stiffness and to significantly increase their efficiency. In the design of composite material structures, a challenge arises due to a large number of design variables, therefore numerical optimization is required for a better design. Given this, the purpose of this study is to propose an optimization methodology for the design of a tapered beam, considering the vibration constrains present in rotating components. This is achieved by coupling a numerical model which considers the bending modes of vibration, with an optimization algorithm, both coded in MATLAB. Five optimization algorithms, heuristic and deterministic, are coded and compared and the most efficient method is selected. Because the ply orientation angles can assume an infinite number of possible angles, or follow the regular 0 / ±45 / 90 degrees approach, four possible tuning approaches are defined. The beam is optimized for the following design cases of boundary conditions and design requirements: the presence or absence of a tensile axial force, the presence or absence of a taper, three taper configurations, four proposed structural tuning approaches and four boundary conditions. Two of these structural tuning approaches are compared for its influence in the dynamic behavior of the structural component and in achieving better values of in-plane and out-of-plane stresses. The results demonstrate the Genetic Algorithm is an efficient method for optimization, a design analysis is an important step

in optimization, and an appropriate tuning approach can improve the overall efficiency of the optimized structure.

ACKNOWLEDGEMENTS

I want to express my deep gratitude to Almighty God for accomplishing this work in engineering research. I also express my gratitude to my supervisor Dr. Ganesan for this opportunity, his great knowledge, inspiration, motivation and support. To my parents, for their great example of dedication and hard work, and to all my family, whom I dearly love. I am thankful also to all my colleagues at the research office, for their friendship, guidance, inspiration and wisdom, and to Dr. Bath, for his valuable contributions in blade design.

Thank you.

Table of Contents

List of Figures

List of tables

Nomenclature

D_{ij}	Generic bending stiffness coefficient
$\bar{Q}_{ij}$	Transformed reduced stiffness
CFEM	Conventional finite element
HFEM	Hierarchical finite element method
x	Longitudinal direction of the laminated beam
y	Transverse direction of the laminated beam
z	Thickness direction of the laminated beam
u	The longitudinal displacement
w	The displacement along thickness direction
N	Number of hierarchical terms
W	Global displacement in the z direction
Θ	Rotation about the y-axis
$[N^w]$	Shape functions of the beam
$[N^d]$	First derivatives of shape functions of the beam

$[N^m]$	Second derivatives of shape functions of the beam
$[k]$	Element stiffness matrix
[m]	Element mass matrix
$[K]$	Global stiffness matrix
[M]	Global mass matrix
$\{u\}$	Nodal displacement matrix of the beam
H	Height of the laminate
H_p	Equivalent height of the ply in element
H_r	Equivalent height of the resin in element
L	Length of the beam
le	Length of the element
b(x)	Beam width along *x* axis
E	Elastic modulus of resin
G	Shear modulus of resin
N	Poisson's ratio of resin
ν_{12}	Major Poisson's ratio of ply
ν_{21}	Minor Poisson's ratio of ply
E_1	Longitudinal modulus
E_2	Transverse modulus

G	In-plane shear modulus
ρ	Density
ρ_p	Density of ply
ρ_r	Density of resin
ϕ	Taper angle
w_p	Blade passing frequency
w_o	Turbine operational frequency
N_b	Number of blades per fan
w_{c1}	First closet natural frequency to w_p
w_{c2}	Second closet natural frequency to w_p
dw	Band amplitude
$\overline{w_e}$	Band centerline error
θ	ply orientation angle
RMA	Regular manufacturing tuning approach
PA	Polynomial approximation tuning approach
FPOA	Free ply orientation angle tuning approach
PA&RMA	Polynomial approximation and regular manufacturing tuning approach
HC	Hill climb

BC	Bisection method
RND	Random method
SA	Simulated annealing
GA	Genetic algorithm
PSM	Particle swarm method
GA	Genetic algorithm
Fit	Fitness or objective function
ζ_i	Individual selection probability
δ_1	Step value
δ_2	Precision
$F(X)$	Objective function
$P(n)$	Initial population of solution
$Q(n)$	Generated population of solution
$R(n)$	Resulting population of $P(n) \cup Q(n)$
rnd	Random value between 0 and 1
ζ_i	Probability of selection of each individual solution
m	PSM algorithm constant of inertia
σ_{11}	Stress in the direction 1,1

σ_{12}	Stress in the direction 1,2
σ_{13}	Stress in the direction 1,3
σ_{23}	Stress in the direction 2,3
ΔH_T	Top half laminate height variation due to the taper
m	Number of plies in the top half higher thickness
n	Number of plies in the top half lower thickness
t	Ply thickness
M	Taper slope
L	Taper length
$D_{m_{ij}}(x)$	$D_{ij}(x)$ component related to the oblique plies
$D_{u_{ij}}(x)$	$D_{ij}(x)$ component related to the horizontal plies
$D_r\ (x)$	$D_{ij}(x)$ component related to the resin pockets
l_1	Resin pocket length for taper configuration B and C
l_2	Resin pocket length for taper configuration D
$H_r(x)$	Resin equivalent height
$H_l(x)$	Laminate

CHAPTER 1 – Motivation, introduction, literature survey, thesis objectives and layout

---

With the advent of numerical models such as Finite Element Method (FEM), product development processes of many industries greatly benefit by substituting physical prototyping by numerical simulations. With this, the development phases of several products gained increased speed to evaluate a possible design configuration. In order to test a greater number of design variations, numerical optimization methods are applied to work in conjunction with numerical models.

Numerical optimization algorithms are defined by a set of mathematical procedures applied to a solution or a population of solutions inside a given mathematical space, aiming to maximize or minimize a particular objective value. Usual design practices operated by a designer are limited in the number of possible variations and therefore also in the overall achieved efficiency. An optimization algorithm however, can generate a greater number of design variations where each design configuration is evaluated with greater speed by the related mathematical model. In the design of composite material components, numerical optimization has also proven to provide very good results, since as an orthotropic material, it has a larger number of design variables than a related isotropic component: ply orientation angles, ply thickness, among others. In the design of tapered laminates, there are also different possible taper configurations, which significantly increase the design space. The large number of variables of composite material structures generates a larger optimization space when compared to similar isotropic components, which is a substantial challenge for design practices supported by regular FEM analysis. Composite material components designed by numerical optimization algorithms coupled with FEM models have proven in several studies to provide superior results and to be a feasible option, especially for systems where efficiency is an important factor [1],[2],[3],[4].

1.1 Motivation

In several industries, a single digit of efficiency increase can represent large financial amounts or greater shares of the market. A study shows that each kilogram of material in the structure of the aircraft A330, costs 2000 US$/ kg in fuel consumption on lifetime, according Kaufmanna 2008 [5] and in the case of a satellite, US$ 36,000 US$ per kg per GEO (Geosynchronous Orbit) mission according Koelle [6], 2002. By substituting aeronautical alloys by composite materials, an important aircraft manufacturer achieved double digit performance increase [7].

The objective of this optimization study is to generate optimized design configurations for vibration of a tapered composite material beam, which is a rotating structural component present in wind turbines, gas turbine, or helicopter blades. The beam has to have limited deformations in the main vibration modes, in order to assure aerodynamic and structural efficiency. For this purpose, one possible criterion for optimization is to move the natural frequencies further from the operational frequencies of the blade in order to avoid resonance, while maximizing the band of operational frequencies free from resonance.

There are several optimization algorithms available in scientific literature, and selecting the best algorithm for a given task is a significant challenge, for selecting the appropriate algorithm can significantly improve the overall results of the optimization study. This study presents some of the most popular optimization methods, and describes an algorithm selection methodology applied to the present design case. In this study several leading edge optimization algorithms are studied, coded and have their efficiency compared in terms of its speed and accuracy of achieving improve designs. The best method is then selected and applied to optimize the beam with several design variations, loading cases and boundary conditions.

1.2 Introduction

The numerical model hereby applied has been created in a previous study conducted by Fazili [8], which considers the out-of-plane bending modes of vibration of a tapered composite beam, with two degrees of freedom at each node: displacement and rotation. This model provides the natural frequencies of the beam for a set of ply orientation angles and three taper configurations. The Hierarchical Finite Element Method (HFEM) formulation was used by Fazili and has generated improved results when compared with Conventional Finite Element Method (CFEM) for the numerical analysis of composite material laminates, [8]. It should be noted that Fazili's model was created following the formulation for tapered composite material laminates, derived by Lin [9].

To ease discussions, a brief introduction to the methodologies of analysis and design optimization is presented, and a comprehensive literature survey is herein provided. Several optimization algorithms were researched, and significant scientific publications related are listed. These algorithms have proven its efficiency in optimizing complex engineering systems with broad optimization space.

1.2.1 Composite materials

Composite material stands for the combination of two or more different materials that together achieve improved quality, as structural stiffness or strength, wear resistance, heat insulation, and other characteristics. In this study the term composite material is used exclusively referring to the combination of advanced graphite fibers with polymeric resin. This combination of materials is used often in the aerospace, automotive and other industries to have more efficient structures to respond to both static and dynamic loads in addition to their lightweight characteristics.

These advanced composite materials have proven to offer superior qualities in several engineering applications, due to their high strength-density ratio.

1.2.2 Internally tapered composite beams

In the case of a generic cantilever beam with distributed or concentrated loads, the flexural stress increases toward the fixed end. This type of beam is used often in airplane wings or rotating blades where tension is evidently greater near the hub and decreases along the length.

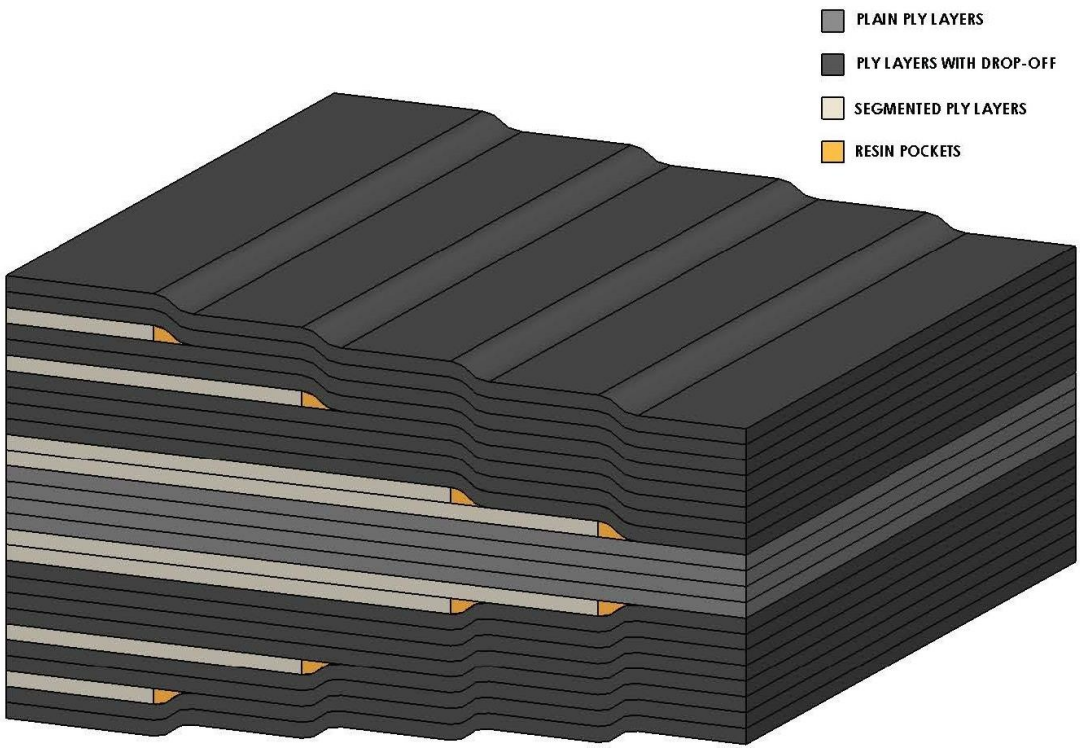

Figure 1.1 *- A schematic of composite tapered beam representation*

Given this, tapered sections offer superior results than non-tapered components, allowing a more efficient stress distribution along its geometry by gradually increasing the cross-section area of the beam as the internal loads are more demanding, therefore granting the component a more

adapted design. An example of tapered beam showing in details the ply drops, segmented plies and resin pockets is displayed in Figure 1.1.

With the advancement of automated manufacturing technologies of composite structures, the creation of more complex structural components, such as tapered composite beams, are facilitated.

1.2.3 Beam optimization for vibration

In many mechanical engineering applications, cantilever beams are required to withstand several static and dynamic loads. One important criterion for the design of rotating structural components, is that the forcing frequency of the system is not the same or close to the natural frequencies, when in operation or in any relevant transient frequency. In the case the operational driving frequency and resonant frequencies of the structure match or are close enough, resonance occurs, which can lead to the excessive vibrations. Another similar phenomenon occurs with structural components under aerodynamic load like airplane wings or rotating blades. These loads can vary due to the deformation of the airfoil shape, which in turn modify the aerodynamic loads. This phenomenon can happen in a resonant way called flutter, which must be prevented by an aeroelastic analysis during design. Current design practices require a window free from resonance between the natural frequencies of the structure and the operational forcing frequencies. In the case of rotating blades, the forcing frequency will be related to the downwash near the supporting structure, which will depend on the number of blades and the rotation speed. For any rotating structure, the natural frequencies vary due to gyroscopic forces. Campbell proposed in 1924 a method to analyze the spectrum of natural frequencies along the rotation speed of the forcing frequency, which was applied to the development of gas turbine blades. A

thorough blade design requires the analysis of the main vibration modes, with maximum stresses and stationary deformation verification. In most cases the optimization of a structural component subjected to dynamic loads aims to reduce the overall weight of the structure while maintaining safe and efficient operational conditions. More specifically, the optimization for vibration is intended to assure that the natural frequencies of the structure are further located from the forcing frequency related to the downwash of the blades, or any other forcing frequency present in the system operation. This present work is focused on the analysis and optimization for vibrations in out-of-plane bending modes with two degrees of freedom: deflection and rotation. A tapered beam is considered and is optimized for vibration by defining the ply orientation angles which will maximize the band free from natural frequencies, while centering the band with the blade passing frequency.

1.2.4 Finite element method

Many systems and processes can be represented by mathematical models which simulate its natural behavior with significant accuracy. A mathematical model can be analytical or numerical. An analytical model is defined by the derivation of the governing equations of the studied system or process, up to its overall representation, generally with more complex or larger equations than a generic FEM, with much fewer or even one single element. A numerical model is a term used to define those models where the domain is subdivided into several sub-domains, where each subdomain can be represented by simplified equations also called interpolation functions. Analytical models are more difficult to obtain, however have faster calculation, while numerical

models in its turn have fast and robust methods for its generation, while requiring more processing time on its evaluation.

Among the numerical methods, there are different variations: Finite Difference Method (FDM), Conventional Finite Element Method (FEM or CFEM) and Finite Volume Method (FVM). The oldest is FDM which basically approximates the PDE by the expansion of Taylor Series on each sub domain. In order to facilitate the analysis of more complex geometries, boundary conditions and non-linarites, CFEM was created. HFEM is a variation of CFEM which has proved to give more precise results for laminate analysis with singularities such as resin pockets generated in taper configurations, by adding trigonometric terms in the interpolation function [8].

Non-linearities such as the presence of a resin pocket following the segmented ply, can cause larger errors in conventional interpolation functions, where these interpolation functions are represented by a polynomial in the FEM method. The addition of trigonometric terms to the interpolation function, as in the HFEM, has proven in previous studies to give enhanced precision, and HFEM is the method applied in this work.

1.2.5 Optimization algorithms

There are several types of optimization algorithms applied to design, yet for the present design task are considered basically two main differentiated categories, which are determinist algorithms and heuristic algorithms. Deterministic optimization methods started in the 17th century, together with the advent of Newton's mechanics laws and differential calculus. One of the most basic deterministic algorithm is called Hill Climb (HC) and it can be compared to a blind person trying to find the highest point of a delimited region, by evaluating the most

inclined direction at each step. Global optimization algorithms are a type of heuristic methods which work with a population of solution and generates a subsequent population by combining the best evaluated points inside a delimited mathematical space. Both deterministic and global optimization methods improve the overall performance of the solution, or population of solutions, until it reaches a threshold and the optimization is completed. Hybrid algorithms use a combination of global algorithms and gradient methods.

1.2.6 Previous contributions

This study is conducted as a continuation of two previous research projects. These projects have generated the composite tapered beam formulation, created the numerical model in MATLAB with the HFEM methodology, and performed several analyses of its dynamic behavior in the bending modes of vibration.

These are the main contributions of the related research:

I. Lin [9] , in 2004 generated a study with the following results:
    a. Formulation of a thickness-tapered beam to be applied to FEM and HFEM methodologies.
    b. Created the numerical models in MATLAB and compared the results of FEM and HFEM methodologies.
    c. Studied the free vibration response of tapered beams with different taper angles.
    d. Studied the free vibration response with axial force, using both classical laminate theory and first-order shear deformation theory.

II. Fazili [8], in 2013:

a. Created a tapered beam model in MATLAB for the three main taper configurations using HFEM methodology.
b. Performed an analysis on the effect of the number of elements in the tapered beam model.
c. Studied free and the forced vibration response of symmetric thickness-tapered and width-tapered laminated composite beams.
d. Determined the natural frequencies, mode shapes and forced vibration response of different types of internally-tapered composite beams.
e. Compared the HFEM results with Rayleigh-Ritz results.

1.3 Literature survey

This section provides an up-to-date survey report with the state-of-the-art of topics related to this study, as available in the main scientific journals and communities. Some of the latest and most significant studies related to this work are herein listed.

1.3.1 Tapered composite beams and hierarchical finite element method

Surprisingly not much work has been developed for tapered composite beam until present time. He, Hoa and Ganesan [10] provides an extensive review on laminated composite structures. Ganesan and Zabihollah [11], [12] studied the vibration of tapered composite beams using a high-order finite element that allows better results than conventional FEM, as it better conforms with the discontinuities at ply drop-off locations. The stiffness coefficients are determined based on stress-strain transformation. A formulation was developed for undamped vibration and they

performed a parametric study. Lin [9] defined the bending stiffness coefficients for the four main taper configurations for composite laminates, studied the dynamic behavior of thickness-tapered composite beam, and also conducted a parametric study of tapered composite beams. Ahmed [13] performed experimental and numerical studies of tapered composite beams and compared conventional and high-order finite elements, in the analysis of tapered composite laminates, describing the response under several configurations and boundary conditions, and performed a parametric analysis. Vijay [14] investigated the free and forced vibration response and buckling response of tapered composite beams with a parametric analysis of width ratio, taper configuration and several boundary conditions and laminate configurations. Fazili [8] studied the response of tapered composite beams with several boundary conditions as simply-supported, clamped-clamped, clamped-free and free-clamped beams using hierarchical finite element method, considering beams thickness-tapered, width-tapered, and width-and-thickness tapered. Salajegheh [15] studied the dynamic response of tapered composite beams with rigid and elastic supports, conducted an extensive parametric study, compared results from both usual and advanced finite element methods, and also studied the response of forced vibration. Khedeir and Reddy [16] have studied the free vibration of laminate with arbitrary boundary conditions. Abarcar [17] have analyzed the vibration of cantilever beam providing natural frequencies and mode shapes for several fiber orientations. Babu [18] has studied the dynamic characterization of thickness-tapered composite laminated plates. Ghaffari, Zabihollah and Saeedi [19] studied the damage detection based on natural frequencies variations of non-uniform thickness laminated composite beams. Roy and Ganesan [20] verified the influence of different types of thickness profiles on dynamic response of tapered composite beams, with different boundary conditions, and compared the results with non-tapered beam. Gupta and Rao [21] analyzed the eigenvalues

of stiffness and mass matrix of Timoshenko beam with taper and twisted profiles. Hodges [22] performed a free vibration analysis of composite beams to predict the natural frequencies and modes by both numerical and analytical methods. Houmat [23] has used a polynomial with added trigonometric terms, or so-called hierarchical finite element method to analyze Timoshenko beams and compared the results with regular FEM. Çalim [24] investigated the effects of taper angle and ply orientation of composite beams on their dynamic behavior using Timoshenko beam theory. Javirad and Nazari [25] proposed a novel stochastic method and applied to the optimization of a composite laminate structure. Also Javirad and Nazari [26] applied a hybrid method of Simulated Annealing (SA) with Particle Swarm Optimization (PSO) to improve PSO optimization of laminate, defining improved configurations of ply orientation angles and layer thickness of composite material structures.

1.3.2 Beam vibration analysis and beam optimization for vibration

Many authors contributed to this field. Niordison [27] provides an overview in different cases of cantilever beams optimization for vibration, where the objective is the maximization of the first fundamental frequencies. He specifies that tapering the beam is an effective way to maximize the lower natural frequencies. Mabie and Rogers [28] conducted a study of the dynamic response of tapered beams under different boundary conditions, comparing the results to non-tapered beams. Khan, Thornton and Willmert [29] present two optimal criterion techniques for the minimum weight of structural systems subjected to natural frequencies limitations. Gupta and Rao [21] describe a procedure to obtain stiffness and mass matrices for a twisted beam with varied cross-section, in order to calculate the natural frequencies. Carrera [30] presented the free vibration analysis of beam with arbitrary cross sections, using hierarchical finite element. Rakesh, 1989,

[31] provides an overview on wave propagation on many laminated beams and plates under several boundary conditions and geometries, using both analytical and numerical analyses. Nixon [32] proposes a methodology to design minimal weight composite rotor blades, first the blade is designed, followed by a design correction to assure the natural frequencies are not close to the operational frequencies. Bassiouni [33] investigated theoretically and experimentally the dynamic behavior of laminated composite beams. First using FEM methodology, and then comparing with experimental values. Chen and Bian [34] proposed a new approach for the dynamic analysis of laminated beams combining the state method and the differential quadrature method. Grandhi [35] reviewed several surveys and papers in structural optimization with dynamic frequency constrains, with references to composite structures, and beams. Jun [36] proposed a finite element method for general laminated composite beam, based on the first-order shear deformation theory. Hajianmaleki and Qatu [37] gave a review on straight and curved composite beams, commenting on research done between 1989 to 2012, related to composite beam vibration analysis. Fatmi and Ghazouani [38] describe a new high order composite beam theory that can be viewed as an extension of Saint-Venant's theory. Khdeir and Reddy [16] derived the analytical solutions of refined beam theories to study the free vibration of cross-ply rectangular beam with arbitrary conditions. Machado and Cortínez [39] investigated the influence of initial in-plane deformations generated by the actions of external loadings as well the effect of shear flexibility on the dynamic behavior of bisymmetric thin-walled composite beams. Song and Librescu [40] focused on the formulation of thin and thick-walled laminated composite beams free vibration theory. Banerjee [41] demonstrated exact expressions for the frequency equations and mode shapes of composite Timoshenko beams with cantilever boundary

conditions. Koshmatka and Friedman [42] modeled analytically the free vibration characteristics of advanced composite turbo propellers.

1.3.3 Finite element method for structural analysis and global optimization

Cook [43] and Bathe [44] provided a comprehensive reference for FEM with several examples. Goldberg [45] describe the functionality of the Genetic Algorithm methodology. Koza [46] applied the GA to genetic programming, adaptive systems and other topics which can be applied to structure optimization. Mitchel [47] also gave a good reference for the same methodology, with a comprehensive survey on interesting related work developed. Kennedy [48] described a global optimization methodology called Particle Swarm Optimization, based on how animals move in flocks, as seen in nature. Marini and Walczak [49] provide a tutorial in the subject. Ghiasi, et al [50] described several optimization methods that can be applied to define the staking sequence of a composite material laminate with constant and variable stiffness. These methods include gradient-based, direct search, and also heuristic optimization and specialized design optimization algorithms. Nik, et al [51] generated a surrogated-based multi-objective optimization of a composite laminate with curvilinear fibers. Hajela [52] applied parallel genetic algorithm in the multidisciplinary optimization of a rotor blade. Irisarri [53] have searched for optimum design of tapered laminate composite structures using staking sequence tables. Also he optimized the ply drop order of laminates with variable stiffness using a gradient based method [1]. Keller [4] performed an optimization of ply angles in a composite laminated structure using a hybrid evolutionary algorithm. Coello [54] applies a GA-based optimization algorithm for the design of a robot arm. Zehnder and Ermanni [2] describe a methodology for the global optimization of composite structures. Hansel [55] uses a genetic topology optimization for

weight reduction of composite structures. Ghiasi, Fayazbakhsh, Pasini and Lessard [56] describe several optimization processes to define optimum stacking sequence of composite structures, proposing techniques such as multi-level optimization, hybrid methods and topology optimization. Adeli [57] applied GA for the optimization of truss structures. Nagendra [58], Todoroki [59] and Narayana [60] applied GA to the optimization of composite structures. Almeida and Awruch [3] applied genetic algorithm and finite element analysis to the optimization of composite laminated structures. Scollen and Hargraves [61] have compiled several optimization studies applying Simulate Annealing optimization in diversified scientific fields. Esfandiari [62] provides a tutorials and a sample for the bisection method. Arora [63] provides a description of gradient-based optimization applied to structures. Yang [64] describes several optimization methods including the Bisection Method, Simulated Annealing and Particle Swarm Optimization.

1.4 Thesis objectives

As previously stated the usual design optimization of structural components subjected to rotation, like a helicopter, windmill or gas turbine blades must assure stresses do not surpass maximum values and the deformations are inside allowed limits. This deformation limit considers the maximum allowed values for the main modes of vibration of the blade. In addition, it is necessary to assure the natural frequencies of the component, in all the main vibration modes, are further from the operational frequencies of the system in order to avoid resonance, which can cause excessive vibrations. All these constrain must be considered during a thorough optimization design task. The present study is focused in the beam design optimization for

vibration, considering solely the out-of-plane bending modes of vibration of a composite material tapered beam.

Lin [9] generated a study on the formulation of a thickness-tapered beam to be applied to numerical models and compared the results of FEM and HFEM methodologies. Fazili [8] applied this study to create a numerical model in MATLAB for the tapered beam using HFEM methodology. He also performed a study defining the necessary number of elements of the HFEM model to achieve required precision for analysis with minimal computation cost. This HFEM model is here applied to work in conjunction with the optimization algorithm to generate near-optimum solutions for the component.

This thesis has the objective to contribute to the advance of scientific knowledge by listing and describing several optimization algorithms commonly applied in optimization studies, and providing the basic guide lines of each algorithm to facilitate its coding in further applications. In addition, is demonstrated a procedure for the design analysis of a tapered composite material beam, and an optimization process applied in the design of a composite material structure is also showcased.

In order to study the optimization of tapered composite beams for vibration, the defined objectives of the thesis are:

i. Study, test and describe the process to optimize a composite structure for vibration by coupling a HFEM numerical model of a tapered composite beam with a selected optimization algorithm, both coded in MATALB.
ii. Research, test and describe several heuristic and gradient-based optimization algorithms for single objective optimization (SOO).

iii. Suggest an algorithm selection methodology, and apply the most suited for the particular design task.

iv. Generate optimized design configurations for the tapered composite beam, for several tuning approaches with different degrees of freedom. Achieve optimized results, considering:

- Four boundary conditions
- Two loading cases: pre-stressed and a free-vibration
- The three main taper configurations and a non-tapered beam
- Possible and viable laminated structure tuning approaches

v. Generate a design analysis of the structural component, to evaluate the influence of the main design variables in the overall dynamic behavior of the laminates.

vi. Use ANSYS software to measure maximum stresses in the laminates with optimized design configurations. Evaluate near-optimum designs related to the two main tuning approaches, in terms of in plane and out-of-plane stresses.

vii. Summarize study achievements and propose future works.

1.5 Thesis layout

Chapter one has an introduction to the subject of this study, the methodologies applied in this work and its overall application in the optimization of tapered composite beams. This first chapter also describes a literature survey with many important scientific research papers related to this topic, giving an overview of the state-of-the-art of the research field.

Chapter two conducts a review of the numerical model formulation for the tapered composite beam. The optimization for vibration problem is defined, in terms of design criteria and

optimization objective. A visual representation of the optimized laminate is proposed, and several structural tuning approaches are considered for each optimization experiment. Also several optimization algorithms are described, having their efficiency compared.

In chapter three, a design analysis is performed and the main design parameters are evaluated and compared in their influence on the natural frequencies of the tapered beam. The influence of ply angle orientation along the thickness of the beam, beam length and the presence of a tensile axial load are some of the analyzed parameters.

Chapter four displays the optimization results for free vibration and pre-stressed vibration for two selected tuning approaches, and the in-plane and out-of-plane stresses are evaluated with ANSYS software. These stresses are evaluated from two main tuning approach samples, and are compared to evaluate the influence of each tuning approach in the efficiency of the designed structure.

In chapter five a conclusion is presented, the main results are evaluated and summarized, and future works are suggested.

The tapered composite material laminate in general has intrinsic characteristics that differentiate it from regular isotropic tapered structures. One of the most important is the possibility to orient the fibers along a preferred or principal stress direction. Once there is a discontinuity in one of the plies of the laminate due to the taper, a resin rich region may form which is referred to as a resin pocket. The resin pockets can be placed in different positions of the thickness or length of the laminate according each to taper configuration. These design variables: ply orientation angle and the resin pocket locations, can be adjusted during the optimization process to tailor the dynamic behavior of the beam.

2.1. Numerical model formulation

As mentioned, to each taper configuration the beam formulation is presented by Lin [9], and the numerical models have been created by Fazili [8] in MATLAB, following the hierarchical finite element method (HFEM) formulation, for each of the main taper configurations. These models are adapted in the present work to have non-tapered laminate elements at the extremities of the tapered beam as illustrated at figure 2.1.

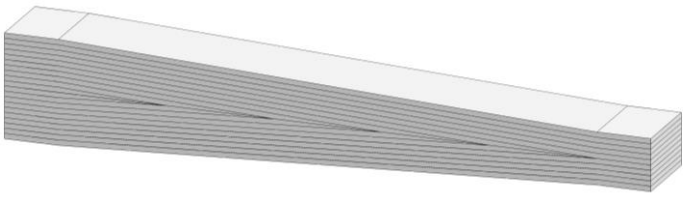

Figure 2.1 *– A thickness tapered beam with non-tapered sections*

2.1.1. Tapered composite beam free vibration formulation

In order to increase the thickness of the laminate while maintaining the original number of plies in the numerical model, each ply is substituted by a unitary ply-up of four plies with 0.125 mm each. This adaptation is necessary in order to evaluate a structure with larger dimensions while maintaining the numerical model's main characteristics. With this, each ply in the numerical model is here represented by a ply-up of four plies with identical ply orientation angles, giving a total of 0.5 mm of thickness per unitary ply-up. The beam's numerical model evaluates a total of thirty-six ply-ups with 0.5 mm thickness each, at one extremity of the beam, with a total of twelve ply-ups at the opposite extremity. For the sake of simplification, each ply-up of 0.5 mm with identical orientation angles is hereby referred to as a regular ply. The number of plies of the laminate decreases along the length, as the beam is tapered thickness-wise. As the laminate is symmetric and balanced to the horizontal plane, only nine ply orientation angles are considered as optimization variables. The equations of motion of the laminate follows the classical laminate theory and cylindrical bending theory.

2.1.2. Tapered laminate formulation

As the stresses and deformations considered are only of out-of-plane bending modes, the stiffness matrix of the laminate model will depend solely on the bending stiffness coefficient D_{11}. There are four possible taper configurations, as illustrated at figure 2.2.

Configuration A stands for a resin core in taper geometry, overlaid with continuous plies. Because the internal resin core of the taper configuration A do not offers good mechanical properties for the structure, this taper configuration is considered only as a theoretical model.

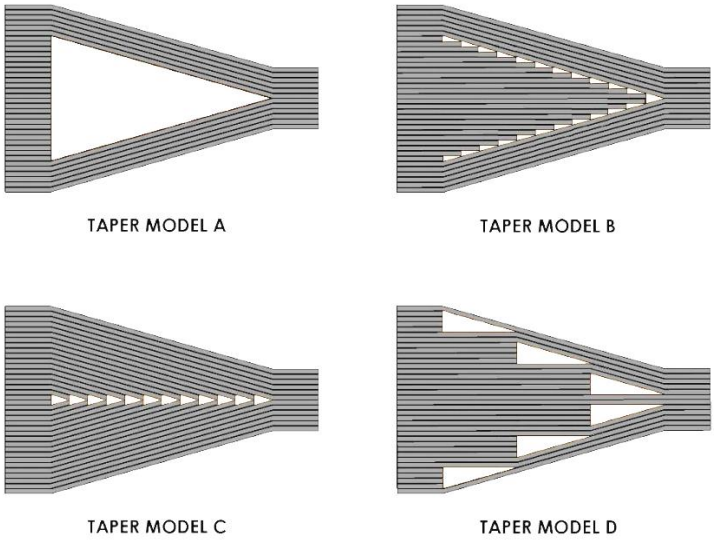

Figure 2.2 *– The four laminate taper configurations*

The formulation for configuration A is given by eq. (2.1):

$$D_{ij} = \frac{1}{3}\left[\sum_{k=1}^{R} \bar{Q}_{ij_k}(z_k^3 - z_{k-1}^3) + \sum_{k=2N-R+1}^{2N} \bar{Q}_{ij_k}(z_k^3 - z_{k-1}^3) - 2Q_{r_{ij}}\, z_R^3\right] \qquad (2.1)$$

The variable D_{ij} represents a generic bending stiffness coefficient of composite plates, in the fourth quadrant of the ABD matrix, and $\bar{Q}_{ij_k}$ is the transformed reduced stiffness of the k^{th} layer, as described by Hyer [65]. The variables i and j are the coefficients related to the direction indexes, referring to each one of the global coordinate axis. As the laminate is symmetric on the horizontal plane, only the top half is considered in the calculation. The variables N and R define the half layer numbers of plies on the left end and right end, and z stands for the height of each ply interface, measured from the center line.

The formulation for the taper configuration B is given by equation (2.2), where the core is constituted by horizontal ply layups in staircase format, with ply layups on the external side of the core. In this configuration, resin pockets are located at intermediate heights along the beam.

$$D_{ij} = \frac{1}{3}\left[\sum_{k=1}^{R} \bar{Q}_{ij_k}(z_k^3 - z_{k-1}^3) + \sum_{k=R+m+1}^{2N-R-m} \bar{Q}_{ij_k}(z_k^3 - z_{k-1}^3) + \sum_{k=2N-R+1}^{2N} \bar{Q}_{ij_k}(z_k^3 - z_{k-1}^3) + 2Q_{r_{ij}}\,(z_{R+m}^3 - z_R^3)\right] \tag{2.2}$$

The height of the horizontal plies decreases linearly along the x axis at each ply-drop, due to the staircase geometry. This variation is included in the formulation by the variable m, which defines the index of each ply-drop on the beam, along the direction of the x axis. Configuration C is defined by the center line position of small resin pockets after each ply drop along the beam, and its D_{ij} coefficient is given by eq. (2.3).

$$D_{ij} = \frac{1}{3}\left[\sum_{k=1}^{N-m} \bar{Q}_{ij_k}(z_k^3 - z_{k-1}^3) + \sum_{k=N+m+1}^{2N} \bar{Q}_{ij_k}(z_k^3 - z_{k-1}^3) + 2Q_{r_{ij}}\, z_{N-m}^3\right] \tag{2.3}$$

Taper configuration D shows the interlaying of continuous and segmented ply layers in defined intervals of ply drop along the beam. In this configuration, resin pockets are located both at center and near external plies, see eq. (2.4).

$$D_{ij} = \frac{1}{3}\left\{ \sum_{n=1}^{m} \left[\left(\bar{Q}_{ij}{}_{2n-1} + \bar{Q}_{ij}{}_{2N-2n+2} \right) (z_{2n-1}^3 - z_{2n-2}^3) \right] + \sum_{k=2m+1}^{2N-2m} \bar{Q}_{ij}{}_{k}(z_k^3 - z_{k-1}^3) + 2Q_{r}{}_{ij}(z_{2m}^3 - z_{2m-1}^3) \right\} \tag{2.4}$$

As the HFEM model has two non-tapered elements, the formulation for plain laminate is included. According to Hyer [65] it is defined as:

$$D_{ij} = \frac{1}{3}\left[\sum_{k=1}^{m} \bar{Q}_{ij}{}_{k}(z_n^3 - z_{k-1}^3) \right] \tag{2.5}$$

A more detailed calculation of the bending stiffness coefficient is given at the appendix C.

2.1.3. Equations of motion for composite laminate

The derivation of the equations of motion for the tapered laminated follows the classical laminate theory which defines the stresses due to pure bending deformations. The beam has a total of 18 mm in the higher thickness, with a total of 1 m length. This gives a thickness-length ratio of 1.8%, which is lower than the limit of 10% for a slender beams classification. With this, the modeled beams can be considered as a slender beam, in which is the error due to the transversal shear stresses and deformations are of low amplitude, which are not required to be calculated. After deriving the equations of kinetic and potential energies, the Hamilton principle is applied and the equation of motion for a composite laminated beam is defined:

$$\int_0^L b(x)D_{11}(x)\left(\frac{d^2w}{dx^2}\right)\left(\frac{d^2\delta w}{dx^2}\right)dx - \int_0^L b(x)N_x\left(\frac{dw}{dx}\right)\left(\frac{d\delta w}{dx}\right)dx - \omega^2\int_0^L\int_{-H/2}^{H/2}\rho b(x)w\delta w dx dz = 0 \tag{2.6}$$

Here the variable $D_{11}(x)$ is the bending stiffness coefficient along the center line of the beam and w is the vertical displacement. N_x represents the compressive axial force if present, $b(x)$ is the width of the beam along the length, ρ is the density of the laminate and ω represents the natural frequencies of the system. Another form to express the bending stiffness coefficient for cylindrical bending, according to Hyer [65] is:

$$D_{11}(x) = \int_{-H/2}^{H/2}\overline{Q}_{11}z^2dz \tag{2.7}$$

The variable H stands for total thickness of the beam, and $\overline{Q}_{ij}$ is the coefficient of transformed reduced stiffness. The deflection is in the z direction can be given as:

$$w(x,t) = W(x)e^{i\omega t} \tag{2.8}$$

2.1.4. Conventional finite element model

Based on the formulation for tapered composite beam, and the equations of motion for cylindrical bending of composite laminate derived by Lin [9], a numerical model following the HFEM concept in MATLAB was created by Fazili [8] for the three main selected taper configurations B, C and D. In this study, the ideal number of elements for best performance of

the model of the tapered beam is defined as six elements, following the HFEM formulation. This model has been adapted to have two non-tapered sections at each extremity of the beam.

The HFEM model in this study is divided into eight elements joined horizontally. This follows the same element-sizing configuration from previous study, where six elements are joined horizontally for the tapered section of the beam, and one extra element is added at each extremity of the model at each non-tapered section. Each element has two nodes, and each node has two degrees of freedom, deflection *w* and rotation θ, as displayed at figure 2.3. The beam dimensions are presented at figure 2.4, where the taper angle ϕ is calculated as 0.458 degrees.

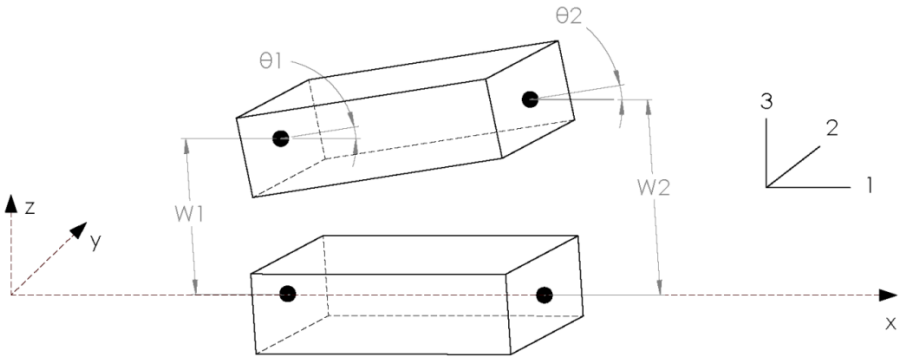

Figure 2.3 *–Degrees of freedom of a single element*

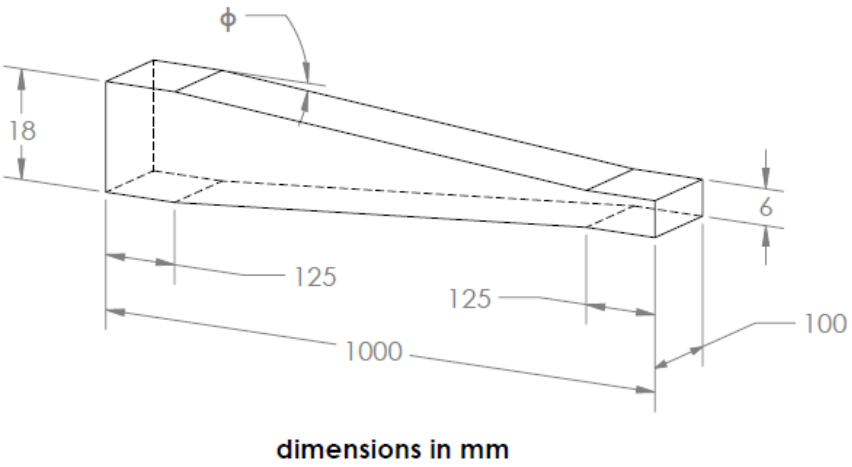

Figure 2.4 *– HFEM tapered beam model dimensions*

In order to understand the HFEM concept, the conventional finite element method (CFEM) is presented. Assuming the deflection of the beam along the axis x is approximated to a third degree polynomial, we can define,

$$W(x) = c_1 + c_2 x + c_3 x^2 + c_4 x^3 \tag{2.9}$$

Another form to express this polynomial is,

$$W = [K_w][c] \tag{2.10}$$

where,

$$[K_w] = [1 \quad x \quad x^2 \quad x^3] \tag{2.11}$$

and,

$$[c] = \begin{bmatrix} c_1 \\ c_2 \\ c_3 \\ c_4 \end{bmatrix} \tag{2.12}$$

We can define the notation for the angle at each node as,

$$\theta = [K_\theta][c] \tag{2.13}$$

Where,

$$[K_\theta] = \frac{d([K_w])}{dx} = [0 \quad 1 \quad 2x \quad 3x^2] \tag{2.14}$$

With the boundary coordinates $x_{(1)} = 0$ and $x_{(2)} = l_e$, where l_e is the length of each element.

$$\{u\} = \begin{Bmatrix} w_1 \\ \theta_1 \\ w_2 \\ \theta_2 \end{Bmatrix} = [K_u]\{c\} \tag{2.15}$$

Where,

$$[K_u] = \begin{bmatrix} 1 & 0 & 0 & 0 \\ 0 & 1 & 0 & 0 \\ 1 & l_e & l_e^2 & l_e^3 \\ 0 & 1 & 2l_e & 3l_e^2 \end{bmatrix} \tag{2.16}$$

From a given local displacement $\{u\}$, is possible to quantify the displacement of each node in global coordinates, defined by the variable W,

$$\{c\} = [K_u]^{-1}\{u\} \tag{2.17}$$

Where,

$$W = [K_w][K_u]^{-1}\{u\} \tag{2.18}$$

If we call N^w an interpolation function matrix, we can defined it as,

$$[N^w] = [K_w][K_u]^{-1} \tag{2.19}$$

Combining equations (2.10) and (2.19), the global displacement is given by,

$$W = [N^w]\{u\} \tag{2.20}$$

Using the following notation,

$$[N^d] = \frac{d[N^w]}{dx} \tag{2.21}$$

$$[N^m] = \frac{d^2[N^w]}{dx^2} \tag{2.22}$$

And applying equations (2.20) to (2.22) into equation (2.6), we have the governing equation of motion of the laminated composite beam as,

$$\left[\int_0^{l_e} b(x)\left[D_{11}[N^M]^T[N^M]\right] - N_x[N^d]^T[N^d]\,dx - \omega^2 \int_0^{l_e} b(x)(\rho_P H_P + \rho_r H_r)\left[[N^w]^T[N^w]\right] dx\right]\{u\} = 0 \tag{2.23}$$

Equations (2.23) is the classical harmonic equation, from which we define the rigidity or stiffness $[k]$ and mass $[m]$ matrices as,

$$[k] = \int_0^{l_e} b(x)\left[D_{11}[N^M]^T[N^M]\right] - N_x[N^d]^T[N^d]\,dx \tag{2.24}$$

$$[m] = \int_0^{l_e} b(x)(\rho_P H_P + \rho_r H_r)\left[[N^w]^T[N^w]\right] dx \tag{2.25}$$

In equation (2.26) the term $(\rho_P H_P + \rho_r H_r)$ can be defined as,

$$\int_{-H/2}^{H/2} \rho dz = \rho_P H_P + \rho_r H_r \tag{2.26}$$

From this equation, ρ_P is the density of the ply, ρ_R is the resin density, H_P is the equivalent ply height, and H_R is the resin height, which are used to calculate the mass distribution along the beam length. A detailed formulation for H_P and H_r along the x axis is given at the appendix C. From equations 2.25 and 2.26, we generate the global mass $[M]$ and stiffness $[K]$ matrices, with the assembling algorithm [8]. The equation (2.23) becomes a generic eigenvalue problem, which will give the natural frequencies as the eigenvalues of the system ω, and the eigenvectors as the vibration modes $\{u\}$,

$$\left[[K] - \omega^2[M]\right]\{u\} = 0 \tag{2.27}$$

2.1.5. Hierarchical finite element method

In the hierarchical finite element method (HFEM), the approximation function W(x) has the same polynomial from CFEM, added with a set of trigonometric functions, which in this case are sinusoidal functions, as we can see in equation (2.28).

$$W(x) = c_1 + c_2 x + c_3 x^2 + c_4 x^3 + \sum_{i=1}^{N} c_{i+4} \sin \frac{i\pi x}{l_e}, \quad i = 1,2,3 \ldots \tag{2.28}$$

In the equation (2.29), l_e stands for each element length, and N is the number of hierarchical terms. The function can also be expressed as:

$$W = [K_w][c] \tag{2.29}$$

$$K_w = \begin{bmatrix} 1 & x & x^2 & x^3 & \sin \frac{\pi x}{l_e} & \ldots & \sin \frac{N\pi x}{l_e} \end{bmatrix} \tag{2.30}$$

$$[c] = \begin{bmatrix} c_1 \\ c_2 \\ c_3 \\ \vdots \\ c_{N+4} \end{bmatrix} \tag{2.31}$$

As performed for the displacement W we can also define for θ:

$$\theta = [K_\theta][c] \tag{2.32}$$

$$K_\theta = \frac{d(K_w)}{dx} = \begin{bmatrix} 0 & 1 & 2x & 3x^2 & \frac{\pi}{l_e} \cos \frac{\pi x}{l_e} & \ldots & \frac{N\pi}{l_e} \cos \frac{N\pi x}{l_e} \end{bmatrix} \tag{2.33}$$

By defining the displacement matrix {u}, we have:

$$\{u\} = \begin{Bmatrix} w_1 \\ \theta_1 \\ w_2 \\ \theta_2 \\ A_3 \\ \vdots \\ A_N \end{Bmatrix} \tag{2.34}$$

The HFEM requires a different procedure than CFEM to assemble the global mass $[M]$ and stiffness $[K]$ matrices, from local mass matrices $[m]$ and stiffness matrices$[k]$, [8].

2.1.6. Finite element model for vibration analysis of the particular studied case

Figure 2.5 presents the four cases of boundary conditions considered in this study.

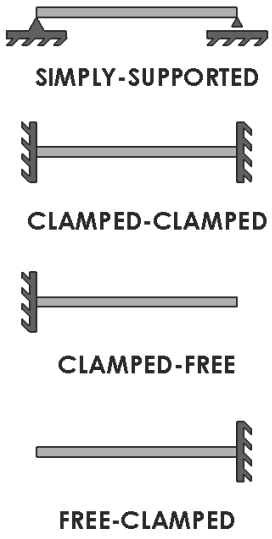

Figure 2.5*- Boundary conditions applied to the tapered beam*

The beam at Figure 2.4 has 36 layers with a symmetric configuration to the horizontal plane, each layer with 0.5 mm of thickness, giving a total of 18 mm of thickness (H). The length (L) is defined as 1 m and width is 0.1 m, and each extremity has a non-tapered segment of 0.125 m. The maximum taper slope is given by a decrease of the thickness from 36 layers worth a total thickness of 18 to 12 layers in the opposite edge, with 6 mm total thickness, as displayed in figure 2.4. The total length of the tapered section is 0.75 m. The material used in the composite laminate beam is the NCT-301 graphite-epoxy prepreg, its properties are given at Tables 2.1 and 2.2, for ply and resin.

Longitudinal modulus (E_1)	0.1139e3 GPa
Transverse modulus (E_2)	0.7986e1 GPa
$E_3 = E_2$	0.7986e1 GPa
In-plane shear modulus (G_{12})	0.3138e1 GPa
Major Poisson's ratio (ν_{12})	0.288
Minor Poisson's ratio (ν_{21})	0.178
Density of ply (ρ_p)	0.1480e4 kg/m3

Table 2.1 *- Mechanical properties of ply* [66]

Elastic modulus (E)	0.3930e1 GPa
Shear modulus (G)	0.1034e1 GPa
Poisson's ratio (ν)	0.37
Density of resin ((ρ_r)	0.1000 e4 kg/m3

Table 2.2*- Mechanical properties of resin* [66]

At table 2.1, E_1 is the extensional modulus in the direction one, which is the direction of the carbon fibers. E_2 and E_3 are the extensional modulus in the direction two and three, which are the directions related to the resin, as displayed at Figure 2.3.

2.1.7. Case comparison

To define some of the operational parameters of the blade as the rotating speed, dimensions, among other variables, the design case chosen for this work is similar to the fan blade of a commercial turbofan gas turbine.

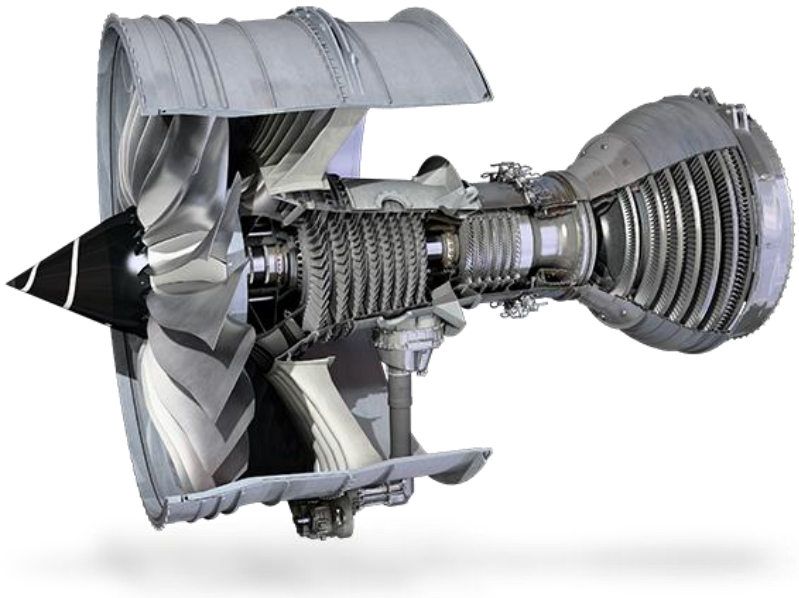

Figure 2.6 *– A commercial turbofan gas turbine* [67]

Some design and operational parameters are defined for a rectangular and tapered beam, with approximate values of the commercial turbofan engine, as displayed at Table 2.3:

	Commercial turbofan blade	Numerical model
Fan rotating speed	~2700 RPM	~2700 RPM
Blade length	~1 m	1 m
Blade maximum thickness	~20 mm	18 mm
Blade width	~0.1 m	0.1 m
Number of fan blades	20	20

Table 2.3 *– Commercial turbofan blade and tapered composite beam parameters*

With these specifications the design parameters of the HFEM tapered beam model are defined. Figure 2.7 shows the D_{11} calculated value for each taper configuration, with all ply orientation angles with the beam centerline equal to zero. The taper configurations B, C and D are represented by the curves with nomenclature TC-B, TC-C and TC-D. The non-tapered beam is represented by the curve TC-N, as seen at figure 2.6.

Applying these values to the numerical model of the thickness tapered beam, the D_{11} coefficient is exemplified in figure 2.7 for all plies with zero degree for the ply orientation angles.

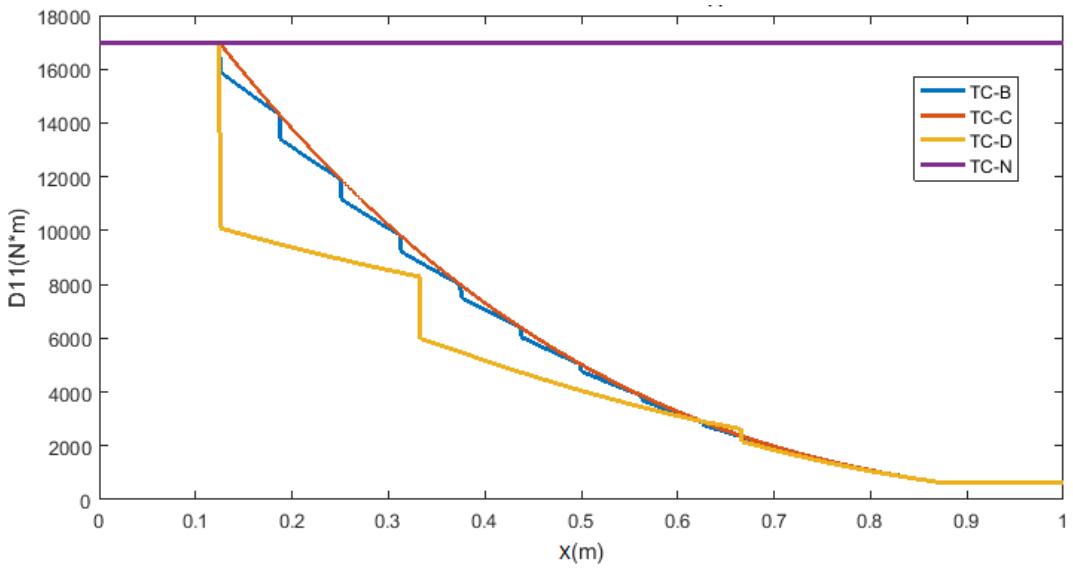

Figure 2.7 *– Bending stiffness coefficient D_{11} vs X in the HFEM model*

At figure 2.7, is displayed the influence of each taper configuration in the bending stiffness of the beam along its length X. The D_{11} coefficient of taper configuration B shows much similarity with of taper configuration C, where configuration B, in blue line, has smaller drops along the slope, which are related to the resin pockets in the intermediate position of the beam. Because the resin pockets of taper configuration C are located near the center line of the laminate, it has lower influence in the overall bending stiffness coefficient. In this same figure, the D_{11} value of taper configuration D along the length represented by the yellow line shows greater drops in the curve, which are related to its larger resin pockets along its thickness.

2.2. Optimization for vibration

The objective of the present optimization work is to determine near-optimum design configurations for vibration of the tapered composite beam. To design a blade for a helicopter, a gas turbine or a windmill, it is necessary to follow some design requirements. In general, the

blade must be dynamically stable in all the modes of vibration, and stresses must not exceed allowable values. Also for helicopters, the stationary deformation of the blade must not exceed a maximum value for safety reasons. To assure the dynamic stability of the system, the structure in all the main vibration modes must be far from resonant frequencies during operation to avoid excessive vibrations. In this present study only the out-of-plane bending modes of vibration are considered by the HFEM model of the beam, and its related optimization for vibration is hereby described.

In order to optimize a blade for out-of-plane bending modes of vibration, as in the case of a gas turbine, helicopter or windmill blades, is necessary to calculate the blade passing frequency. This frequency is related to the downwash from the blades reaching the supporting structure, which will be the forcing frequency of the system. The blade passing frequency w_p can be calculated as:

$$w_p = w_o * N_b \tag{2.35}$$

At equation 2.35, w_o is the operational frequency and N_b is the number of blades of the rotor. In rotordynamical systems, the natural frequencies often depend on the rotation speed due to centrifugal and gyroscopic forces. Campbell [68] created a technic by plotting the system response as a function of the rotation speed, where the spectrum of each natural frequency together and the forcing frequency value are defined along the speed axis. When these curves intersect there is the chance of occurring resonance, as demonstrated in Figure 2.8.

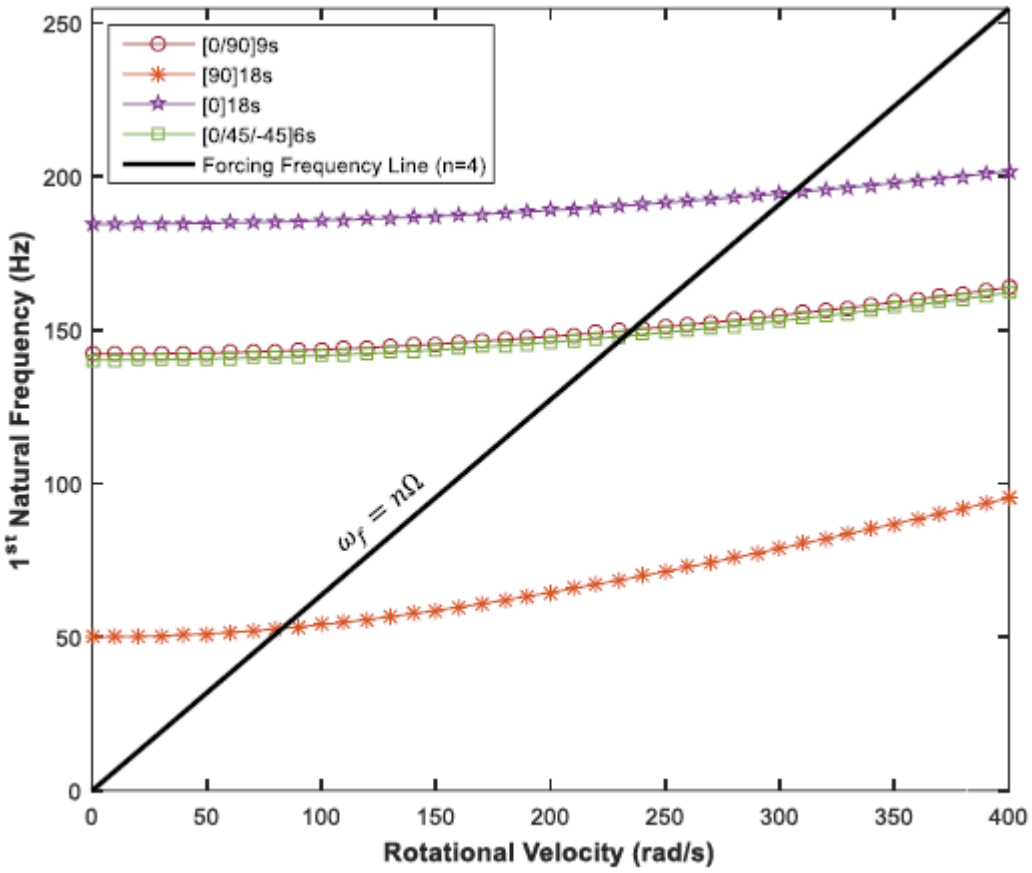

Figure 2.8 *– An example of application of the Campbell diagram* [69]

Due to simplifications in the numerical model, the natural frequencies are hereby considered independent of the rotation speed.

2.2.1. Optimization problem definition

During regular operation, it is required that the blade passing frequency will not match the blade or the system natural frequency. For this is necessary during the blade design, to assure a resonance-free band in the proximity of w_p. Also as a design requirement, this band must be maximized and also centered with w_p. Defining w_{c1} and w_{c2} as the closest natural frequencies of the beam to the passing frequency w_p, we have:

$$if:\ w_{c1} < w_p\ < w_{c2} \tag{2.36}$$

$$dw = |w_{c2} - w_{c1}| \tag{2.37}$$

$$\overline{w_e} = \left| w_p - \left(\frac{w_{c2} + w_{c1}}{2} \right) \right| \tag{2.38}$$

where dw is the resonance-free band amplitude to be maximized, and $\overline{w_e}$ is the error of the centerline of the band with the operational passing frequency w_p, as illustrated on figure 2.9:

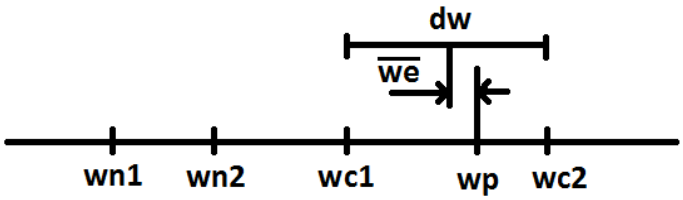

Figure 2.9 *– Graphical representation of dw and* $\overline{w_e}$

2.2.2. Objective value definition

In single objective optimizations it is required to define an objective value, by which each possible solution will be evaluated and ranked. In the present study the goal is to maximize the band amplitude dw, and minimize the center line error of the band $\overline{w_e}$.

The objective function is created following the weighted sum method [70] that accommodates distinct objective values into one. This objective value is here defined as Fit, an abbreviation of the term "fitness", which is desired to be maximized:

$$Fit = dw - 10 * \overline{w_e} \tag{2.39}$$

The coefficient of 10 multiplying the variable $\overline{w_e}$ has been defined by trial and error while testing the optimization algorithm. With this, the sorting procedure of the algorithm will prioritize the possible solutions with larger resonance-free band and low offset error with the blade passing frequency.

2.3. Graphical representation of a symmetric and balanced laminate

As a manufacturing restriction to avoid warpage, the laminate must be symmetric and balanced, [53] or an approximation of these characteristics. In the case of the tapered laminated beam, this means that its representation is:

$$[\pm\theta_1;\ \pm\theta_2; \ldots;\ \pm\theta_N;]_{sym} \tag{2.40}$$

While the vector that will define the laminate's ply orientations angles, is here defined as the representative vector $\overrightarrow{v_r}$:

$$\overrightarrow{v_r} = [\theta_1;\ \theta_2; \ldots;\ \theta_N] \tag{2.41}$$

As an example we can define a possible symmetric and balanced laminate as $[\pm 30;\ \pm 35; \pm 60; \pm 75;]_{sym}$. The ply layup representation is given in figure 2.10., where the colors represent:

black	Positive angles on top half of the laminate
blue	Negative angles on top half of the laminate
red	Positive angles on bottom half of the laminate
green	Negative angles on bottom half of the laminate

Table 2.4 *– Symmetric and balanced laminate color code*

The graphical representation of the laminate is here proposed, where the curves are defined by the points in the same quadrant. Following the same color code, the laminate is defined and displayed in Figure 2.10:

PLY LAYER #	
8	-75
7	75
6	-60
5	60
4	-35
3	35
2	-30
1	30
-1	30
-2	-30
-3	35
-4	-35
-5	60
-6	-60
-7	75
-8	-75

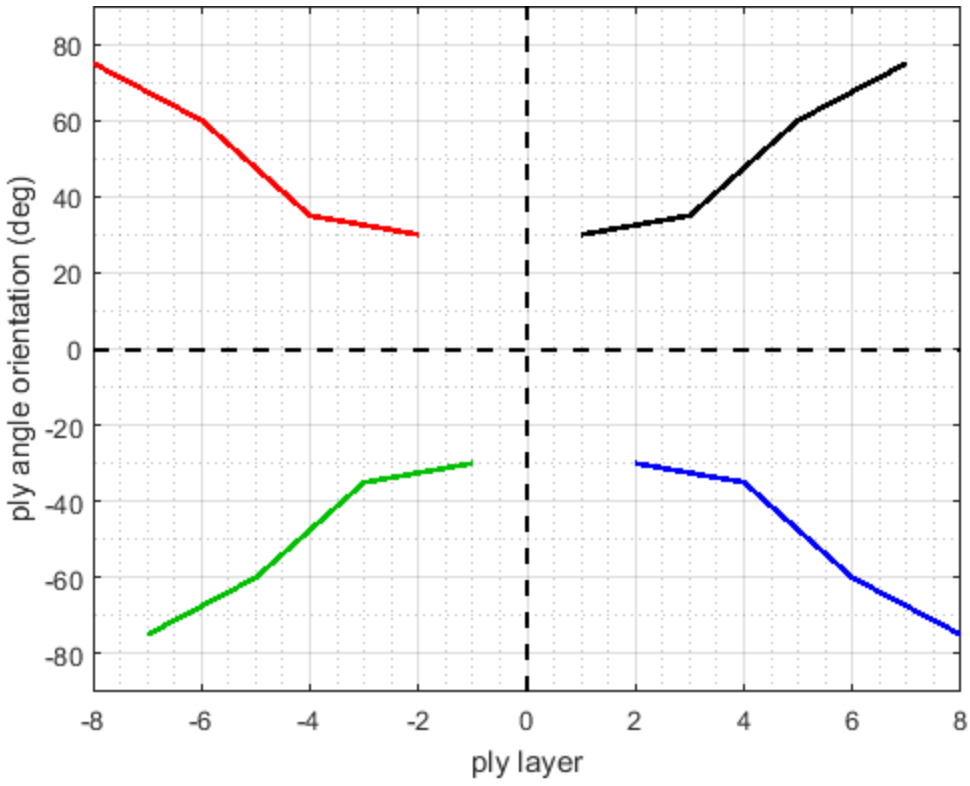

Figure 2.10 *– Example of a possible symmetric and balanced laminate*

The HFEM model of the tapered beam previously created has a total of 36 plies. Because the laminate is balanced and symmetric, the total of 36 ply orientation angles will be defined by the 9 ply orientation angles of the representative vector $\overrightarrow{v_r}$.

For simplification, all the optimization results of the symmetric and balanced laminate will be represented only by the points in the upper right of the quadrant, which is also the representative vector.

2.4. Composite material structural tuning approaches

Current manufacturing practices in several industries often consider four possible ply orientation angles during design: 0 / $\pm$45 / 90 degrees. With the advancement of composite material manufacturing technology, a greater design space can be considered with other ply orientation angles. In order to define the ply orientation angles of the optimized laminate it is necessary to consider which structural tuning approach will be applied, as it defines the set of possible orientation angles of the laminate.

2.4.1. Regular manufacturing approach (RMA)

As mentioned, an usual approach in composite material manufacturing considers the 0 / $\pm$45 / 90 degrees as possible orientation angles. This is a very practical approach to reduce the number of variables to simplify the design process and facilitate manufacturing. Increasing the number of possible ply orientation angles makes manufacturing and design more challenging for current technics.

2.4.2. Polynomial approximation approach (PA)

By reducing the number of possible ply orientation angles, design can be facilitated, however it discards several plausible configurations in having angles different of 0, $\pm$45 or 90 degrees. To solve this problems, another design option is hereby created and defined as polynomial approximation approach (PA), in which the representative vector curve (equation 2.41) shown at the upper right quadrant of figure 2.10 is approximated by a polynomial. With recent developments in automated fiber placement technologies, PA becomes a feasible design approach for several applications with more advanced manufacturing technology. Together with the taper configurations for laminates, it offers a greater number of design configurations. This larger design space could represent a challenge for regular design procedures supported by FEM analysis due to the intricacy of the achieved solutions, however, for automated design tasks such numerical optimization it is a viable and a more interesting challenge, allowing development of more tailored solutions.

2.4.3. Free ply orientation angle approach (FPOA)

Another possible design / tuning approach is to consider any ply orientation angle between zero and ninety degrees. This approach greatly increases the number of possible design configurations, which is interesting for optimization. The downside however, is that it can generate large orientation angle gradients between each layer of the laminate, what can generate increased out-of-plane stress values.

2.4.4. Polynomial approximation and regular manufacturing approach (PA&RMA)

This methodology follows the same procedure as PA, as to approximating the orientation angle values to a polynomial curve at a first step, and then defining the ply orientation angles to its

closest values of the RMA, in 0 / ±45 / 90 degrees. With this, regular manufacturing practices are maintained, and the ply orientation angles along the thickness of the laminate are derived from the center line of the polynomial.

2.5. Optimization algorithms

There are many optimization algorithms available, each one with its advantages and disadvantages. In order to select the most appropriate method for the particular task, several algorithms are researched, coded in MATLAB and have its speed and accuracy measured and compared. The average convergion curves and speed are considered as the selecting criteria. The algorithm which has achieved the best solution in a feasible time is selected for the optimization task.

2.6. Deterministic optimization algorithms

Gradient based algorithms, or deterministic algorithms [63] are very well known in many numerical analysis R&D engineering centers. Some examples of gradient methods are: hill climb (or gradient descent), bisection method, Gauss–Newton algorithm, Newton–Raphson method, among others. Those methods were first developed in the 17th century at same time of the mechanics laws of physics and are greatly useful until now as it often delivers improvements at each iteration, until the algorithm reaches desired precision. The downside of gradient methods is that when it is not used in conjunction with a combinatorial analysis tool that efficiently explores the overall optimization space, it has the tendency to converge to local optimum points.

2.6.1. Hill climb method (HC)

If we would consider the optimization space as a delimited geographic region with several hills and valleys, this method would be compared to a blind person, that at each step would sense which would be the steepest direction, in order to find the highest point. This method calculates the gradient of the function or model at the initial guess point, for each one of the design variables.

Once the gradient is calculated, a step is given from the initial guess toward the gradient direction. If the position achieved is better than the previous, this position is recorded, and this procedure is repeated several times until the algorithm converges. For a maximization problem, we can define the hill climb method (HC) as:

> (10) Define step value δ_1 and desired precision δ_2;

> (20) Calculate gradient $\overrightarrow{\nabla F}$ at initial point $X(n)$, for each variable:

$$\overrightarrow{\nabla F}(X) = \overrightarrow{\nabla F}(x_1, x_2, \dots, x_k) = \left(\left| \frac{\overrightarrow{\partial F}}{\overrightarrow{\partial x_1}} \right| \hat{\imath}_1 + \left| \frac{\overrightarrow{\partial F}}{\overrightarrow{\partial x_2}} \right| \hat{\imath}_2 + \cdots + \left| \frac{\overrightarrow{\partial F}}{\overrightarrow{\partial x_k}} \right| \hat{\imath}_k \right)$$

> (30) calculate $X(n+1) = X(n) + \overrightarrow{\nabla F} * \delta_1$;

> (40) evaluate $F(X(n+1))$;

> (50) calculate $\Delta F = F(X(n+1)) - F(X(n))$, and define $n := n+1$;

> (60) If $F(X(n)) > F(X(n-1))$ & $\Delta F > \delta_2$, go to (30), else go to (70);

> (70) converge algorithm, plot and save results;

2.6.2. Bisection method (BM)

The most basic procedure to numerically find a root of an equation is the bisection method [71]. It consists in repeatedly dividing the interval where the root is located by evaluating its middle position.

As it consistently gives an improved answer, it is a simple, yet very robust optimization tool. This method applied in finding roots of an equation (i.e. a polynomial) is not as fast as other gradient methods, nevertheless it always converges, differently than other methods that may diverge depending on the function. It can be applied to find the maximum or minimum values of a given function.

This algorithm can be used in conjunction with the hill climb method. Once the local optimum is reached by hill climb, the bisection method can refine the solution by subdividing the step interval where the solution is expected to be located. The bisection method for a maximization problem can be expressed as follow:

> (10) define initial parameters:

- Number of maximum bisection steps n_{max};
- Initial bisection step length δ_1
- bisection iteration $n \coloneqq 1$;
- $\delta(m) = \delta_1$;

> (20) define: $\begin{cases} X1 = X(n) + \delta(n); \\ X2 = X(n) - \delta(n); \end{cases}$

> (30) If $F(X1) > F(X(n))$, then $X(n) = X1$; and go to (50), else go to (40);

> (40) if $F(X2) > F(X(n))$, then $X(n) = X2$; and go to (50), else go to (60);

> (50) $X\ (n+1) := X(n)$;

> (60) $n \coloneqq n + 1$, and bisection step is defined as $\delta(\mathrm{n}) = \delta(\mathrm{n}-1) \,/\, 2$;

> (70) if $n = n_{max}$ converge algorithm, plot and save results; else go to (20);

2.7. Global optimization algorithms

In many engineering optimization tasks, often the optimization space is broad, represented by a large number of variables. As the number of variables increases, the size of the design space expands exponentially. With this the option to discretize it and evaluate all possible combinations, becomes expensive in terms of number of evaluations. Making use of gradient methods to find optimum values in these cases is not the best alternative also, as it might have an early convergion to local optimums closer to the initial guess, and the derivate calculation becomes more expensive as the number of design variables increase. Another alternative to this problem is to apply a global optimization algorithm (GOA), which are population based

methods. As most of the global optimization methods, it starts with an initial random population, and generates at each iteration a population with better performance by following simple governing rules defined by the method. Due to its gradient-free intrinsic characteristic, it has the same evaluating speed in problems with many or few of variables, differently from gradient based optimization.

2.7.1. Random method (RND)

The most basic global optimization method is the random method, also denominated Monte Carlo algorithm, which consists in creating a random population at each iteration, and storing the best recorded positions. It does not have a very efficient exploration capacity as it does not concentrate in more promising areas of the optimization space. Nevertheless, it provides a population of solutions with equal density distribution in the optimization space, which can be in sequence explored in conjunction with a precise local optimum method like HC.

The algorithm starts with the iteration index n equal to one, and an initial population with random distribution $P(n)$ is generated and each individual solution is evaluated according the single objective value. In sequence, a second population denominated $Q(n)$ is also generated with random distribution inside the optimization space, and evaluated.

The populations $P(n)$ and $Q(n)$ are added creating population $R(n)$. In sequence, population $R(n)$ is sorted according the objective value and the best individuals are selected, generating $P(n+1)$. The iteration index is increase by one and this process is repeated until the algorithm reaches the maximum number of generations.

> (10) Iteration step $n := 1$;

> (20) Generate initial population $P(n)$ with random distribution;

> (30) Evaluate $P(n)$ according the single objective value;

> (40) Generate population $Q(n)$ with random distribution;

> (50) Evaluate $Q(n)$ according the single objective value;

> (60) Generate population $R(n) = P(n) \cup Q(n)$. Sort and select $R(n)$, generating $P(n+1)$;

> (70) $n := n + 1$;

> (80) If $n = n_{max}$ then plot and save results, else go to (40);

2.7.2. Simulated annealing method (SA)

Created by Kirkpatrick in 1983 [72], Simulated Annealing is a GOA that mimics the metallurgical process of annealing, where liquid metal has its temperature slowly decreased until solid state. In this slow-cooling process, the atoms have the possibility to travel inside the cast and find lower-energy positions. This process is a crystallization process, which allows the metal to become stronger and more durable for several applications.

With simple coding this algorithm is a viable option for a global exploration method with fast implementation. The simulated annealing method description is given:

> (10) define initial parameters:

- Define k_1, k_2, k_3 and n_{max};
- Iteration step $n := 1$;

> (20) Generate initial population $P(n)$, of particles i of possible solutions, with random distribution;

> (30) Evaluate $P(n)$ according the single objective value;

> (40) Calculate temperature $T(n)$, and define translation amplitude $\left\|\overrightarrow{\Delta S_i}(n)\right\|$and direction $\widehat{\Delta S_i}(n)$:

$$\begin{cases} T(n) = k_1 * e^{-k_2 n} \\ \left\|\overrightarrow{\Delta S_i}(n)\right\| = k_3 * T(n) \\ \widehat{\Delta S_i}(n) = rnd_1 * \overrightarrow{\imath_1} + rnd_2 * \overrightarrow{\imath_2} + \ldots + rnd_m * \overrightarrow{\imath_m} \end{cases}$$

Where rnd is a random value between 0 and 1,

then calculate the translation vector for each point as:

$$\overrightarrow{\Delta S_i}(n) = \left\|\overrightarrow{\Delta S_i}(n)\right\| * \widehat{\Delta S_i}(n)$$

> (50) for each particle i, assign the new position $\overrightarrow{S_i}(n+1) = \overrightarrow{S_i}(n) + \overrightarrow{\Delta S_i}(n)$, generating the population $Q(n)$;

> (60) Evaluate $Q(n)$ according the single objective value;

> (70) Generate population $R(n) = P(n) \cup Q(n)$. Sort and select $R(n)$, generating $P(n+1)$;

> (80) $n := n + 1$;

> (90) If $n = n_{max}$ then plot and save results, else go to (40);

In the numerical algorithm, an initial population $P(n)$ of solution with random distribution in the optimization space is created and evaluated, where $n = 1$. To each solution it is added a translation or variation vector $\overrightarrow{\Delta S_i}(n)$, with random direction defined by the variable $\widehat{\Delta S_i}(n)$ and

step length $\left\|\overrightarrow{\Delta S_i}(n)\right\|$ proportional to the system temperature. The system temperature $T(n)$ is calculated at each iteration, which has a logarithm decrease along the generations. By adding a translation vector $\overrightarrow{\Delta S_i}(n)$ to each individual solution of $P(n)$, the population $Q(n)$ is generated, being then also evaluated. These two populations are added to generate the population $R(n)$, which is sorted according the main objective value and the best individual solutions are selected generating population $P(n+1)$. This process is repeated until the maximum number of generations is reached.

2.7.3. Genetic Algorithm (GA)

Originally created by J.H. Holland in 1975 [73], this algorithm mimics the theory of evolution stated by Charles Darwin, particularly applied to organisms that reproduce by mating. It states that beneficial mutations tend to accumulate in living organisms along the generations, thus generating its evolution.

As other GOAs, it starts with an initial population $P(n)$ of solution randomly distributed in the optimization space, where $n = 1$. At each iteration, population $Q(n)$ is generated though the genetic operators of mutation and crossover, and then is evaluated by the objective value. These two populations are added to generate population $R(n)$ which is then sorted and the best individual solutions are selected to create the generation $P(n+1)$. This process is repeated consecutively until the maximum number of generations is reached.

The term "fitness" is commonly used in the field of optimization where GA is applied. It is related to the objective value, which is to be maximized or minimized, according to the optimization requirements. It can be defined as equal to the objective value for a maximization problem, else the negative or inverse of the objective value in minimization problems. In the

algorithm, the problem variables are sequentially set in a vector called chromosome. In the permutation process or "cross-over", each pair of vectors or chromosomes has their values exchanged, to generate a new pair of solution, as in the biologic process of mating. The mutation process consists in a "copy error" of the chromosome, which error has its probability of occurrence and maximum amplitude as pre-defined parameters. Goldberg [45] provides a comprehensible tutorial for the algorithm.

	INITIAL VECTORS						
VECTOR 1	**0.35007**	**0.8991**	**0.81963**	**0.27797**	**0.70852**	**0.70475**	**0.22668**
VECTOR 2	0.04014	0.70203	0.13485	0.35682	0.41615	0.43146	0.27032
	PERMUTATED VECTORS						
VECTOR 3	**0.35007**	0.70203	**0.81963**	**0.27797**	0.41615	**0.70475**	0.27032
VECTOR 4	0.04014	**0.8991**	0.13485	0.35682	**0.70852**	0.43146	**0.22668**

Table 2.5 *– Permutation representation*

	INITIAL VECTOR						
VECTOR 1	0.04014	0.70203	0.13485	0.35682	0.41615	0.43146	0.27032
	MUTATED VECTOR						
VECTOR 2	0.04014	0.70203	0.13485	0.35682	**0.75294**	0.43146	0.27032

Table 2.6 *– Mutation representation*

After the recombination, all possible solutions are sorted and selected according to its fitness, and again recombined, until the algorithm converges. From literature references, there are three possible processes of pair selection in the GA algorithm, in which only one can be applied:

- Random selection: a simple randomly pair selection from the population of solutions.
- Roulette wheel selection: in this pair selection process, each individual solution has the probability to be selected proportional to its objective value. If we call the fitness of each solution as Fit_i , we can define the probability of selection of each individual solution ζ_i as:

$$\zeta_i = \frac{Fit_i}{\sum_{j=1}^{n} Fit_j} \tag{2.42}$$

- Tournament selection: in this selection process, an arbitrary number of solutions are randomly selected from the population, and the pair of solutions with greater fitness is chosen.

An overall description of the Genetic Algorithm is as follow:

> (10) Define initial GA operation parameters:

- Mutated / Permutated population ratio;
- Mutation probability per bit;
- Maximum mutation amplitude, in percentage of maximum delta value of each bit;
- Maximum number of iterations n_{max};
- Quantity of selected solutions $P(n)$;
- Quantity of recombined solutions $Q(n)$;

> (20) Define iteration step $n := 1$, and generate initial population of solutions $P(n)$ with random distribution;

> (30) Evaluate $P(n)$ according the single objective value;

> (40) Generate recombined population of solution $Q(n)$, applying crossover and mutation operators at $P(n)$;

> (50) Evaluate $Q(n)$ according the single objective value;

> (60) Generate population $R(n) = P(n) \cup Q(n)$;

> (70) Sort $R(n)$ by the single objective value;

> (80) Sort and select by objective value $R(n)$, generating $P(n+1)$ and define $n := n + 1$;

> (90) if $n = n_{max}$ then converge algorithm and go to (100), else go to (40);

> (100) plot results and save;

2.7.4. Particle swarm method (PSM)

This method created by Kennedy and Eberhart, in 1995 [48], is based in the flocking behavior of birds and schooling of fish, as observed in nature.

It also starts with an initial population $P(n)$ with random distribution in the optimization space, with $n = 1$. The movement of each candidate solution in the design space is defined by a vectorial summation of the best individual position recorded by each individual solution $B_i(n)$, the best global position recorded at each generation $G(n)$, and a vector with random direction.

All these vectors are multiplied by a coefficient with random value before being added, giving to each of the particles (or each candidate solution) a roaming and a converging direction in the optimization space. Each individual solution has the particle position, which has a roaming characteristic in the optimization space, and also the best recorded value. This procedure is repeated until the algorithm reaches the maximum number of steps. Marini and Walczak [49] give a clear overview of the method.

A simplified description of the Particle Swarm Method (PSM) is:

> (10) Define m_0, and set $n := 1$;

> (20) Generate initial population $P(n)$, of possible solutions (particles) i, with random distribution;

> (30) Evaluate $P(n)$ according the single objective value;

> (40) for each particle i, assign the particle or individual best recorded position, $B_i(n)$ as its initial position;

> (50) for each particle i, assign the individual speed, $v_i = 0$;

> (60) For population $P(n)$, save the global best solution of the population $G(n)$;

> (70) To each particle i, assign new speed $\overrightarrow{v_i}(n+1)$ according three components: inertia, global best and individual best:

$m = m_0 * (0.99)^n$, where m is the inertia value;
$\overrightarrow{v_i}(n+1) = \overrightarrow{v_i}(n) * m + rnd_{i1}\left(\overrightarrow{B_i}(n) - \overrightarrow{X_i}(n)\right) + rnd_{i2}\left(\vec{G}(n) - \overrightarrow{X_i}(n)\right)$;
Where rnd is a random number between 0 and 1;

> (80) To each particle i, assign new particle position $\overrightarrow{X_i}(n+1)$, defining new swarm position $\vec{P}(n+1)$

$$\overrightarrow{X_i}(n+1) = \overrightarrow{X_i}(n) + \overrightarrow{v_i}(n+1)$$

> (90) $n := n + 1$;

> (100) Evaluate particle population $\vec{P}(n)$ according the single objective value;

> (110) Update individual particle best position $\overrightarrow{B_i}(n)$ and global best position $\vec{G}(n)$;

> (120) If $n = n_{max}$ then plot and save results, else go to (70);

2.8. Hybrid algorithm

In order to improve the algorithm efficiency, global optimization algorithms (GOA) and gradient-based methods can be used together as a hybrid method. With this is possible to evaluate global optimum regions of the design space and also perform localized optimization in the more promising regions. The hybrid method here applied also starts with a population with random distribution in the optimization space denominated $P(n)$, where $n = 1$. To generate the population $Q_1(n)$, a GOA is applied to $P(n)$ which is also evaluated by the single objective value. Subsequently a gradient method is applied to $Q_1(n)$ to generate $Q_2(n)$. Because the gradient method also evaluates the population, no further evaluation is required. These three populations are added to generate $R(n)$, which is sorted and have the best individuals selected to create population $P(n+1)$. The variable n is increased by one, and this process is repeated until the algorithm reaches the maximum number of iterations.

>(10) Iteration step $n := 1$;

>(20) Generate initial population $P(n)$ with random distribution;

>(30) Evaluate $P(n)$ according the single objective value;

>(40) Apply a GOA to $P(n)$ to generate population of solution $Q_1(n)$;

>(50) Evaluate $Q_1\ (n)$ according the single objective value;

>(60) Apply a gradient method to $Q_1(n)$ to generate $Q_2(n)$;

>(70) Generate population $R(n) = P(n) \cup Q_1(n) \cup Q_2(n)$;

>(80) Sort $R(n)$ and select best values to generate population of solutions $P(n+1)$;

>(90) $n := n + 1$;

>(100) If $n = n_{max}$ then plot and save results, else go to (40);

2.9. Algorithms selection

It is an important consideration, to note that the main characteristics of the optimization space vary according to its function. As mentioned, a good analogy is to compare an optimization space to a delimited geographic region with hills and valleys, where the algorithm seeks to find the overall maximum height. In this analogy, depending on the functions which generates it, some optimization spaces would have several hills and valleys, others would have less height variation, while others could present discontinuities as cliffs, which would not be appropriate for gradient-based optimization methods. Therefore, each algorithm can show different values of efficiency for each objective function, as each function can generate an optimization space with different characteristics.

In order to select the best algorithm for the particular optimization task, the methods are tested for its efficiency in achieving the best solution and speed of convergion. For this purpose, the average convergion curve is calculated from 30 optimizations. The sample size of 30 is defined based on previous scientific publications of optimization studies where the average curve is also evaluated from this sample size.

Because the heuristics methods and the hybrid method have stochastic variables along its procedure, fluctuations related to the objective value achieved are expected at each optimization run.

Therefore the algorithm with greater average for the final objective value should be considered as the one with best response for the particular task. Also, it is desirable the method would reach this value as fast as possible to reduce computation time.

For this purpose the test problem is defined as the maximization of the Fit value (eq.2.39) for the beam with the following configuration:

- fixed-fixed boundary condition
- taper configuration B
- free-vibration
- polynomial approximation (PA) tuning approach
- Blade passing frequency w_p equal to 5600 rd/s

With this the optimization is performed with five different algorithms, and the average convergion curve is displayed in figure 2.11.

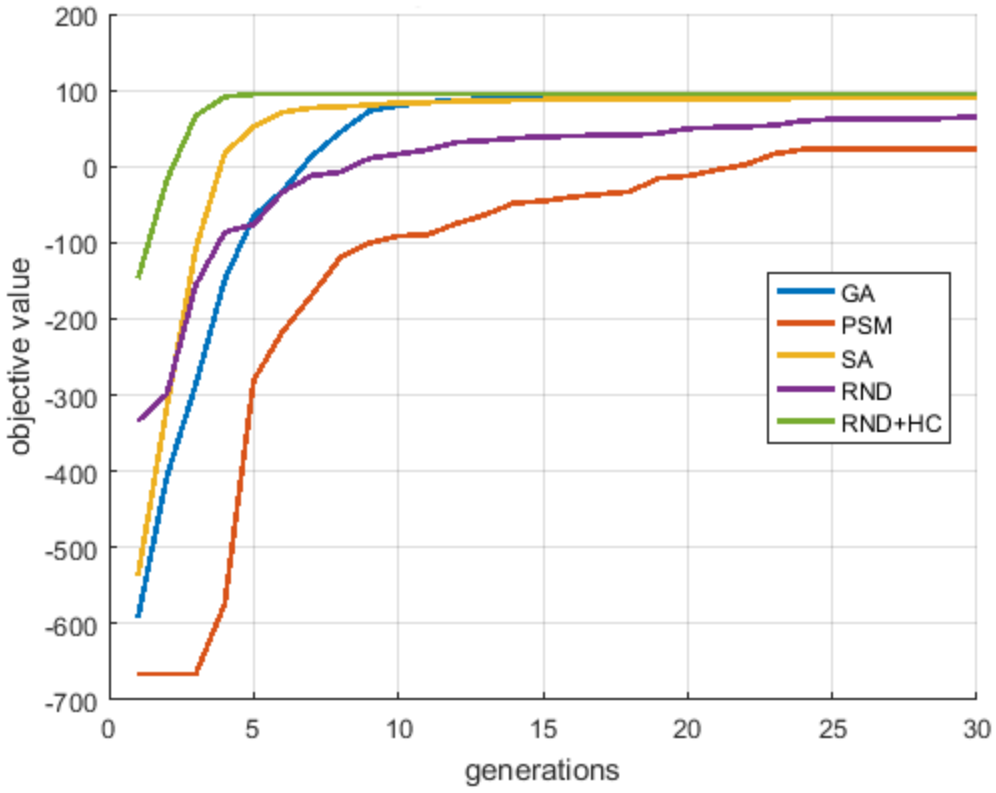

Figure 2.11 *– 30 Average convergion curve comparison*

The hybrid method chosen is RND+HC, and the conversion curves comparison of the algorithms are displayed in figure 2.11.

The best algorithm is the Random method combined with Hill Climb (RND+HC), followed by the Genetic Algorithm (GA), for the present numerical model and selected sub-space of optimization. Figure 2.12 and table 2.5 displays the optimized objective value according to each method, where GA, SA and RND+HC have achieved similar results.

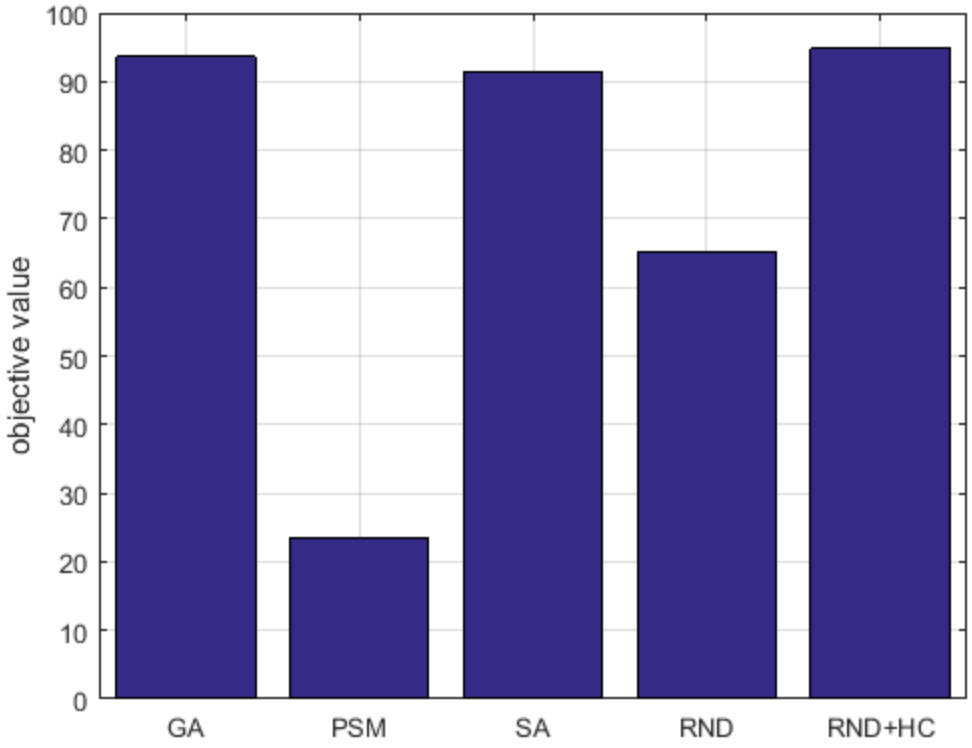

Figure 2.12 *– Objective value achieved by each method*

Table 2.7 quantify precisely the results of figure 2.12, where is possible to verify the optimization algorithm GA achieved better performance than SA.

GA	93.590
PSM	23.382
SA	91.458
RND	65.302
RND+HC	94.808

Table 2.7 *– Final objective value per optimization algorithm*

The particle swarm method (PSM) achieved the lowest value, even lower than the random method (RND), which is used as a reference. This can be caused by the coefficients of the PSM not being properly adjusted. The RND method did not achieve good results due to the fact that at each iteration it is created another population of random position in the optimization space, without any procedure to work and improve the already optimized solutions. Simulated annealing (SA) performs a mutation of each improved solution, achieving a good level of efficiency among the algorithms, yet among the GOAs it has achieved the second best value. Genetic algorithm (GA) also improves the best solutions by applying the operators of mutation and permutation, what demonstrated to provide good results. RND+HC is the best method, yet is very time consuming due to the gradient calculation at each iteration. Therefore the selected method for the present optimization study is the Genetic Algorithm with random selection of the chromosome pair.

As mentioned, these efficiency values can vary for different optimization problems or objective function. Also by changing the set of operational coefficients of each method, these methods can perform with different accuracy and speed. A complete evaluation of each algorithm efficiency would require the test of several objective functions and sets of operational parameters of these methods.

In order to better understand the influence of several variables in the dynamic response of a composite tapered beam, the natural frequencies are calculated and displayed as a function of the following variables:

- **Ply orientation angles** – The orientation angle of the fibers can modify the rigidity of the beam in a given direction, and therefore the structure's natural frequencies. In the design of a composite material structure, the deformations must be limited in all the main modes of vibration, and the influence of the fibers orientation in the dynamic behavior of the structure must be considered in order to evaluate or generate a possible design configuration.
- **Boundary conditions –** There are several applications for rotating structural components, which have varied boundary conditions. Some blades like the fan blade of a turbo fan engine are built in the clamped-free (CF) boundary condition, while other compressor blades are built with the clamped-clamped (CC) boundary condition. In order to consider several rotating beam designs, the four main boundary conditions previously mentioned are considered in the design analysis.
- **Thickness-taper configuration –** It is possible to generate a large number of taper configurations, by selecting the position of the ply drops along the thickness and the length of the beam. The three main configurations mentioned in chapter 2 are applied as a design variable.
- **Beam length –** By modifying the length of a rotating structural component, the natural frequencies related to the bending mode of vibration also are modified. The amount by

which the length variable influences the dynamic behavior of a tapered composite material beam is here evaluated.

- **Tensile axial loading –** A rotating beam can be deformed by centrifugal force or carry other structural components in its extremity. These are an example where the effect of an axial loading must be considered during project.

By verifying how these variables influence in the dynamic behavior of the tapered beam, it is expected to gain an insight and understanding of a possible tapered beam design configuration.

3.1. Design analysis nomenclature and laminate sections

Having defined the beam geometry, taper configuration and the number of layers, the bending stiffness coefficient D_{11} of the symmetric and balanced laminate will depend solely on the ply orientation angles. These angles are defined by the herein named representative vector $\overrightarrow{v_r}$, eq. (2.41), as seen in chapter 2. In order to differentiate three main sections of the half thickness laminate, the representative vector can also be defined as,

$$\overrightarrow{v_r} = [\alpha_3;\ \beta_3;\ \gamma_3] \tag{3.1}$$

When with identical angles, the same vector is defined as,

$$\overrightarrow{v_r} = [\lambda_9] \tag{3.2}$$

These laminate sections can be independently varied from 0 to 90 degrees to evaluate their influence on the dynamic behavior of the beam. The positions of each of these sections in the laminate are indicated in fig 3.1.

Specifically, Figure 3.1 represents the upper half thickness of a laminate, where the internal, intermediate and external sections of the laminate are respectively denominated by the variables α, β and γ, according to equation 3.1. In the case the orientation angles of all plies of the laminate are defined by the same angle, this angle is denominated λ. These variables are used to identify the portions of the plies under analysis in the plots.

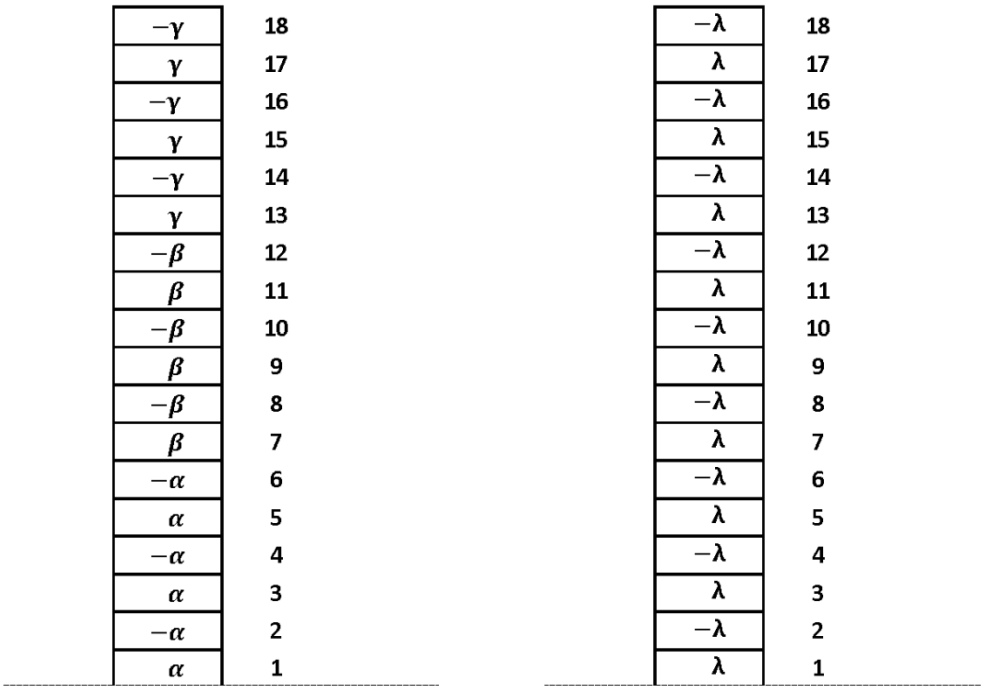

Figure 3.1 *– Ply sections of the laminate*

In order to identify the numerical optimization results, some abbreviations are applied:

TC-B	Taper configuration B
TC-C	Taper configuration C
TC-D	Taper configuration D
TC-N	Non-tapered beam
SS	Simple-supported boundary condition
CC	Clamped-clamped boundary condition
CF	Clamped-free boundary condition
FC	Free-clamped boundary condition
ω_1 to ω_8	Natural frequencies 1 to 8

Table 3.1 *– Abbreviations for data analysis*

To compare the tapered beam efficiency for several design cases, a regular non-tapered composite material beam with same dimensions is used as a reference for the dynamic response. The mechanical properties applied in this design analysis for the optimization study are the same as those provided at Tables 2.1 and 2.2.

3.2. Design analysis – first three natural frequencies of a cantilever beam

Figure 3.2 shows the influence of the ply orientation angles on the first three natural frequencies of the clamped-free tapered laminate, for each one of the main taper configurations and a non-tapered laminate with same dimension.

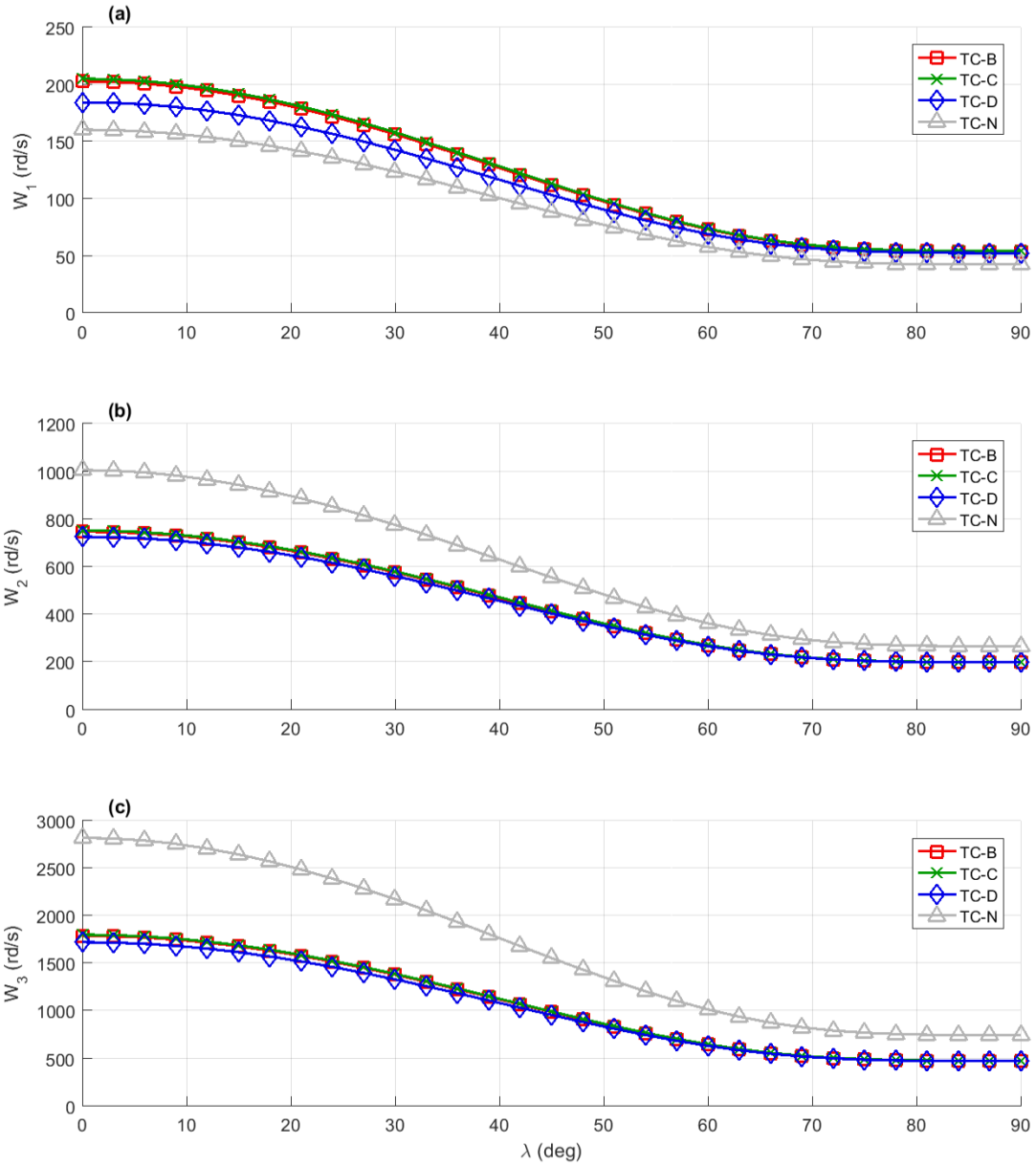

Figure 3.2a – *First natural frequency vs λ – clamped-free boundary condition*

Figure 3.2b – *Second natural frequency vs λ – clamped-free boundary condition*

Figure 3.2c – *Third natural frequency vs λ – clamped-free boundary condition*

Figure 3.2a shows that the non-tapered beam has lower fundamental frequencies than the tapered configurations, and this difference is reduced as the λ orientation angle increases. Interestingly, the non-tapered beam presents higher values for the second and third natural frequencies. This occurs due to the fact that the higher mass in the extremity of the non-tapered beam causes to decrease the values for the fundamental frequency, yet the higher bending stiffness of the non-tapered beam increases the natural frequencies values for the second and third natural frequencies.

For the tapered beams, it is noted the taper configuration D has lower fundamental frequency than configurations B and C, where configuration B and C show very similar values. This is a consequence of the presence of greater resin pockets in the configuration D along its thickness which reduces the overall rigidity of the structure.

Due to the fact that resin pockets have lower deformation resistance, it decreases the overall bending stiffness coefficient of the beam and reduces the fundamental natural frequency value. Observing the results for second and third natural frequencies in Figs. 3.2b and 3.2c, it is noted that there is not much difference between the tapered configurations. In addition, both tapered and non-tapered configurations have lower natural frequencies for higher angles.

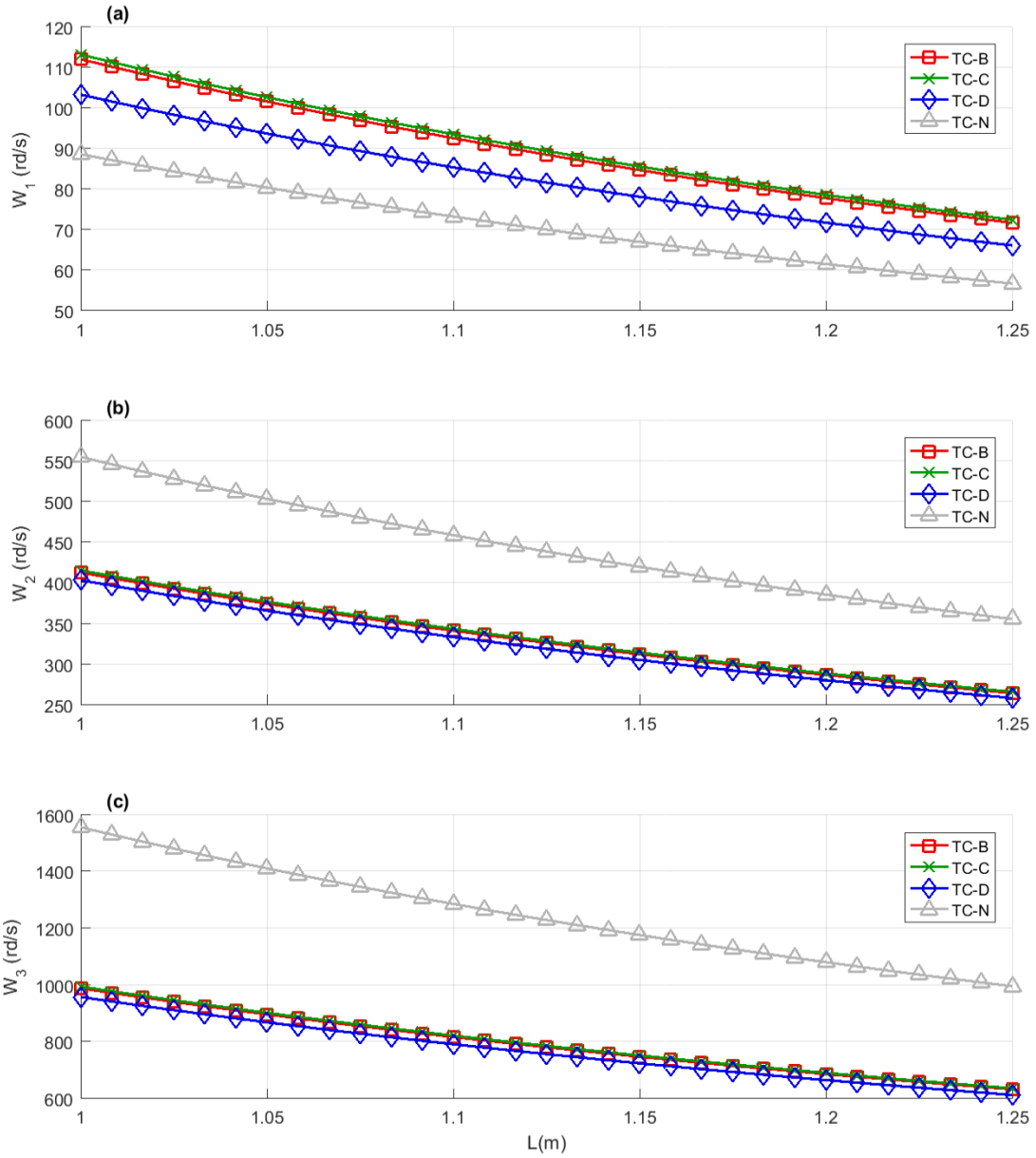

Figure 3.3a – *First natural frequency vs L – clamped-free boundary condition*

Figure 3.3b – *Second natural frequency vs L – clamped-free boundary condition*

Figure 3.3c – *Third natural frequency vs L – clamped-free boundary condition*

In figure 3.3a to figure 3.3c the first three natural frequencies of a cantilever beam are evaluated along a variation on the length of the beam, while the ply orientation angles λ remain at the default value of 45 degrees.

In an overall analysis the frequencies are higher for lower beam lengths and this is equally observed for the tapered and non-tapered configurations.

Also, it is noted in figure 3.3a, that the curves of fundamental frequencies are higher for the tapered configurations B and C than the taper configuration D.

In figure 3.3b and at figure 3.3c, the second and third natural frequency curves are higher for the non-tapered configurations, while all tapered configurations present similar values. This is caused by the fact that the non-tapered beam has higher overall bending stiffness coefficient. It is noted the non-tapered beam has higher mass also, which reduces the fundamental natural frequency values, yet for second and third bending modes, the natural frequencies of the non-tapered beam are increased, and are also more influenced by the higher stiffness generated by the greater thickness of the non-tapered configuration.

It is observed configurations B and C have higher natural frequency values than configuration D.

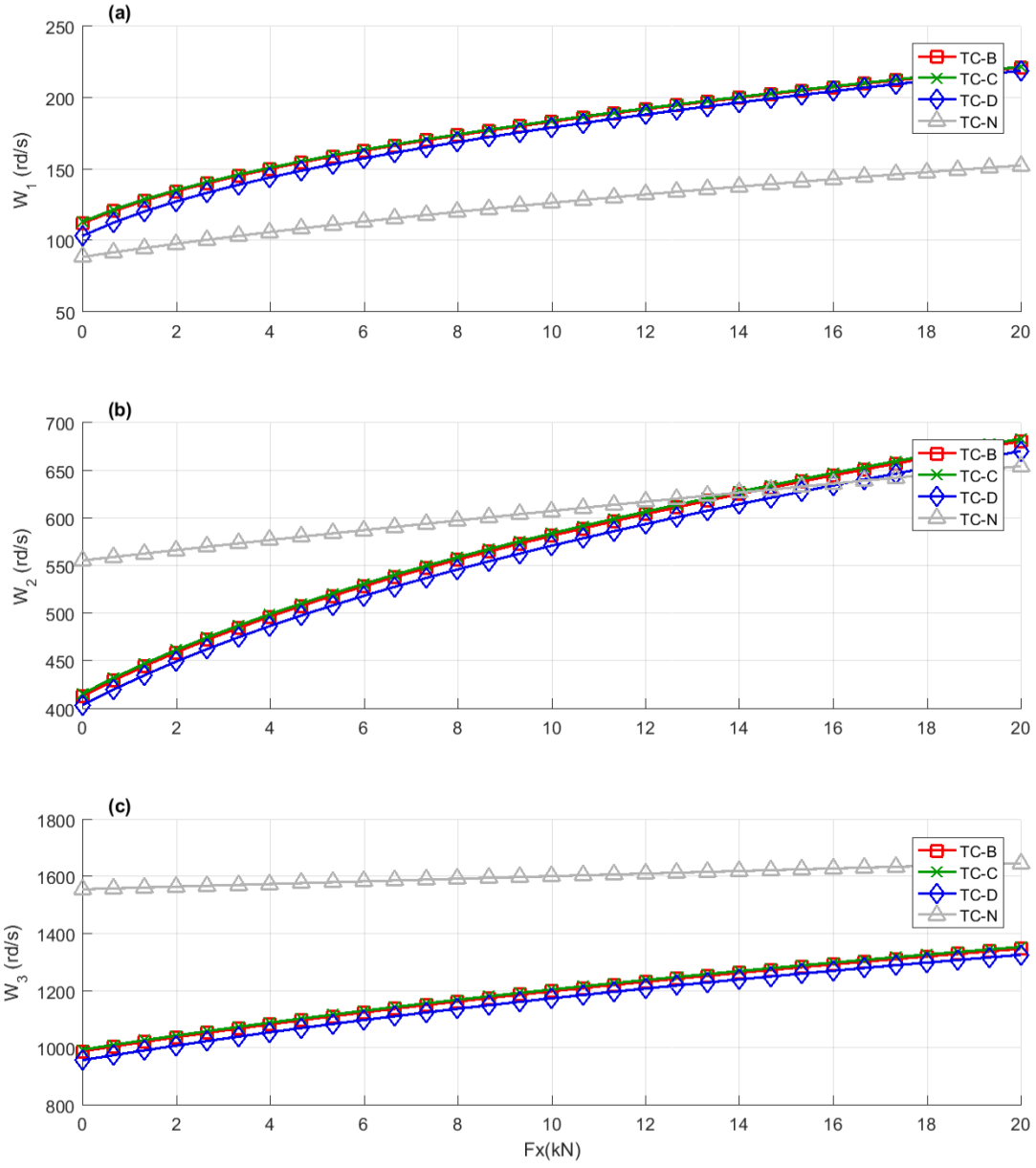

Figure 3.4a – *First natural frequency vs Fx – clamped-free boundary condition*

Figure 3.4b – *Second natural frequency vs Fx – clamped-free boundary condition*

Figure 3.4c – *Third natural frequency vs Fx – clamped-free boundary condition*

The effect of an axial tensile force on the natural frequencies of tapered and non-tapered laminates is displayed in figure 3.4, with the ply orientation angles of all the plies λ assuming the default value of 45 degrees. In an overall analysis it is possible to infer that a tensile axial force increases the natural frequencies of the beam. It is possible to note that tapered laminates are more influenced by a tensile axial force than a non-tapered laminate, due to the fact that in a tapered geometry the cross-section area decreases along the length, causing greater strain to same load values, These strain values increase the rigidity of the structure, which increase the natural frequencies. The fundamental frequency values are greater for tapered beams, while the second and the third natural frequencies are greater for non-tapered laminates, in most of these evaluated cases.

As stated by Niordson and Grandhi [27], [74], we can verify that by tapering a cantilever beam the fundamental frequencies are maximized. In the cases evaluated, is possible to infer that the second natural frequency is generally minimized for the tapered beams – with the exception of some cases in the pre-stressed configuration. This is an important design study that must be considered for cantilever components with axial loading that operate with blade passing frequencies greater than the fundamental frequency. The third natural frequencies are lower for the tapered configurations in all mentioned design configurations.

3.3. Design analysis - four boundary conditions of a tapered beam

Figure 3.5 displays the effect in all the natural frequencies under 7000 rad/s, for a given ply orientation angle, with all ply orientation angles of the laminate varying from 0 to 90 degrees. This angle is represented by the variable λ, where the natural frequencies are measured for the three taper configurations and the four boundary conditions, for a free-vibration condition and a default beam length of 1 m.

In an overall evaluation of the figures, the dynamic behavior of the tapered beam does not differ much from each taper configuration, and an angle increase demonstrates to significantly decrease all the natural frequencies. This decrease shows to be more significant to the higher natural frequencies, especially in the region between 30 and 60 degrees.

It is possible to note that the in the higher the natural frequencies, there is a greater reduction generated from a ply orientation angle increase.

It is also possible to understand from the plots at figures 3.5 that a variation in the boundary condition significantly modifies the natural frequencies values, while a taper configuration variation does not change the natural frequencies in a macro scale.

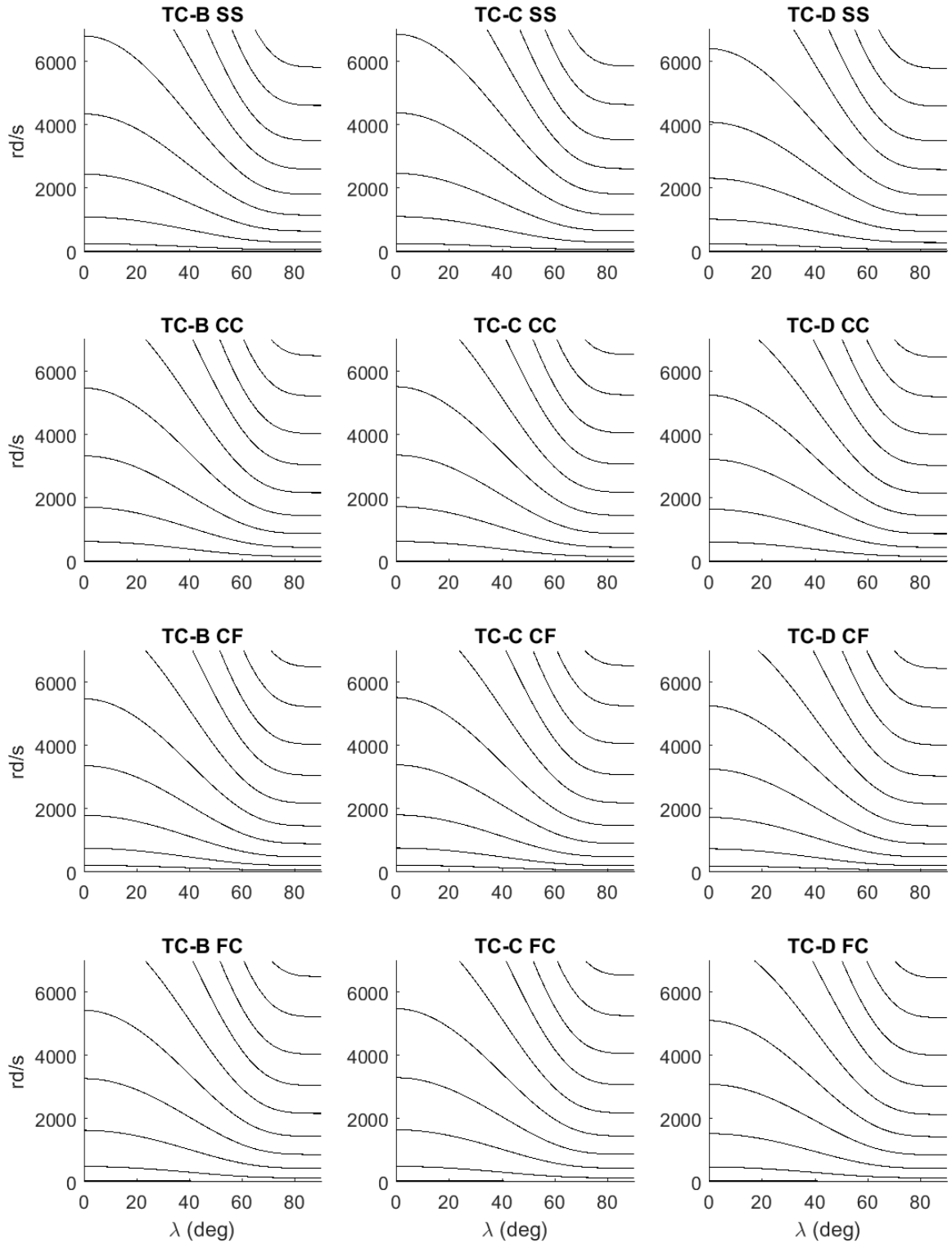

Figure 3.5 – *Natural frequencies vs λ angle variation*

The effect of the length of a tapered beam in the natural frequencies is shown in figure 3.6, where it is seen that the natural frequencies are higher for smaller beam lengths. Also for this design analysis, it can be seen that a taper configuration variation does not modify in a macro scale the natural frequencies, while the boundary condition does significantly change these values.

For the taper configuration D, in the boundary condition clamped-clamped (CC), clamped-free (CF) and free-clamped (FC), is possible to note in the top right part of the curves, the presence of an extra natural frequency, which is not seen in the other taper configurations B and C for the same boundary conditions. This greater number of natural frequencies up to 7000 rd/s for greater beam lengths indicates the taper configuration D presents a greater number of vibration modes for the same design configuration, if compared with the other taper configurations, which indicates it has lower bending stiffness coefficient. This hypothesis is possible to confirm due to the fact the taper configuration D has a larger volumes of resin in its structure, which does reduces the overall bending stiffness of the structure. Interestingly taper configuration B and C show very similar results in a macro scale analysis.

These curves demonstrate the beam length variation follows the same principle of the harmonic pendulum equation, in which the natural frequency is reduced for greater values of length.

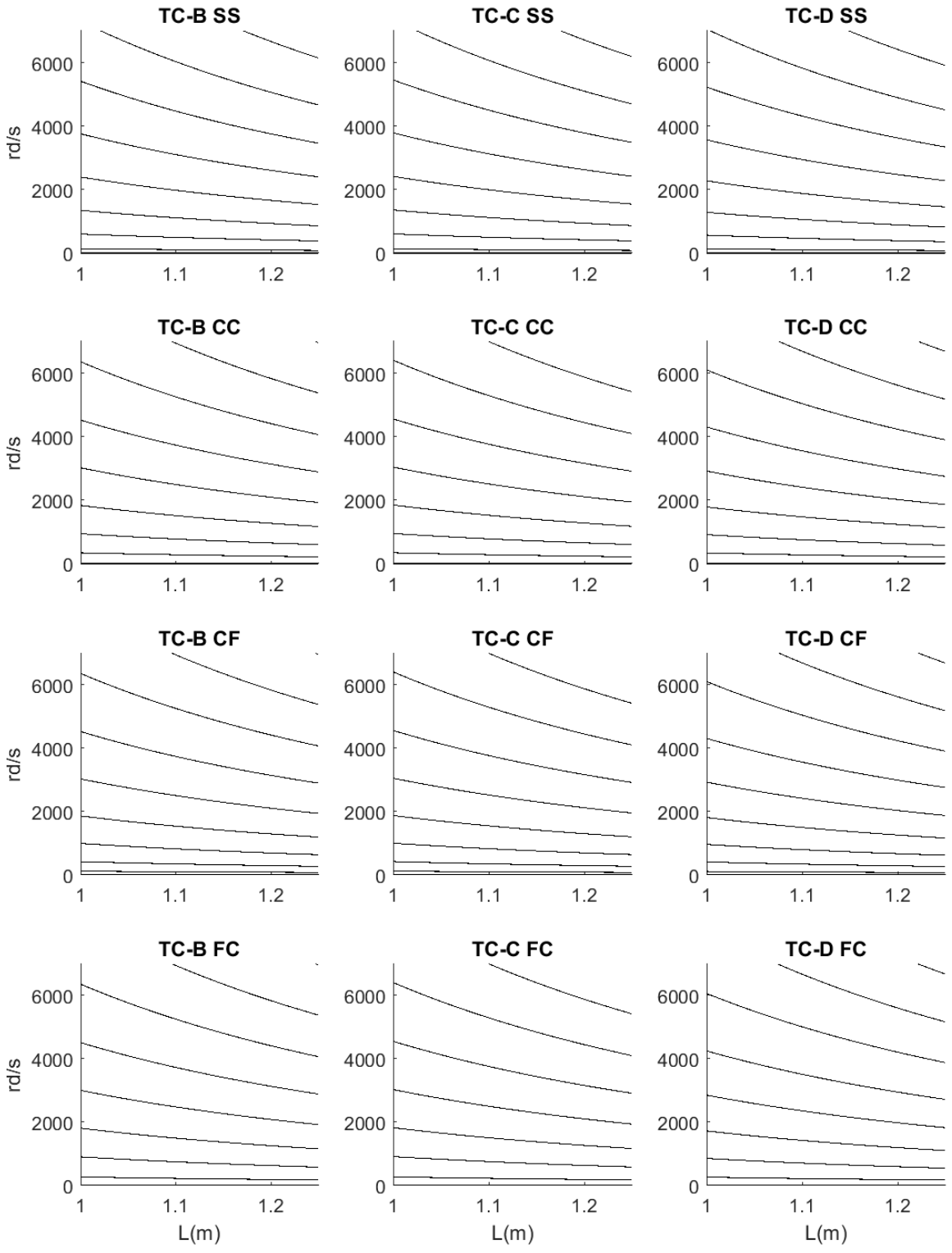

Figure 3.6 – *Natural frequencies vs length L*

The effect of a tensile axial force in the tapered beam is displayed at figure 3.7. It is demonstrated it has the overall effect of increasing the natural frequencies, due to the fact that a tensile loading modifies the rigidity of the structure, which changes also its natural frequencies.

It is understood from the curves the boundary conditions do significantly modify the natural frequency values, while a variation in the taper configuration do not have much influence in the overall dynamic behavior of the beam.

When comparing the natural frequencies from taper configuration D with configuration B and C, however, is possible to see it has lower values for same loading and boundary condition. This can also be referred to the fact of larger resin pockets which reduces the bending stiffness coefficient, reducing also all the natural frequencies.

In an overall analysis, the natural frequencies related to the bending modes of vibration seem to linearly rise with an axial tensile load.

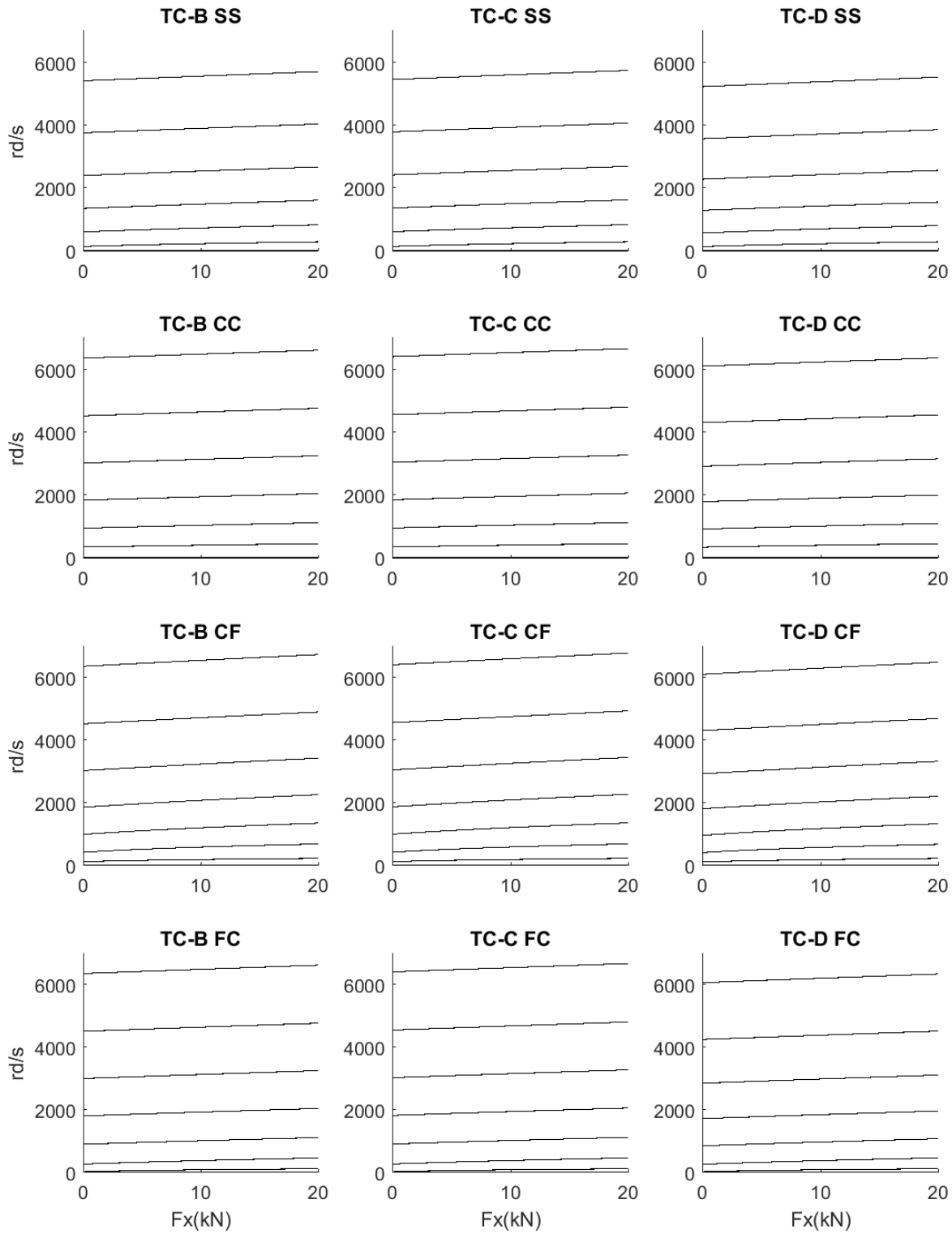

Figure 3.7 – *Natural frequencies vs tensile axial force Fx*

3.4. Design analysis – 3D analysis curves of a cantilever beam

Due to the fact that many tapered beams applications as windmill blades, helicopter blades and others, are in the clamped-free boundary condition, this is the focus of the 3D design analysis. In order to compare the effect of some design variables, 3D curves of the first and second natural frequencies are generated, varying several design variables. Figure 3.8 shows the influence of the ply orientation angles on the intermediate and external layers of the laminate $\beta, \gamma,$ eq. (3.1).

Any ply orientation angle not mentioned in the plots remains with the default angle of forty five degrees. If we consider the curve related to the first natural frequency ($w_n 1$) of the taper configuration B, is possible to note that when β and γ assume values near 90 degrees, the natural frequencies are lower than when both coefficients assume values near zero degrees. This can be understood due to the fact that when the fibers of the external and intermediate layers are aligned with the main axis of the beam, the coefficient D_{11} has greater values, what increases the natural frequencies of the structure. Also is possible to note that when β is increased there is a lower frequency rise than when γ is increased, what leads to the assumption the external plies of the laminate represented by the variable γ have more contribution in the dynamic behavior of the beam than the intermediate plies of the laminate represented by the variable β. The same pattern is observed in all the plots of figure 3.8, where some differences are observed between each taper configuration. For the first natural frequency, in the region where β and γ have the value of zero-degrees, taper configuration B displays a natural frequency around 190 rd/s, taper configuration C around 200 rd/s and taper configuration D around 170 rd/s, from what we understand the taper configurations does have an influence in the natural frequencies. Taper configuration C again displays higher values due to its resin pockets being located in the horizontal plane of symmetry.

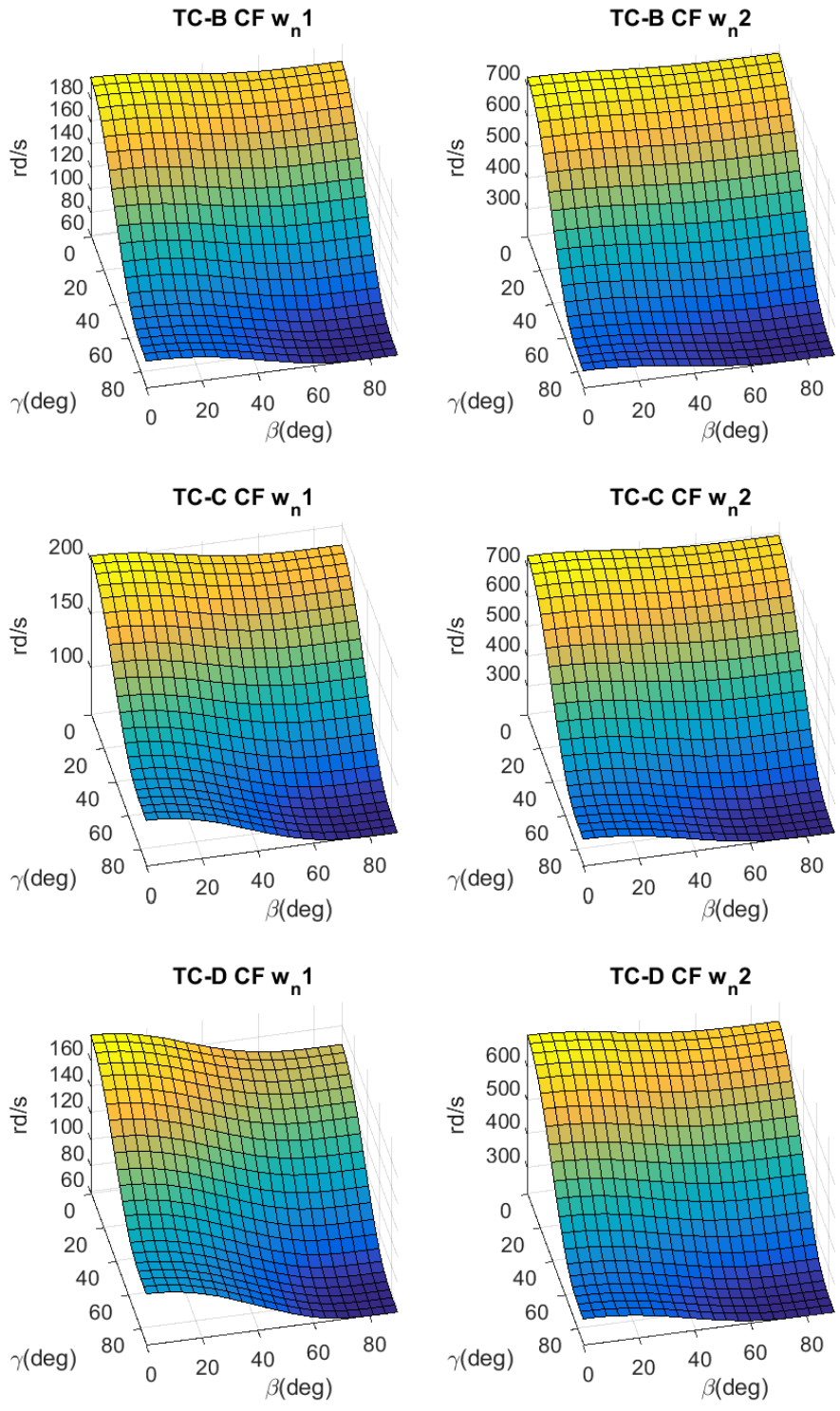

Figure 3.8 – *Clamped-free tapered beams – first and second natural frequencies vs β vs γ*

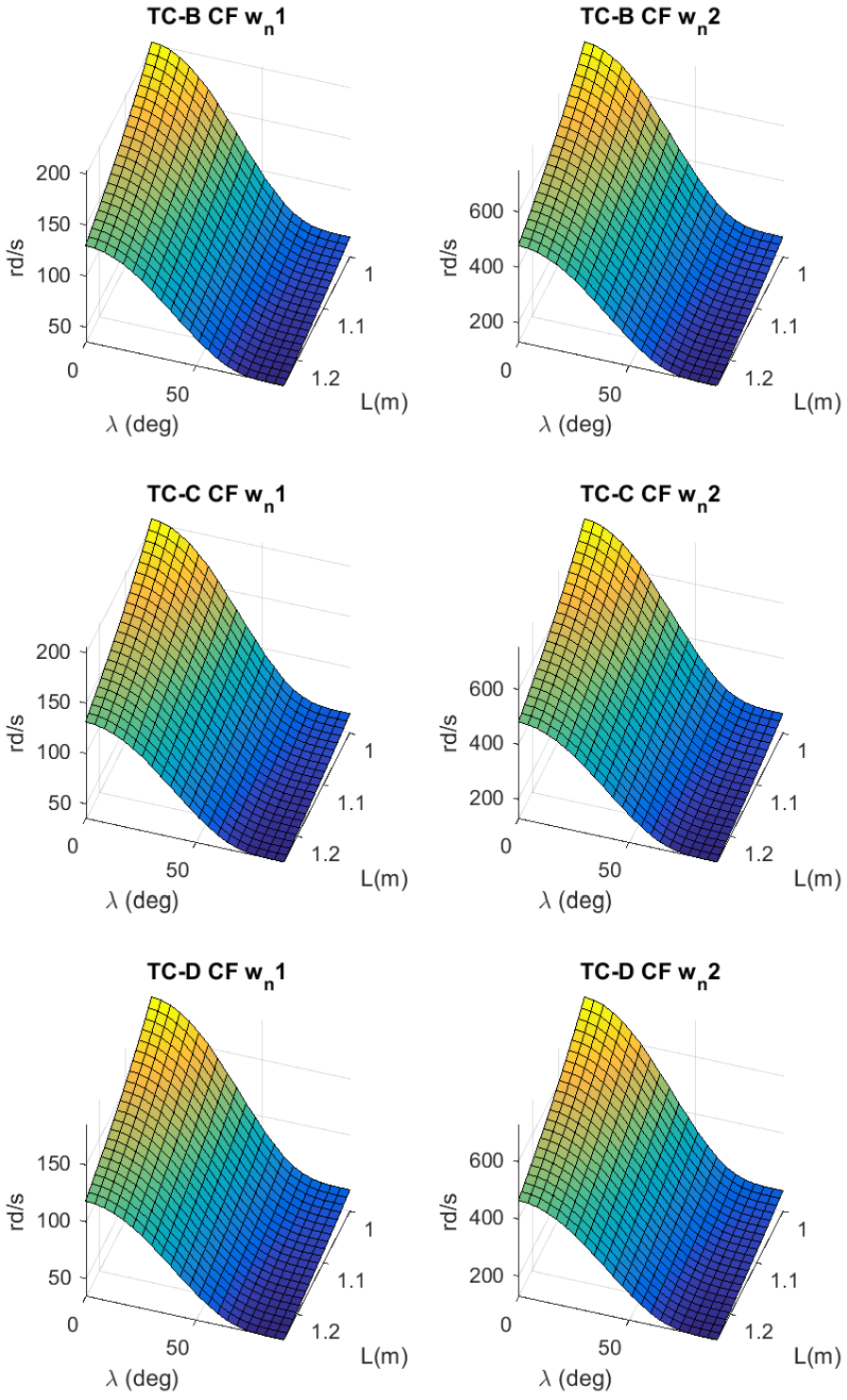

Figure 3.9 – *Clamped-free tapered beams – first and second natural frequencies vs λ vs L*

Figure 3.9 compares the effect on the first and second natural frequencies with a variation of the ply orientation angle for all the layers of the laminate, which angle is represented by the variable λ, along with the effect of a length variation L, varying from 1 meter to 1.25 meters. It is shown in the curves that both variables are important in the dynamic behavior of the beam in the given intervals, and the natural frequencies significantly decrease for greater lengths and higher ply orientation angles.

It is possible to note at any of the curves from figure 3.9, that at the point where λ assumes the value of 90 degrees and L is equal to 1.25 m, the natural frequencies have a lower value. From this point, a decrease of ply orientation angles λ toward zero-degrees contributes to increase the natural frequency more than when decreasing the length to 1 m. From this is possible to understand the given length variation has less influence in the dynamic behavior of the structure than the variation of the ply orientation angle from 90 to 0 degrees.

Another inference can also be made from the point where λ is equal to zero-degrees and the length is 1.25 m, for any taper configuration or boundary condition of figure 3.9. A reduction of the length toward the value of 1 m has greater influence in increasing the natural frequencies, than when the length has the same length reduction while λ is equal to 90 degrees. This is due to the fact that when the ply orientation angles are aligned with the beam main axis, the D_{11} value of the structure is increased, what contributes to higher natural frequencies. And with D_{11} having greater values, a length variation has more influence in the dynamic behavior of the beam that when D_{11} has lower values. It is possible to note also that when λ is in the zero-degree region and L is equal to 1.25 m, the natural frequencies for the taper configuration D are lower than for configurations B and C, which is also related to the presence of greater resin pockets at configuration D.

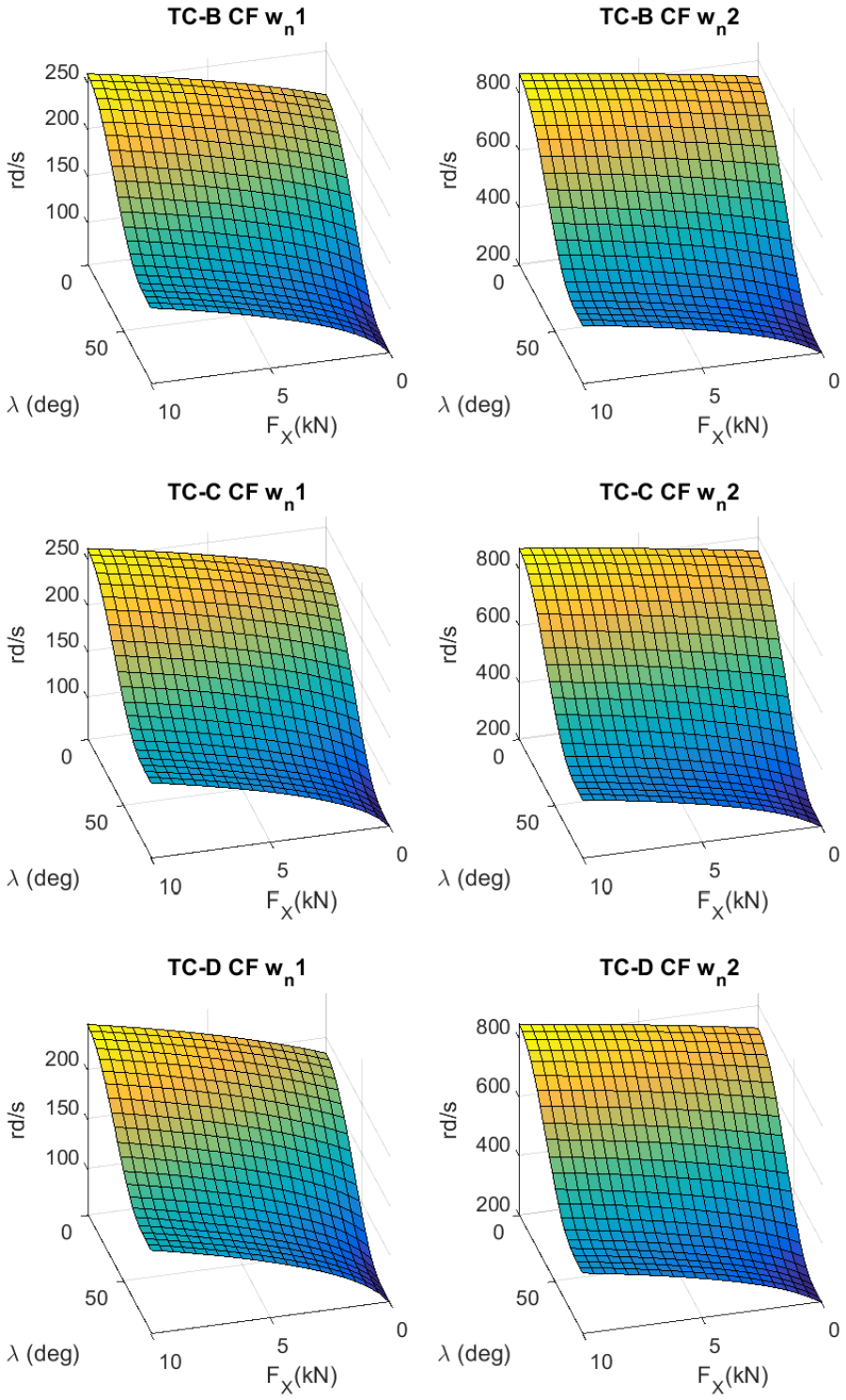

Figure 3.10 – *Clamped-free tapered beams – first and second natural frequencies vs λ vs Fx*

The curves from figure 3.10 compare the influence of angle variation in all the plies of the laminate, represented by the variable λ, with an axial tensile force F_x in the interval of 0 to 10 kN. It is possible to see from all the curves at figure 3.10, that both variables are important in the determination of the natural frequencies. It is noted in all the curves for the first and second natural frequencies, however, that the variable representing the ply orientation angle λ shows greater influence in all the considered configuration of the tapered beam, than the axial force F_x in its given interval.

In the same figure for the fundamental frequency of configuration D, in the point where λ is equal to zero-degrees and F_x is equal to 10 kN, is possible to see this frequency is lower than the other taper configurations. This can be deduced again from the fact of greater resin pockets present at the taper configuration D, which reduces the stiffness of the beam.

Also in all the curves it is noted there is a greater frequency increase when F_x goes from 0 to 10 kN while λ is equal to 90 degrees, than when it is equal to zero degrees. This is due to the fact that when the laminate has all ply orientation angles equal to 90 degrees, the structure has lower stiffness than when the ply orientation angles are equal to zero degrees. With this. the presence of a tensile axial force increases the stiffness of the structure in a greater amount when λ is equal to 90 degrees than when it is equal to zero degrees, what is reflected in the natural frequencies.

The extended results of all the design analysis performed in this study are presented in the Appendix A.

CHAPTER 4 - Optimization results

The genetic algorithm demonstrated good conversion speed and accuracy in the convergion comparison test at chapter 2, and is the algorithm chosen in the optimization for vibration of the tapered beam and the non-tapered beam, for several design requirements and boundary conditions. The optimization algorithm aims to maximize the objective function stated at equation 2.39, by defining a set of ply orientation angles which will provide satisfactory dynamic response in the bending modes of vibration.

Each optimization task must achieve a near-optimum design configuration following the respective manufacturing approach. This optimization design study aims to maximize a band free from resonance, and to maintain this band centered with the blade passing frequency, which is related to the operational frequency of the system. This optimization study considers the dynamic behavior of the laminated beam related to the bending modes of vibration only, and is a partial design requirement of a comprehensive blade design study.

For the optimization study are considered the four structural tuning approaches described in chapter 2, and the presence and the absence of a tensile axial force. The design configurations for the optimizations displayed at table 4.2 are applied to all boundary conditions, taper configurations B, C and D, and a non-tapered beam.

4.1. Selected design cases

To identify the numerical optimization results, the nomenclature follows the table 3.1 with some added acronyms at table 4.1:

RMA	Regular manufacturing approach
PA	Polynomial approximation approach
FPOA	Free ply orientation angle approach
PA&RMA	Polynomial approximation &regular manufacturing approach

Table 4.1 *– Nomenclature for manufacturing approaches*

The results are sub-divided as in the presence or absence of a constant axial tensile force F_x of 10 kN tensioning the beam (pre-stressed or free vibration), and also by the four types of structural tuning approach, as displayed in table 4.2:

	free vibration	**pre-stressed vibration**
FPOA	Result group 1	Result group 2
RMA	Result group 3	Result group 4
PA	Result group 5	Result group 6
PA&RMA	Result group 7	Result group 8

Table 4.2 *– Result groups distribution*

Each result group is defined by the combination of the four boundary conditions and a total of three taper configurations and a non-tapered configuration. Table 4.3 shows the structure of each result group:

	TC-B	TC-C	TC-D	TC-N
SS	OUTCOME SET 01	OUTCOME SET 05	OUTCOME SET 09	OUTCOME SET 13
CC	OUTCOME SET 02	OUTCOME SET 06	OUTCOME SET 10	OUTCOME SET 14
CF	OUTCOME SET 03	OUTCOME SET 07	OUTCOME SET 11	OUTCOME SET 15
FC	OUTCOME SET 04	OUTCOME SET 08	OUTCOME SET 12	OUTCOME SET 16

Table 4.3 *– Result group structure*

Each outcome set consists of five consecutive optimizations for the same design requirements, giving as output five optimized representative vectors. The complete results of the optimizations are presented in the appendix B, for all the eight result groups. In this chapter only result groups 5 to 8 for tapered beams are presented.

4.2. Optimization results

The beam is optimized for vibration by the described methodology, giving as output the ply orientation angles of the symmetric and balanced laminate defined by the upper right curve at fig. 2.10, which is the representative vector. To each result group the outcome set of five optimization curves are displayed according to its boundary condition and taper configuration.

From all the optimization achieved according to table 4.2, the result groups related to PA and PA&RMA are chosen for an in depth analysis, which are result groups 5 to 8. These outputs are reviewed in what is related to its optimized design configuration and dynamic response characteristics.

4.2.1. Optimization results for PA

The optimized solutions of the result groups 5 and 6 related to the PA structural tuning approach for free vibration and pre-stressed vibration, are presented in figures 4.1 and 4.2, respectively. The curves show the graphical representation of the optimized beam, showing the representative vector, which defines all ply orientation angles of the laminate.

From these results is possible infer that several of the optimizations achieved similar near-optimum configurations, due to the fact that the set of five repetitive optimizations converged for approximated curves for several cases. For the taper configuration simply-supported (SS) in figure 4.1, more specifically the optimization results for taper configurations B and C, the curves are mostly in the zero to fifty degrees' region for all the laminates, with few exceptions, with some representative vectors near the zero-degree region. This accounts for greater values of D_{11} which increases the overall natural frequency values. For the taper configuration D, it is noted that all the curves diverge from the zero degree region in the external plies of the laminate γ (θ_7 to θ_9). This same pattern is also seen in the pre-stressed results (fig. 4.2), for the simply-supported boundary condition, demonstrating the structure with taper configuration D has different dynamic characteristics than the structures with taper configuration B and C. This same pattern seen in taper configuration D, of diverging from the zero-degree region in the external plies of the laminate, and also having different outcomes from taper configuration B and C, can be noted in all boundary conditions, at figures 4.1 and 4.2.

For taper configuration B and C for the boundary condition clamped-clamped (CC) at figure 4.1 it is noted some fluctuation in the internal layers of the laminate, with the intermediate layers with several ply orientation angles near the 90 degree region, and the external layers near the

zero-degree region. This is a particular design configuration which seems to describe most curves with same boundary condition and taper configurations, where the external plies show a greater contribution in the bending stiffness coefficient than the intermediate plies of the laminate, which demonstrated satisfactory results in the optimizations.

It is interesting to note that for the boundary condition clamped-clamped (CC) for the taper configuration D, the intermediate and external layers fluctuate in the 50 degree region, differently than the average values observed for taper configuration B and C. This accounts for lower bending stiffness coefficient for taper configuration D than for taper configuration B and C. Due to the presence of large resin pockets the structure presented with taper configuration D presents also a different dynamic behavior, and achieved a tuned design configuration with different ply orientation angles. Because the band free from natural frequency maximized by the algorithm can be defined between any consecutive pair of natural frequencies (equation 2.37), the accentuated structural differences of taper configuration D can lead the optimization to achieve a design configuration maximizing the band free from natural frequencies with a different pair of natural frequencies, what would generate much dissimilarities in the optimizations outcomes from taper configurations B and C, even with similar design parameters.

In figure 4.1, the results for clamped-free boundary condition (CF), for the taper configuration B and C, demonstrate that the ply orientation angles of the intermediate laminate section β (θ_4 to θ_6) are mostly defined in the range between forty and one hundred degrees, while the external laminates, γ section (θ_7 to θ_9), are mostly defined near the zero and fifty degree region. The same pattern is also seen in figure 4.2 for the pre-stressed results, for the same boundary condition and taper configuration.

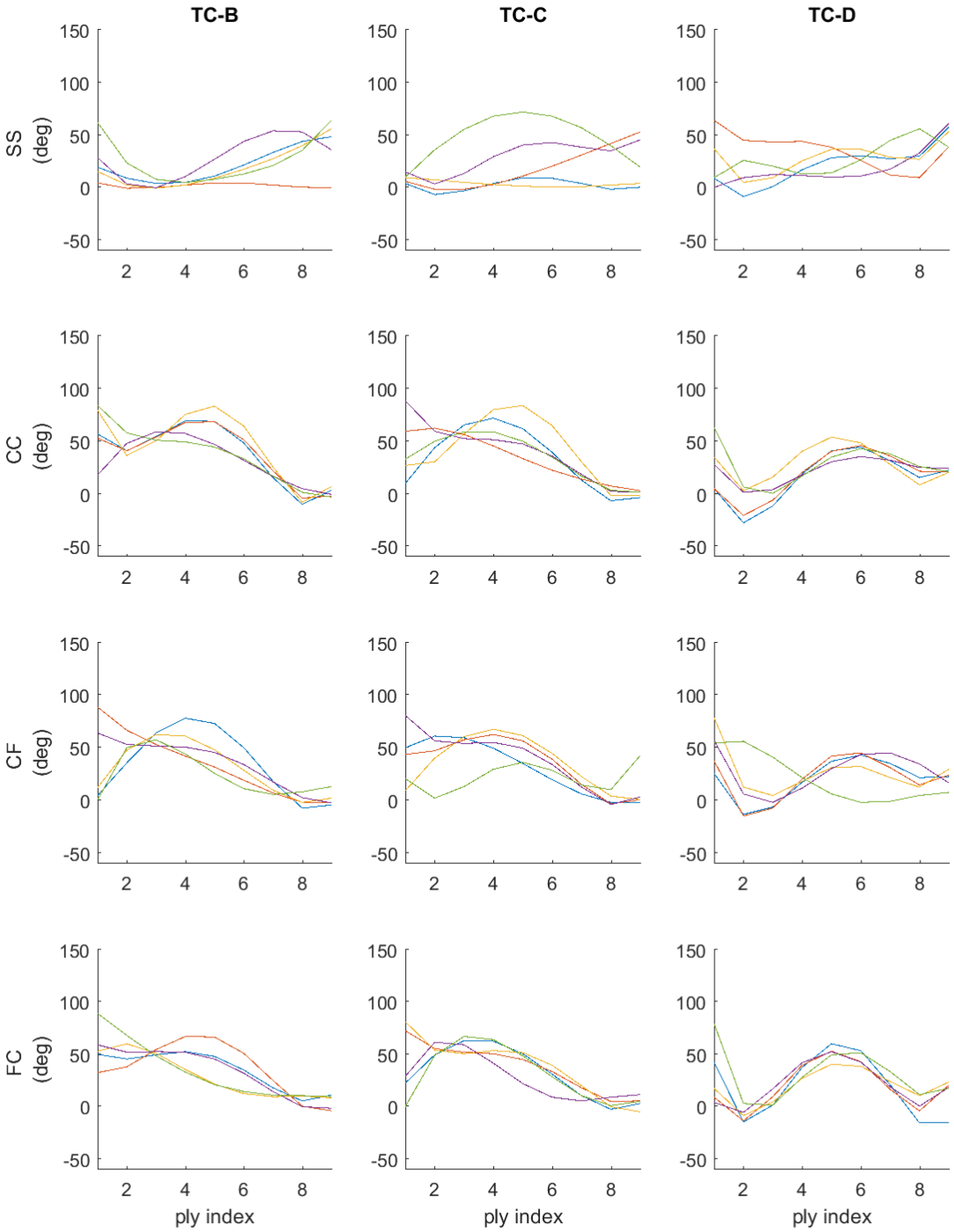

Figure 4.1 *– Tapered beam optimization results - result group 5*

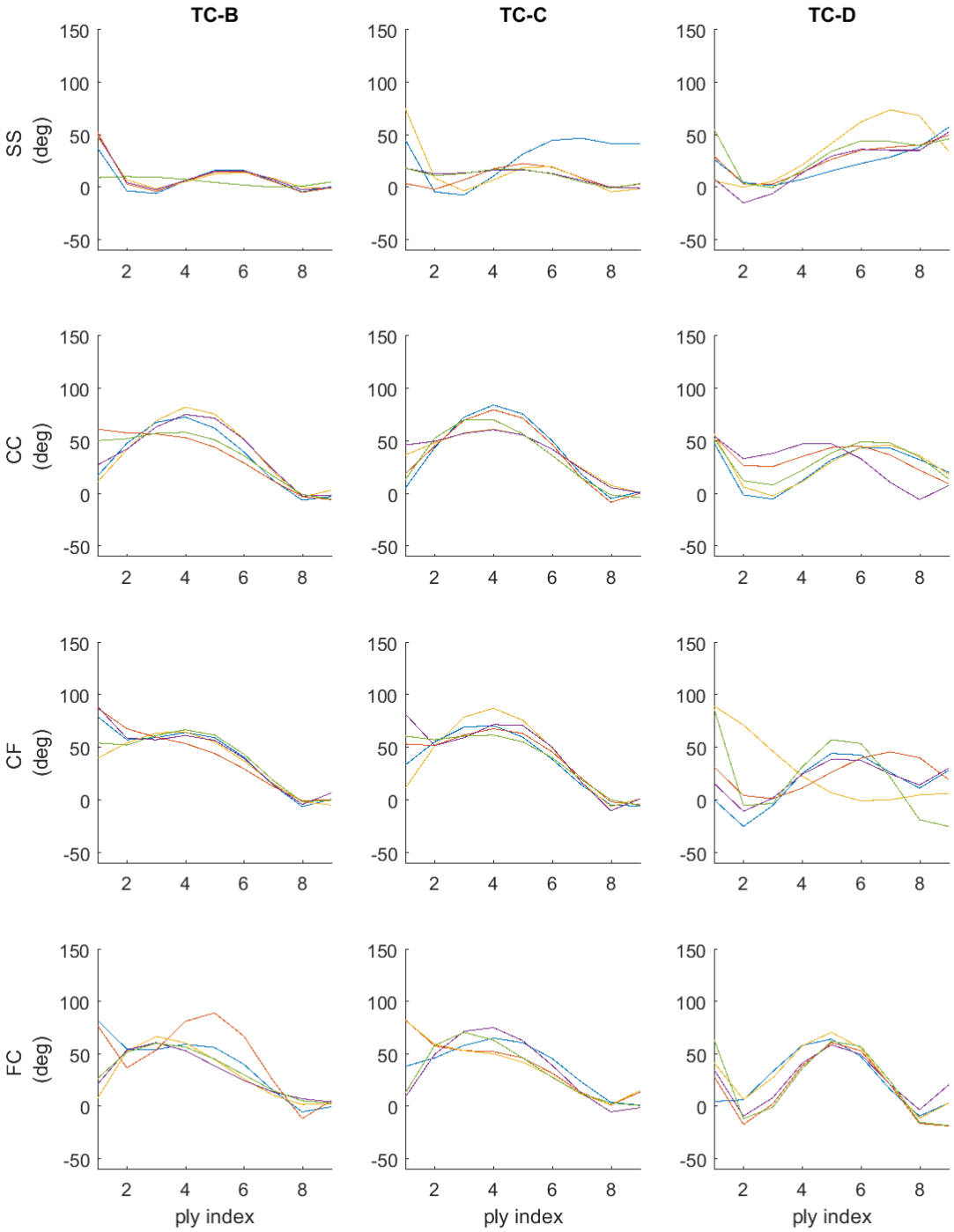

Figure 4.2 *– Tapered beam optimization results - result group 6*

From equations 2.2 to 2.5 is possible to infer that ply orientation angles near the ninety degrees region account for lower values of D_{11}, and lower angles account for higher values of D_{11}. It is noted that the orientation angles of internal plies in the α section (θ_1 to θ_3) are the plies with greater variance in all the optimization results. This is occasioned due to the fact that the internal plies of the laminate have lower contribution to the bending stiffness coefficient D_{11}, therefore, it assumes different values during optimization. For the clamped-free boundary condition (CF) and the taper configuration D, also in figure 4.1, the external plies γ (θ_7 to θ_9) assume values near to the 40 degrees region. This large difference from taper configurations B and C can be caused by the larger resin pockets in the taper configuration D, what greatly modifies the structural characteristics of the beam.

In figure 4.1, and figure 4.2, are observed for the clamped-free boundary condition (CF) and taper configurations B and C similar results, while for taper configuration D the optimized values again are fairly different from configurations B and C.

For the results of the free-clamped boundary condition (FC) of PA tuning approach, interestingly the results are similar, for pre-stressed and free vibration optimization results (figures 4.1 and 4.2), with some slight differences accounted for the load presence.

The results for the taper configuration D diverge from the region of zero-degree in the external plies of the beam, γ section (θ_7 to θ_9), for several of the boundary conditions, from what is possible to infer that the near optimum regions for this taper configuration are located near lower D_{11} values. For the result group 6 and 8 (figures 4.2 and 4.4) the beam is subjected to an axial tensile force of N_x equal to 100 kN/m. As the beam width is 0.1m, the total axial force F_x is equal to 10 kN. Comparing both structural tuning approaches with and without the presence of a

load, it is possible to note that the pre-stressed condition modifies the rigidity of the structure, which amounts for some differences between the ply orientation angles.

In order to achieve solutions with greater precision it is possible to apply a more powerful algorithm like RND+HC. The downside of this algorithm, however, would be that this method is more time consuming.

4.2.2. Optimization results for PA&RMA

From result group 7, in figure 4.3, it is noted that in the simply-supported boundary condition (SS), all the ply orientation angles of the intermediate and external plies, sections β (θ_4 to θ_6) and γ (θ_7 to θ_9), are lower than 90 degrees, while some curves have several angles in the zero degree region. This amounts to greater D_{11} values, reducing the structure flexibility, where a structure with greater rigidity has increased natural frequency values. Also for the same boundary condition, it is seen that some curves have converged to fairly similar values in the same set of results, from what is possible to understand that the optimization has reached to similar near-optimum location in several cases. These observations for the simply-supported boundary condition in the result group 7 also can be applied to result group 8, in figure 4.4, for the same boundary condition. At figure 4.3, for the result group 7, in the clamped-clamped boundary condition (CC) it is observed several design configurations, where for the taper configuration B, C and D the intermediate layers of the beams display ply orientation angles between zero and ninety degrees, while for the external layers of the beam it displays ply orientation angles between zero and forty five degrees.

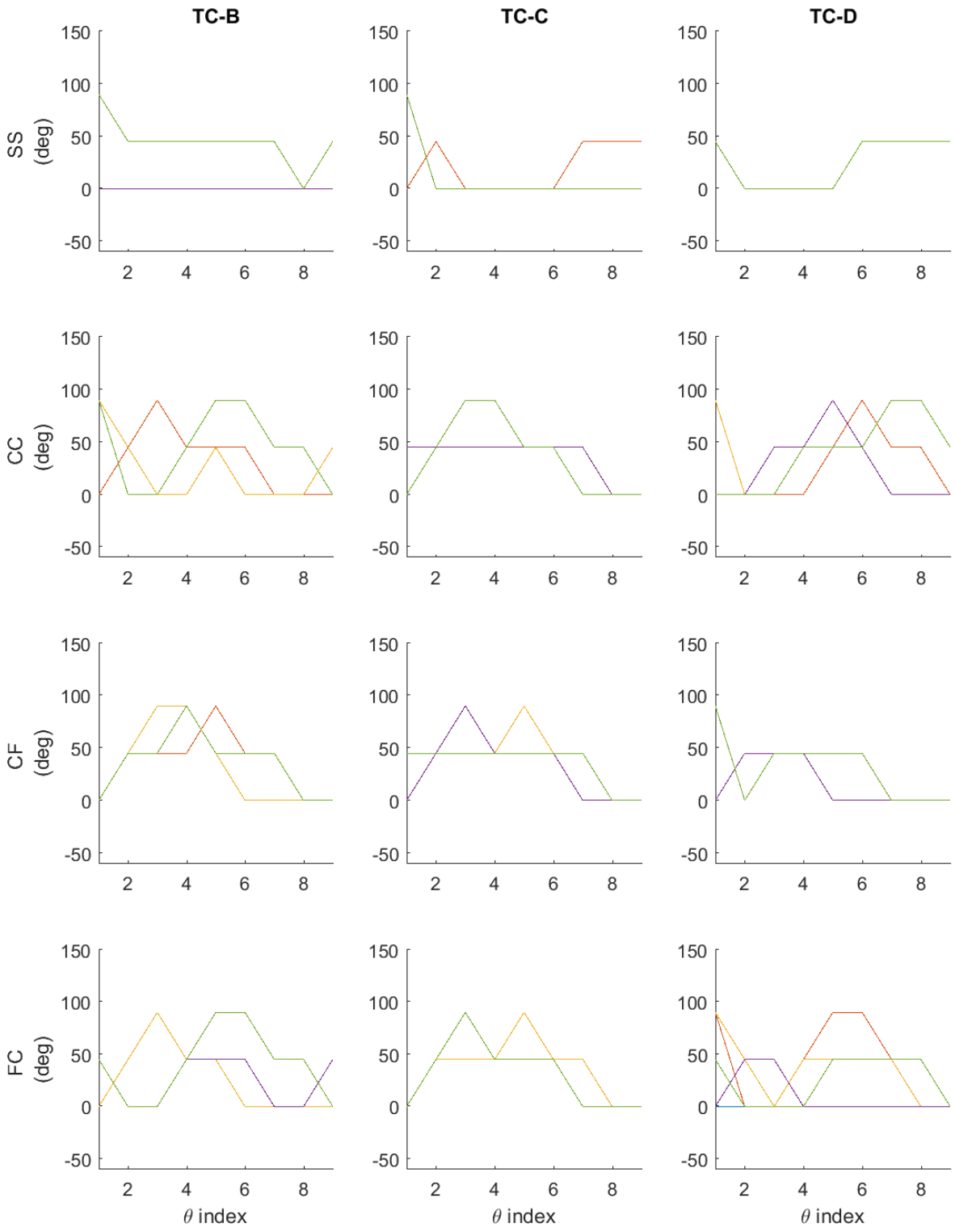

Figure 4.3 *– Tapered beam optimization results - result group 7*

This observation can also be applied to the result group 8 at figure 4.4, where the only exception is for the taper configuration D where all angles are between zero and forty five degrees and the external layers are close to the zero-degree region. What can be interpreted from these results is that also for these cases, taper configuration D has a different structural characteristics, which also for the PA&RMA tuning approach displays distinct near-optimum design configurations with the same design functionality than the other taper configurations.

For the clamped-free (CF) and free-clamped (FC) boundary conditions of result group 7 (figure 4.3), is possible to observe that the external plies of the laminate have converged to the zero-degrees region, in most cases, and also the same can be said for the curves of result group 8, with the same boundary conditions. From this it is possible to understand that for the given blade passing frequency w_p in the given optimization design space, the near-optimum values are near regions where the bending stiffness coefficient D_{11} has increased values, since the external layers of the laminate have increased contribution in the D_{11} coefficient.

It is not very clear how the tensile axial force interacts in the optimized design for PA&RMA. It is possible to infer however, that for both free and pre-stressed vibration optimizations, the load condition does modify the optimized design configurations. Also is possible to infer that there are several achieved solutions with coincident near-optimum configurations.

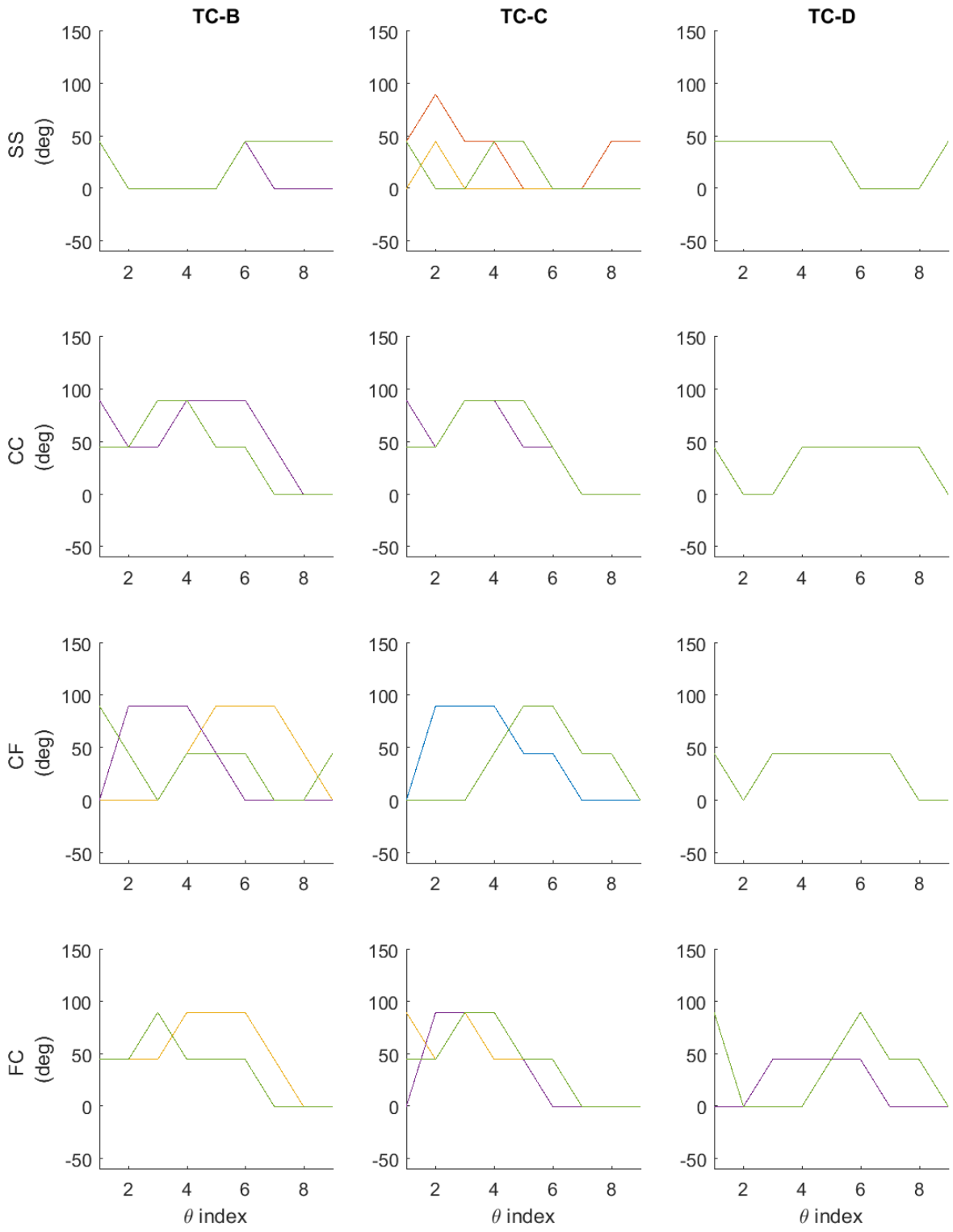

Figure 4.4 *– Tapered beam optimization results - result group 8*

4.3. In-plane and out-of-plane stresses comparison

From the previous optimizations groups analyzed, it is sampled results for the taper configuration B, and an in depth review is made to access the efficiency of the manufacturing approaches PA and PA&RMA in term of important internal stresses for laminated structure, as the in-plane and out-of-plane stresses.

In order to evaluate the in-plane and out-of-plane stresses of the tapered beams optimized with the polynomial approximation and regular manufacturing approach (PA&RMA) and the polynomial approximation approach (PA), the beams are modeled using the ACP composite module of the software ANSYS v17.

Figure 4.5a display the ANSYS model of the beam with taper configuration B, where the thickness is increased 20 times for visualization. Figure 4.5b displays the center line of each ply of the same beam, also with increased thickness.

Figure 4.6a displays the beam with actual thickness dimension, and figure 4.6b displays the out-of-plane stresses analysis of a single ply, showing the screen display of ANSYS, while acquiring the internal stresses of the tapered beam. The layers are considered as a single surface in the model of the ACP module, and in the structural module the element applied is the cubical element of 40 by 33.33 millimeters, with the same height as the thickness of the beam.

(a)

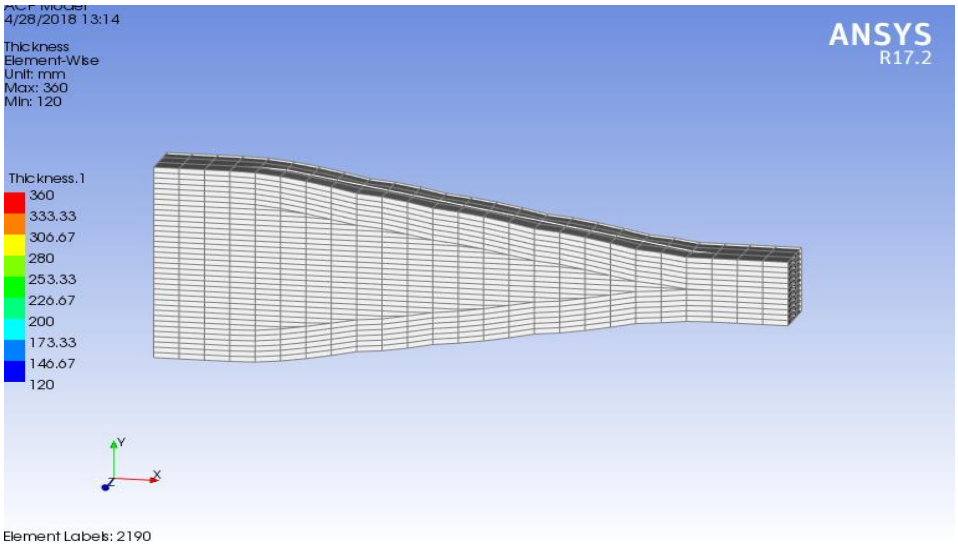

(b)

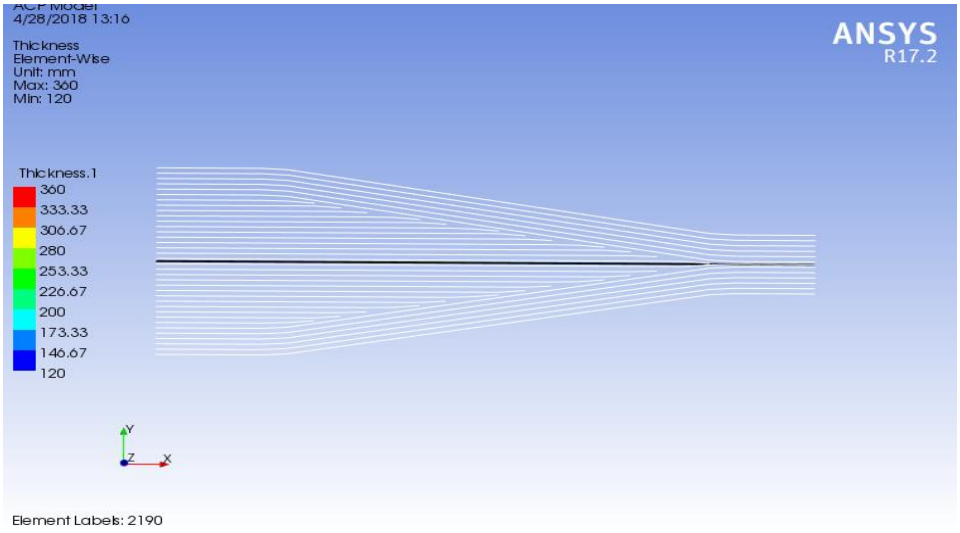

Figure 4.5a – *Tapered beam with thickness increased 20x – model*

Figure 4.5b – *Tapered beam with thickness increased 20x – ply centerline*

(a)

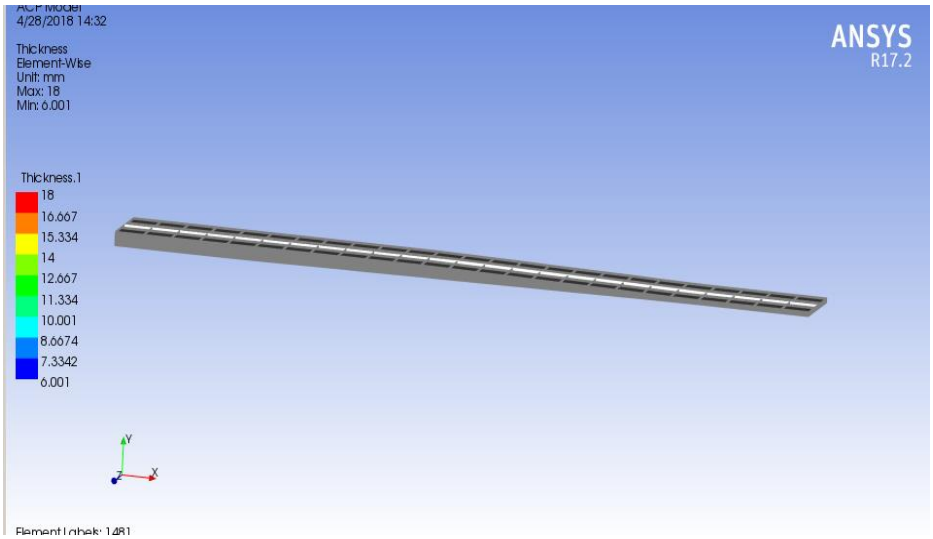

(b)

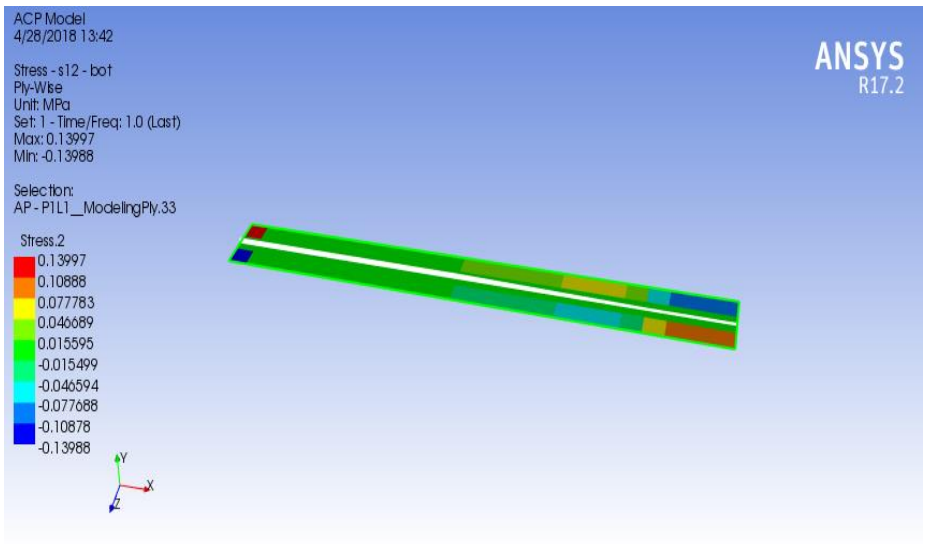

Figure 4.6a – *Tapered beam modeled in ANSYS*

Figure 4.6b – *Single ply stress analysis*

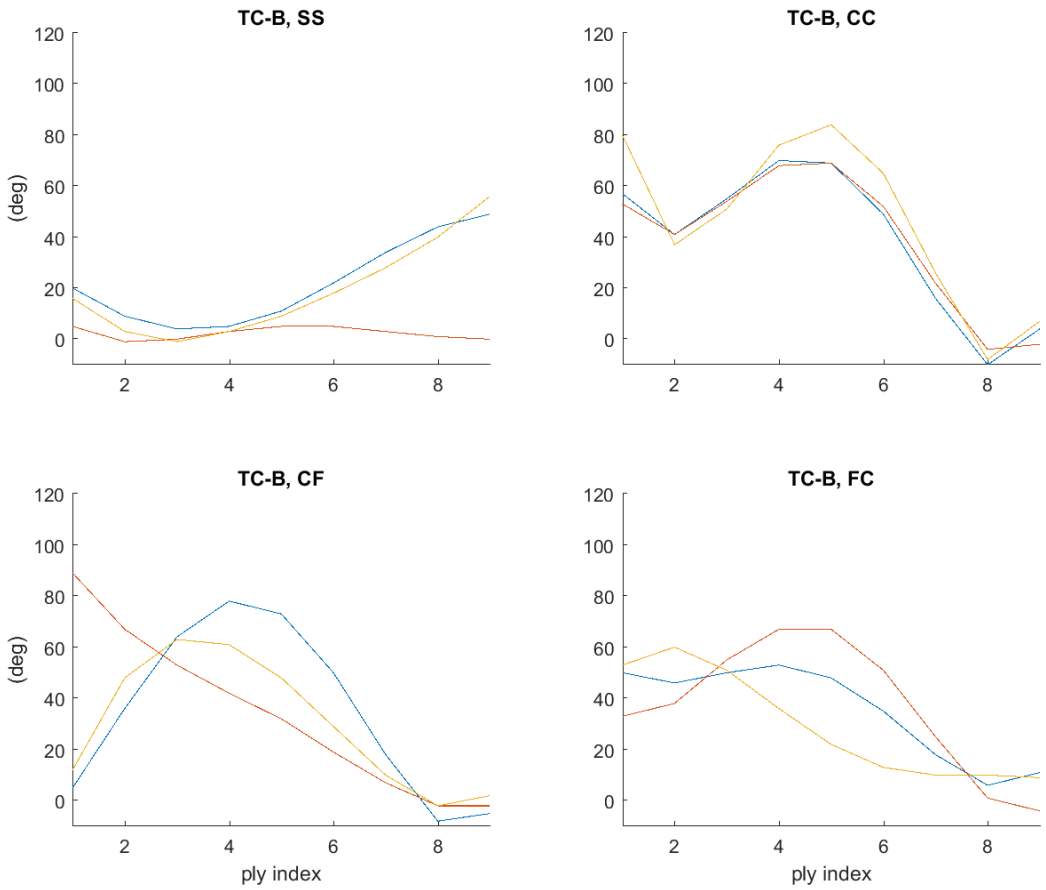

***Figure 4.7** – Plot of selected samples from result group 5 – PA*

From result groups 5 (fig. 4.7) and 7 (fig. 4.8), three samples from each outcome set of taper configuration B are selected, for all the four boundary conditions, giving a total of twenty-four optimized beams sampled. These solutions are evaluated to determine the maximum in-plane stresses σ_{11} and σ_{12}, and out-of-plane stresses σ_{13} and σ_{23}, when one of the extremity of the

beam is subjected to a vertical displacement of the same magnitude as the higher thickness. These values and other details such as the overall fitness value and boundary condition of the selected samples of result group 5 are given in table 4.4, and those of the result group 7 are given in table 4.5. These stress values are evaluated by ANSYS from the optimized solutions for free vibration.

In figure 4.7 the selected samples of result group 5 are related to the optimizations performed with the polynomial approximation approach (PA). In the same figure, for the boundary condition clamped-clamped (CC) it is noted that the curves are very similar, with ply orientation angles near seventy degrees in the intermediate layers of the laminate and angles near zero degrees in the external layers, with much similarity between the results.

In table 4.5, for items 21, 22 and 23, which are the results for the CC boundary condition, we see that the fitness value (FIT) achieved in the optimizations are fairly similar also, in the range of 2220 to 2250, which is significantly a high value among the samples. Interestingly, the fitness values are also close for the curves of the boundary conditions clamped-free (CF) and free-clamped (FC), however the fitness value of these curves are not so close as those for the clamped-clamped (CC) boundary condition. This demonstrates that the optimization problem of the present study has multiple local optimum regions, which are represented by the different curves, which have often achieved similar near-optimum objective values.

For the boundary condition simply-supported (SS) at figure 4.7, the three curves have similar ply orientation angles for the internal plies of the laminate, while one sample shows different values for the intermediate and external plies, assuming ply orientation angles near the zero-degree region to all plies of the laminate, which accounts for greater D_{11}values.

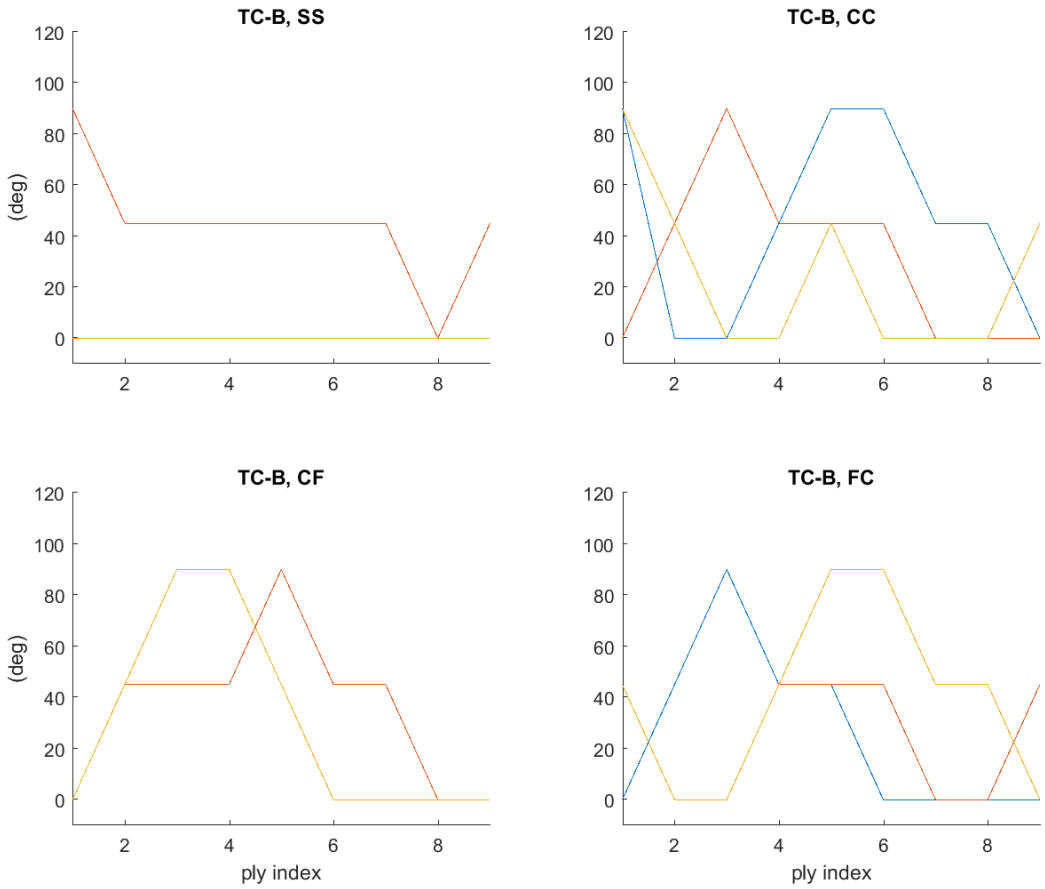

Figure 4.8 – *Plot of selected samples from result group 7 – PA&RMA*

In table 4.5, for the simply-supported (SS) boundary condition, we see that the laminate with the external plies presenting orientation angles near the zero-degree region is the item 2, which has greater fitness value than the two other samples for the same boundary condition.

The laminate represented by the item 2 in table 4.4 presents all the ply orientation angles of the representative vector equal or lower than five degrees.

ITEM	1	2	3	21	22	23	41	42	43	61	62	63
TC	b	b	b	b	b	b	b	b	b	b	b	b
BC	SS	SS	SS	CC	CC	CC	CF	CF	CF	FC	FC	FC
CURVE#	1	2	3	1	2	3	1	2	3	1	2	3
FIT	1948.57	2079.53	1964.72	2249.39	2248.8	2220	2246.36	2272.63	2271.63	2251.46	2259.98	2293.58
L 18	-49	0	-56	-4	2	-7	5	2	-2	-11	4	-9
L 17	49	0	56	4	-2	7	-5	-2	2	11	-4	9
L 16	-44	-1	-40	10	4	8	8	2	2	-6	-1	-10
L 15	44	1	40	-10	-4	-8	-8	-2	-2	6	1	10
L 14	-34	-3	-28	-16	-22	-26	-18	-7	-10	-18	-25	-10
L 13	34	3	28	16	22	26	18	7	10	18	25	10
L 12	-22	-5	-18	-49	-52	-65	-50	-19	-29	-35	-51	-13
L 11	22	5	18	49	52	65	50	19	29	35	51	13
L 10	-11	-5	-9	-69	-69	-84	-73	-32	-48	-48	-67	-22
L 9	11	5	9	69	69	84	73	32	48	48	67	22
L 8	-5	-3	-3	-70	-68	-76	-78	-42	-61	-53	-67	-36
L 7	5	3	3	70	68	76	78	42	61	53	67	36
L 6	-4	0	1	-55	-54	-51	-64	-53	-63	-50	-55	-51
L 5	4	0	-1	55	54	51	64	53	63	50	55	51
L 4	-9	1	-3	-41	-41	-37	-36	-67	-48	-46	-38	-60
L 3	9	-1	3	41	41	37	36	67	48	46	38	60
L 2	-20	-5	-16	-57	-53	-80	-5	-89	-12	-50	-33	-53
L 1	20	5	16	57	53	80	5	89	12	50	33	53
L -1	20	5	16	57	53	80	5	89	12	50	33	53
L -2	-20	-5	-16	-57	-53	-80	-5	-89	-12	-50	-33	-53
L -3	9	-1	3	41	41	37	36	67	48	46	38	60
L -4	-9	1	-3	-41	-41	-37	-36	-67	-48	-46	-38	-60
L -5	4	0	-1	55	54	51	64	53	63	50	55	51
L -6	-4	0	1	-55	-54	-51	-64	-53	-63	-50	-55	-51
L -7	5	3	3	70	68	76	78	42	61	53	67	36
L -8	-5	-3	-3	-70	-68	-76	-78	-42	-61	-53	-67	-36
L -9	11	5	9	69	69	84	73	32	48	48	67	22
L -10	-11	-5	-9	-69	-69	-84	-73	-32	-48	-48	-67	-22
L -11	22	5	18	49	52	65	50	19	29	35	51	13
L -12	-22	-5	-18	-49	-52	-65	-50	-19	-29	-35	-51	-13
L -13	34	3	28	16	22	26	18	7	10	18	25	10
L -14	-34	-3	-28	-16	-22	-26	-18	-7	-10	-18	-25	-10
L -15	44	1	40	-10	-4	-8	-8	-2	-2	6	1	10
L -16	-44	-1	-40	10	4	8	8	2	2	-6	-1	-10
L -17	49	0	56	4	-2	7	-5	-2	2	11	-4	9
L -18	-49	0	-56	-4	2	-7	5	2	-2	-11	4	-9
max σ11 (Mpa)	1.6556	3.49	1.7171	3.0845	3.1317	3.137	3.0832	3.1863	3.0704	2.9385	3.0073	3.1312
max σ12 (Mpa)	0.31958	0.19689	0.043165	0.095664	0.095189	0.089157	0.091145	0.093393	0.092489	0.11231	0.095833	0.097238
max σ13 (Mpa)	0.045055	0.037969	0.039676	0.029343	0.027838	0.027184	0.031156	0.033499	0.035744	0.039217	0.030715	0.036881
max σ23 (Mpa)	0.038691	0.043751	0.023587	0.028024	0.028027	0.0237	0.027966	0.038014	0.031717	0.037322	0.032648	0.036058

Table 4.4 – *Selected samples from result group 5 – PA*

In figure 4.8 and table 4.5, are presented the selected samples for the polynomial approximation and regular manufacturing approach (PA&RMA), without the presence of a tensile axial force.

For the boundary condition simply-supported (SS) we see from table 4.6 at items 1 and 4, that this tuning approach presented two curves with all the ply orientation angles equal to zero, with angles approximated to item 2 of table 4.4 of the PA tuning approach. This is a particular case that can help understand the effect on the in-plane and out-of-plane stresses, when a laminate presents a ply orientation angle gradient along the laminate thickness equal to zero, and all the fibers are oriented in the main stress direction.

At figure 4.8 for the sample PA&RMA results, in the boundary conditions clamped-clamped (CC), clamped-free (CF) and free-clamped (FC), it is noted that the ply orientation angles of the representative vector vary from zero to ninety degrees in most of the plies, and only in the external plies of these laminates the angles are between zero and forty-five degrees, which accounts for increased bending stiffness coefficient of the beam from the external plies, which have greater contribution in the overall bending stiffness coefficient of the beam. Because the optimization objective considers only the maximization of the band free from natural frequencies near the blade passing frequency, the overall stiffness of the component is not an optimization objective. Yet, in an optimization study considering also maximum deformation under loading and vibration, maximum deformation amplitude should be an important design parameter.

For the boundary condition clamped-free (CF) at figure 4.8 the plies are set with varied ply orientation angles between zero and ninety degrees in the internal and intermediate layer of the component, and follow a zero degree ply orientation angle in the external plies. These results show a pattern, which is related to a particular near-optimum configuration which maximizes the objective function. For the boundary condition free-clamped (FC) the same observations can be made, with the difference that it presents ply orientation angles between zero and forty five degrees in the external plies, differently from the PA tuning approach, which has all the external

plies near the zero degrees region. One possibility this occurs is because the PA&RMA tuning approach has less degrees of freedom than the PA approach, and overall approximations achieve different solutions with lower fitness value, as confirms the items 63, 64 and 65 from table 4.5 and items 61, 62 and 63 from table 4.4.

ITEM	1	3	4	21	22	23	41	42	43	63	64	65
TC	b	b	b	b	b	b	b	b	b	b	b	b
BC	SS	SS	SS	CC	CC	CC	CF	CF	CF	FC	FC	FC
CURVE#	1	3	4	1	2	3	1	2	3	3	4	5
FIT	2112.47	1890.69	2112.47	2084.4	2229.8	2106.13	2159.07	2159.07	2233.13	2191.62	2155.48	2114.52
L 18	0	-45	0	0	0	-45	0	0	0	0	-45	0
L 17	0	45	0	0	0	45	0	0	0	0	45	0
L 16	0	0	0	-45	0	0	0	0	0	0	0	-45
L 15	0	0	0	45	0	0	0	0	0	0	0	45
L 14	0	-45	0	-45	0	0	-45	-45	0	0	0	-45
L 13	0	45	0	45	0	0	45	45	0	0	0	45
L 12	0	-45	0	-90	-45	0	-45	-45	0	0	-45	-90
L 11	0	45	0	90	45	0	45	45	0	0	45	90
L 10	0	-45	0	-90	-45	-45	-90	-90	-45	-45	-45	-90
L 9	0	45	0	90	45	45	90	90	45	45	45	90
L 8	0	-45	0	-45	-45	0	-45	-45	-90	-45	-45	-45
L 7	0	45	0	45	45	0	45	45	90	45	45	45
L 6	0	-45	0	0	-90	0	-45	-45	-90	-90	0	0
L 5	0	45	0	0	90	0	45	45	90	90	0	0
L 4	0	-45	0	0	-45	-45	-45	-45	-45	-45	0	0
L 3	0	45	0	0	45	45	45	45	45	45	0	0
L 2	0	-90	0	-90	0	-90	0	0	0	0	-45	-45
L 1	0	90	0	90	0	90	0	0	0	0	45	45
L -1	0	90	0	90	0	90	0	0	0	0	45	45
L -2	0	-90	0	-90	0	-90	0	0	0	0	-45	-45
L -3	0	45	0	0	45	45	45	45	45	45	0	0
L -4	0	-45	0	0	-45	-45	-45	-45	-45	-45	0	0
L -5	0	45	0	0	90	0	45	45	90	90	0	0
L -6	0	-45	0	0	-90	0	-45	-45	-90	-90	0	0
L -7	0	45	0	45	45	0	45	45	90	45	45	45
L -8	0	-45	0	-45	-45	0	-45	-45	-90	-45	-45	-45
L -9	0	45	0	90	45	45	90	90	45	45	45	90
L -10	0	-45	0	-90	-45	-45	-90	-90	-45	-45	-45	-90
L -11	0	45	0	90	45	0	45	45	0	0	45	90
L -12	0	-45	0	-90	-45	0	-45	-45	0	0	-45	-90
L -13	0	45	0	45	0	0	45	45	0	0	0	45
L -14	0	-45	0	-45	0	0	-45	-45	0	0	0	-45
L -15	0	0	0	45	0	0	0	0	0	0	0	45
L -16	0	0	0	-45	0	0	0	0	0	0	0	-45
L -17	0	45	0	0	0	45	0	0	0	0	45	0
L -18	0	-45	0	0	0	-45	0	0	0	0	-45	0
max σ11 (Mpa)	3.4779	2.5325	3.4779	3.1638	3.0669	3.0867	3.1278	3.1278	3.1475	3.1475	2.9138	3.16
max σ12 (Mpa)	0.013625	0.18787	0.013625	0.14589	0.10151	0.19897	0.11941	0.11941	0.080707	0.080707	0.22582	0.14678
max σ13 (Mpa)	0.03797	0.034005	0.03797	0.033628	0.037742	0.043581	0.36496	0.36496	0.033941	0.033941	0.052584	0.034229
max σ23 (Mpa)	0.01838	0.048486	0.01838	0.033676	0.036483	0.042336	0.032772	0.032772	0.021856	0.021856	0.03728	0.024335

Table 4.5 – *Selected samples from result group 7 – PA&RMA*

From an overall analysis of tables 4.4 and 4.5, we note that the fitness values are greater for the result group 5, which is related to the structural tuning approach PA, than for the result group 7, related to the structural tuning approach PA&RMA. From this it is possible to infer that the best tuning approach for optimization for vibration, from these two cases and for this particular sample, is the PA tuning approach, giving greater length of band free from natural frequencies dw and lower offset error $\overline{w}_e$, which are the components of the fitness value, given by equation 2.41.

From table 4.5 it is noted that the laminates with all ply orientation angles equal or closer to zero degrees (item 3 from table 4.4 and items 1 and 3 from table 4.5), are the ones with lower values for σ_{12}, however it shows large values for σ_{11}. Considering that having the main stresses in the direction of the fibers is a good design practice, this can be considered as an efficient design solution.

Figure 4.9 shows the maximum σ_{11} stress value for the samples solutions, where it is noted some fluctuation for both manufacturing approaches for the results related to the simply-supported (SS) boundary condition, and similar values for the other boundary conditions. As these values do not show much difference, a better inference is further made with average values at table 4.7.

At figure 4.10 it is noted σ_{12} with similar and reduced values for the boundary conditions clamped-clamped (CC), clamped-free (CF) and free-clamped (FC) related to the PA tuning approach. This can indicate the high ply orientation angle gradient related to the PA&RMA tuning approach can cause great fluctuation in the internal stresses of the laminate, when compared with the PA tuning approach. From table 4.6, items 1 and 4 present an optimized

laminate with all orientation angles equal to zero-degrees, and at image 4.10 at boundary condition simply-supported (SS) these design configurations show lower values for σ_{12}.

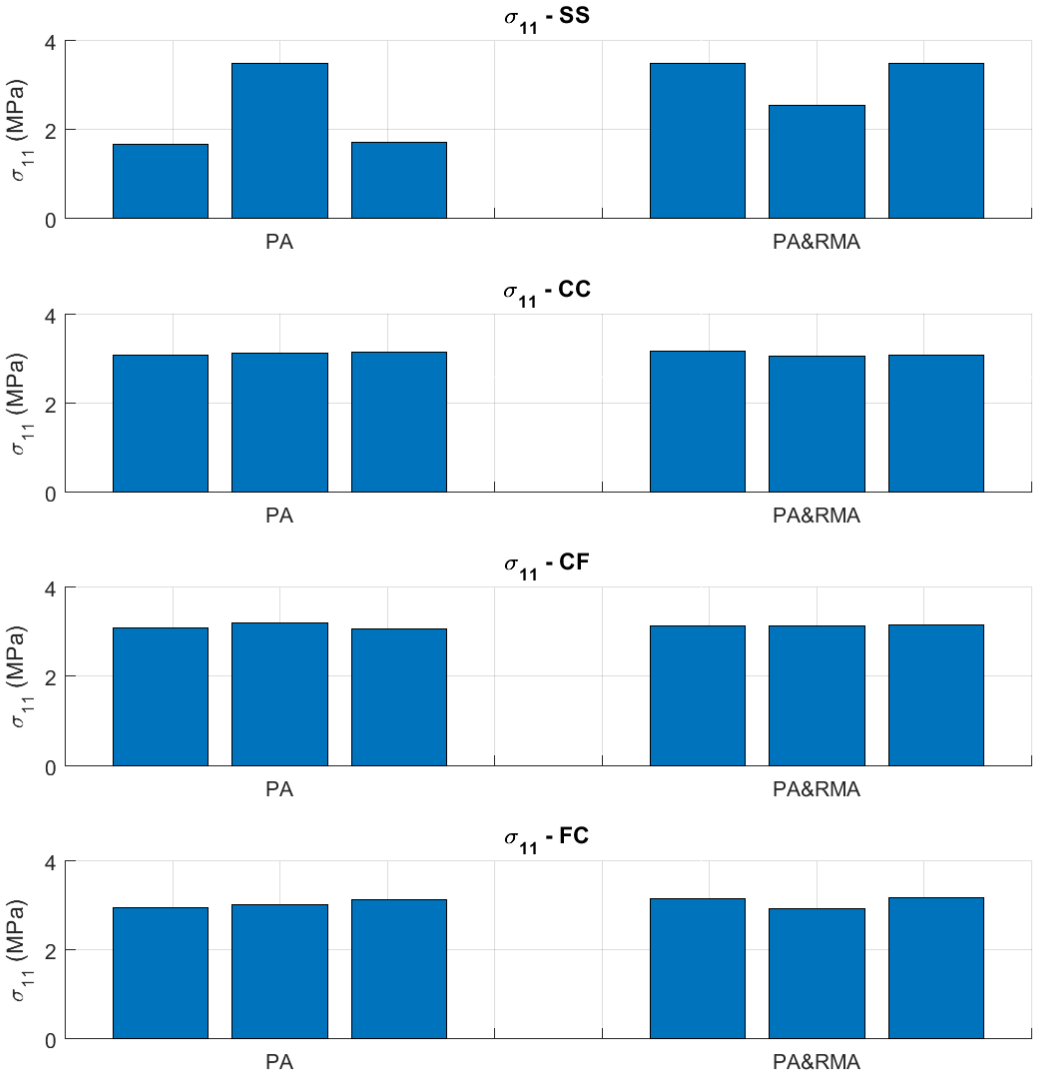

Figure 4.9 *– σ_{11} values for optimized sample for various boundary conditions*

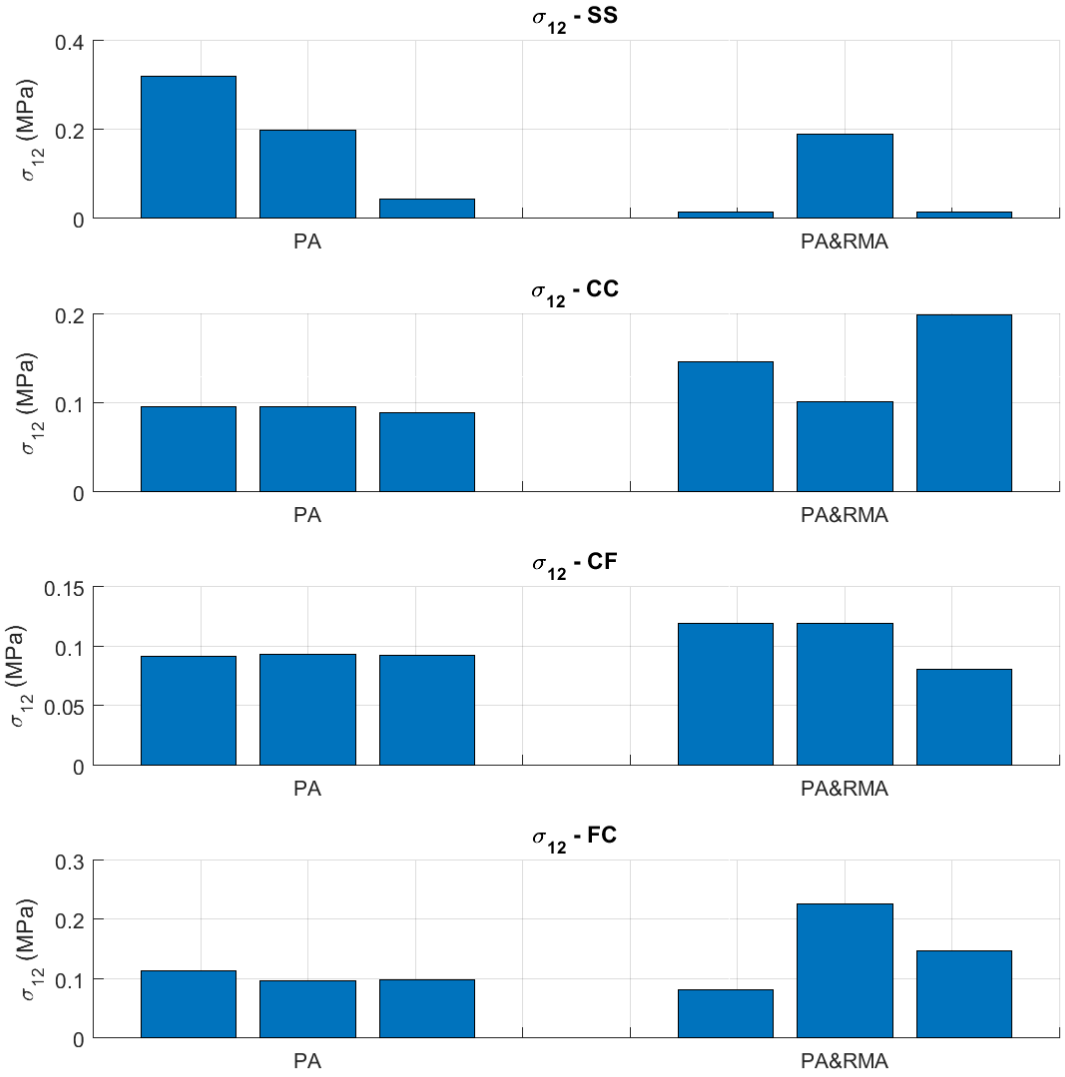

Figure 4.10 – *σ_{12} values for optimized sample for various boundary conditions*

From figure 4.9, it is noted that all the solutions for the boundary conditions CC, CF and FC show similar values for σ_{11} for both tuning approaches. In figure 4.10, is possible to see that with the exception of the SS boundary condition, all samples of the PA tuning approach show similar values for σ_{12} near to 0.1 MPa, while for the PA&RMA tuning approach there is greater variance.

Interestingly, the maximum values for σ_{13} and σ_{23} in figures 4.11 and 4.12 show large variance among the boundary conditions, ranging from 0.03 to 0.05 MPa for σ_{13}, and from 0.02 to 0.05 MPa for σ_{23}, for both tuning approaches. The samples with lower values for σ_{23} are the items 1 and 3 from table 4.6 and item 3 from table 4.5, which present ply orientation angles near or equal to zero-degrees, having σ_{23} around 0.02 MPa, which are have lower values among the samples.

The greater value of σ_{23} of the present sample is related to the item 3 of table 4.5, with the boundary condition SS for the PA&RMA tuning approach. As there is much variance among the samples, more precise conclusions on the in-plane and out-of-plane stresses can be made with the evaluation of larger samples.

The objective value that has been maximized by the optimization, which is also called fitness (FIT) shows similar amplitude for each one of the 24 samples, as observed from figure 4.13. However, for several structural components that are required to be very efficient, even an efficiency increase in the amount of 2 or 3% can be meaningful for related applications.

At figure 4.14 the fitness value achieved in the optimizations show much similarity in all boundary conditions, where the values related to the PA tuning approach show a slight increase. Yet the similarity of the achieved fitness between all the configurations shows the optimizations have produced solutions with the same level of efficiency.

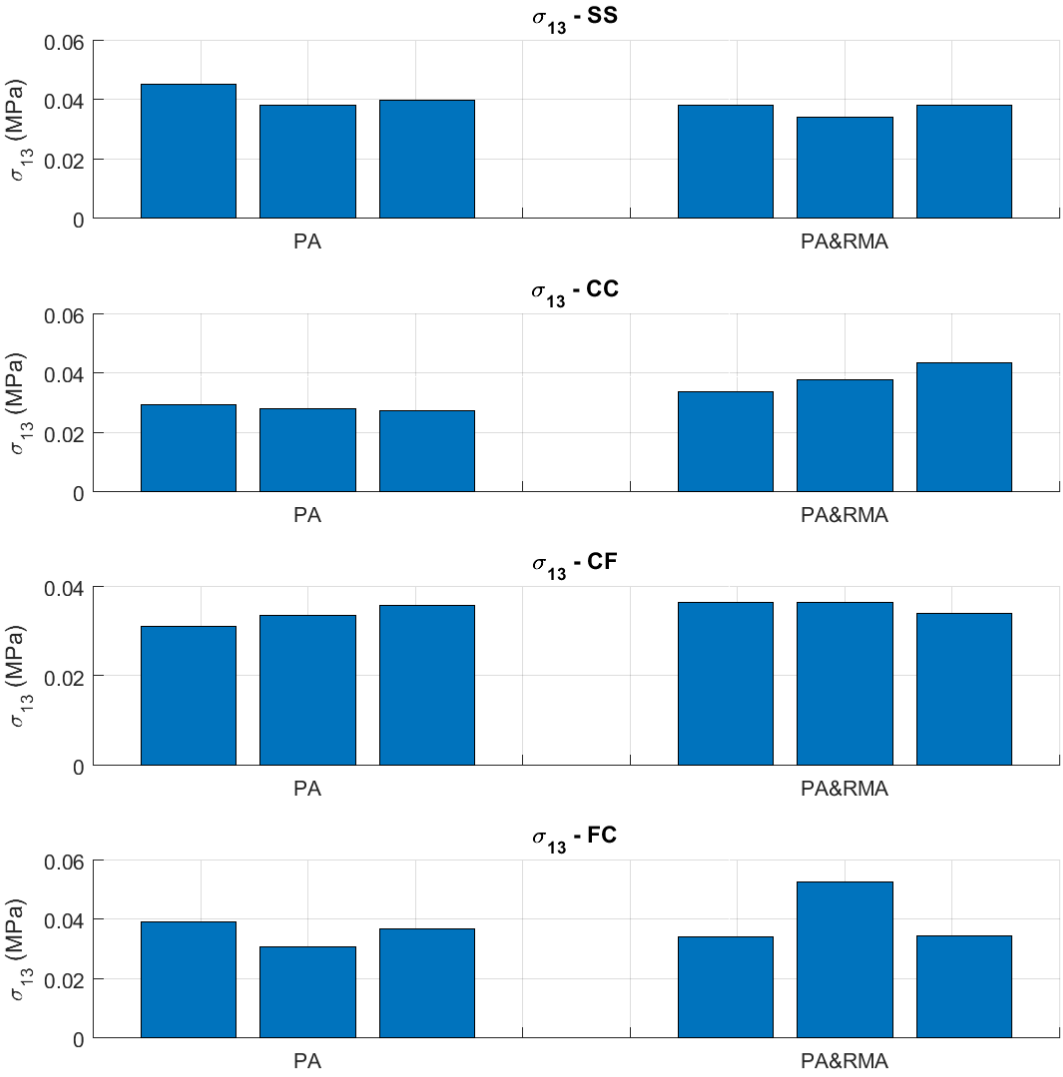

Figure 4.11 *– σ_{13} values for optimized sample for various boundary conditions*

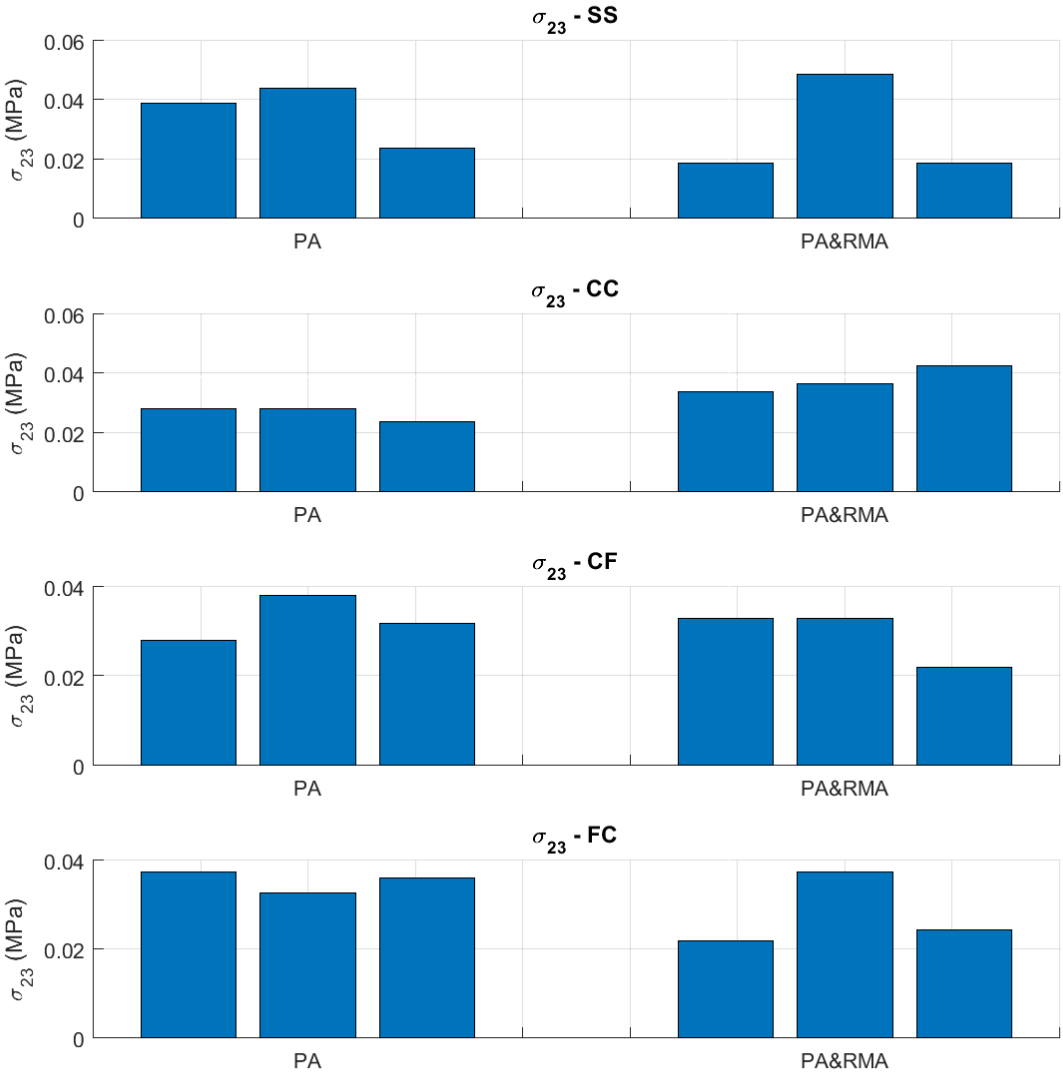

Figure 4.12 *– σ_{23} values for optimized sample for various boundary conditions*

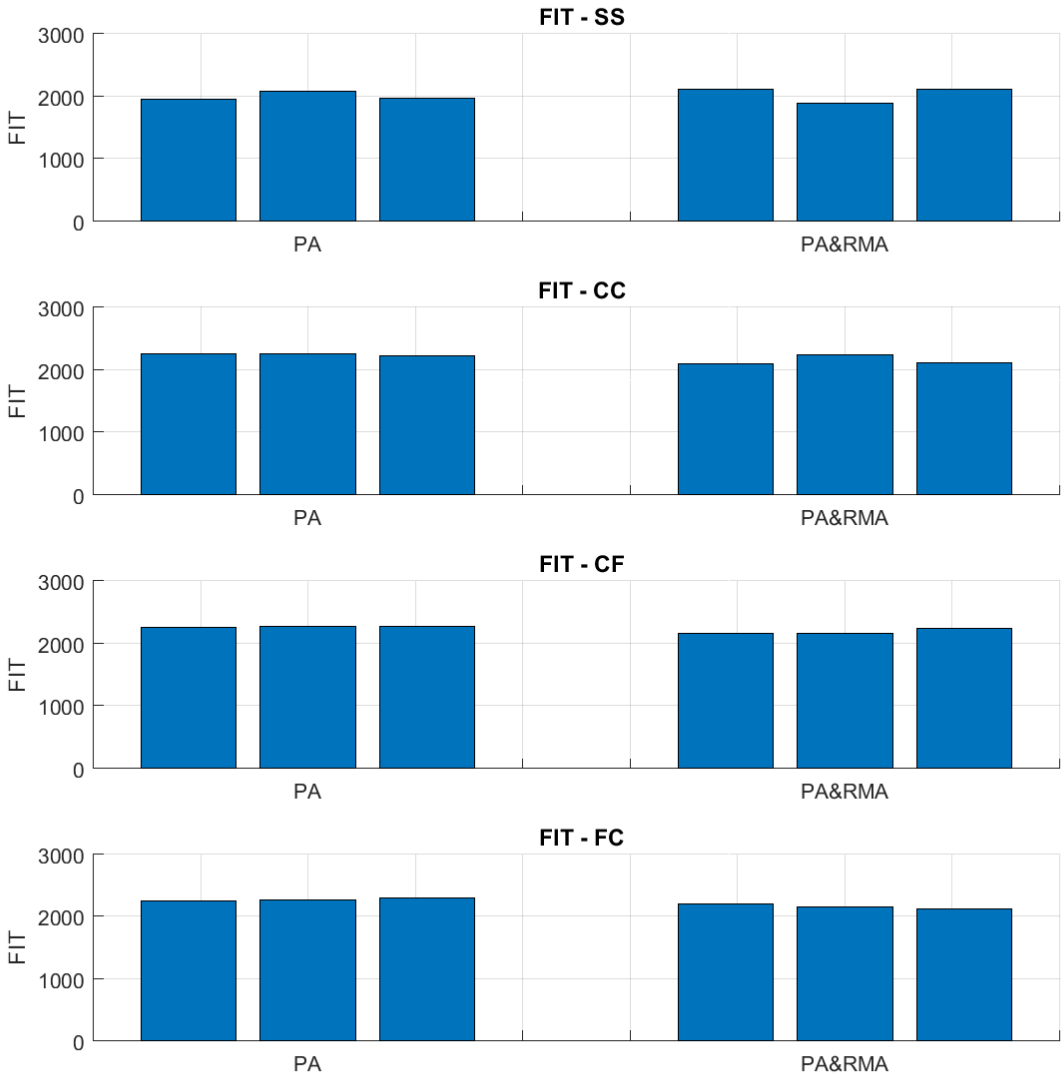

Figure 4.13 – *Fitness values for optimized sample for various boundary conditions*

For the stress values of σ_{13}, the PA tuning approach has presented some values with lower amplitude than for PA&RMA, which suggest that the tuning approach does influence the out-of-plane stresses.

For the out-of-plane stress σ_{23} it is noted that both approaches present large variance, and some lower values for σ_{23} are presented.

From figure 4.14 the samples repeatedly achieved similar levels of efficiency by the optimization process, according to the FIT value, indicating that the optimization process is consistent, and although there are different possible solutions for the same optimization problem, the algorithm reached similar FIT values.

Figure 4.14 presents all the samples result for PA and PA&RMA, in the same sequence order as in the tables 4.5 and 4.6. The stress values for σ_{11} are very similar for both tuning approaches. For the stress values of σ_{12}, the samples of the tuning approach PA showed an average value near to the 0.1 MPa region for most cases, which indicate σ_{12} could be significantly lower for PA tuning approach.

From figure 4.14 is also possible to note there is a large fluctuation among many maximum stresses, which indicate the variations of boundary conditions, and the multiple solutions for this optimization problem reflects also a large variation among the main stresses of the beam. In this figure is also possible to note a similar fitness distribution, with a slight increase in the average for the PA tuning approach.

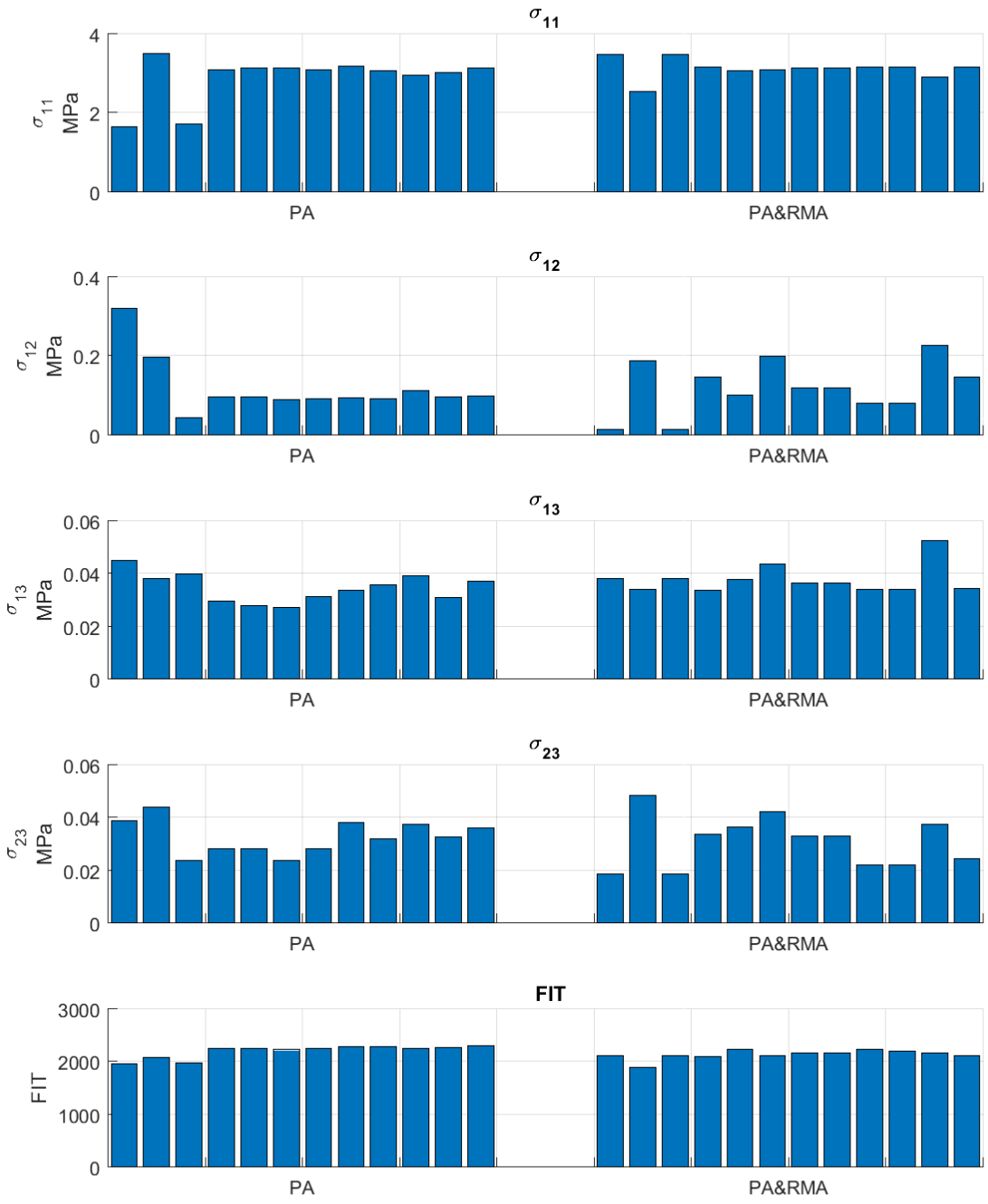

***Figure 4.14** – Overall values for optimized sample*

Table 4.6 displays the overall average values of each analyzed tuning approach, from which values is possible to draw more significant conclusions. For the maximum in-plane stresses, the values for σ_{11} are 7.5% lower for the PA tuning approach, and σ_{12} presents almost the same value for the overall average.

	PA	**PA&RMA**
σ_{11} (MPa)	2.8861	3.1192
σ_{12} (MPa)	0.1185	0.1195
σ_{13} (MPa)	0.0345	0.0377
σ_{23} (MPa)	0.0325	0.0307
FIT	2192.2208	2129.0708
σ_{11} (%)	92.53	100.00
σ_{12} (%)	99.16	100.00
σ_{13} (%)	91.54	100.00
σ_{23} (%)	100.00	94.64
FIT (%)	100.00	97.12

Table 4.6 *– Average results for PA and PA&RMA approaches*

The same table also shows that for the maximum out-of-plane stresses, the samples of PA have values almost 10% lower for σ_{13}, indicating that this tuning approach could be an option to significantly reduce important out-of-plane stresses values. However the PA&RMA presents σ_{23} values almost 5% lower also, and further conclusions would benefit from the inference of larger samples. In the overall optimization efficiency, the value Fit is 2.88% higher for PA tuning approach than PA&RMA, which indicates a greater design space, as present in the PA tuning approach, can increase in the efficiency of the solution achieved by numerical optimization procedures.

CHAPTER 5 – Conclusion

In the present study several tasks related to the design analysis and numerical optimization of a tapered composite beam have been accomplished.

Algorithms with important contributions in the field have been coded in MATLAB, and were tested for the present optimization task, having its accuracy and speed compared.

The previous numerical models of the three taper configurations have been adapted for a different geometry, by the addition of non-tapered sections, and a design study was created displaying the influence of the main design variables in the dynamic behavior of the tapered composite beam.

Several tuning approaches have been defined, and the beam has been optimized under several boundary conditions, tuning approaches and two loading cases. Two of these tuning approaches have been evaluated in terms of maximum in-plane and out-of-plane stresses by replicating the optimized structures in ANSYS.

A summary of the accomplished tasks in the present work is presented:

a. Research and coding of several optimization algorithms, heuristic and deterministic. An algorithm selection methodology was created and applied, and the most efficient optimization algorithm has been selected to the present study.
b. Revision of the bending stiffness coefficient for the tapered laminate, equations of motion and HFEM methodology. Adaptation of the numerical model of the tapered beam to have non-tapered segments at each extremity, as displayed at figure 2.4.

c. A design analysis study of the tapered and non-tapered beam to determine the influence of the main design variables on the dynamic behavior of the component.

d. Definition of several structural tuning approaches for laminated beams.

e. Definition of a graphical representation of the ply orientation angles of a symmetric and balanced laminate.

f. Numerical optimization of the tapered composite beam for vibration for several design configurations, considering:

- Four tuning approaches:
    1. Regular manufacturing approach (RMA)
    2. Free ply orientation angle approach (FPOA)
    3. Polynomial approximation (PA)
    4. Polynomial approximation and regular manufacturing approach (PA&RMA)
- Four boundary condition:
    1. Clamped-clamped (CC)
    2. Simply-supported (SS)
    3. Clamped-free (CF)
    4. Free-clamped (FC)
- Three taper configuration B,C and D, and a non-tapered beam.
- Presence or absence of an axial tensile load.

g. Evaluation of two sampled tuning approach's efficiency in terms of average of maximum values of in-plane and out-of-plane stresses using ANSYS software.

The adapted numerical model of the tapered beam with non-tapered sections has been coded in the MATALB software. This model considers as input values the composite material coefficients, beam geometry, ply orientation angles, three main taper configurations, a non-tapered configuration, and four possible boundary conditions, giving as output the natural frequencies of the beam. This model evaluates the bending modes of vibration only, with two degrees of freedom at each node: deflection and rotation.

A design analysis study has been generated, to evaluate the effect of the design variables or loading on the natural frequencies. The variables considered are: length (L), ply orientation angle variation in the intermediate and external sections of the laminate (β and γ) or in all plies of the laminate (λ), boundary conditions (BC), thickness taper configuration (TC) and axial tensile loading (N_x).

As the number of design variables is significantly greater for a laminated component than for an isotropic component, design procedures are challenged to efficiently and precisely adjust these variables, while the level of precision will depend on the capability of the manufacturing processes applied. Four possible structural tuning approaches have been proposed, and each one has been applied to the optimization as a design specification.

In order to efficiently adjust the large number of design variables for near-optimal configurations for vibration, several optimization algorithms have been coded to work in conjunction with the numerical model of the composite tapered beam, which are divided into two categories: heuristic and deterministic. These algorithms have been tested and compared for their efficiency to achieve near-optimum solutions, and the selected algorithm for this optimization task is the genetic algorithm (GA).

Each design configuration has been optimized five times, and the main objective value FIT reached similar values for several of these outcome sets. The optimization results for all the boundary conditions and taper configurations were grouped in eight result groups, which are defined by the structural tuning approach and presence or absence of a tensile axial force.

Two of these result groups, 5 and 7, which are related to the PA and PA&RMA tuning approach under free-vibration, were sampled and used to evaluate in plane and out-of-plane stresses, and the efficiency of the two related tuning approaches in terms of these stresses: polynomial approximation (PA) and polynomial approximation and regular manufacturing approach (PA&RMA).

After generating the optimized beams in ANSYS, the maximum in-plane stresses σ_{11} and σ_{12}, and the maximum out-of-plane stresses σ_{13} and σ_{23} were measured for a given deflection, providing significant insights about each related tuning approaches.

The main conclusions of this study are:

- The choice of the optimization algorithm does influence the overall outcome of the optimization, and an appropriate selection of the most efficient method has great importance in the efficiency of the overall optimization study.
- Design analysis is an important phase in pre-design, to better interpret the achieved solutions, and to have a better understanding of the model's behavior according to its variables.

- Each taper configuration presented a small difference in the dynamic behavior, which can be an option in tuning a tapered beam during the design process.
- A tapered beam has the fundamental natural frequency increased when compared to a non-tapered beam.
- A tensile axial loading proved to increase all the natural frequencies of the beam.
- The external plies of the laminate have greater influence on the dynamic behavior related to the bending modes of vibration.

- Gradient based algorithms have greater localized precision; however, have the tendency to converge to optimum regions close to the initial guess.
- Global heuristic algorithms can explore the overall space efficiently, however are not as efficient to achieve localized and precise results as gradient methods.
- Genetic algorithm has proven to be very fast for the present task, as other heuristic global optimization methods tested, because these methods do not require derivative calculation. Although GA does not have the same precision of a gradient method, it has provided fairly good results for the present study with great speed.
- The selected structural tuning approach for a laminate can certainly influence the overall efficiency of the structural component. A larger design space, if properly evaluated, can potentially provide better optimization results.
- The tuning approaches here denominated PA&RMA and PA were selected for an in depth analysis, and the related in-plane and out-of-plane stresses are compared. PA has presented a better overall average of the optimization objective value FIT, which variable for this study represents larger band free from natural frequencies and lower center-line offset error of the band with the blade passing frequency w_p. This can be considered as

an indication that a larger design space can potentially provide solutions with greater efficiency.

- PA presented a significantly lower average for the maximum out-of-plane stress value σ_{13}, than the tuning approach PA&RMA, which is an important indicator in the laminate design.
- As consistent results have been achieved in the present work with numerical optimization, the automatic design approach for composite material structures has proven to be a feasible solution in generating efficient near-optimum structural configurations for components with large design space such as a tapered composite beam.

For future work related to composite structures and numerical optimization, the following topics are proposed:

- The verification of structural efficiency and feasibility of different techniques in composite material manufacturing processes with increased design space, as the suggested tuning approach PA, and other possibilities in automatic or semi-automatic manufacturing processes, to work in conjunction with automated design procedures such as numerical optimization.
- Optimization of tapered beams with objective values that include free and forced vibration, especially harmonic steady-state response, which optimization can be performed.

- Generation of greater array of resins and fibers, to be selected during automatic design procedures as numerical optimization.
- Consideration of random variations in material and geometric properties of plies and laminates.

Appendix A – Design analysis results

All the design analysis performed are presented in figures A.1 to figures A.33.

A.1 Design analysis 2D plots

Figures A.1 to figure A.6 display the natural frequencies up to 7000 rad/s, for the tapered and non-tapered beams. The abbreviation follows the acronyms stated at table 3.1 and figure 3.1.

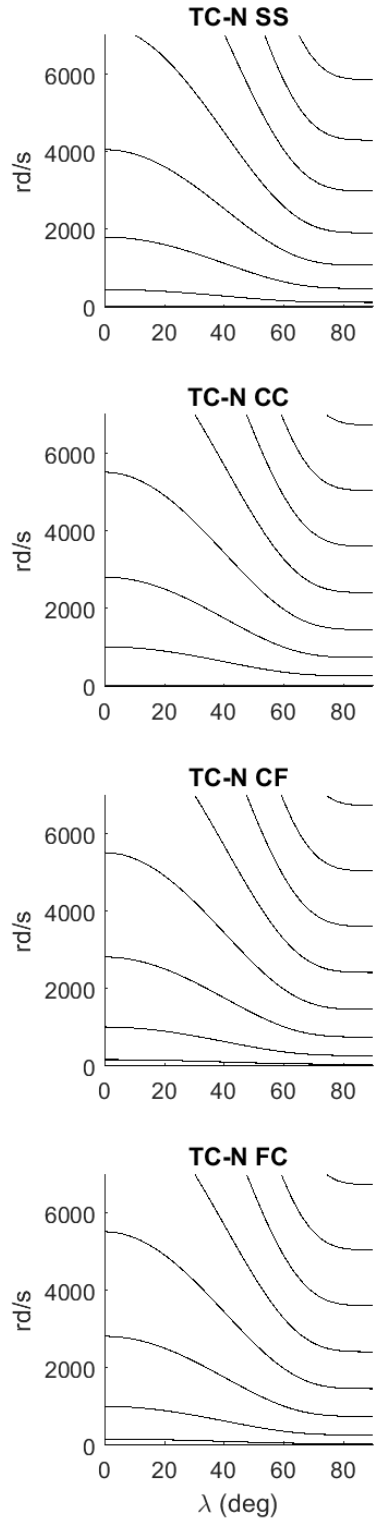

Figure A.1 – *Non-tapered beam – natural frequencies vs λ*

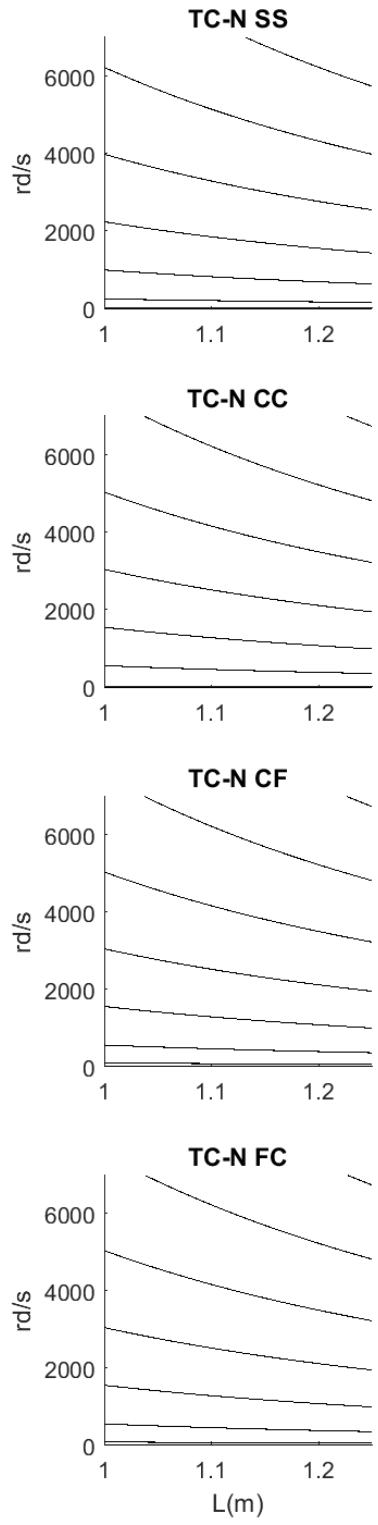

Figure A.2 – *Non-tapered beam – natural frequencies vs L*

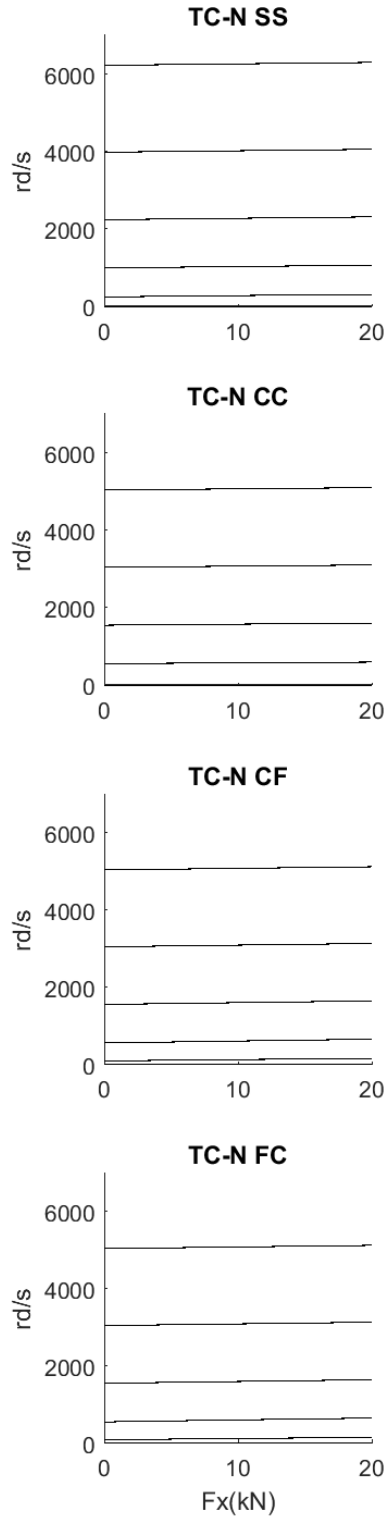

Figure A.3 – *Non-tapered beam – natural frequencies vs Fx*

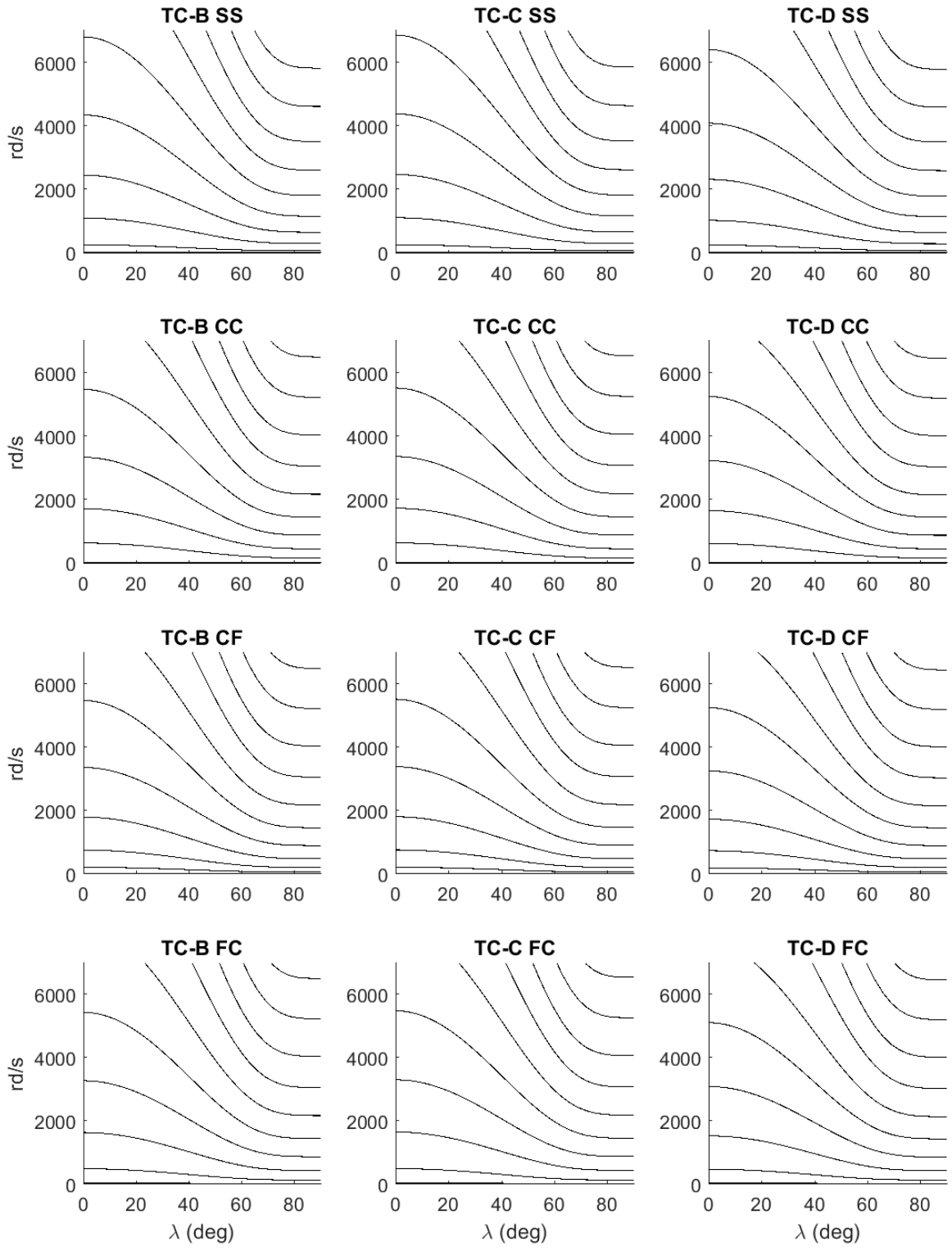

Figure A.4 – *Tapered beams – natural frequencies vs λ*

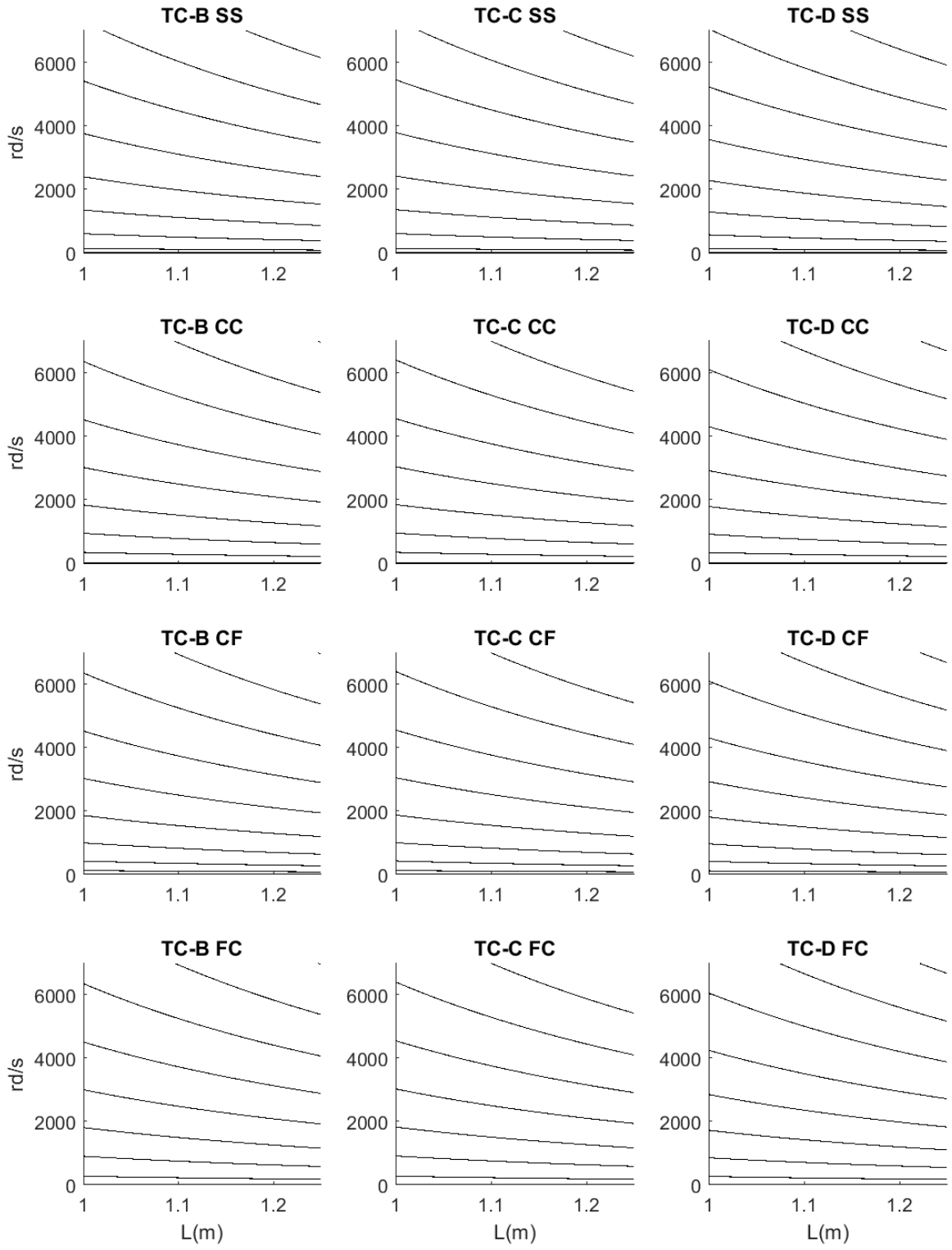

Figure A.5 – *Tapered beams – natural frequencies vs L*

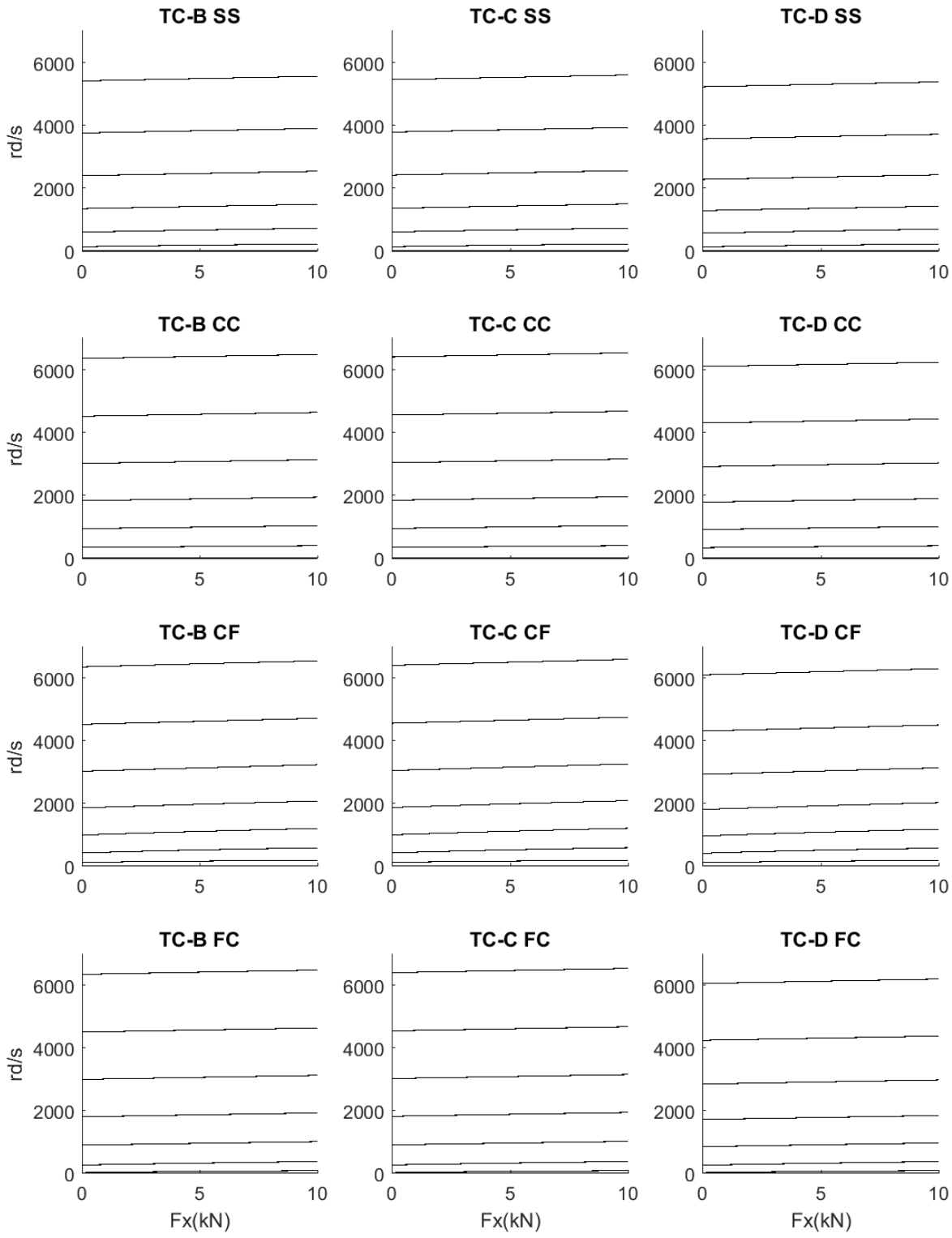

Figure A.6 – *Tapered beams – natural frequencies vs Fx*

A.2. Design analysis 2D plots – first three natural frequencies

Figures A.7 to figures A.18 display the first three natural frequencies to both tapered and non-tapered beams, for all the boundary conditions. The abbreviation applied follows the table 3.1 and figure 3.1.

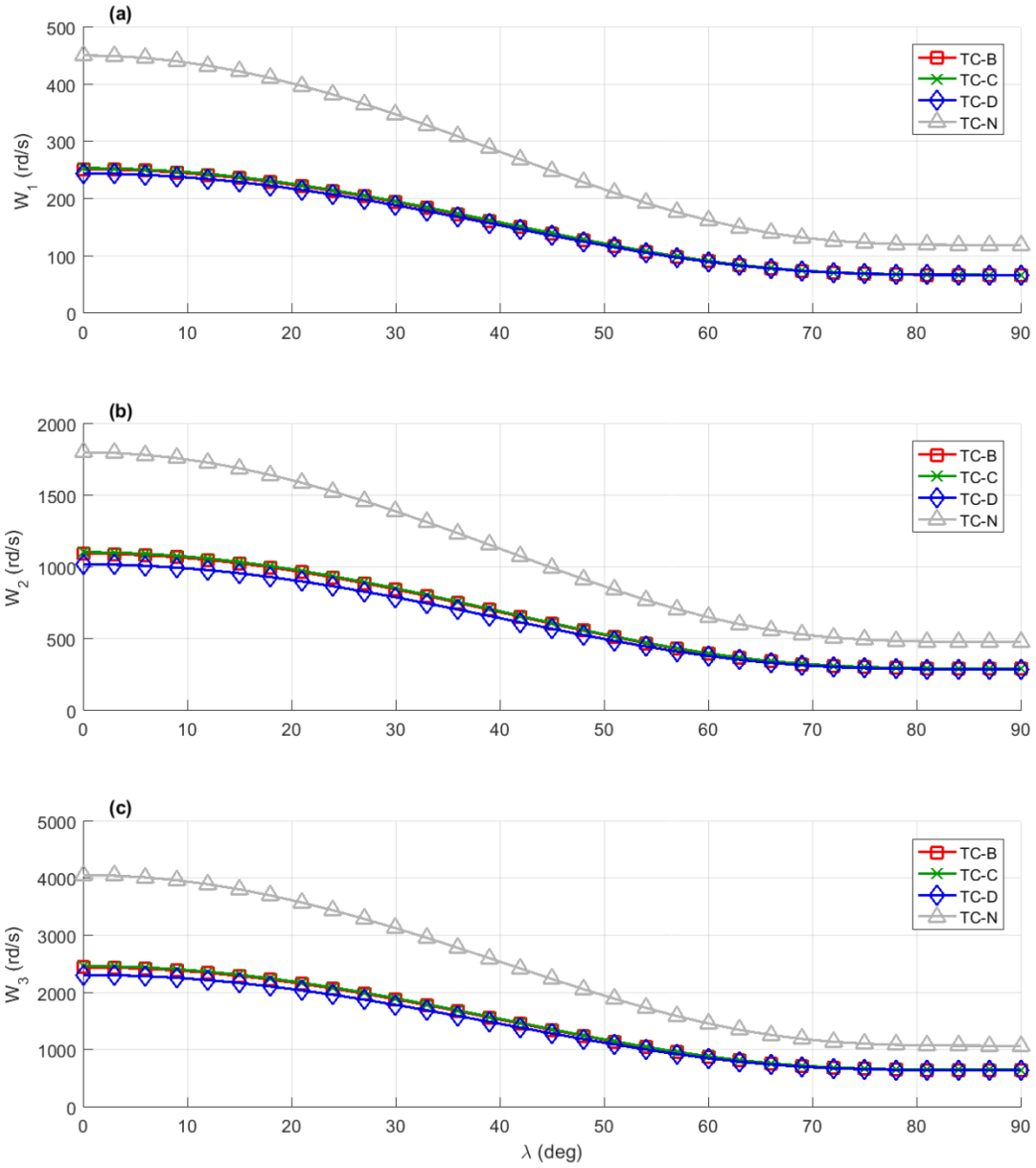

Figure A.7a – *First natural frequency vs λ – simply-supported boundary condition*

Figure A.7b – *Second natural frequency vs λ – simply-supported boundary condition*

Figure A.7c – *Third natural frequency vs λ – simply-supported boundary condition*

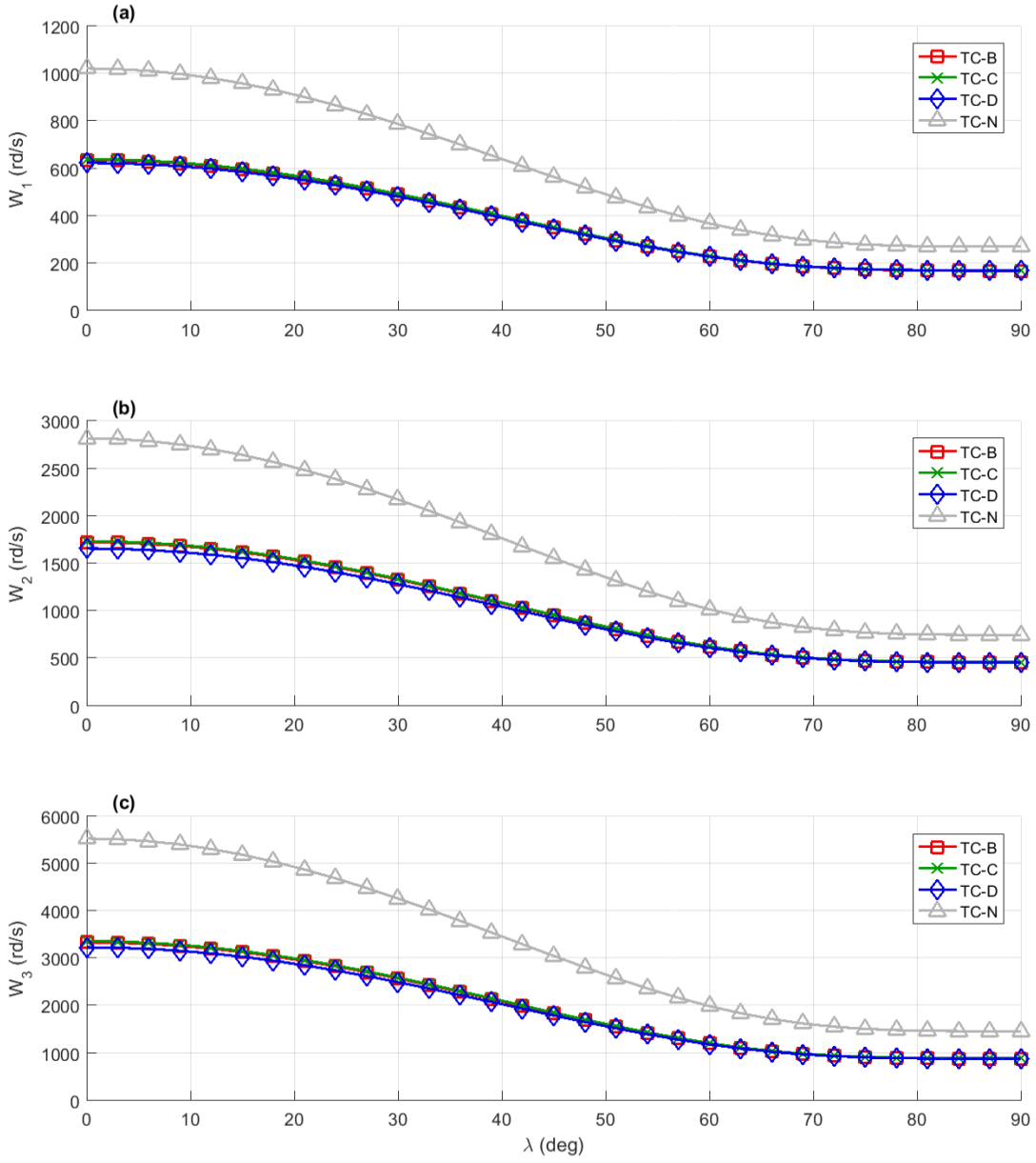

Figure A.8a – *First natural frequency vs λ – fixed-fixed boundary condition*

Figure A.8b – *Second natural frequency vs λ – fixed-fixed boundary condition*

Figure A.8c – *Third natural frequency vs λ – fixed-fixed boundary condition*

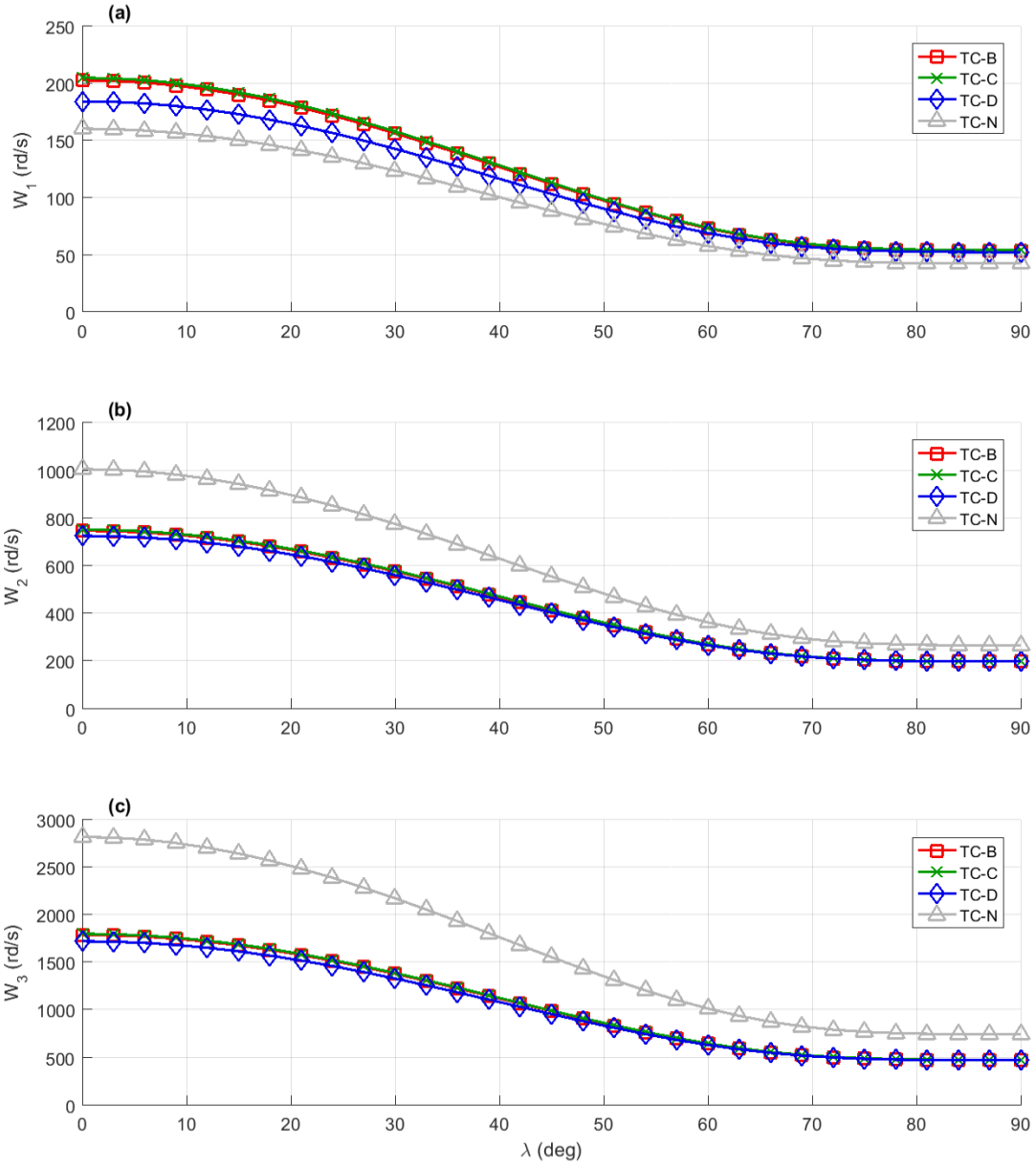

Figure A.9a – *First natural frequency vs λ – clamped-free boundary condition*

Figure A.9b – *Second natural frequency vs λ – clamped-free boundary condition*

Figure A.9c – *Third natural frequency vs λ – clamped-free boundary condition*

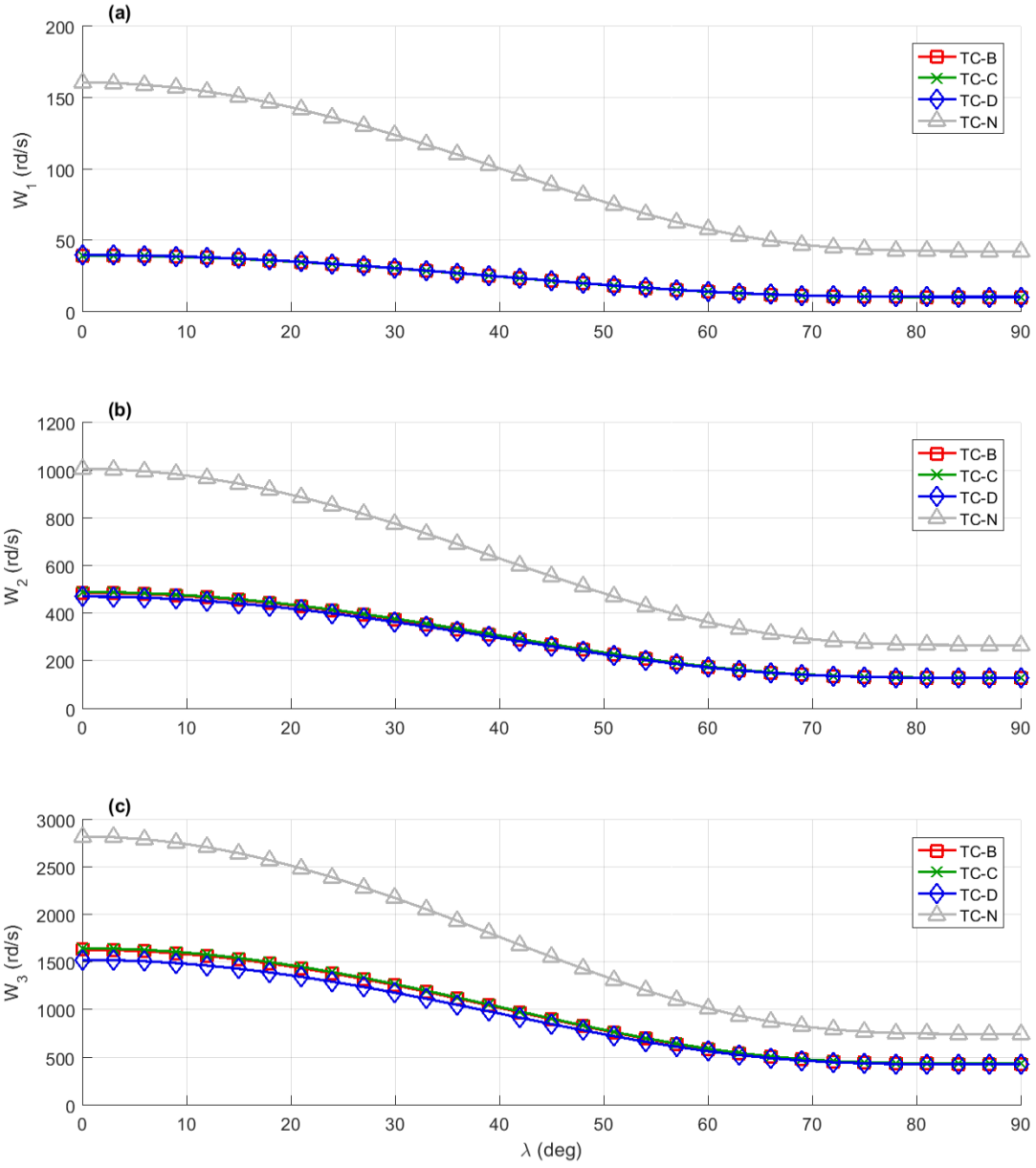

Figure A.10a – *First natural frequency vs λ – free-clamped boundary condition*

Figure A.10b – *Second natural frequency vs λ – free-clamped boundary condition*

Figure A.10c – *Third natural frequency vs λ – free-clamped boundary condition*

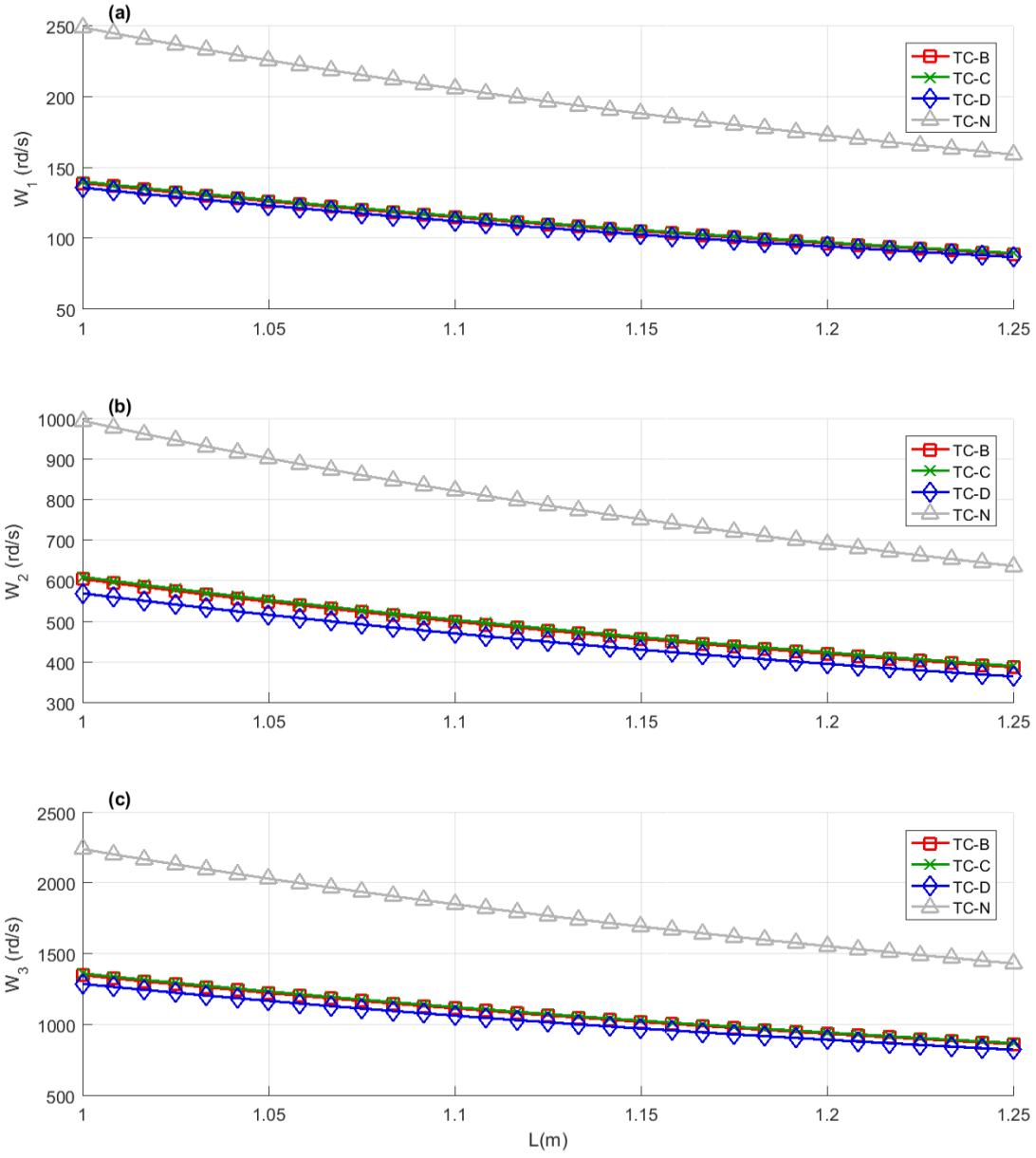

Figure A.11a – *First natural frequency vs L – simply-supported boundary condition*

Figure A.11b – *Second natural frequency vs L – simply-supported boundary condition*

Figure A.11c – *Third natural frequency vs L – simply-supported boundary condition*

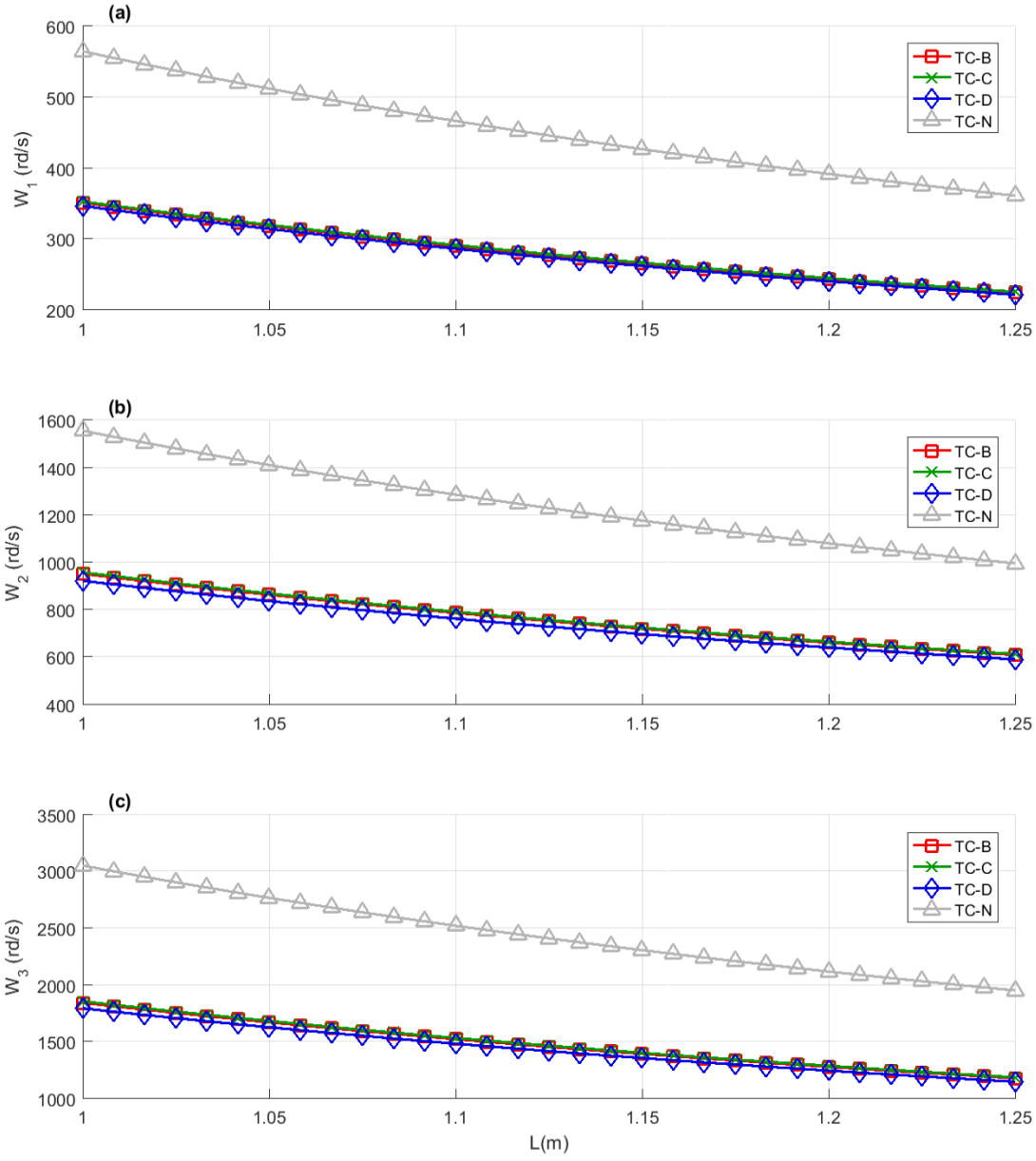

Figure A.12a – *First natural frequency vs L – fixed-fixed boundary condition*

Figure A.12b – *Second natural frequency vs L – fixed-fixed boundary condition*

Figure A.12c – *Third natural frequency vs L – fixed-fixed boundary condition*

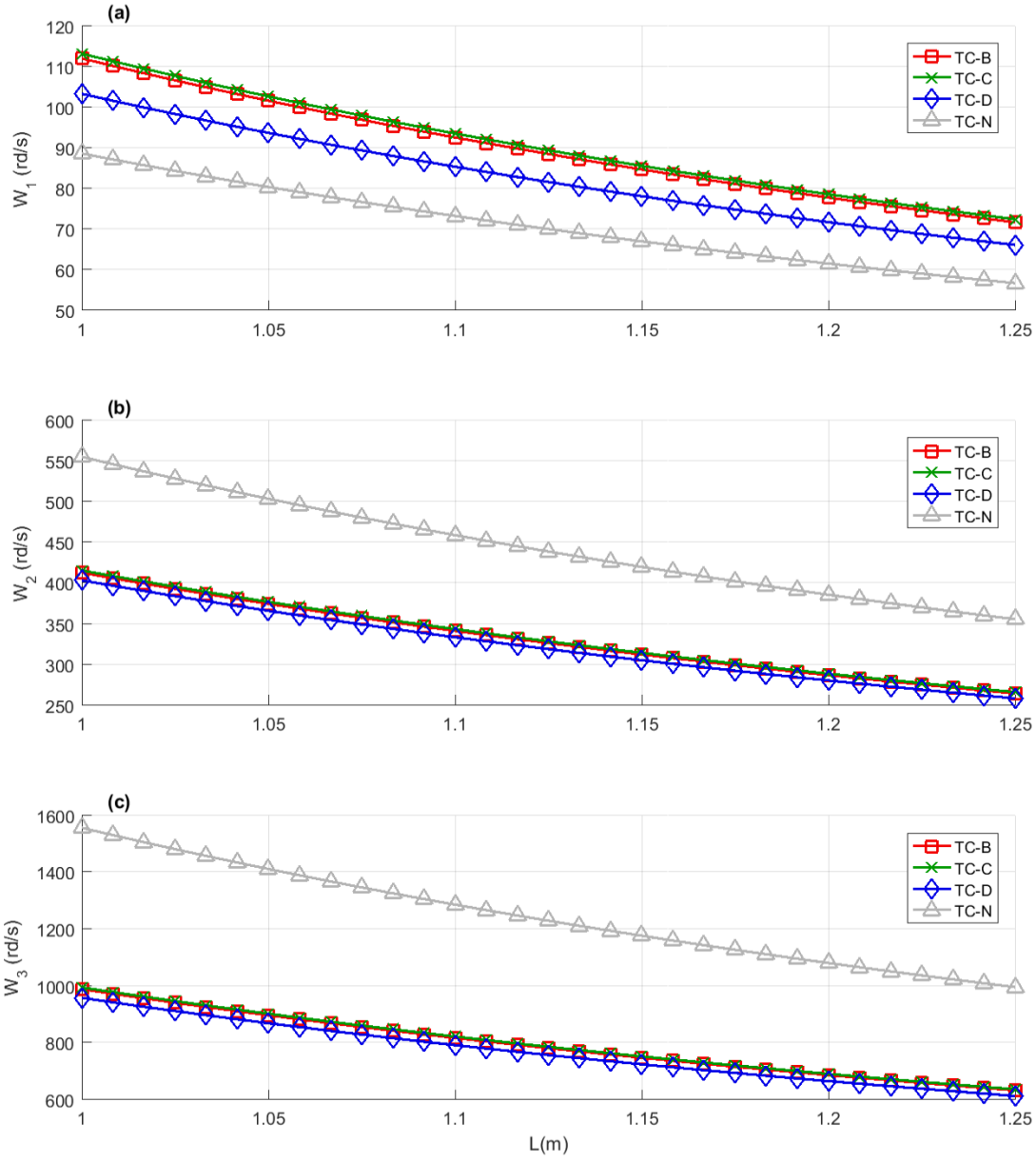

Figure A.13a – *First natural frequency vs L – clamped-free boundary condition*

Figure A.13b – *Second natural frequency vs L – clamped-free boundary condition*

Figure A.13c – *Third natural frequency vs L – clamped-free boundary condition*

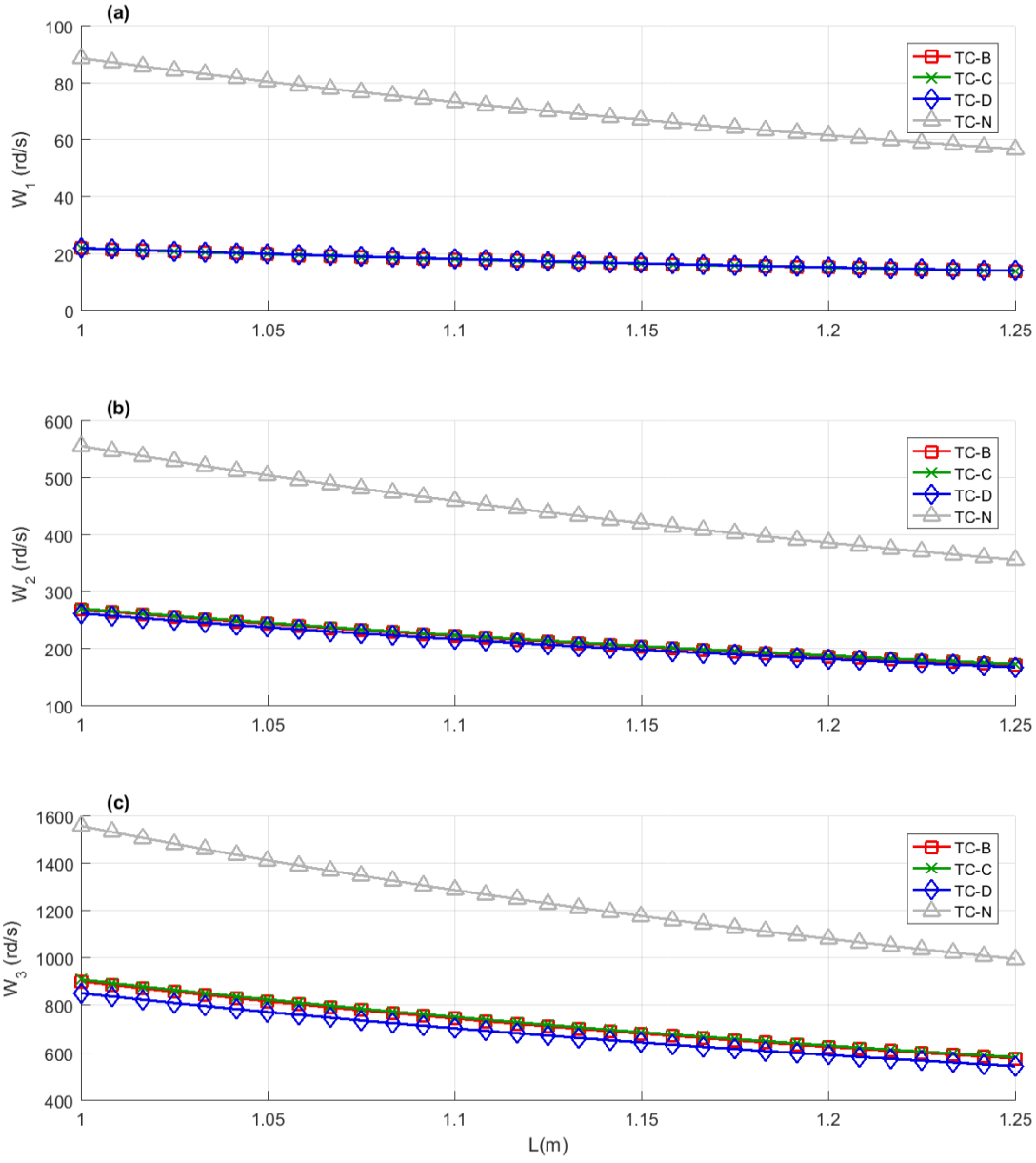

Figure A.14a – *First natural frequency vs L – free-clamped boundary condition*

Figure A.14b – *Second natural frequency vs L – free-clamped boundary condition*

Figure A.14c – *Third natural frequency vs L – free-clamped boundary condition*

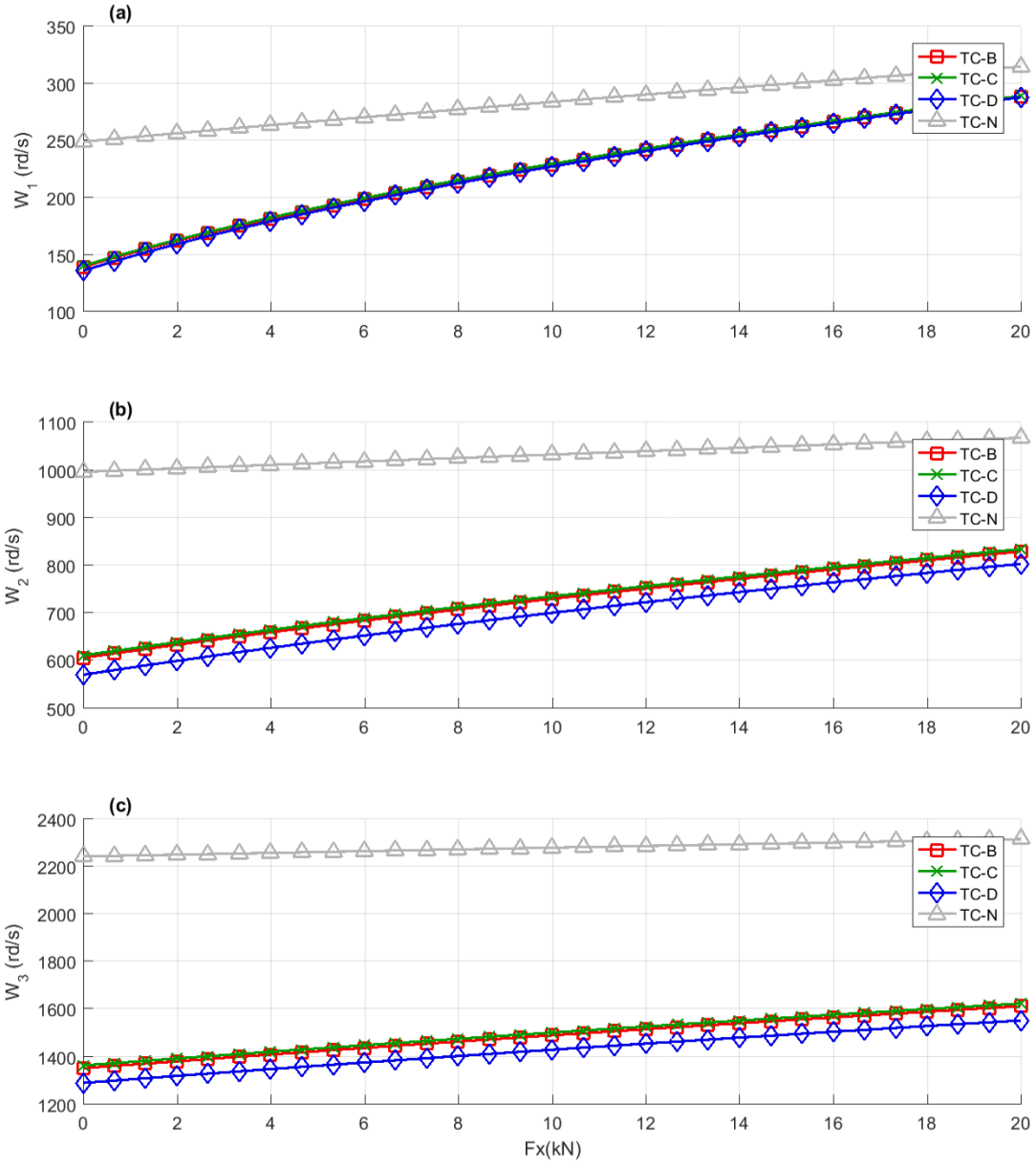

Figure A.15a – *First natural frequency vs Fx – simply-supported boundary condition*

Figure A.15b – *Second natural frequency vs Fx – simply-supported boundary condition*

Figure A.15c – *Third natural frequency vs Fx – simply-supported boundary condition*

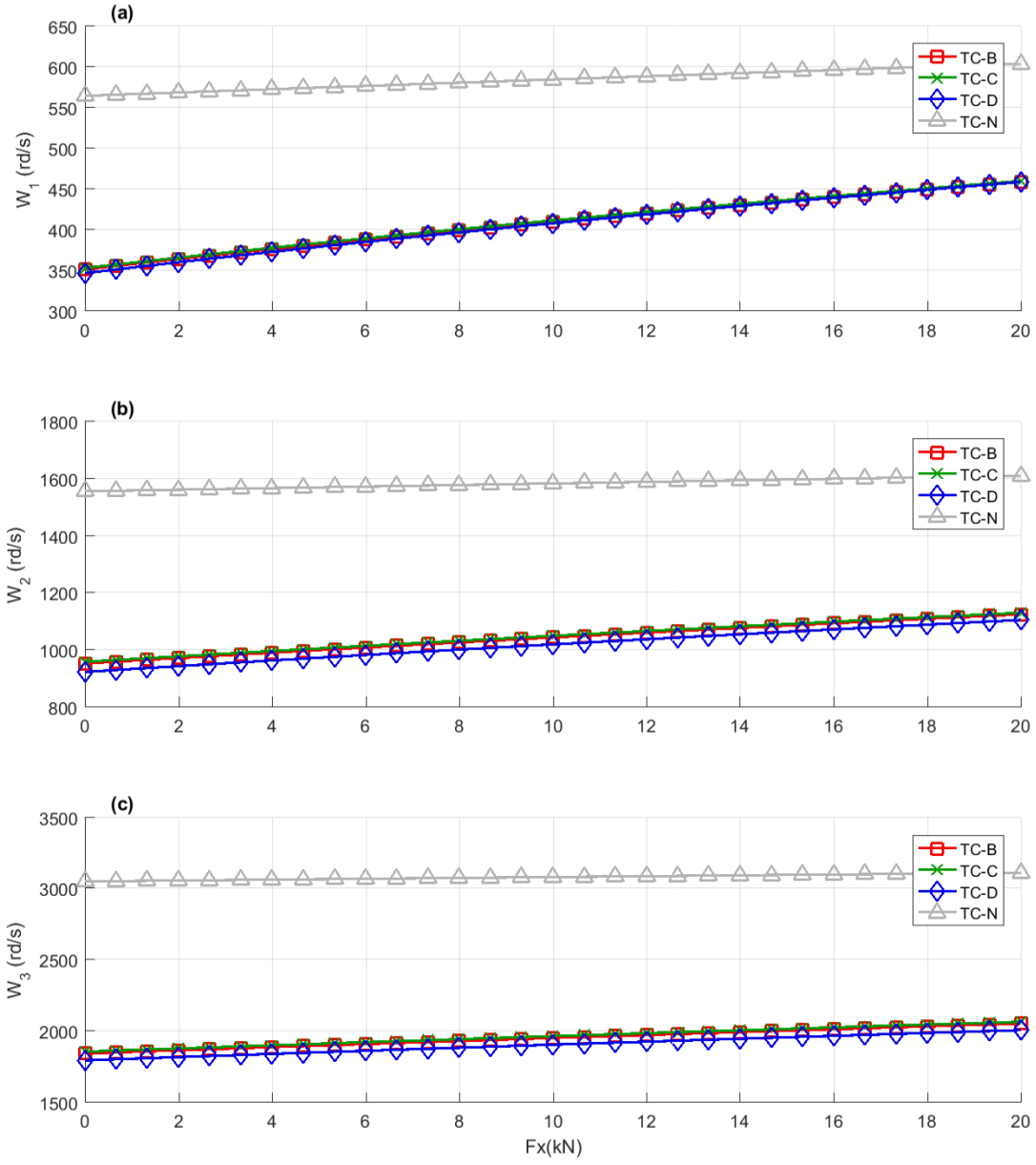

Figure A.16a – *First natural frequency vs Fx – fixed-fixed boundary condition*

Figure A.16b – *Second natural frequency vs Fx – fixed-fixed boundary condition*

Figure A.16c – *Third natural frequency vs Fx – fixed-fixed boundary condition*

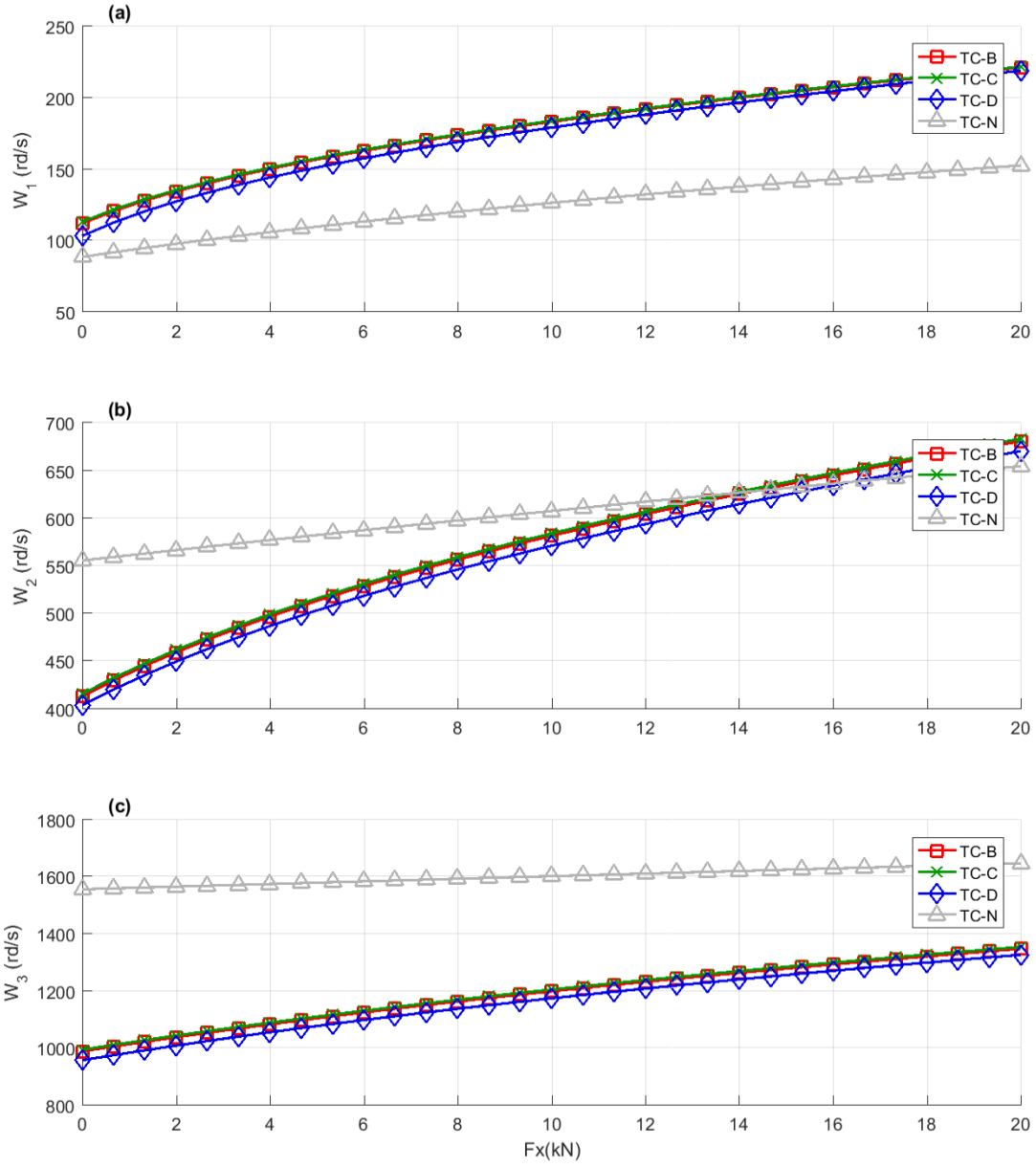

Figure A.17a – *First natural frequency vs Fx – clamped-free boundary condition*

Figure A.17b – *Second natural frequency vs Fx – clamped-free boundary condition*

Figure A.17c – *Third natural frequency vs Fx – clamped-free boundary condition*

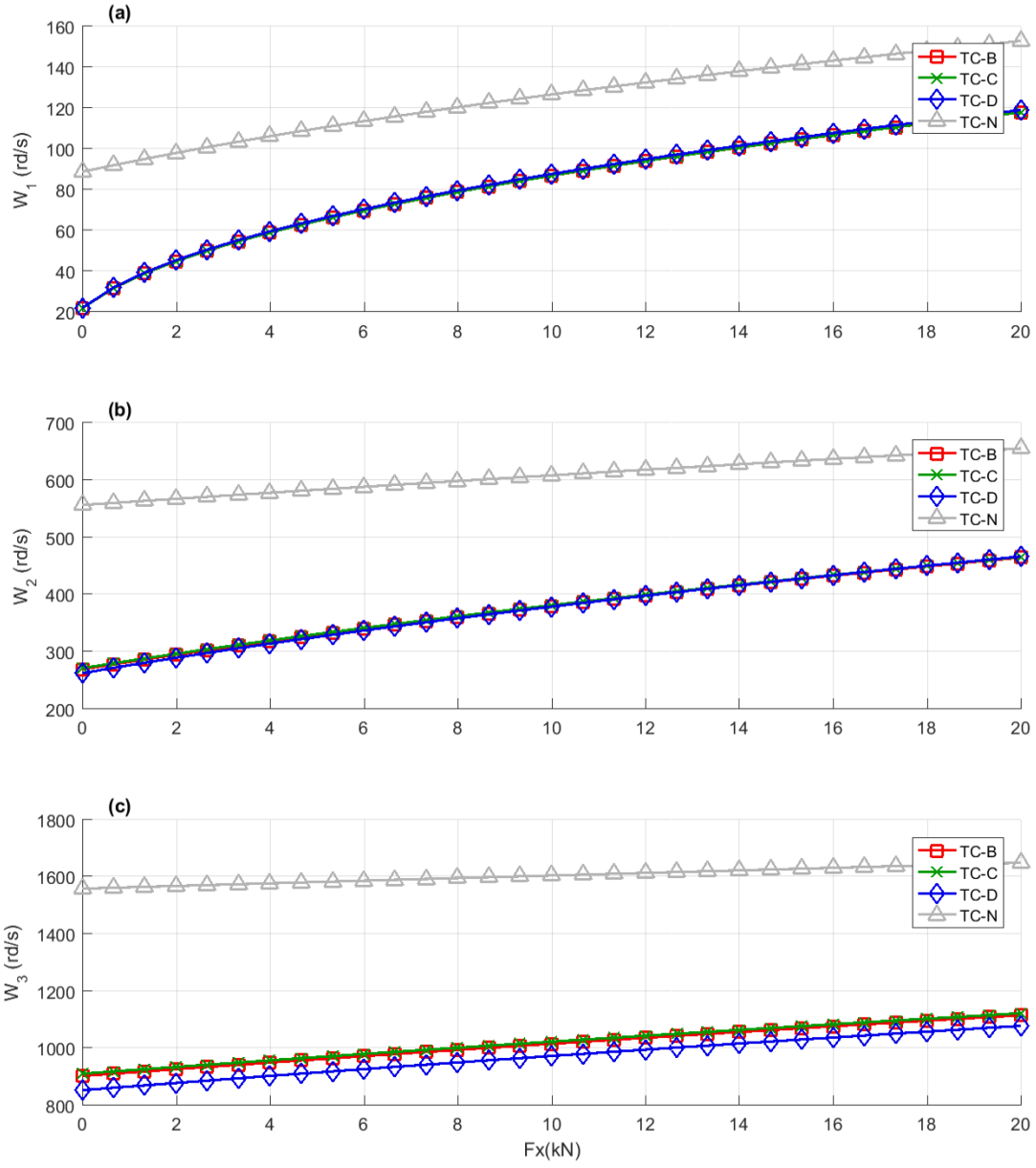

Figure A.18a – *First natural frequency vs Fx – free-clamped boundary condition*

Figure A.18b – *Second natural frequency vs Fx – free-clamped boundary condition*

Figure A.18c – *Third natural frequency vs Fx – free-clamped boundary condition*

A.3. Design analysis 3D plots

All design analysis with the 3D plots are displayed from figures A.19 to figure A.33. The figures A.19 to figure A.21 are related to the non-tapered beam first eight natural frequencies. Figures A.22 to figure A.33 are related to the first eight natural frequencies of the tapered beam. The abbreviation applied follows the table 3.1 and figure 3.1.

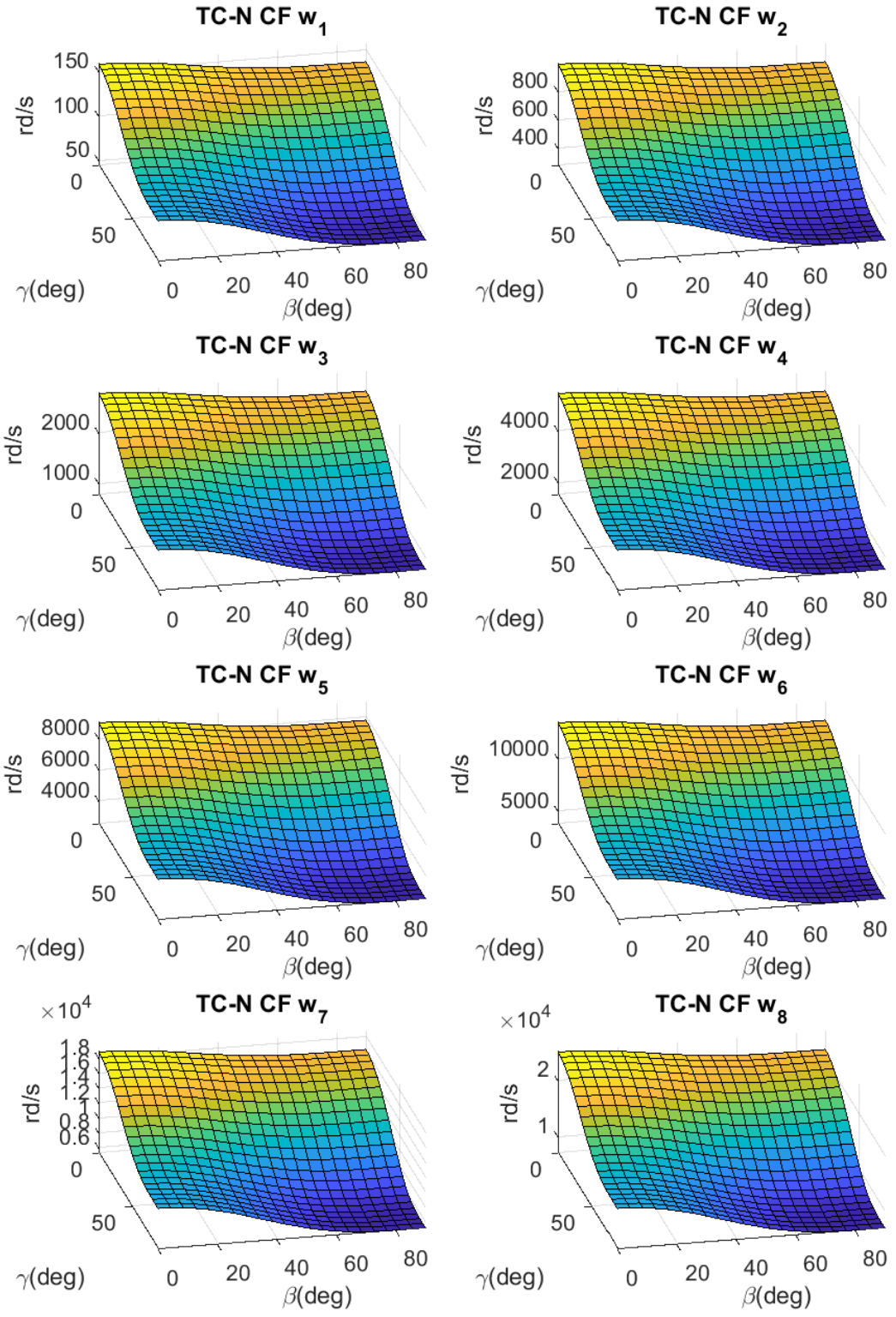

Figure A.19 – *Non-tapered beam – natural frequencies vs β vs γ*

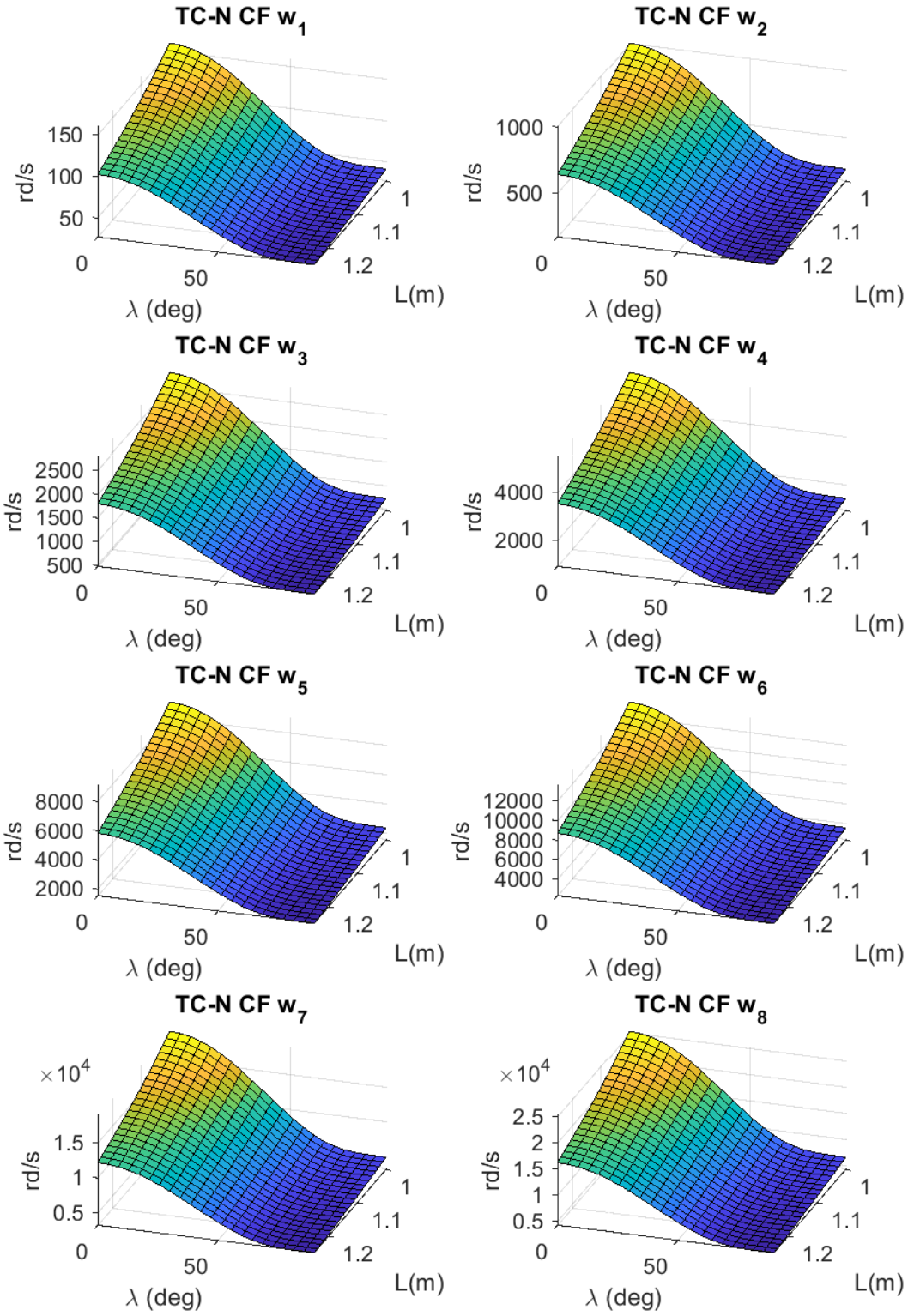

Figure A.20 – *Clamped-free non-tapered beam – natural frequencies vs λ vs L*

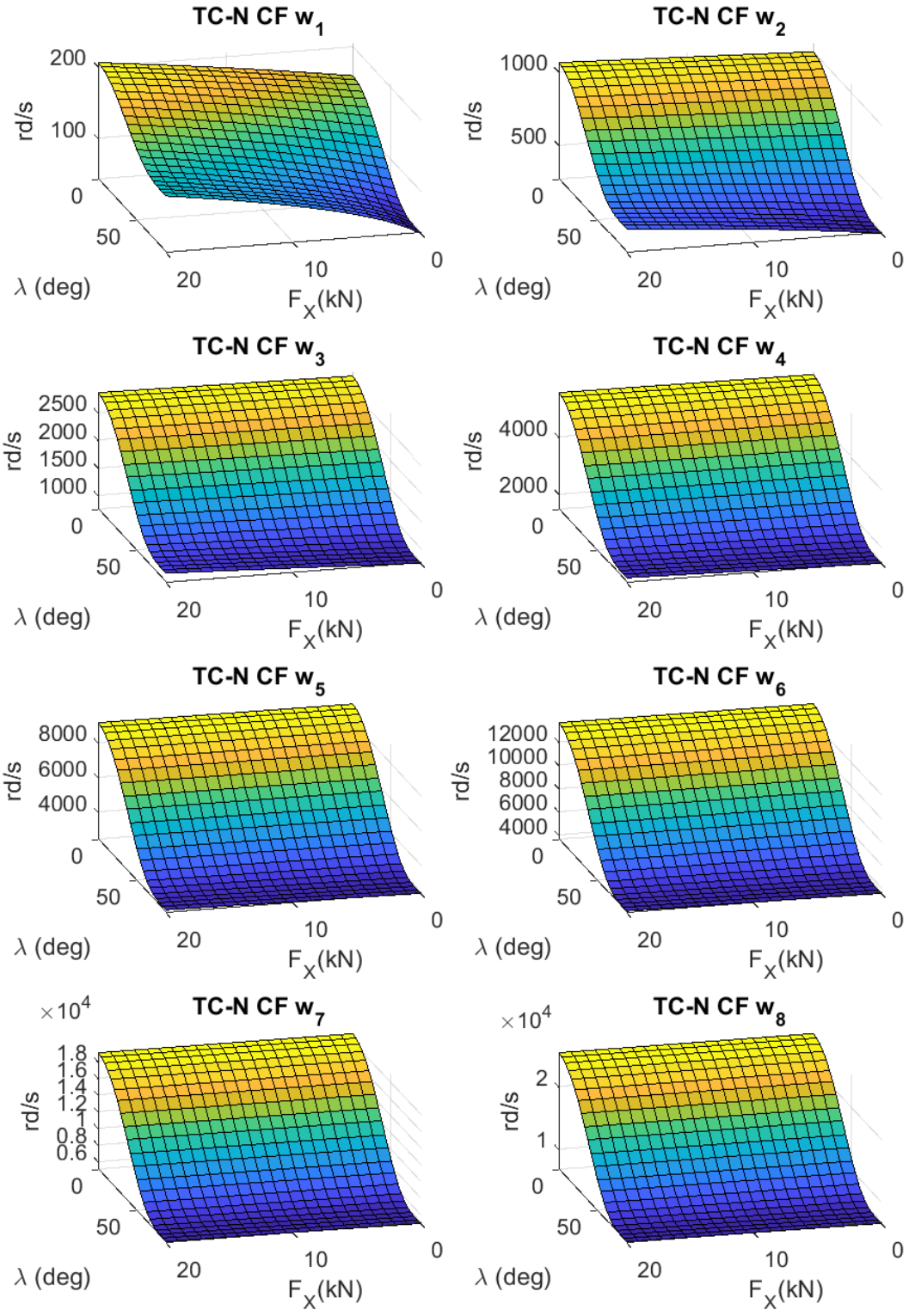

Figure A.21 – *Clamped-free non-tapered beam – natural frequencies vs λ vs Fx*

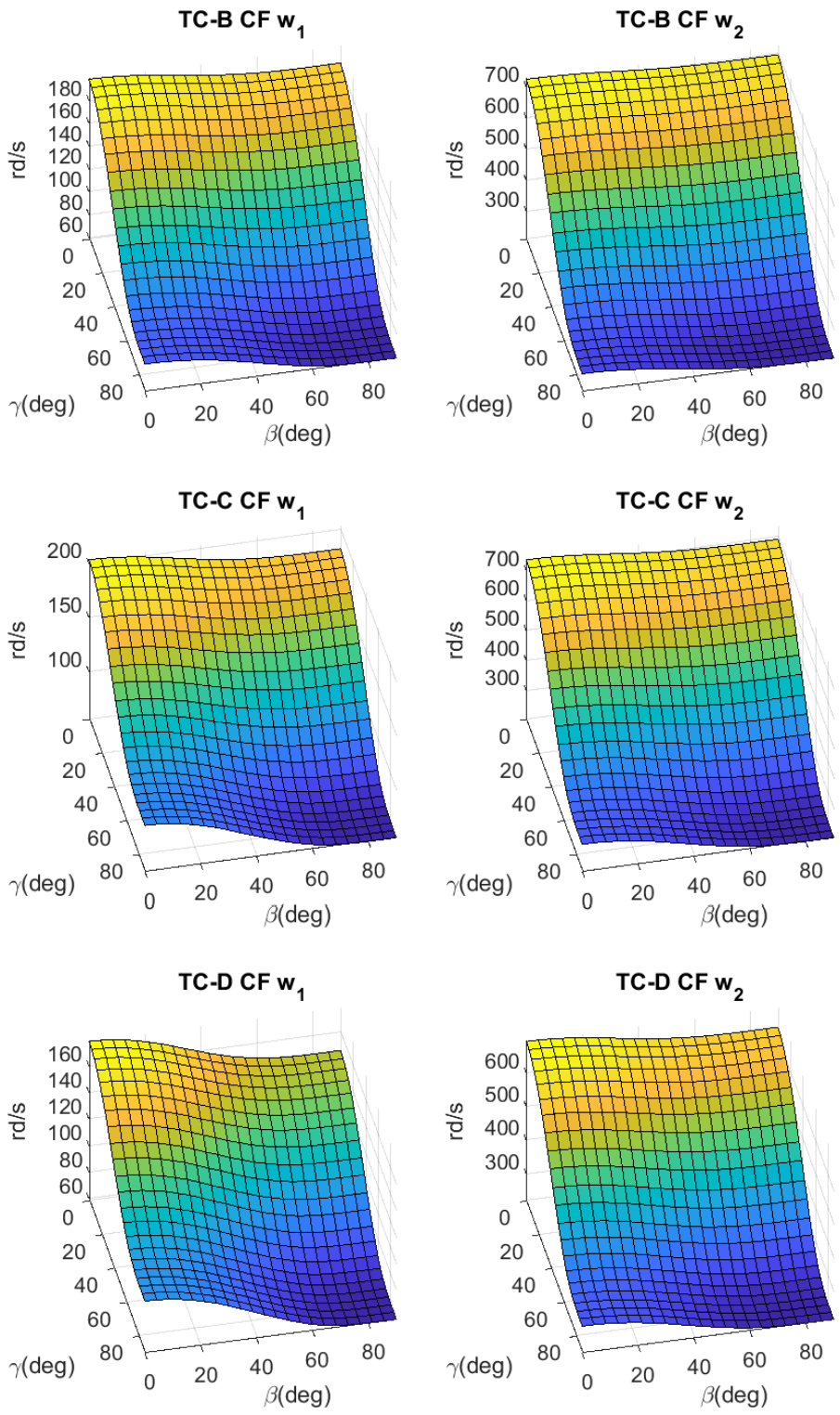

Figure A.22 – *Clamped-free tapered beams – first and second natural frequencies vs β vs γ*

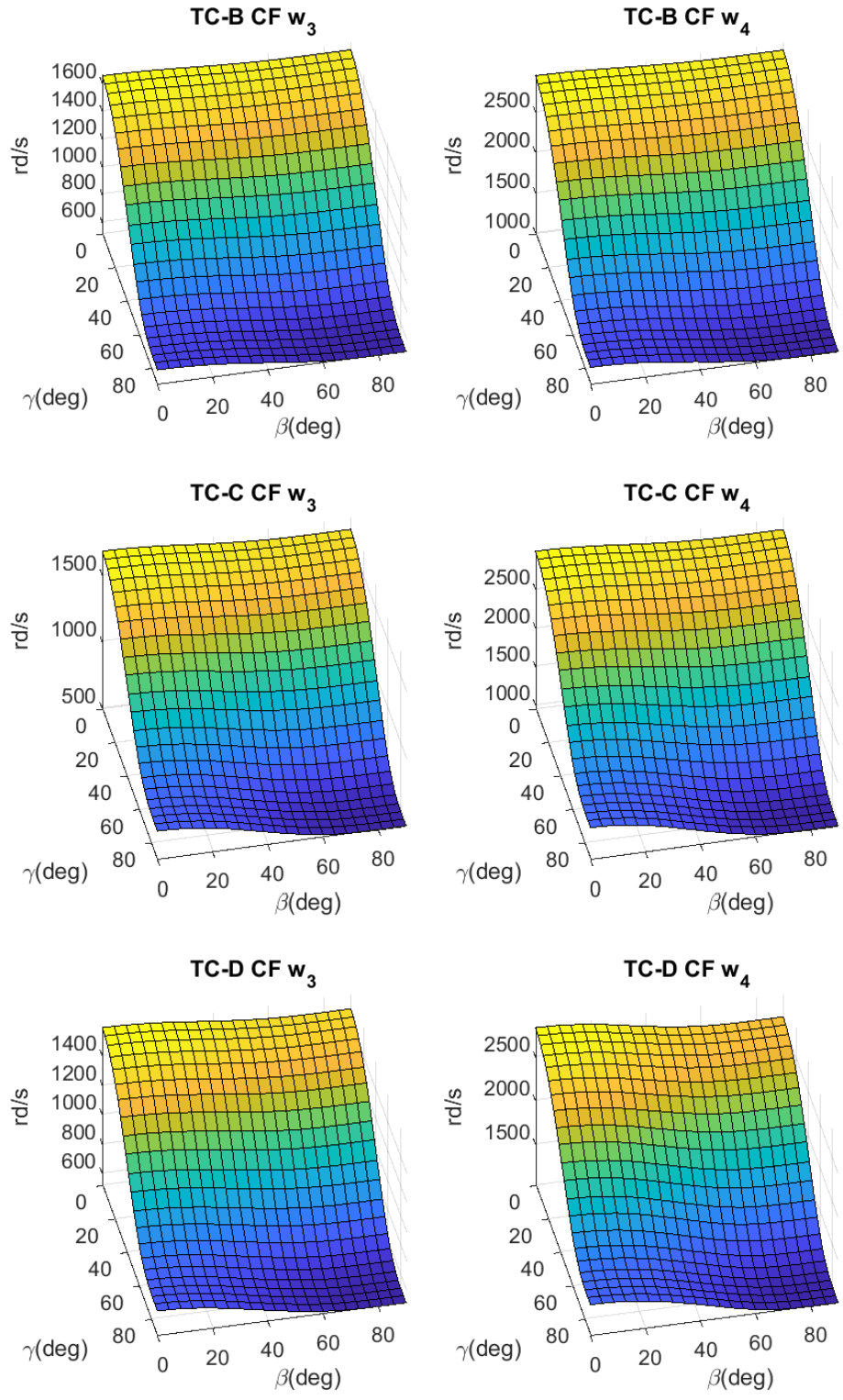

Figure A.23 – *Clamped-free tapered beams – third and fourth natural frequencies vs β vs γ*

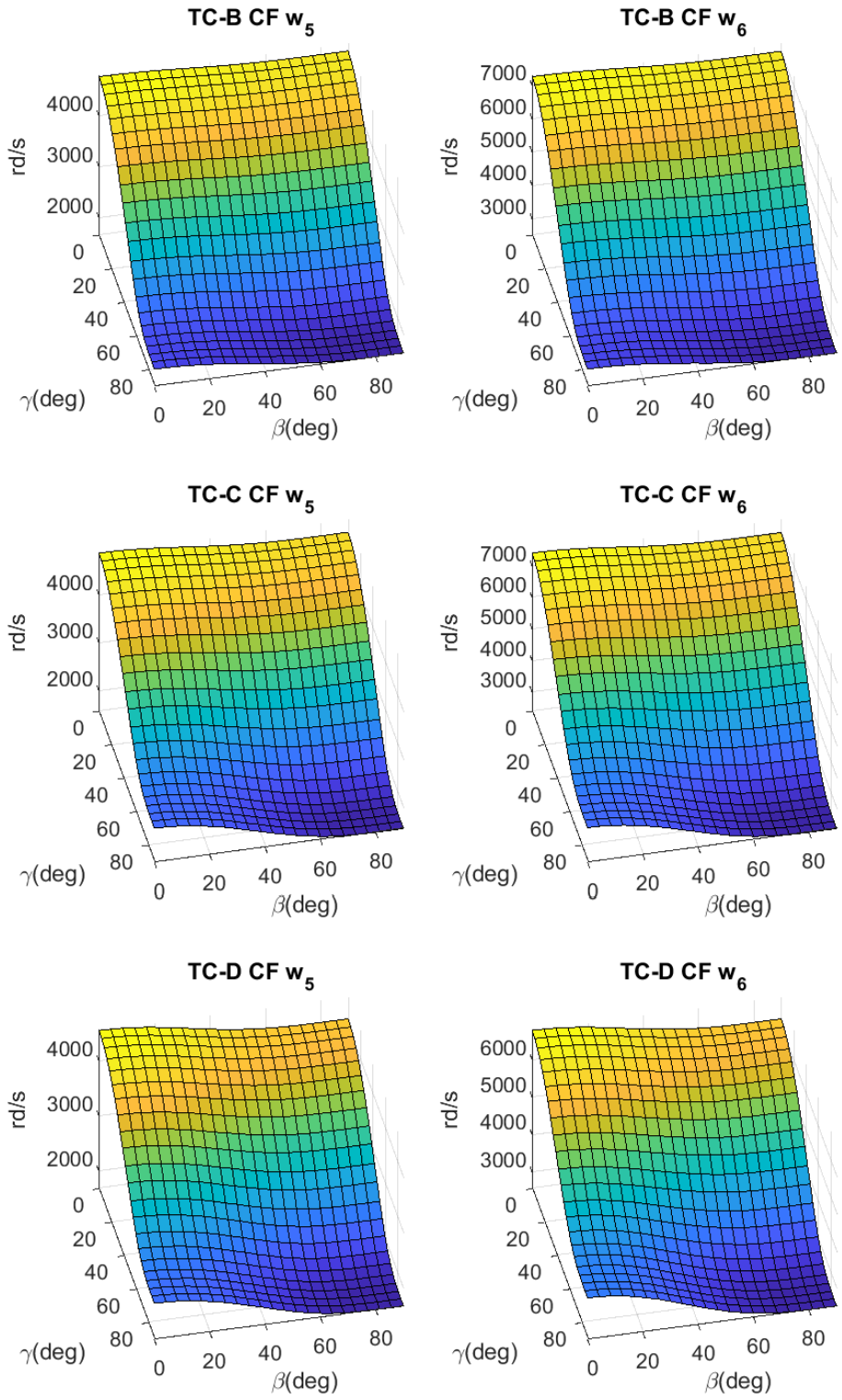

Figure A.24 – *Clamped-free tapered beams – fifth and sixth natural frequencies vs β vs γ*

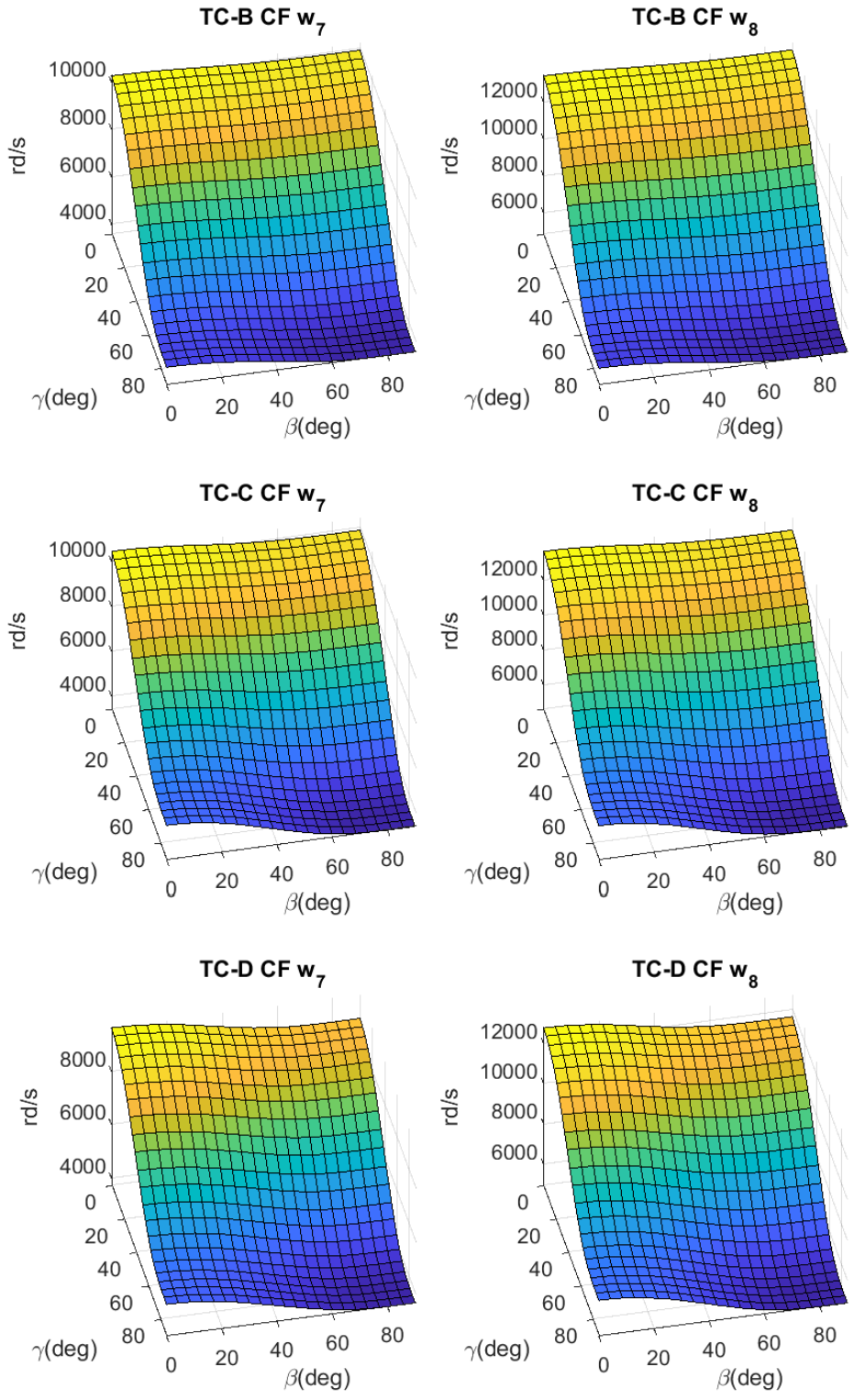

Figure A.25 – *Clamped-free tapered beams – seventh and eighth natural frequencies vs β vs γ*

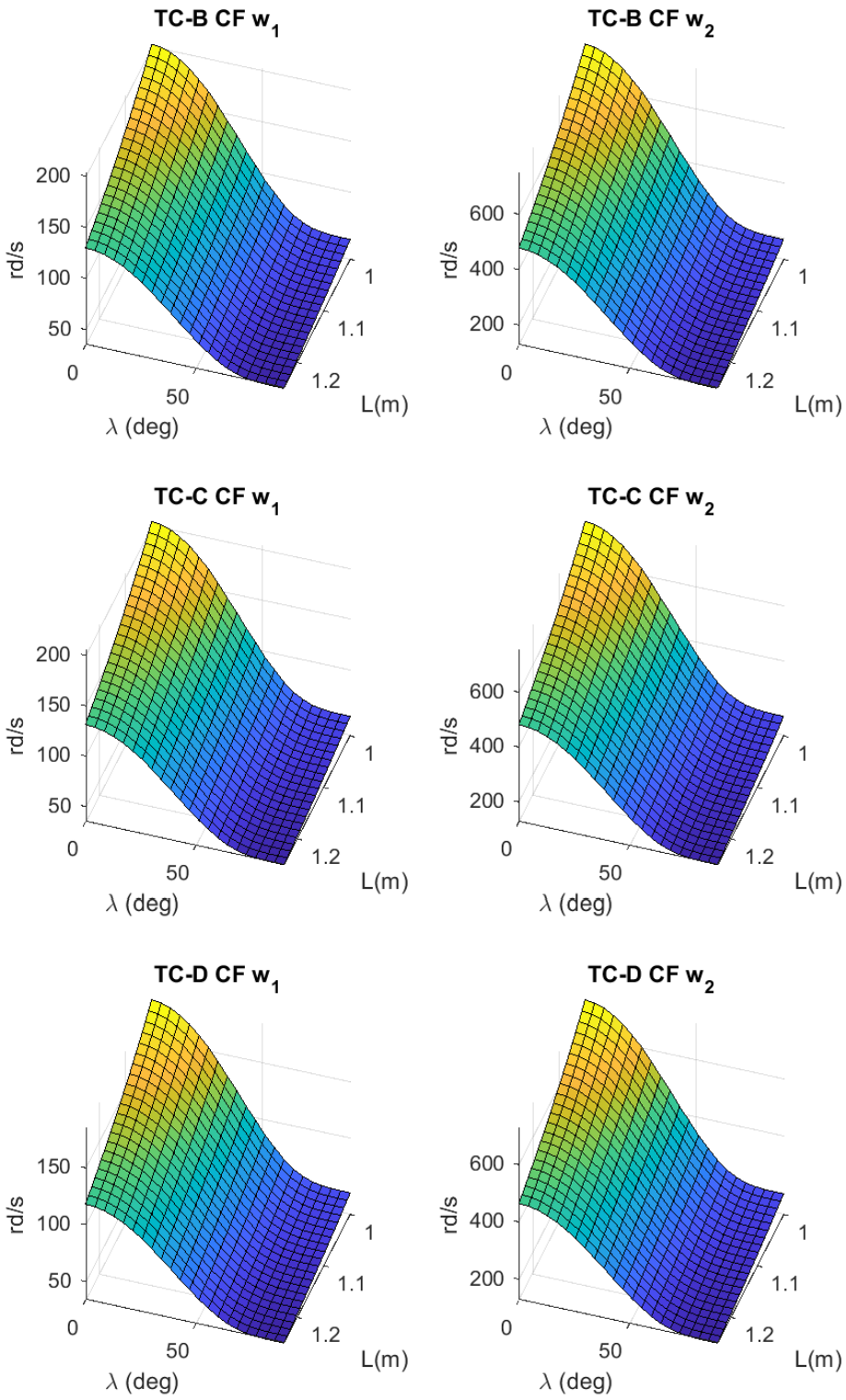

Figure A.26 – *Clamped-free tapered beams – first and second natural frequencies vs λ vs L*

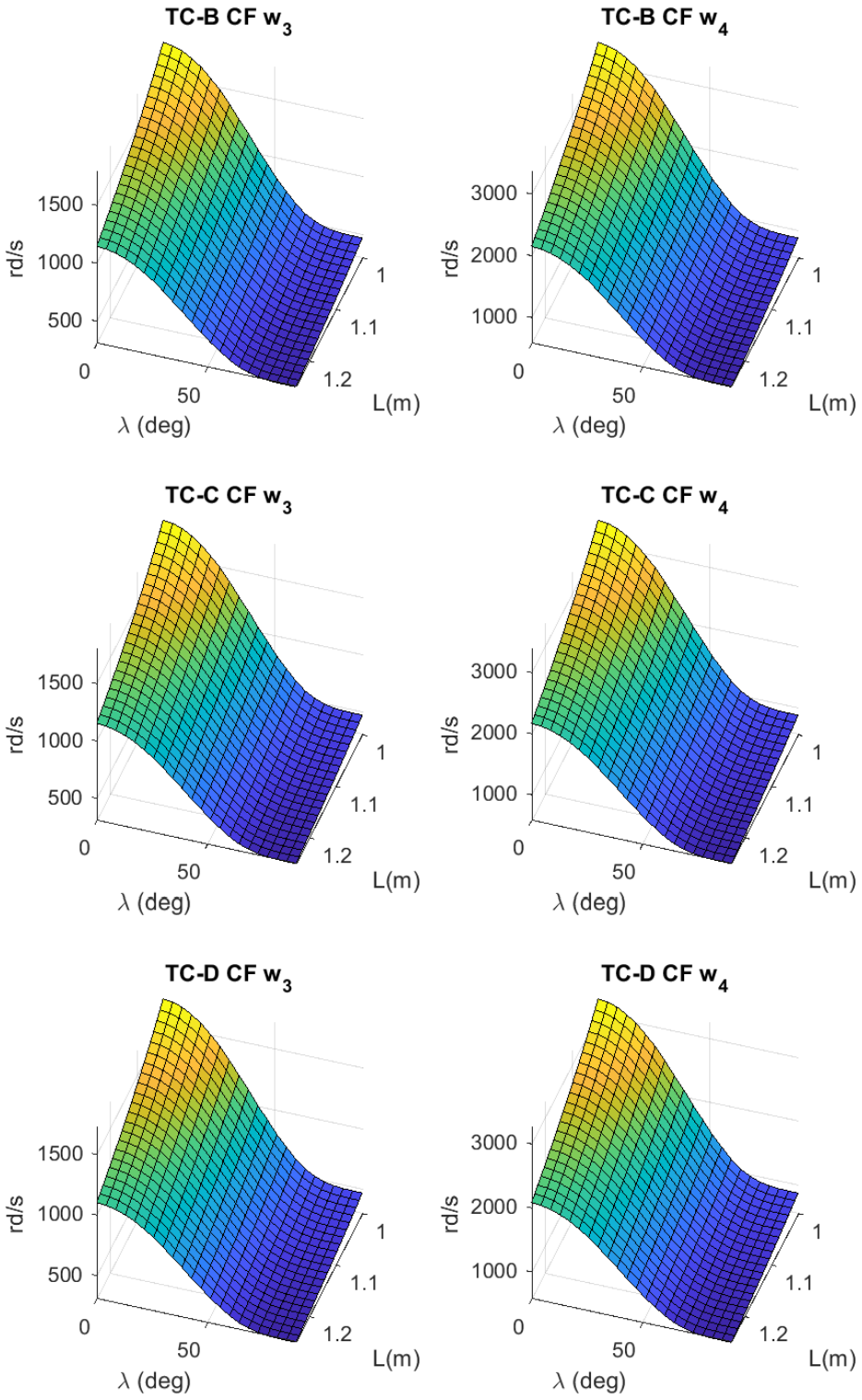

Figure A.27 – *Clamped-free tapered beams – third and fourth natural frequencies vs λ vs L*

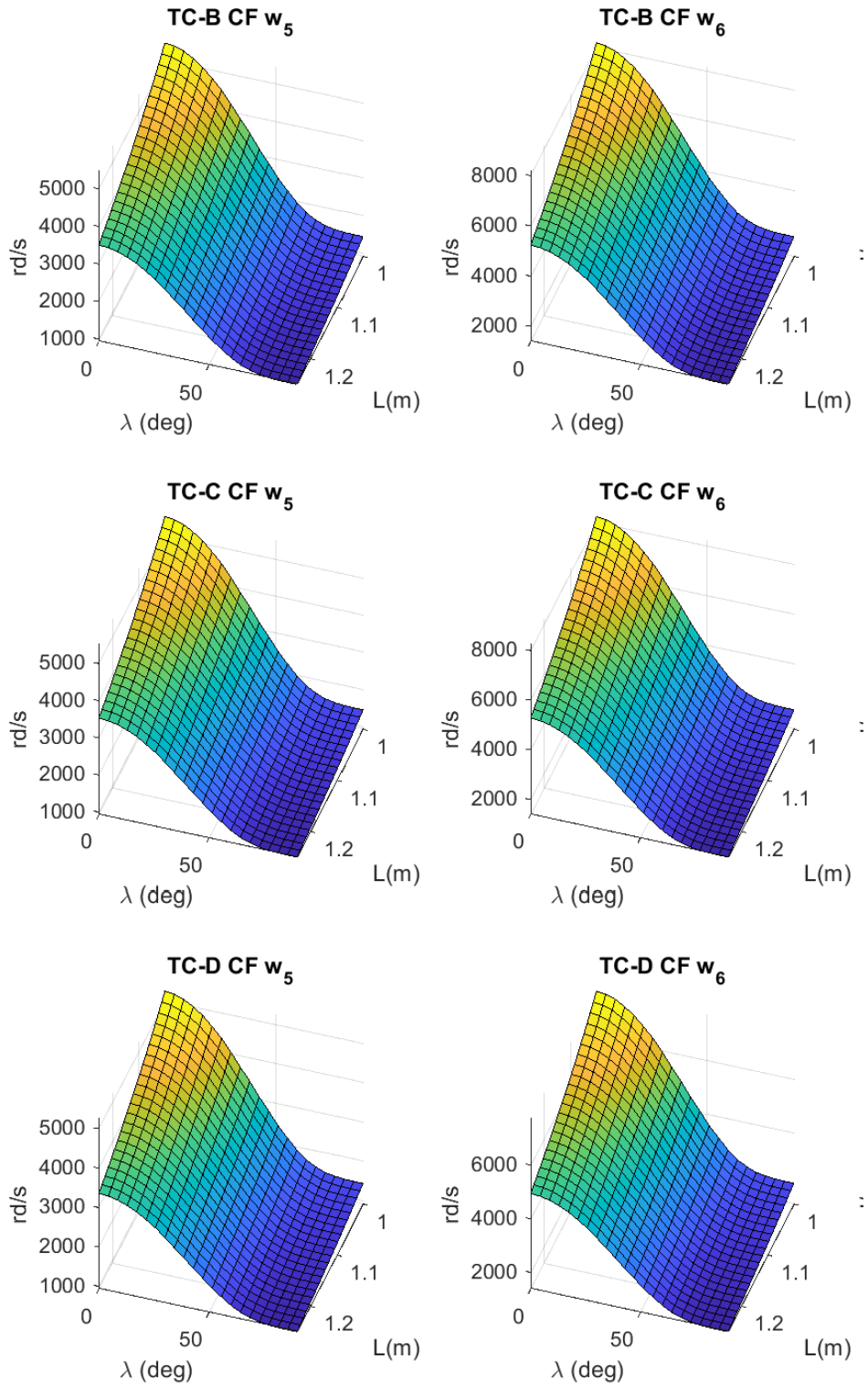

Figure A.28 – *Clamped-free tapered beams – fifth and sixth natural frequencies vs λ vs L*

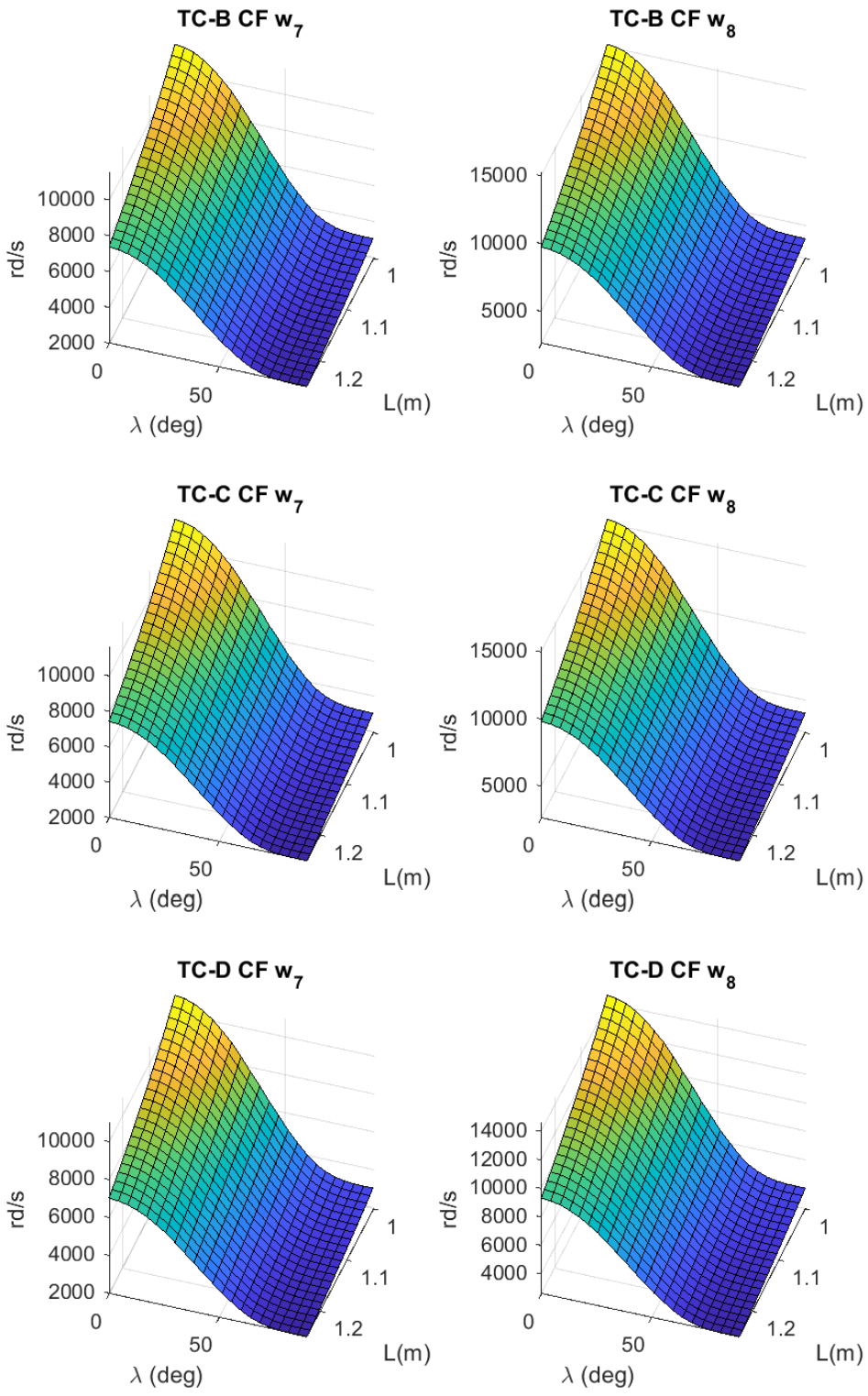

Figure A.29 – *Clamped-free tapered beams – seventh and eighth natural frequencies vs λ vs L*

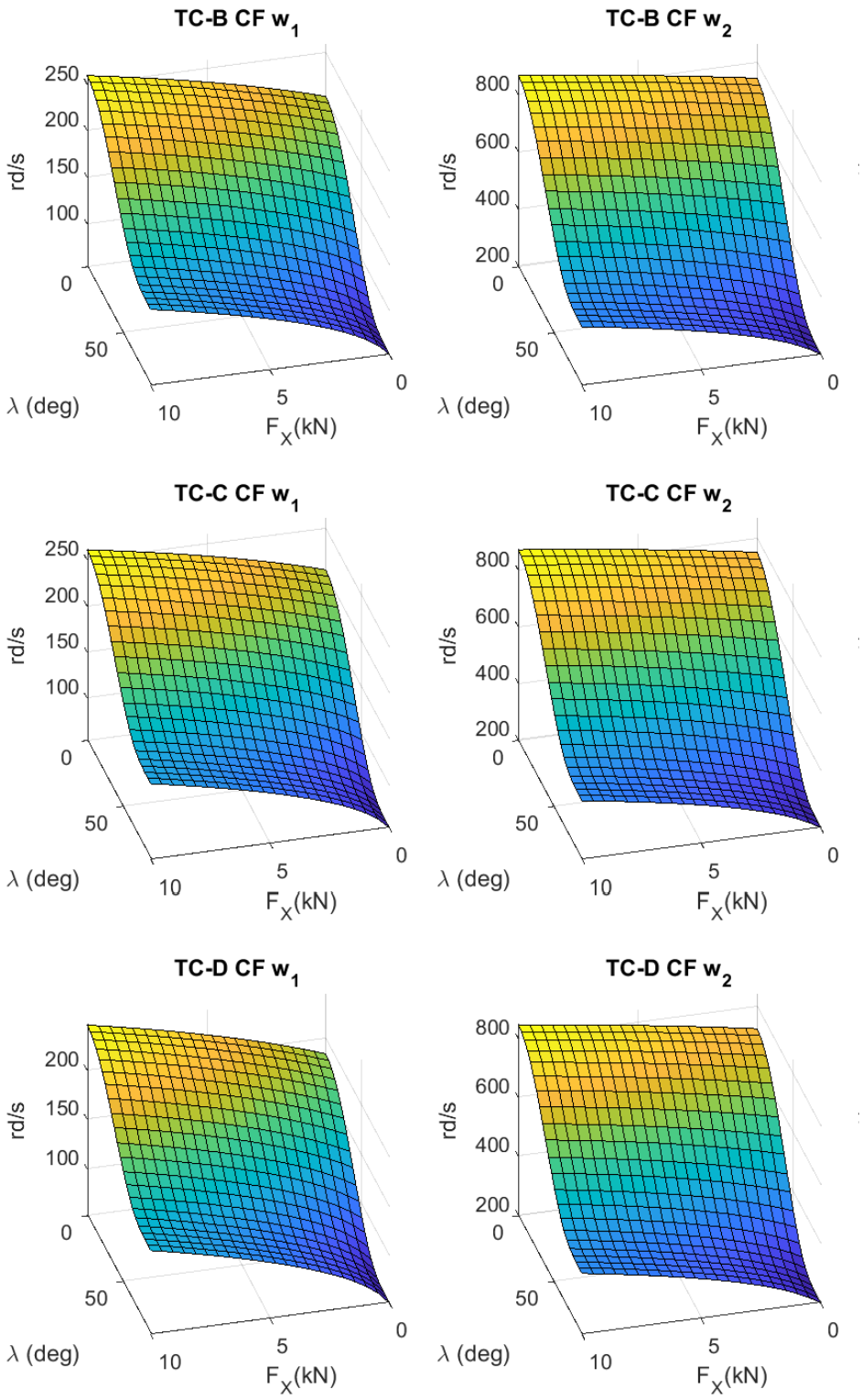

Figure A.30 – *Clamped-free tapered beams – first and second natural frequencies vs λ vs Fx*

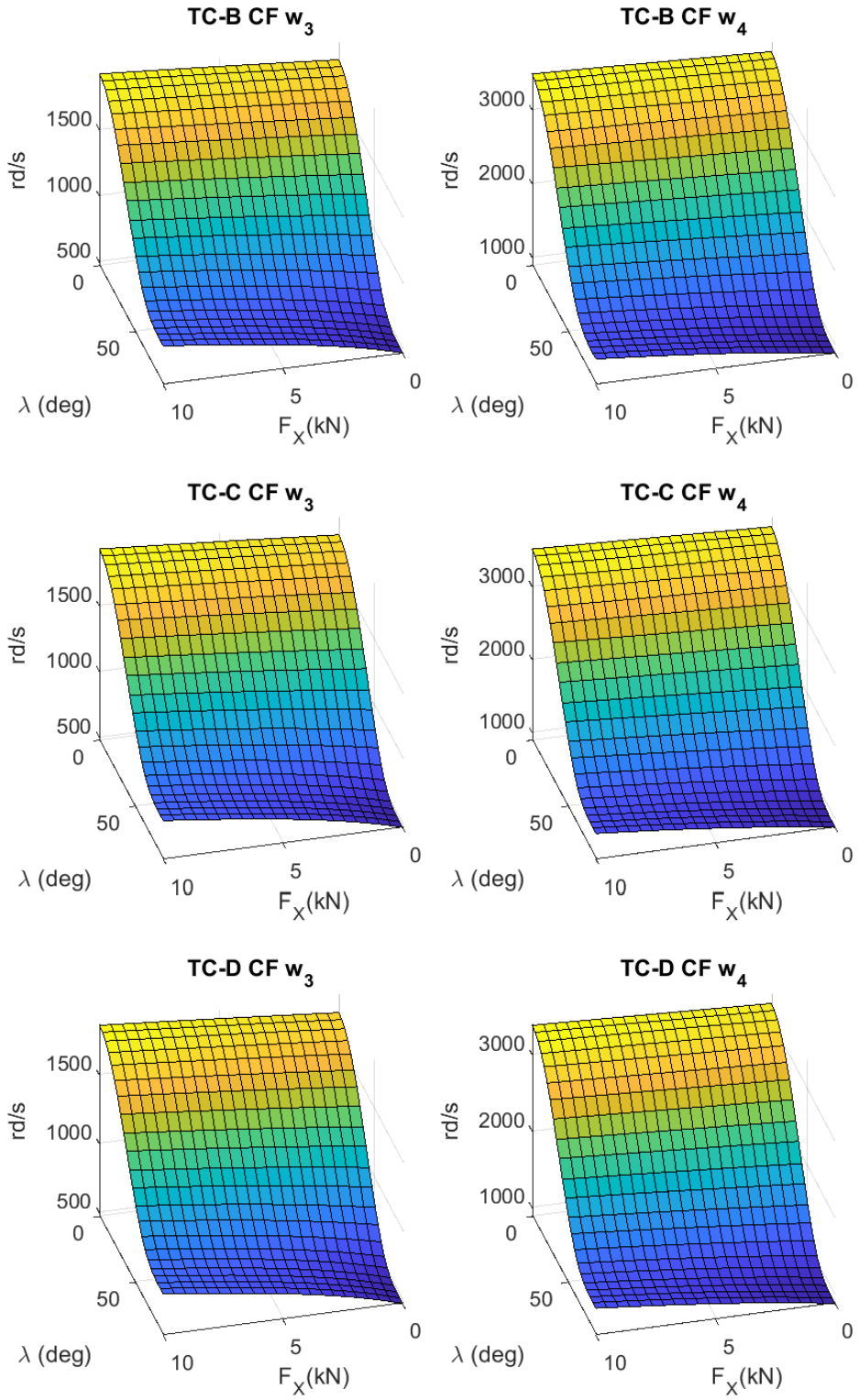

Figure A.31 – *Clamped-free tapered beams – third and fourth natural frequencies vs λ vs Fx*

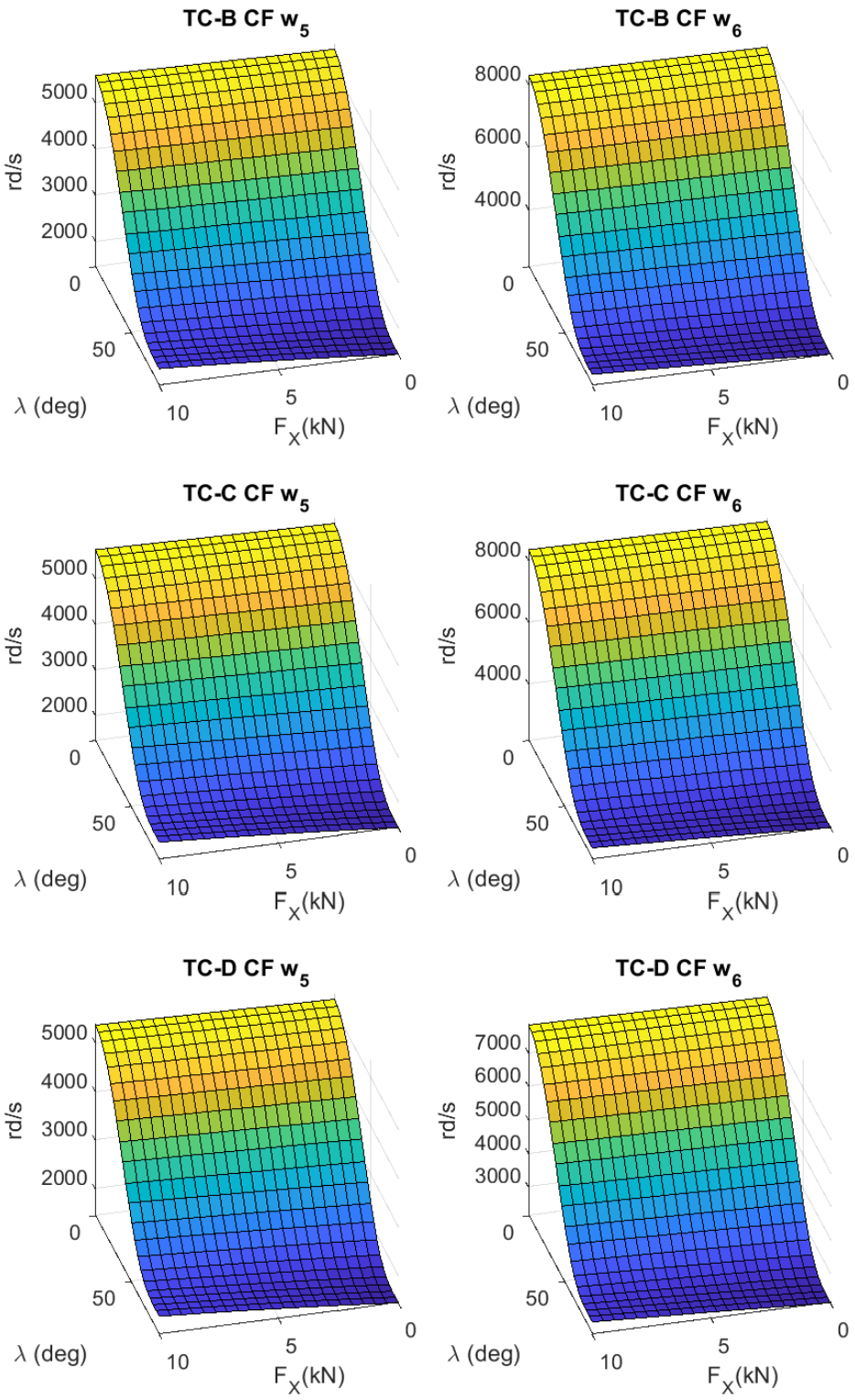

Figure A.32 – *Clamped-free tapered beams – fifth and sixth natural frequencies vs λ vs Fx*

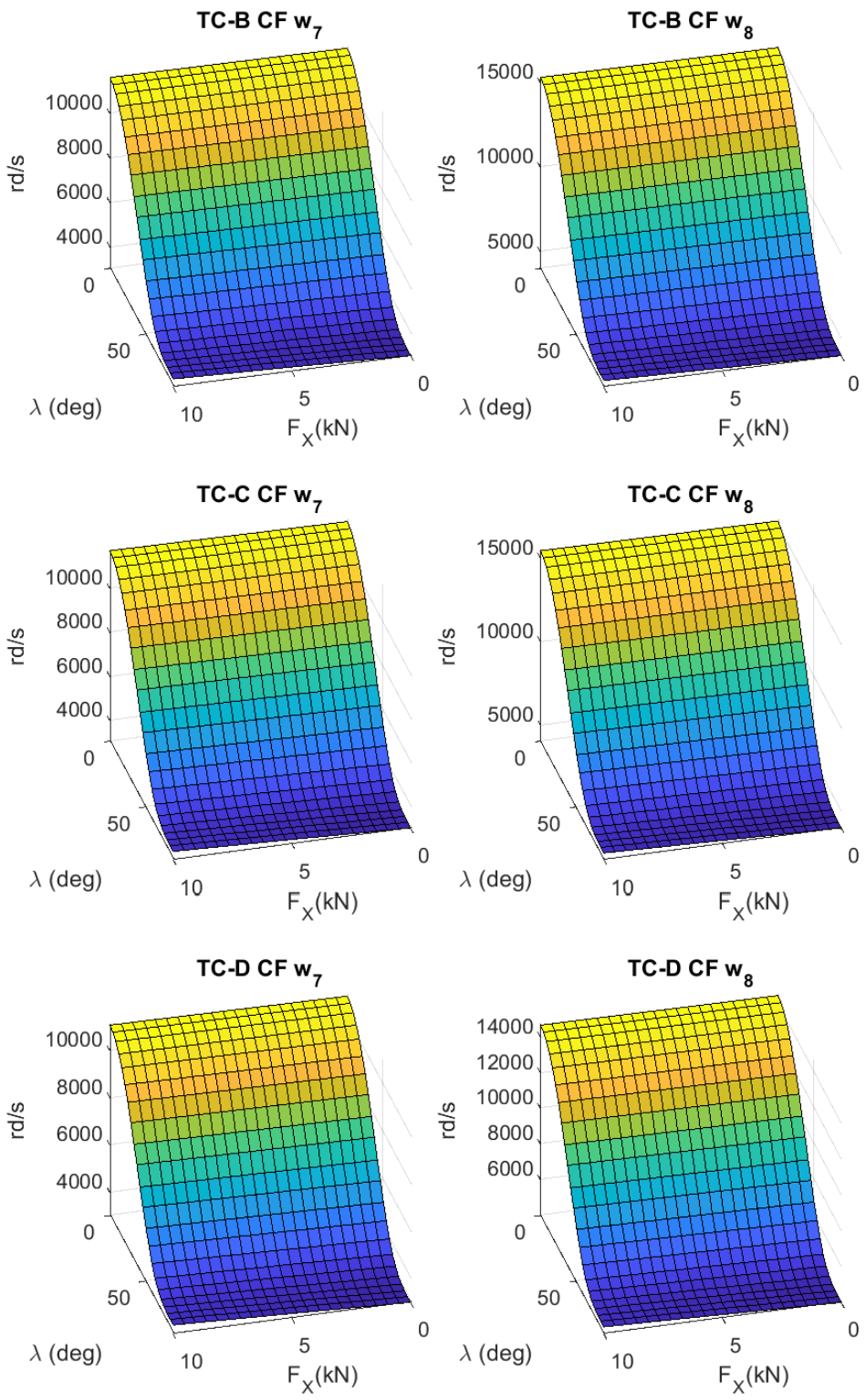

Figure A.33 – *Clamped-free tapered beams – seventh and eight natural frequencies vs λ vs Fx*

Appendix B – Optimization results

The optimization results of all result groups are displayed from figure B.1 to figure B.16.

B.1. Optimization results – representative vector

The optimization results for the non-tapered and tapered configurations are presented at figures B.1 to B.16. The optimizations aim to maximize the single objective value eq. (2.39) and the results are subdivided in eight result groups according the structural tuning approach, and the presence or absence of a tensile force Fx, as displayed on table 4.2.

Table 4.3 displays the optimization results by each result group, where each outcome set consists of five identical optimizations for the same blade passing frequency w_p.

The nomenclature applied to each result group is defined on chapter 4, and follows tables 3.1 and 4.1, and the tuning approaches are described on chapter 2.

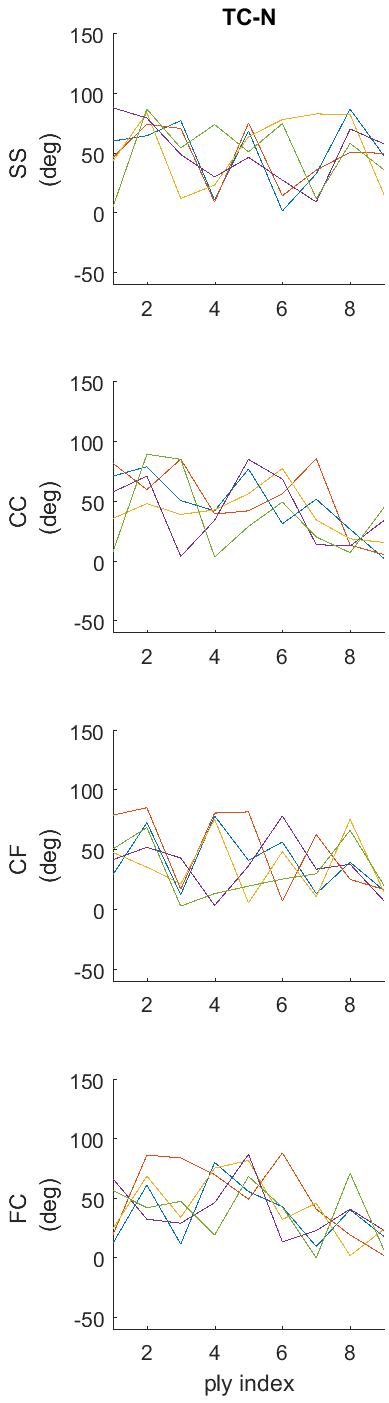

Figure B.1 – *Non-tapered beam optimization results - result group 1*

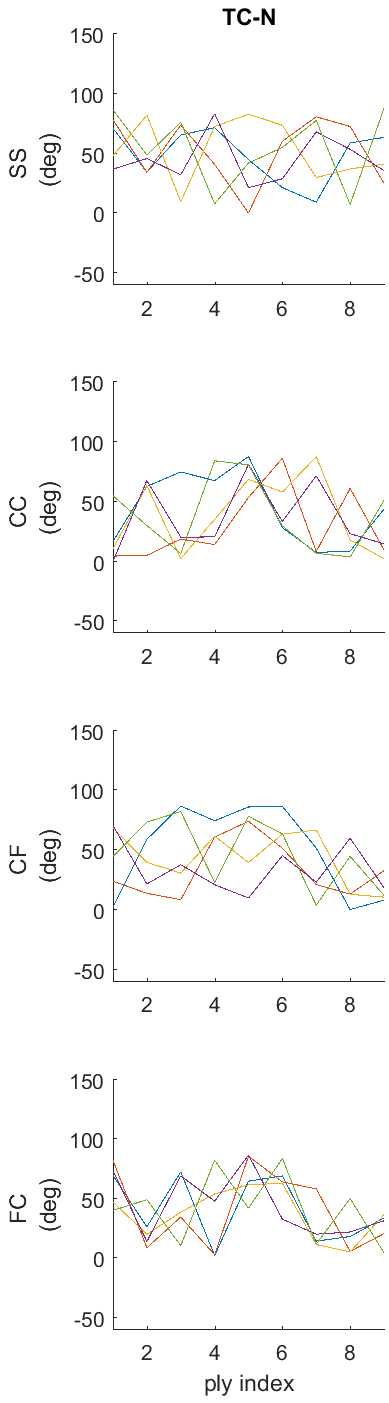

Figure B.2 – *Non-tapered beam optimization results - result group 2*

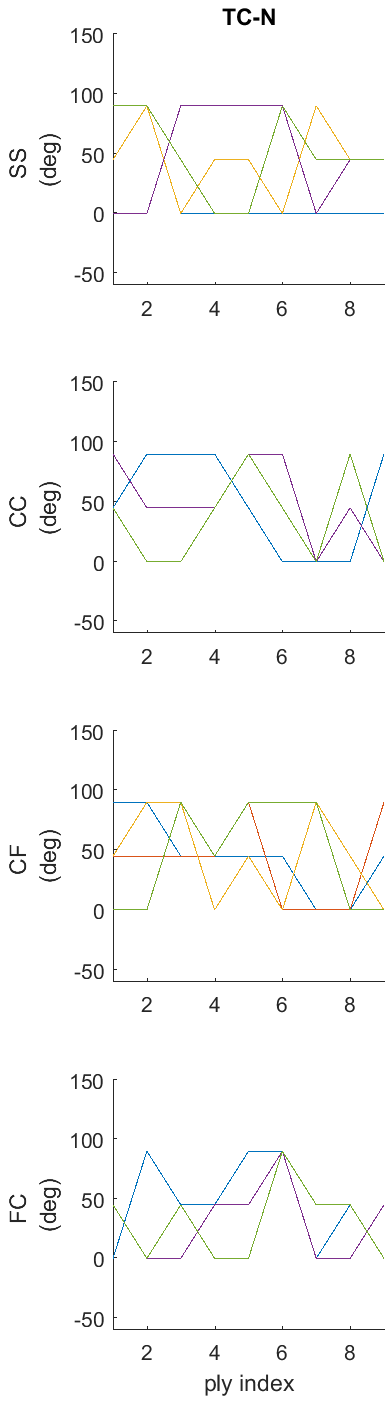

Figure B.3 – *Non-tapered beam optimization results - result group 3*

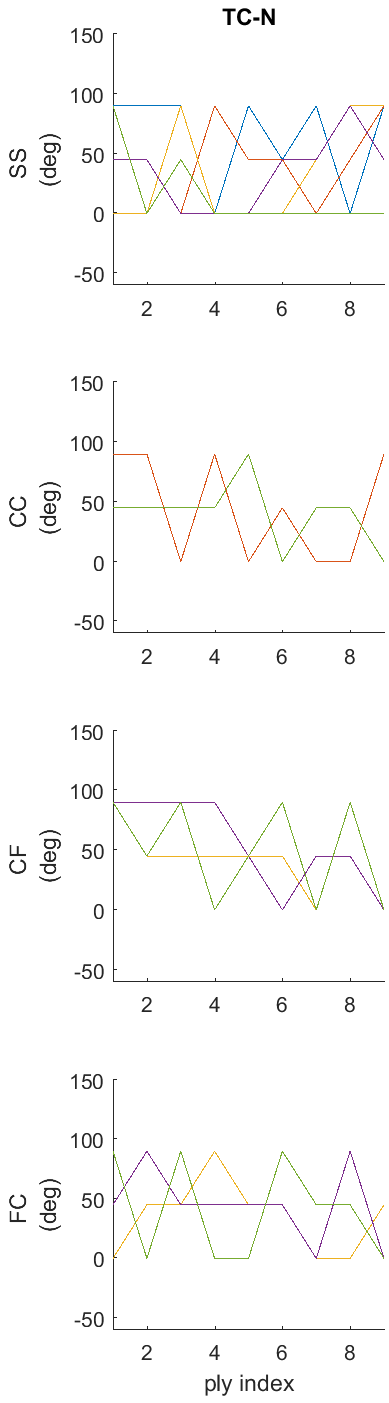

Figure B.4 – *Non-tapered beam optimization results - result group 4*

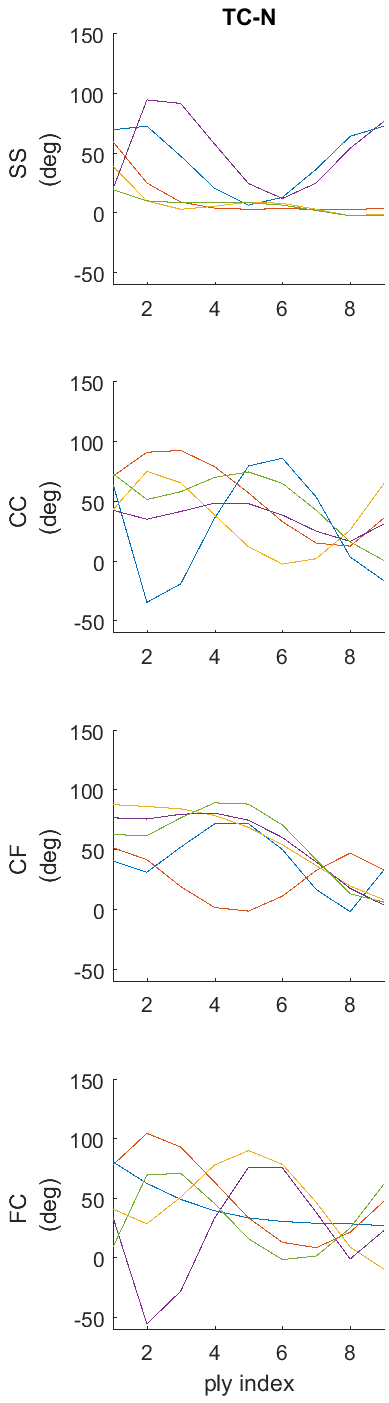

Figure B.5 – *Non-tapered beam optimization results - result group 5*

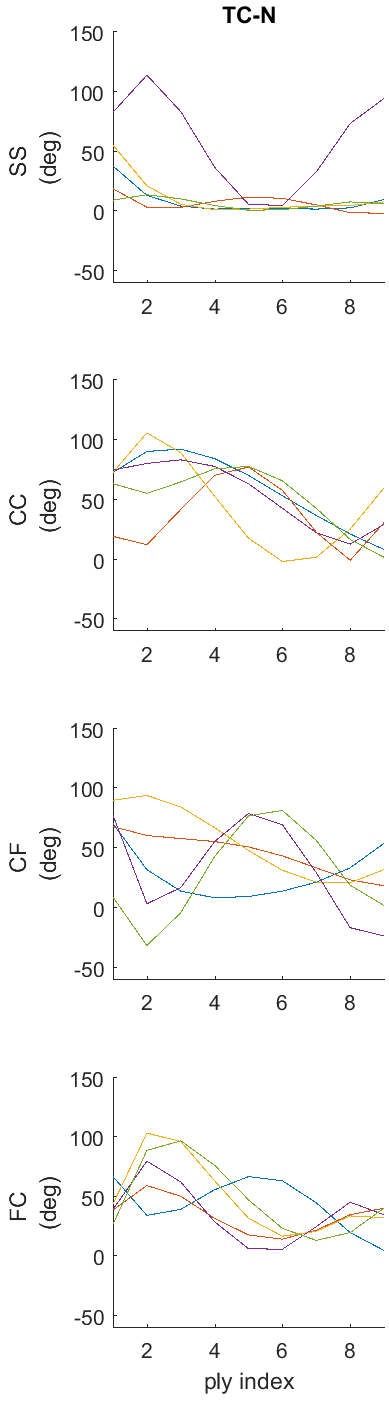

Figure B.6 – *Non-tapered beam optimization results - result group 6*

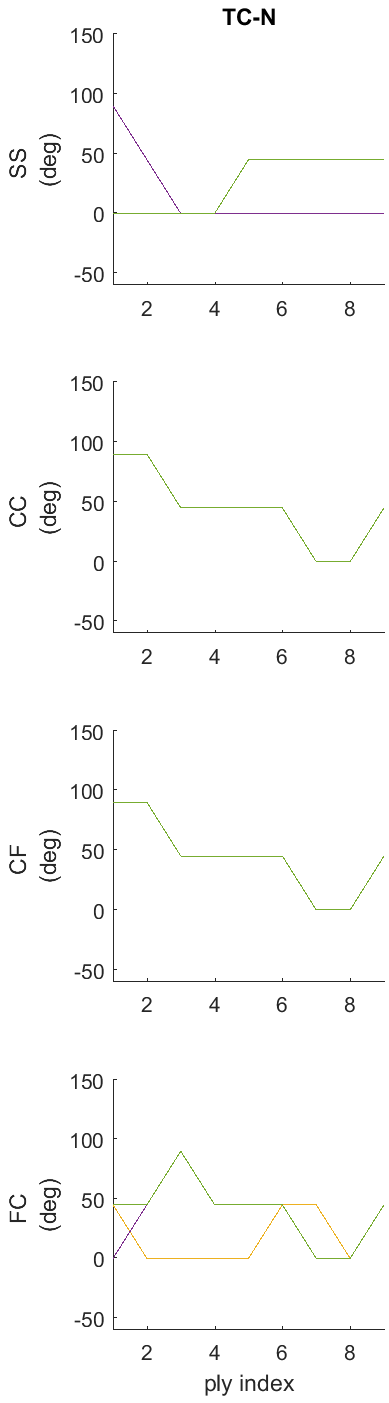

Figure B.7 – *Non-tapered beam optimization results - result group 7*

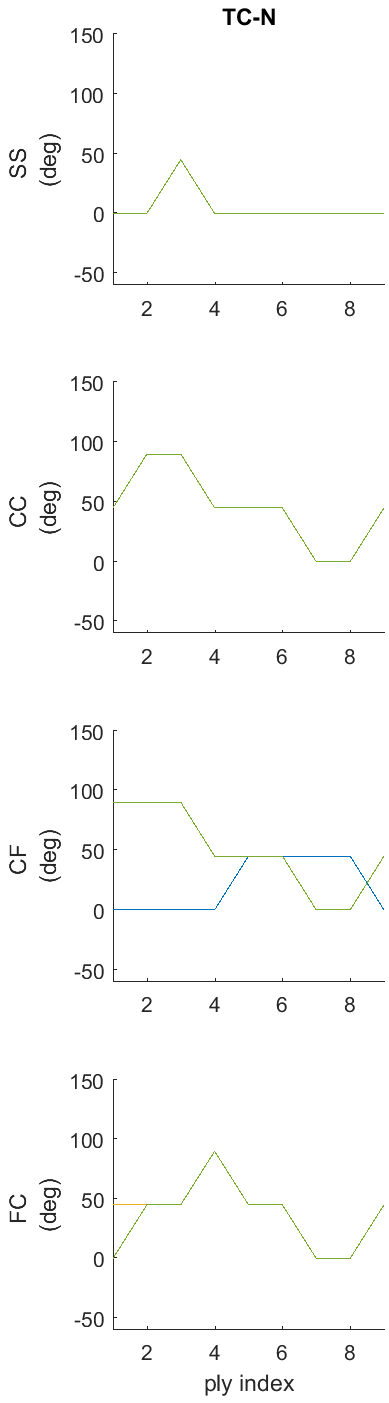

Figure B.8 – *Non-tapered beam optimization results - result group 8*

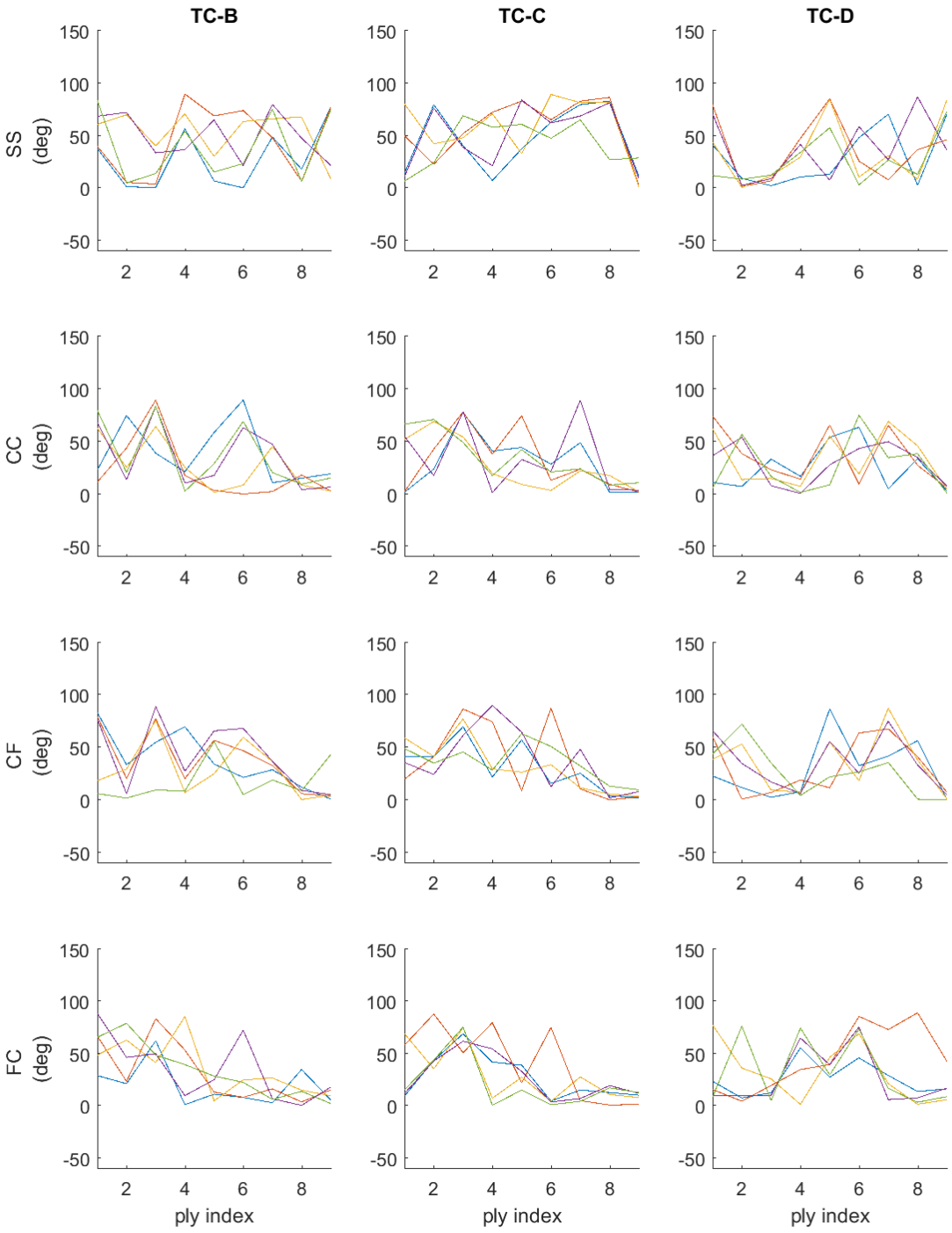

Figure B.9 – *Tapered beam optimization results - result group 1*

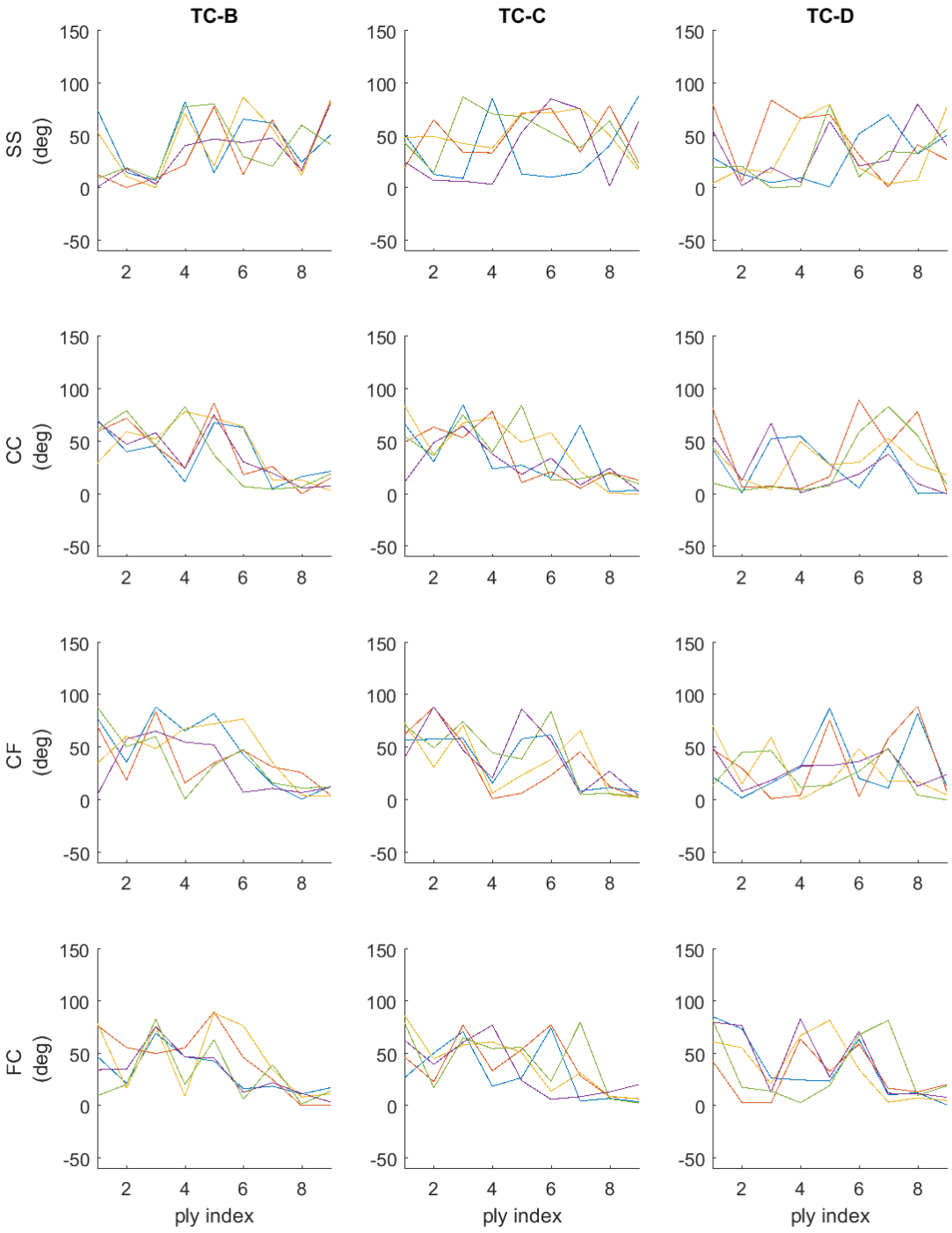

Figure B.10 – *Tapered beam optimization results - result group 2*

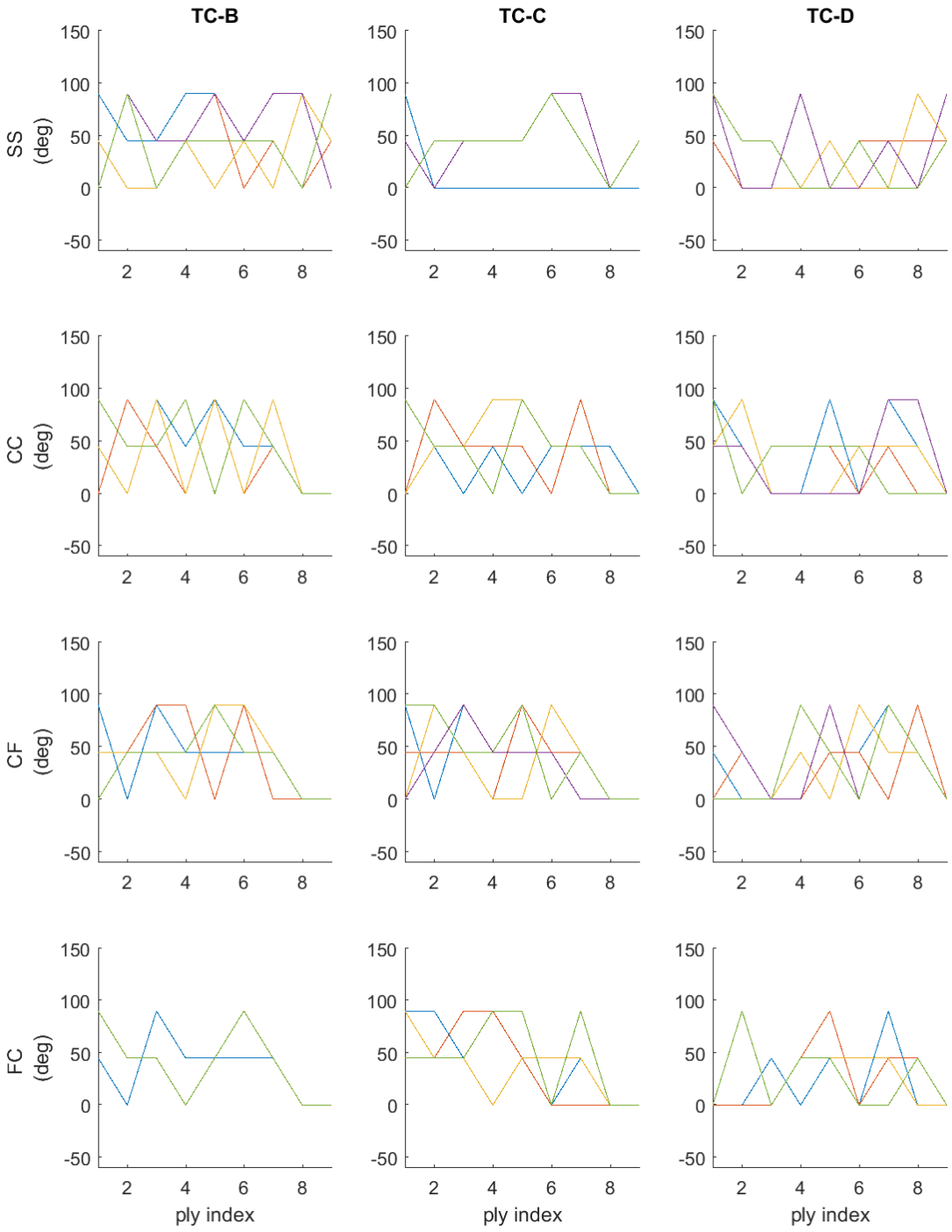

Figure B.11 – *Tapered beam optimization results - result group 3*

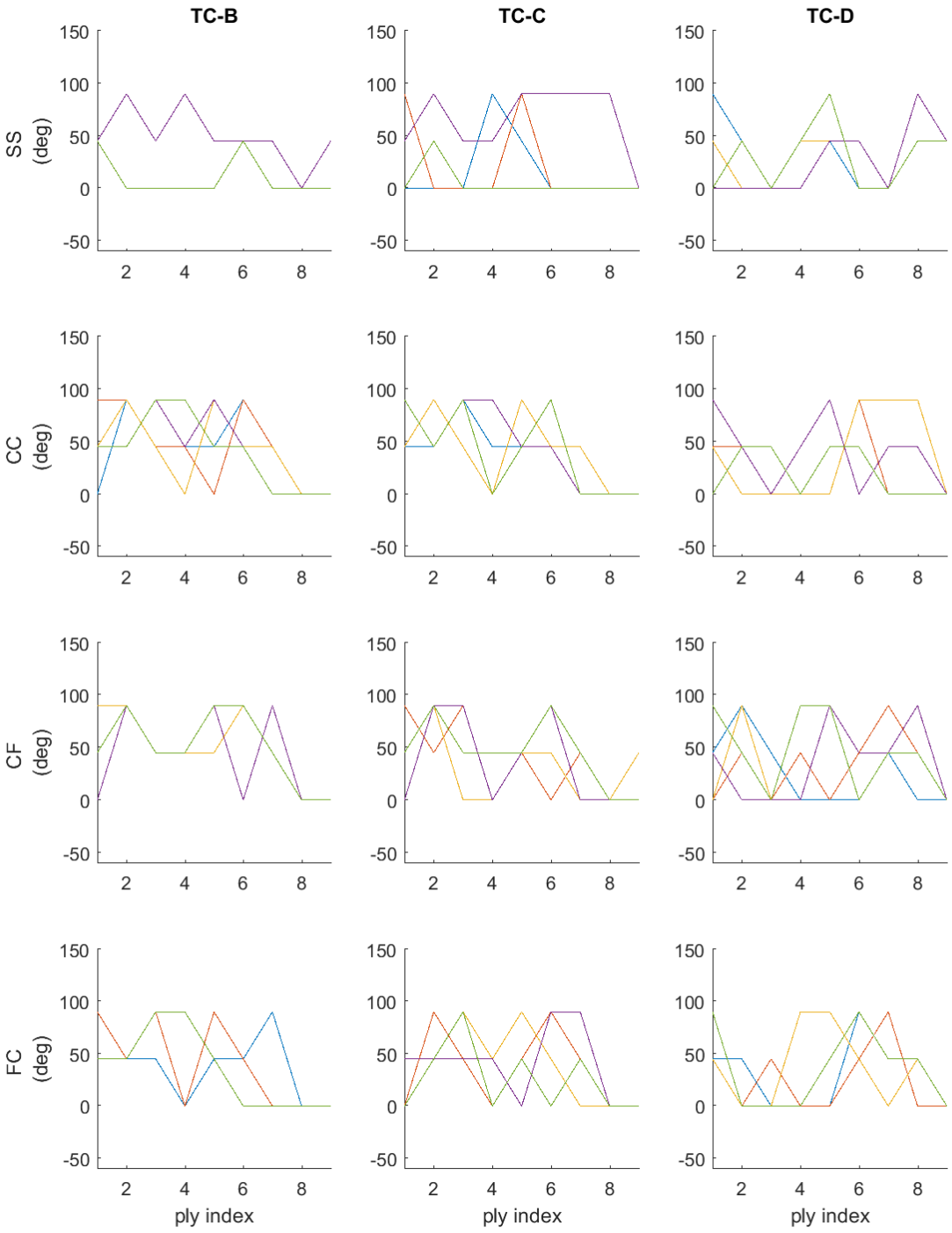

Figure B.12 – *Tapered beam optimization results - result group 4*

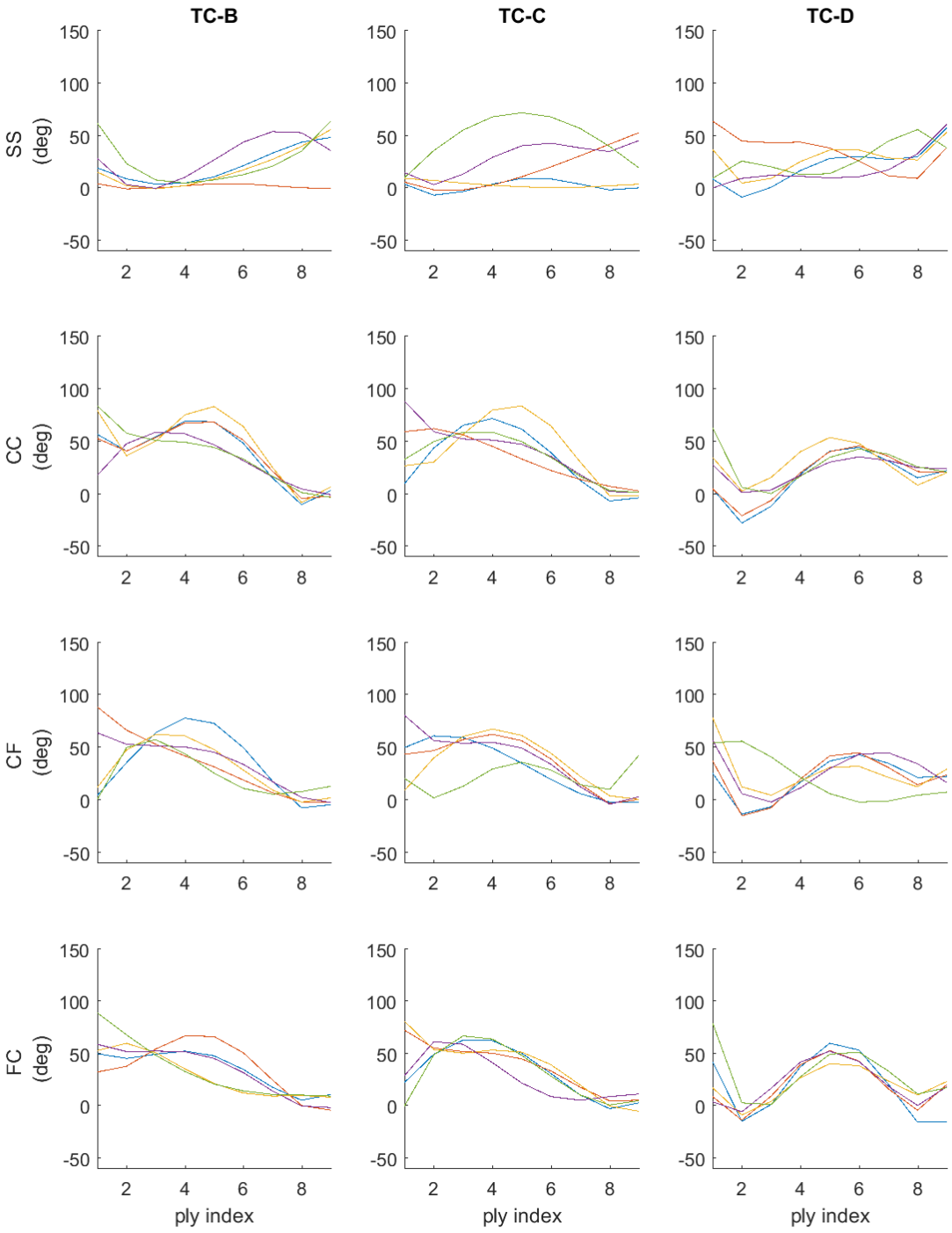

Figure B.13 – *Tapered beam optimization results - result group 5*

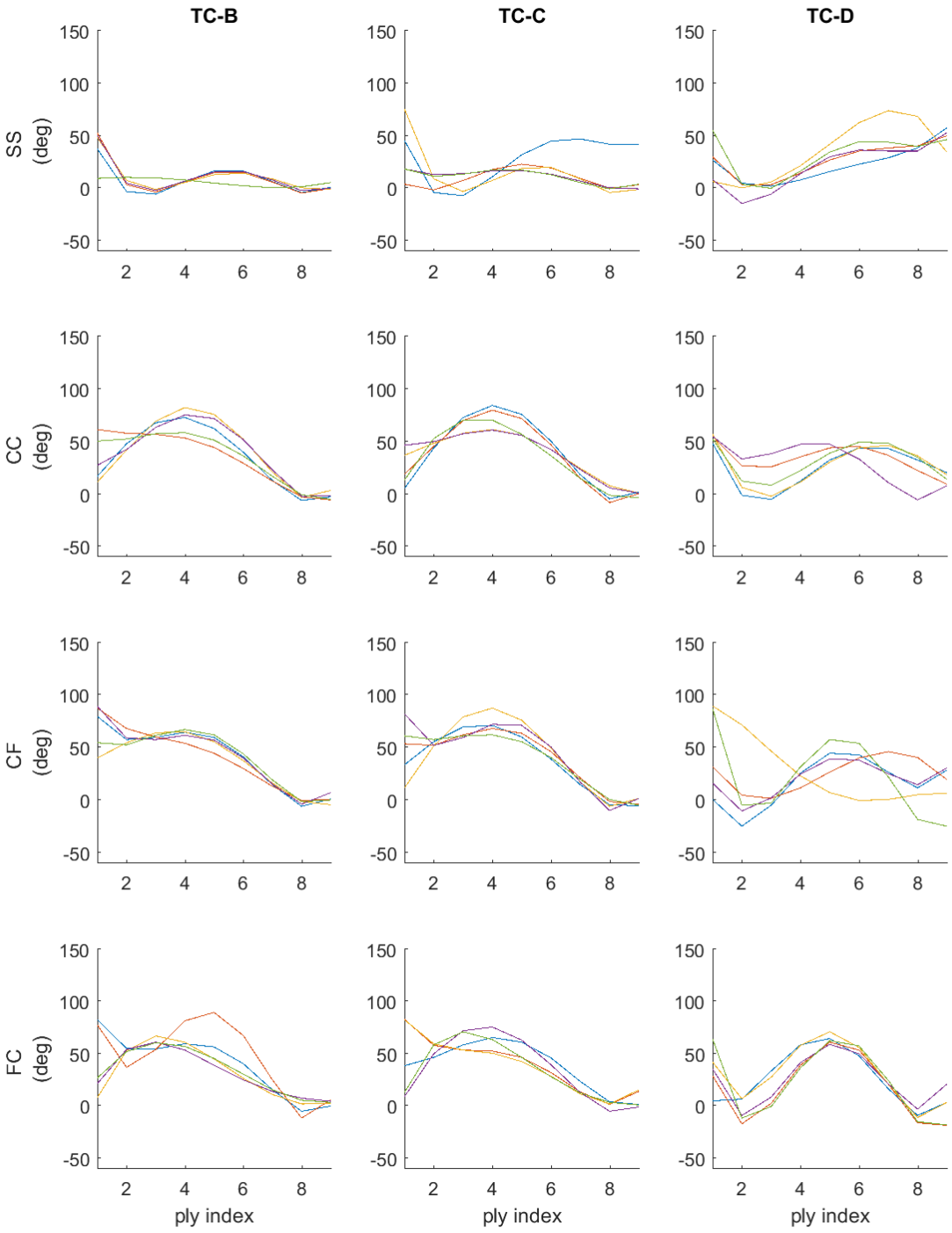

Figure B.14 – *Tapered beam optimization results - result group 6*

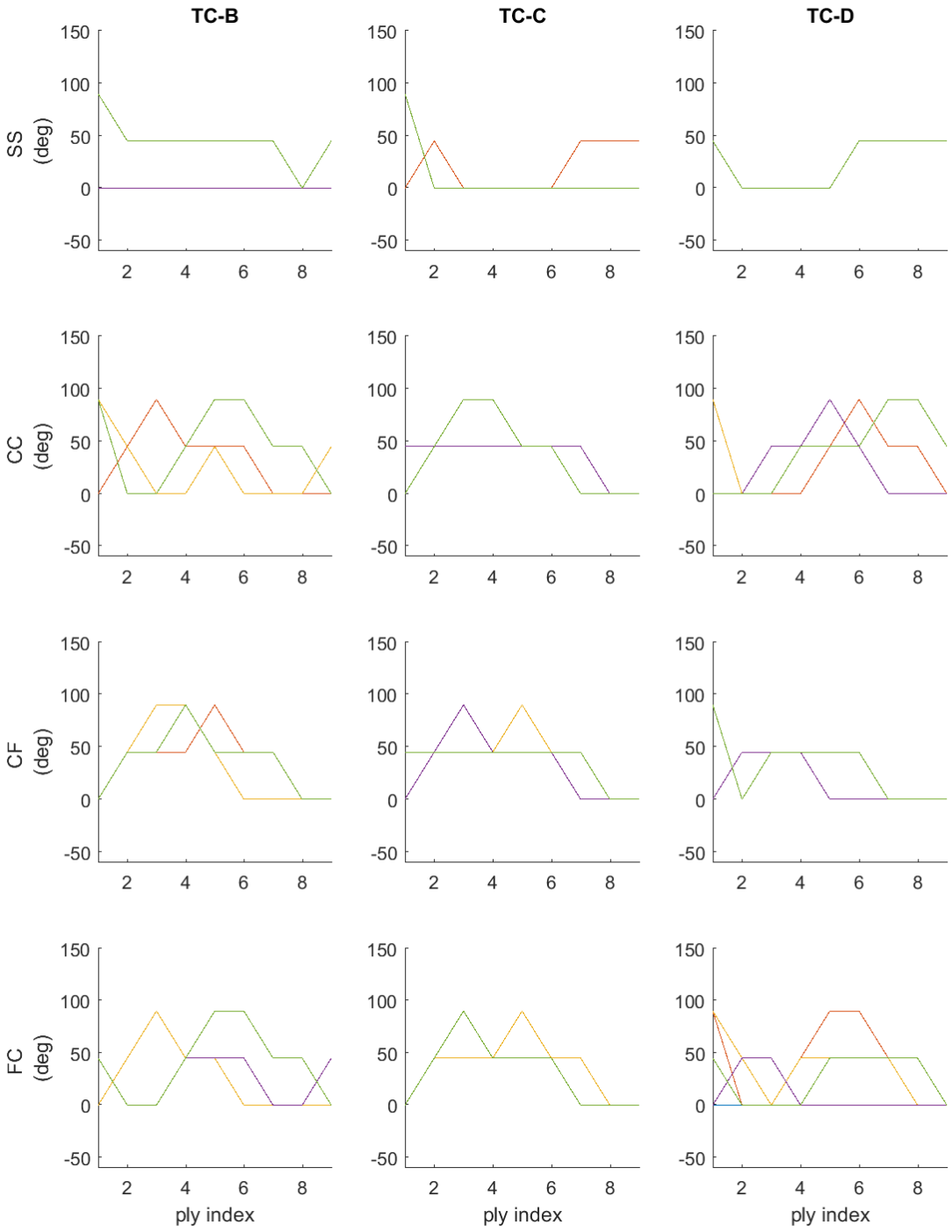

Figure B.15 – *Tapered beam optimization results - result group 7*

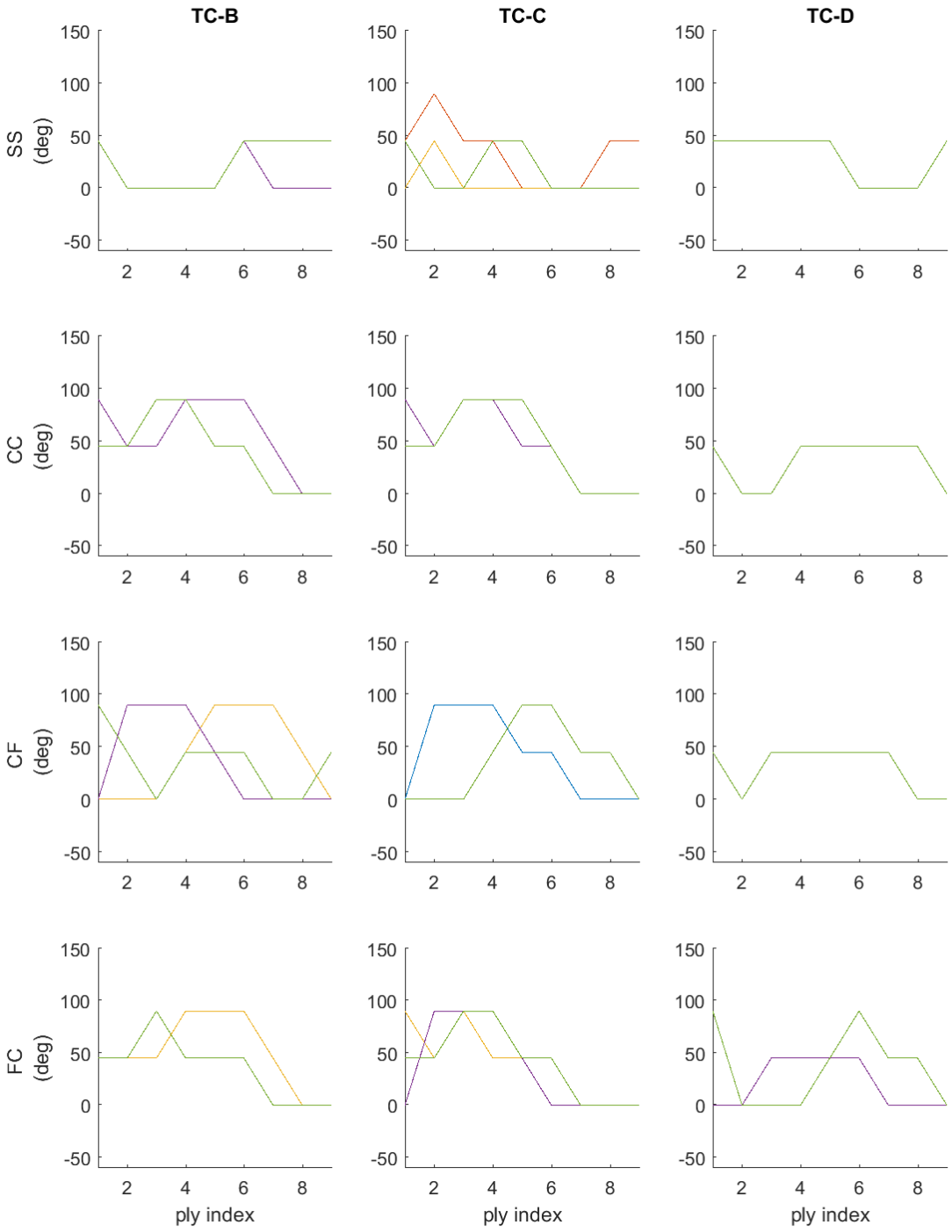

Figure B.16 – *Tapered beam optimization results - result group 8*

B.2 Optimization results – outcome table

Tables B.1 to B.8 display the partial values of optimization results as dw (eq. 2.37), $\overline{w_e}$ (eq. 2.38) and Fit (eq. 2.39), subdivided by each result group as defined in table 4.2.

ITEM	TC	BC	CURVE#	NWC1#	NWC2#	WC1(rd/s)	WC2(rd/s)	Wp(rd/s)	Fx(kN)	dw(rd/s)	wbe(rd/s)	FIT
1	b	SS	1	5	6	4565.7	6634.3	5600	0	2068.58	0.01	1968.51
2	b	SS	2	5	6	4569.2	6631	5600	0	2061.81	0.07	1961.1
3	b	SS	3	5	6	4566.9	6633	5600	0	2066.15	0.07	1965.48
4	b	SS	4	5	6	4573.5	6627	5600	0	2053.5	0.2	1951.48
5	b	SS	5	5	6	4573.7	6626.7	5600	0	2053	0.24	1950.58
6	c	SS	1	5	6	4570.8	6627.6	5600	0	2056.84	0.83	1948.57
7	c	SS	2	5	6	4568.6	6631.3	5600	0	2062.7	0.05	1962.24
8	c	SS	3	5	6	4571.8	6628.4	5600	0	2056.56	0.12	1955.35
9	c	SS	4	5	6	4570.1	6629.8	5600	0	2059.68	0.04	1959.3
10	c	SS	5	5	6	4577.5	6622.1	5600	0	2044.61	0.15	1943.08
11	d	SS	1	5	6	4517.5	6683	5600	0	2165.58	0.25	2063.1
12	d	SS	2	5	6	4508.4	6691.3	5600	0	2182.9	0.14	2081.51
13	d	SS	3	5	6	4508.5	6692.5	5600	0	2184.04	0.48	2079.26
14	d	SS	4	5	6	4515.9	6684.5	5600	0	2168.53	0.2	2066.52
15	d	SS	5	5	6	4503.5	6695.8	5600	0	2192.32	0.38	2088.48
16	n	SS	1	4	5	4370.3	6829.8	5600	0	2459.51	0	2459.47
17	n	SS	2	4	5	4370.2	6829.7	5600	0	2459.5	0	2459.47
18	n	SS	3	4	5	4370.2	6829.8	5600	0	2459.5	0	2459.49
19	n	SS	4	4	5	4370.2	6829.8	5600	0	2459.5	0	2459.5
20	n	SS	5	4	5	4370.2	6829.7	5600	0	2459.5	0	2459.48
21	b	CC	1	4	5	4458.6	6741.5	5600	0	2282.9	0.07	2182.21
22	b	CC	2	4	5	4419.2	6782.9	5600	0	2363.74	1.04	2253.3
23	b	CC	3	4	5	4431.1	6765.6	5600	0	2334.53	1.65	2218.02
24	b	CC	4	4	5	4438.5	6761.9	5600	0	2323.39	0.2	2221.4
25	b	CC	5	4	5	4433.1	6767	5600	0	2333.92	0.05	2233.39
26	c	CC	1	4	5	4437.9	6761.5	5600	0	2323.65	0.31	2220.5
27	c	CC	2	4	5	4416.1	6783.9	5600	0	2367.84	0.01	2267.78
28	c	CC	3	4	5	4418.5	6781.7	5600	0	2363.21	0.06	2262.61
29	c	CC	4	4	5	4438.9	6761.7	5600	0	2322.78	0.27	2220.12
30	c	CC	5	4	5	4420.3	6780	5600	0	2359.64	0.14	2258.21
31	d	CC	1	4	5	4516.4	6683.8	5600	0	2167.38	0.08	2066.59
32	d	CC	2	4	5	4510.2	6690.2	5600	0	2180	0.24	2077.64
33	d	CC	3	4	5	4505.9	6694.2	5600	0	2188.34	0.06	2087.77
34	d	CC	4	4	5	4509.2	6690.3	5600	0	2181.18	0.25	2078.68
35	d	CC	5	4	5	4511.9	6688.1	5600	0	2176.23	0.02	2076.05
36	n	CC	1	3	4	4221.3	6978.7	5600	0	2757.38	0	2757.37
37	n	CC	2	3	4	4221.3	6978.7	5600	0	2757.38	0	2757.34
38	n	CC	3	3	4	4221.3	6978.7	5600	0	2757.38	0.01	2757.3
39	n	CC	4	3	4	4221.3	6978.7	5600	0	2757.38	0.02	2757.23
40	n	CC	5	3	4	4221.3	6978.7	5600	0	2757.37	0.01	2757.28
41	b	CF	1	5	6	4436	6764.7	5600	0	2328.62	0.35	2225.07
42	b	CF	2	5	6	4428.4	6771.2	5600	0	2342.76	0.21	2240.65
43	b	CF	3	5	6	4426.6	6773.1	5600	0	2346.57	0.16	2245
44	b	CF	4	5	6	4444.7	6756.3	5600	0	2311.61	0.49	2206.7
45	b	CF	5	5	6	4462.9	6736.9	5600	0	2274.02	0.11	2172.92
46	c	CF	1	5	6	4411.2	6784.9	5600	0	2373.79	1.95	2254.26
47	c	CF	2	5	6	4412.9	6787.2	5600	0	2374.35	0.05	2273.88
48	c	CF	3	5	6	4415	6785.4	5600	0	2370.38	0.19	2268.44
49	c	CF	4	5	6	4445.5	6755.1	5600	0	2309.53	0.3	2206.56
50	c	CF	5	5	6	4462.5	6737	5600	0	2274.47	0.23	2172.2
51	d	CF	1	5	6	4503.4	6696.5	5600	0	2193.13	0.08	2092.33
52	d	CF	2	5	6	4505.8	6693.8	5600	0	2188.03	0.18	2086.24
53	d	CF	3	5	6	4512.4	6686.3	5600	0	2173.9	0.68	2067.07
54	d	CF	4	5	6	4513.9	6686.2	5600	0	2172.3	0.06	2071.74
55	d	CF	5	5	6	4502.1	6698.6	5600	0	2196.53	0.32	2093.29
56	n	CF	1	4	5	4221.2	6978.8	5600	0	2757.52	0.01	2757.43
57	n	CF	2	4	5	4221.2	6978.7	5600	0	2757.52	0.01	2757.43
58	n	CF	3	4	5	4221.2	6978.8	5600	0	2757.52	0	2757.52
59	n	CF	4	4	5	4221.2	6978.8	5600	0	2757.52	0	2757.51
60	n	CF	5	4	5	4221.2	6978.8	5600	0	2757.53	0.01	2757.46
61	b	FC	1	5	6	4432	6767.1	5600	0	2335.1	0.48	2230.33
62	b	FC	2	5	6	4415.4	6785.2	5600	0	2369.78	0.27	2267.13
63	b	FC	3	5	6	4435.9	6763.3	5600	0	2327.44	0.37	2223.76
64	b	FC	4	5	6	4420.4	6779.7	5600	0	2359.37	0.05	2258.91
65	b	FC	5	5	6	4404	6796.3	5600	0	2392.25	0.15	2290.74
66	c	FC	1	5	6	4404.7	6795.1	5600	0	2390.34	0.09	2289.45
67	c	FC	2	5	6	4402.1	6797.4	5600	0	2395.25	0.27	2292.54
68	c	FC	3	5	6	4403.2	6796.4	5600	0	2393.23	0.22	2291.02
69	c	FC	4	5	6	4410	6788.2	5600	0	2378.17	0.92	2269.01
70	c	FC	5	5	6	4405.1	6795.1	5600	0	2390.06	0.09	2289.12
71	d	FC	1	5	6	4481	6719.2	5600	0	2238.23	0.07	2137.52
72	d	FC	2	6	7	4575	6625	5600	0	2050.02	0.01	1949.88
73	d	FC	3	5	6	4478.2	6722.1	5600	0	2243.84	0.15	2142.39
74	d	FC	4	5	6	4478.2	6722.2	5600	0	2243.97	0.18	2142.14
75	d	FC	5	5	6	4480.8	6719.9	5600	0	2239.08	0.35	2135.58
76	n	FC	1	4	5	4221.2	6978.8	5600	0	2757.67	0.01	2757.61
77	n	FC	2	4	5	4221.2	6978.8	5600	0	2757.66	0.01	2757.55
78	n	FC	3	4	5	4221.2	6978.9	5600	0	2757.68	0.02	2757.52
79	n	FC	4	4	5	4221.2	6978.8	5600	0	2757.67	0	2757.66
80	n	FC	5	4	5	4221.2	6978.8	5600	0	2757.67	0	2757.67

Table B.1 - *Optimization results - result group 1*

ITEM	TC	BC	CURVE#	NWC1#	NWC2#	WC1(rd/s)	WC2(rd/s)	Wp(rd/s)	Fx(kN)	dw(rd/s)	wbe(rd/s)	FIT
1	b	SS	1	5	6	4586.4	6614.1	5600	10	2027.63	0.25	1925.11
2	b	SS	2	5	6	4589.5	6610.3	5600	10	2020.79	0.08	1920.03
3	b	SS	3	5	6	4583	6616.9	5600	10	2033.84	0.05	1933.32
4	b	SS	4	5	6	4587.4	6612.3	5600	10	2024.85	0.13	1923.56
5	b	SS	5	5	6	4589.4	6610.6	5600	10	2021.13	0	1921.11
6	c	SS	1	5	6	4588.2	6611.6	5600	10	2023.34	0.08	1922.53
7	c	SS	2	5	6	4600.6	6599.6	5600	10	1999.09	0.1	1898.05
8	c	SS	3	5	6	4592.9	6610.9	5600	10	2018.09	1.89	1899.15
9	c	SS	4	5	6	4593.6	6606.4	5600	10	2012.85	0.01	1912.78
10	c	SS	5	5	6	4594.9	6604.5	5600	10	2009.61	0.28	1906.85
11	d	SS	1	5	6	4534	6667.1	5600	10	2133.11	0.58	2027.32
12	d	SS	2	5	6	4551.1	6649.8	5600	10	2098.7	0.41	1994.57
13	d	SS	3	5	6	4536	6663.9	5600	10	2127.9	0.04	2027.55
14	d	SS	4	5	6	4538.1	6661.7	5600	10	2123.56	0.09	2022.69
15	d	SS	5	5	6	4521.9	6678	5600	10	2156.11	0.04	2055.66
16	n	SS	1	4	5	4377.7	6822.3	5600	10	2444.61	0.01	2444.48
17	n	SS	2	4	5	4377.7	6822.3	5600	10	2444.61	0.01	2444.49
18	n	SS	3	4	5	4377.7	6822.3	5600	10	2444.61	0	2444.6
19	n	SS	4	4	5	4377.7	6822.3	5600	10	2444.62	0.02	2444.44
20	n	SS	5	4	5	4377.7	6822.3	5600	10	2444.61	0	2444.61
21	b	CC	1	4	5	4470	6729.9	5600	10	2259.89	0.05	2159.44
22	b	CC	2	4	5	4449.8	6750.3	5600	10	2300.47	0.02	2200.29
23	b	CC	3	4	5	4440.7	6759.2	5600	10	2318.49	0.09	2217.64
24	b	CC	4	4	5	4432.4	6767.3	5600	10	2334.9	0.13	2233.58
25	b	CC	5	4	5	4452.7	6747.5	5600	10	2294.82	0.07	2194.07
26	c	CC	1	4	5	4440.8	6758.7	5600	10	2317.96	0.25	2215.47
27	c	CC	2	4	5	4438.8	6758.4	5600	10	2319.64	1.38	2205.87
28	c	CC	3	4	5	4435.3	6764.7	5600	10	2329.4	0.01	2229.33
29	c	CC	4	4	5	4437.6	6762.1	5600	10	2324.5	0.13	2223.18
30	c	CC	5	4	5	4440.8	6763.6	5600	10	2322.75	2.19	2200.89
31	d	CC	1	4	5	4524.9	6674.4	5600	10	2149.45	0.36	2045.89
32	d	CC	2	4	5	4519.7	6680.4	5600	10	2160.65	0.03	2060.38
33	d	CC	3	4	5	4527.8	6672.3	5600	10	2144.52	0.09	2043.65
34	d	CC	4	4	5	4504	6694.4	5600	10	2190.42	0.8	2082.42
35	d	CC	5	4	5	4518.8	6681.4	5600	10	2162.62	0.07	2061.89
36	n	CC	1	3	4	4226.3	6973.7	5600	10	2747.37	0	2747.35
37	n	CC	2	3	4	4226.3	6973.7	5600	10	2747.37	0	2747.35
38	n	CC	3	3	4	4226.3	6973.7	5600	10	2747.37	0	2747.35
39	n	CC	4	3	4	4226.3	6973.7	5600	10	2747.37	0	2747.35
40	n	CC	5	3	4	4226.3	6973.7	5600	10	2747.38	0.02	2747.17
41	b	CF	1	5	6	4462.6	6737.3	5600	10	2274.7	0.02	2174.46
42	b	CF	2	5	6	4491	6708.5	5600	10	2217.47	0.25	2114.98
43	b	CF	3	5	6	4479.6	6719.9	5600	10	2240.31	0.21	2138.22
44	b	CF	4	5	6	4456.7	6739.8	5600	10	2283.08	1.75	2165.63
45	b	CF	5	5	6	4457.8	6742.9	5600	10	2285.06	0.38	2181.26
46	c	CF	1	5	6	4456.5	6743.5	5600	10	2286.98	0.03	2186.71
47	c	CF	2	5	6	4457.3	6741.4	5600	10	2284.13	0.67	2177.48
48	c	CF	3	5	6	4473.8	6726.5	5600	10	2252.63	0.14	2151.25
49	c	CF	4	5	6	4481.8	6719.5	5600	10	2237.63	0.64	2131.24
50	c	CF	5	5	6	4454.7	6739.3	5600	10	2284.64	2.98	2154.87
51	d	CF	1	5	6	4549.2	6650.7	5600	10	2101.42	0.06	2000.83
52	d	CF	2	5	6	4537.2	6663.1	5600	10	2125.84	0.13	2024.5
53	d	CF	3	5	6	4545.5	6654.7	5600	10	2109.18	0.08	2008.4
54	d	CF	4	5	6	4547.8	6652.1	5600	10	2104.27	0.08	2003.5
55	d	CF	5	5	6	4535.7	6664.7	5600	10	2128.97	0.19	2027.05
56	n	CF	1	4	5	4229.5	6970.5	5600	10	2741.07	0	2741.05
57	n	CF	2	4	5	4229.5	6970.5	5600	10	2741.07	0	2741.02
58	n	CF	3	4	5	4229.5	6970.5	5600	10	2741.07	0	2741.06
59	n	CF	4	4	5	4229.5	6970.5	5600	10	2741.07	0	2741.06
60	n	CF	5	4	5	4229.5	6970.5	5600	10	2741.07	0	2741.06
61	b	FC	1	5	6	4446.3	6753.9	5600	10	2307.54	0.1	2206.57
62	b	FC	2	5	6	4430.8	6772.4	5600	10	2341.6	1.6	2225.58
63	b	FC	3	5	6	4446	6754.2	5600	10	2308.26	0.11	2207.16
64	b	FC	4	5	6	4423.5	6776.7	5600	10	2353.16	0.09	2252.24
65	b	FC	5	5	6	4445.7	6754.4	5600	10	2308.69	0.07	2207.99
66	c	FC	1	5	6	4424.5	6775.2	5600	10	2350.74	0.17	2248.99
67	c	FC	2	5	6	4444.1	6755.7	5600	10	2311.57	0.07	2210.91
68	c	FC	3	5	6	4426.9	6773.1	5600	10	2346.23	0.02	2246.04
69	c	FC	4	5	6	4435.2	6763.7	5600	10	2328.45	0.54	2223.07
70	c	FC	5	5	6	4455.6	6744.6	5600	10	2289.04	0.09	2188.09
71	d	FC	1	5	6	4494.5	6705	5600	10	2210.56	0.25	2108.04
72	d	FC	2	5	6	4494.6	6705.1	5600	10	2210.55	0.12	2109.3
73	d	FC	3	5	6	4497.1	6702.8	5600	10	2205.68	0.05	2105.16
74	d	FC	4	5	6	4497.6	6701.9	5600	10	2204.35	0.26	2101.73
75	d	FC	5	5	6	4499.6	6700.4	5600	10	2200.81	0.02	2100.64
76	n	FC	1	4	5	4229.4	6970.6	5600	10	2741.2	0	2741.17
77	n	FC	2	4	5	4229.4	6970.6	5600	10	2741.21	0.01	2741.08
78	n	FC	3	4	5	4229.4	6970.6	5600	10	2741.2	0	2741.2
79	n	FC	4	4	5	4229.4	6970.6	5600	10	2741.2	0.01	2741.07
80	n	FC	5	4	5	4229.4	6970.6	5600	10	2741.21	0	2741.16

Table B.2 - *Optimization results - result group 2*

ITEM	TC	BC	CURVE#	NWC1#	NWC2#	WC1(rd/s)	WC2(rd/s)	Wp(rd/s)	Fx(kN)	dw(rd/s)	wbe(rd/s)	FIT
1	b	SS	1	5	6	4568.7	6632.6	5600	0	2063.92	0.61	1957.82
2	b	SS	2	5	6	4583.4	6616.3	5600	0	2032.88	0.16	1931.32
3	b	SS	3	5	6	4568.4	6632.7	5600	0	2064.3	0.51	1959.18
4	b	SS	4	5	6	4569.8	6627.7	5600	0	2057.9	1.29	1945.03
5	b	SS	5	5	6	4582.5	6623.2	5600	0	2040.65	2.83	1912.31
6	c	SS	1	4	5	4367	6841	5600	0	2473.94	4.01	2433.82
7	c	SS	2	5	6	4583.7	6612.2	5600	0	2028.49	2.04	1908.06
8	c	SS	3	5	6	4583.7	6612.2	5600	0	2028.49	2.04	1908.06
9	c	SS	4	5	6	4589	6612.5	5600	0	2023.52	0.76	1915.94
10	c	SS	5	5	6	4583.7	6612.2	5600	0	2028.49	2.04	1908.06
11	d	SS	1	5	6	4515.6	6687.1	5600	0	2171.43	1.34	2058.06
12	d	SS	2	5	6	4515.6	6687.1	5600	0	2171.43	1.34	2058.06
13	d	SS	3	5	6	4506.2	6686.6	5600	0	2180.47	3.6	2044.43
14	d	SS	4	5	6	4504.9	6705.7	5600	0	2200.79	5.34	2047.38
15	d	SS	5	5	6	4525.5	6676.6	5600	0	2151.12	1.07	2040.38
16	n	SS	1	3	4	4038.6	7180.1	5600	0	3141.52	9.36	3047.96
17	n	SS	2	4	5	4370.4	6830	5600	0	2459.6	0.23	2457.35
18	n	SS	3	4	5	4370.4	6830	5600	0	2459.6	0.23	2457.35
19	n	SS	4	4	5	4370.3	6829.9	5600	0	2459.56	0.12	2458.36
20	n	SS	5	4	5	4369.5	6828.5	5600	0	2459.06	1	2449.02
21	b	CC	1	4	5	4446.8	6757.9	5600	0	2311.11	2.38	2187.34
22	b	CC	2	4	5	4438.5	6774.5	5600	0	2335.94	6.48	2171.1
23	b	CC	3	4	5	4443.1	6762.6	5600	0	2319.57	2.85	2191.11
24	b	CC	4	4	5	4449.4	6751	5600	0	2301.65	0.18	2199.83
25	b	CC	5	4	5	4449.4	6751	5600	0	2301.65	0.18	2199.83
26	c	CC	1	4	5	4490.8	6711.5	5600	0	2220.75	1.13	2109.45
27	c	CC	2	4	5	4439.3	6766.1	5600	0	2326.77	2.73	2199.45
28	c	CC	3	4	5	4453.1	6747.6	5600	0	2294.49	0.32	2191.28
29	c	CC	4	4	5	4444.5	6757	5600	0	2312.49	0.74	2205.04
30	c	CC	5	4	5	4444.5	6757	5600	0	2312.49	0.74	2205.04
31	d	CC	1	4	5	4508.4	6695.4	5600	0	2186.97	1.93	2067.7
32	d	CC	2	4	5	4511.5	6687.6	5600	0	2176.18	0.46	2071.61
33	d	CC	3	4	5	4510.2	6689.2	5600	0	2179.04	0.32	2075.81
34	d	CC	4	4	5	4511.9	6686.4	5600	0	2174.54	0.84	2066.17
35	d	CC	5	4	5	4514.2	6685.3	5600	0	2171.07	0.24	2068.63
36	n	CC	1	3	4	4221.5	6979	5600	0	2757.48	0.22	2755.33
37	n	CC	2	3	4	4221.2	6978.6	5600	0	2757.33	0.1	2756.29
38	n	CC	3	3	4	4221.2	6978.6	5600	0	2757.33	0.1	2756.29
39	n	CC	4	3	4	4221.2	6978.6	5600	0	2757.33	0.1	2756.29
40	n	CC	5	3	4	4221.1	6978.4	5600	0	2757.26	0.23	2754.92
41	b	CF	1	5	6	4447	6750.4	5600	0	2303.4	1.3	2190.38
42	b	CF	2	5	6	4419	6788.8	5600	0	2369.79	3.91	2230.73
43	b	CF	3	5	6	4445.5	6755.3	5600	0	2309.8	0.4	2205.77
44	b	CF	4	5	6	4459.5	6746	5600	0	2286.58	2.75	2159.07
45	b	CF	5	5	6	4459.5	6746	5600	0	2286.58	2.75	2159.07
46	c	CF	1	5	6	4453.2	6750.5	5600	0	2297.32	1.81	2179.2
47	c	CF	2	5	6	4452.9	6755	5600	0	2302.04	3.97	2162.34
48	c	CF	3	5	6	4436.5	6758.7	5600	0	2322.16	2.42	2197.93
49	c	CF	4	5	6	4409.4	6783	5600	0	2373.69	3.8	2235.65
50	c	CF	5	5	6	4425.5	6770.3	5600	0	2344.85	2.12	2223.69
51	d	CF	1	5	6	4504.1	6695.3	5600	0	2191.2	0.31	2088.11
52	d	CF	2	5	6	4514.8	6680.7	5600	0	2165.93	2.26	2043.38
53	d	CF	3	5	6	4507.3	6688.6	5600	0	2181.31	2.06	2060.68
54	d	CF	4	5	6	4509.3	6689.2	5600	0	2179.91	0.79	2071.98
55	d	CF	5	5	6	4509.8	6691	5600	0	2181.19	0.38	2077.4
56	n	CF	1	4	5	4221.5	6979.2	5600	0	2757.7	0.36	2754.06
57	n	CF	2	4	5	4220.6	6977.7	5600	0	2757.1	0.86	2748.45
58	n	CF	3	4	5	4221.5	6979.1	5600	0	2757.67	0.3	2754.71
59	n	CF	4	4	5	4221.4	6979	5600	0	2757.63	0.23	2755.35
60	n	CF	5	4	5	4221.4	6979	5600	0	2757.63	0.23	2755.35
61	b	FC	1	5	6	4435.5	6767.1	5600	0	2331.68	1.29	2218.74
62	b	FC	2	5	6	4428.5	6767.1	5600	0	2338.63	2.19	2216.73
63	b	FC	3	5	6	4428.5	6767.1	5600	0	2338.63	2.19	2216.73
64	b	FC	4	5	6	4428.5	6767.1	5600	0	2338.63	2.19	2216.73
65	b	FC	5	5	6	4428.5	6767.1	5600	0	2338.63	2.19	2216.73
66	c	FC	1	5	6	4416.7	6788.2	5600	0	2371.58	2.45	2247.05
67	c	FC	2	5	6	4412.7	6786.7	5600	0	2373.94	0.32	2270.77
68	c	FC	3	5	6	4435.8	6774.7	5600	0	2338.96	5.24	2186.58
69	c	FC	4	5	6	4434.6	6763.8	5600	0	2329.14	0.8	2221.17
70	c	FC	5	5	6	4434.6	6763.8	5600	0	2329.14	0.8	2221.17
71	d	FC	1	5	6	4474.2	6725.4	5600	0	2251.23	0.23	2148.91
72	d	FC	2	5	6	4489	6712.6	5600	0	2223.58	0.83	2115.31
73	d	FC	3	5	6	4480	6710.7	5600	0	2230.69	4.67	2084.02
74	d	FC	4	5	6	4504.4	6696.4	5600	0	2192.05	0.42	2087.83
75	d	FC	5	5	6	4504.4	6696.4	5600	0	2192.05	0.42	2087.83
76	n	FC	1	4	5	4220.9	6978.5	5600	0	2757.52	0.3	2754.51
77	n	FC	2	4	5	4220.9	6978.4	5600	0	2757.49	0.36	2753.85
78	n	FC	3	4	5	4220.9	6978.4	5600	0	2757.49	0.36	2753.85
79	n	FC	4	4	5	4220.9	6978.4	5600	0	2757.49	0.36	2753.85
80	n	FC	5	4	5	4220.9	6978.4	5600	0	2757.49	0.36	2753.85

Table B.3 - *Optimization results - result group 3*

ITEM	TC	BC	CURVE#	NWC1#	NWC2#	WC1(rd/s)	WC2(rd/s)	Wp(rd/s)	Fx(kN)	dw(rd/s)	wbe(rd/s)	FIT
1	b	SS	1	4	5	4384.1	6820.3	5600	10	2436.15	2.2	2414.19
2	b	SS	2	4	5	4384.1	6820.3	5600	10	2436.15	2.2	2414.19
3	b	SS	3	4	5	4384.1	6820.3	5600	10	2436.15	2.2	2414.19
4	b	SS	4	5	6	4608.2	6598	5600	10	1989.85	3.12	1858.61
5	b	SS	5	4	5	4384.1	6820.3	5600	10	2436.15	2.2	2414.19
6	c	SS	1	4	5	4381.1	6816.4	5600	10	2435.34	1.27	2422.64
7	c	SS	2	4	5	4382	6818.5	5600	10	2436.48	0.23	2434.14
8	c	SS	3	5	6	4592.9	6608.8	5600	10	2015.9	0.83	1907.57
9	c	SS	4	5	6	4592.9	6608.8	5600	10	2015.9	0.83	1907.57
10	c	SS	5	4	5	4381	6824.4	5600	10	2443.35	2.72	2416.16
11	d	SS	1	5	6	4527.5	6664.8	5600	10	2137.27	3.84	1998.87
12	d	SS	2	5	6	4524.9	6675.3	5600	10	2150.43	0.12	2049.2
13	d	SS	3	5	6	4524.9	6675.3	5600	10	2150.43	0.12	2049.2
14	d	SS	4	5	6	4512.3	6677.7	5600	10	2165.32	5.01	2015.24
15	d	SS	5	5	6	4529.5	6673.4	5600	10	2143.88	1.46	2029.23
16	n	SS	1	4	5	4377.4	6821.9	5600	10	2444.46	0.33	2441.12
17	n	SS	2	4	5	4378.4	6823.4	5600	10	2445.01	0.9	2435.98
18	n	SS	3	4	5	4378.2	6823	5600	10	2444.87	0.59	2438.98
19	n	SS	4	4	5	4376.9	6821	5600	10	2444.15	1.04	2433.73
20	n	SS	5	3	4	4040.5	7167.4	5600	10	3126.93	3.97	3087.27
21	b	CC	1	4	5	4460.4	6740.5	5600	10	2280.11	0.42	2175.93
22	b	CC	2	4	5	4449.9	6741.7	5600	10	2291.84	4.22	2149.6
23	b	CC	3	4	5	4449.5	6756.7	5600	10	2307.24	3.13	2175.92
24	b	CC	4	4	5	4433	6764.7	5600	10	2331.71	1.13	2220.44
25	b	CC	5	4	5	4436.2	6765.1	5600	10	2328.88	0.66	2222.28
26	c	CC	1	4	5	4431.5	6759.2	5600	10	2327.67	4.65	2181.17
27	c	CC	2	4	5	4451.9	6750.6	5600	10	2298.65	1.24	2186.21
28	c	CC	3	4	5	4451.9	6750.6	5600	10	2298.65	1.24	2186.21
29	c	CC	4	4	5	4441.5	6766.7	5600	10	2325.19	4.11	2184.08
30	c	CC	5	4	5	4439.6	6764.1	5600	10	2324.52	1.84	2206.15
31	d	CC	1	4	5	4517.6	6682.2	5600	10	2164.59	0.07	2063.88
32	d	CC	2	4	5	4506.4	6698.9	5600	10	2192.47	2.66	2065.84
33	d	CC	3	4	5	4517.6	6682.2	5600	10	2164.59	0.07	2063.88
34	d	CC	4	4	5	4529	6669.7	5600	10	2140.66	0.62	2034.44
35	d	CC	5	4	5	4506.2	6692.9	5600	10	2186.69	0.41	2082.56
36	n	CC	1	3	4	4226.3	6973.7	5600	10	2747.38	0.01	2747.29
37	n	CC	2	3	4	4226.5	6974	5600	10	2747.5	0.26	2744.89
38	n	CC	3	3	4	4226.3	6973.7	5600	10	2747.38	0.01	2747.29
39	n	CC	4	3	4	4226.3	6973.7	5600	10	2747.38	0.01	2747.29
40	n	CC	5	3	4	4226.3	6973.7	5600	10	2747.38	0.01	2747.29
41	b	CF	1	5	6	4484.5	6716.7	5600	10	2232.16	0.61	2126.1
42	b	CF	2	5	6	4484.5	6716.7	5600	10	2232.16	0.61	2126.1
43	b	CF	3	5	6	4484.5	6716.7	5600	10	2232.16	0.61	2126.1
44	b	CF	4	5	6	4495.6	6706.2	5600	10	2210.6	0.92	2101.37
45	b	CF	5	5	6	4482.4	6708.3	5600	10	2225.92	4.62	2079.67
46	c	CF	1	5	6	4464.9	6738.9	5600	10	2274.06	1.88	2155.23
47	c	CF	2	5	6	4459.2	6751.5	5600	10	2292.33	5.32	2139.11
48	c	CF	3	5	6	4510.8	6693.4	5600	10	2182.54	2.09	2061.66
49	c	CF	4	5	6	4464.9	6738.9	5600	10	2274.06	1.88	2155.23
50	c	CF	5	5	6	4488.8	6718.5	5600	10	2229.76	3.64	2093.34
51	d	CF	1	5	6	4523.4	6674.3	5600	10	2150.91	1.14	2039.5
52	d	CF	2	5	6	4544.2	6652.3	5600	10	2108.08	1.74	1990.65
53	d	CF	3	5	6	4549.3	6655.5	5600	10	2106.17	2.37	1982.43
54	d	CF	4	5	6	4532.9	6664	5600	10	2131.13	1.52	2015.95
55	d	CF	5	5	6	4550.9	6649.8	5600	10	2098.9	0.37	1995.25
56	n	CF	1	4	5	4229.4	6970.4	5600	10	2741.04	0.07	2740.33
57	n	CF	2	4	5	4229.4	6970.4	5600	10	2741	0.14	2739.6
58	n	CF	3	4	5	4230	6971.4	5600	10	2741.42	0.7	2734.44
59	n	CF	4	4	5	4229.4	6970.4	5600	10	2741.04	0.07	2740.33
60	n	CF	5	4	5	4229.4	6970.4	5600	10	2741	0.14	2739.6
61	b	FC	1	5	6	4451.6	6747.2	5600	10	2295.53	0.6	2189.5
62	b	FC	2	5	6	4422.1	6773.7	5600	10	2351.61	2.06	2230.99
63	b	FC	3	5	6	4419.3	6780.1	5600	10	2360.83	0.32	2257.59
64	b	FC	4	5	6	4419.3	6780.1	5600	10	2360.83	0.32	2257.59
65	b	FC	5	5	6	4419.3	6780.1	5600	10	2360.83	0.32	2257.59
66	c	FC	1	5	6	4424.3	6774.9	5600	10	2350.52	0.4	2246.57
67	c	FC	2	5	6	4450.1	6754.8	5600	10	2304.69	2.41	2180.62
68	c	FC	3	5	6	4424.3	6774.9	5600	10	2350.52	0.4	2246.57
69	c	FC	4	5	6	4457.4	6740.8	5600	10	2283.4	0.86	2174.82
70	c	FC	5	5	6	4418.4	6770.9	5600	10	2352.48	5.36	2198.89
71	d	FC	1	5	6	4503.2	6697	5600	10	2193.77	0.12	2092.58
72	d	FC	2	5	6	4490.4	6712.2	5600	10	2221.83	1.29	2108.94
73	d	FC	3	5	6	4501.4	6700.3	5600	10	2198.96	0.83	2090.65
74	d	FC	4	5	6	4502.9	6697	5600	10	2194.04	0.05	2093.54
75	d	FC	5	5	6	4502.9	6697	5600	10	2194.04	0.05	2093.54
76	n	FC	1	4	5	4229.4	6970.6	5600	10	2741.22	0.02	2740.97
77	n	FC	2	4	5	4229.4	6970.6	5600	10	2741.19	0.04	2740.82
78	n	FC	3	4	5	4229.4	6970.6	5600	10	2741.19	0.04	2740.82
79	n	FC	4	4	5	4229.4	6970.6	5600	10	2741.22	0.02	2740.97
80	n	FC	5	4	5	4229.3	6970.5	5600	10	2741.15	0.1	2740.13

Table B.4 - *Optimization results - result group 4*

ITEM	TC	BC	CURVE#	NWC1#	NWC2#	WC1(rd/s)	WC2(rd/s)	Wp(rd/s)	Fx(kN)	dw(rd/s)	wbe(rd/s)	FIT
1	b	SS	1	5	6	4570.4	6627.9	5600	0	2057.5	0.89	1948.57
2	b	SS	2	4	5	4341.2	6802.5	5600	0	2461.27	28.17	2079.53
3	b	SS	3	5	6	4567.5	6632.4	5600	0	2064.9	0.02	1964.72
4	b	SS	4	5	6	4575.8	6624.8	5600	0	2048.98	0.32	1945.76
5	b	SS	5	5	6	4573.9	6624.7	5600	0	2050.77	0.73	1943.48
6	c	SS	1	4	5	4364.2	6835.7	5600	0	2471.49	0.01	2371.41
7	c	SS	2	5	6	4569.5	6630.4	5600	0	2060.88	0.02	1960.71
8	c	SS	3	4	5	4364.2	6835.8	5600	0	2471.59	0.01	2371.52
9	c	SS	4	5	6	4578.6	6620.9	5600	0	2042.29	0.28	1939.52
10	c	SS	5	5	6	4573.1	6624	5600	0	2050.92	1.48	1936.13
11	d	SS	1	5	6	4498.8	6701.4	5600	0	2202.64	0.09	2101.75
12	d	SS	2	5	6	4521.2	6678.9	5600	0	2157.66	0.05	2057.2
13	d	SS	3	5	6	4509.8	6689.4	5600	0	2179.51	0.4	2075.49
14	d	SS	4	5	6	4505.2	6696.2	5600	0	2191.03	0.67	2084.35
15	d	SS	5	5	6	4534.9	6665.4	5600	0	2130.54	0.17	2028.89
16	n	SS	1	4	5	4370.3	6829.8	5600	0	2459.51	0.01	2459.43
17	n	SS	2	3	4	4031.9	7168.1	5600	0	3136.28	0	3136.25
18	n	SS	3	3	4	4031.8	7168.1	5600	0	3136.27	0.03	3136
19	n	SS	4	4	5	4370.3	6829.8	5600	0	2459.51	0	2459.47
20	n	SS	5	3	4	4031.9	7168.2	5600	0	3136.29	0.01	3136.18
21	b	CC	1	4	5	4424.8	6775.5	5600	0	2350.7	0.13	2249.39
22	b	CC	2	4	5	4425.5	6774.5	5600	0	2348.93	0.01	2248.8
23	b	CC	3	4	5	4439.5	6760.8	5600	0	2321.28	0.13	2220
24	b	CC	4	4	5	4418.1	6781.7	5600	0	2363.58	0.14	2262.18
25	b	CC	5	4	5	4417.7	6782.1	5600	0	2364.39	0.08	2263.55
26	c	CC	1	4	5	4416.9	6783.2	5600	0	2366.26	0.04	2265.86
27	c	CC	2	4	5	4419.6	6780.8	5600	0	2361.24	0.18	2259.45
28	c	CC	3	4	5	4440.1	6759.8	5600	0	2319.69	0.08	2218.9
29	c	CC	4	4	5	4415.6	6784.3	5600	0	2368.66	0.05	2268.12
30	c	CC	5	4	5	4415.5	6784.4	5600	0	2368.85	0.07	2268.2
31	d	CC	1	4	5	4516.3	6683.7	5600	0	2167.41	0.03	2067.11
32	d	CC	2	4	5	4514	6686.2	5600	0	2172.17	0.08	2071.42
33	d	CC	3	4	5	4519.2	6680.7	5600	0	2161.56	0.05	2061.1
34	d	CC	4	4	5	4515.3	6684.7	5600	0	2169.44	0.03	2069.16
35	d	CC	5	4	5	4511.9	6687.7	5600	0	2175.89	0.2	2073.93
36	n	CC	1	3	4	4221.3	6978.7	5600	0	2757.38	0	2757.37
37	n	CC	2	3	4	4221.3	6978.7	5600	0	2757.38	0.01	2757.3
38	n	CC	3	3	4	4221.3	6978.7	5600	0	2757.38	0	2757.36
39	n	CC	4	3	4	4221.3	6978.7	5600	0	2757.38	0	2757.37
40	n	CC	5	3	4	4221.3	6978.7	5600	0	2757.38	0	2757.36
41	b	CF	1	5	6	4426.6	6773.5	5600	0	2346.84	0.05	2246.36
42	b	CF	2	5	6	4413.5	6786.6	5600	0	2373.04	0.04	2272.63
43	b	CF	3	5	6	4414.1	6786	5600	0	2371.88	0.03	2271.63
44	b	CF	4	5	6	4417.5	6782.4	5600	0	2364.84	0.05	2264.32
45	b	CF	5	5	6	4421.7	6777.4	5600	0	2355.71	0.46	2251.13
46	c	CF	1	5	6	4421.6	6778.3	5600	0	2356.74	0.06	2256.18
47	c	CF	2	5	6	4414.3	6785.8	5600	0	2371.52	0.07	2270.86
48	c	CF	3	5	6	4424	6777.1	5600	0	2353.12	0.56	2247.54
49	c	CF	4	5	6	4412.8	6787.2	5600	0	2374.42	0.03	2274.11
50	c	CF	5	5	6	4469.2	6730.6	5600	0	2261.43	0.11	2160.29
51	d	CF	1	5	6	4512.6	6688.9	5600	0	2176.28	0.77	2068.58
52	d	CF	2	5	6	4515	6684.8	5600	0	2169.74	0.11	2068.61
53	d	CF	3	5	6	4519	6680.5	5600	0	2161.51	0.26	2058.92
54	d	CF	4	5	6	4506.4	6693.6	5600	0	2187.22	0	2087.21
55	d	CF	5	5	6	4509.9	6692.7	5600	0	2182.85	1.29	2069.96
56	n	CF	1	4	5	4221.2	6978.8	5600	0	2757.52	0.01	2757.45
57	n	CF	2	4	5	4221.2	6978.8	5600	0	2757.52	0	2757.48
58	n	CF	3	4	5	4221.2	6978.8	5600	0	2757.52	0	2757.51
59	n	CF	4	4	5	4221.2	6978.7	5600	0	2757.52	0.01	2757.38
60	n	CF	5	4	5	4221.2	6978.8	5600	0	2757.53	0.01	2757.47
61	b	FC	1	5	6	4418.5	6779.6	5600	0	2361.02	0.96	2251.46
62	b	FC	2	5	6	4420	6780	5600	0	2360.01	0	2259.98
63	b	FC	3	5	6	4403	6796.9	5600	0	2393.94	0.04	2293.58
64	b	FC	4	5	6	4403	6796.6	5600	0	2393.63	0.2	2291.64
65	b	FC	5	5	6	4405.5	6795.4	5600	0	2389.82	0.44	2285.38
66	c	FC	1	5	6	4402.3	6797.8	5600	0	2395.5	0.01	2295.36
67	c	FC	2	5	6	4404.5	6795.3	5600	0	2390.74	0.08	2289.89
68	c	FC	3	5	6	4408.1	6792.7	5600	0	2384.55	0.4	2280.58
69	c	FC	4	5	6	4405.4	6793.6	5600	0	2388.11	0.5	2283.12
70	c	FC	5	5	6	4402.5	6797.6	5600	0	2395.07	0.02	2294.83
71	d	FC	1	5	6	4481.1	6718.9	5600	0	2237.74	0.01	2137.6
72	d	FC	2	5	6	4479.6	6720.5	5600	0	2240.91	0.02	2140.75
73	d	FC	3	5	6	4481.4	6718.4	5600	0	2236.95	0.1	2135.99
74	d	FC	4	5	6	4480.1	6720	5600	0	2239.96	0.04	2139.57
75	d	FC	5	5	6	4482	6718	5600	0	2236.08	0	2136.05
76	n	FC	1	4	5	4221.2	6978.8	5600	0	2757.67	0.01	2757.61
77	n	FC	2	4	5	4221.2	6978.8	5600	0	2757.67	0	2757.63
78	n	FC	3	4	5	4221.2	6978.8	5600	0	2757.67	0	2757.65
79	n	FC	4	4	5	4221.2	6978.8	5600	0	2757.67	0	2757.64
80	n	FC	5	4	5	4221.2	6978.8	5600	0	2757.67	0	2757.65

Table B.5 - *Optimization results - result group 5*

ITEM	TC	BC	CURVE#	NWC1#	NWC2#	WC1(rd/s)	WC2(rd/s)	Wp(rd/s)	Fx(kN)	dw(rd/s)	wbe(rd/s)	FIT
1	b	SS	1	4	5	4379.7	6820.1	5600	10	2440.41	0.11	2339.32
2	b	SS	2	4	5	4379.6	6820.3	5600	10	2440.73	0.02	2340.5
3	b	SS	3	4	5	4379.9	6820.1	5600	10	2440.17	0.01	2340.11
4	b	SS	4	4	5	4379.8	6820.3	5600	10	2440.49	0.09	2339.6
5	b	SS	5	4	5	4380.5	6819.6	5600	10	2439.09	0.02	2338.94
6	c	SS	1	5	6	4595.3	6605.3	5600	10	2010	0.28	1907.25
7	c	SS	2	4	5	4381.9	6818	5600	10	2436.14	0.03	2335.85
8	c	SS	3	4	5	4381.7	6818.4	5600	10	2436.69	0	2336.66
9	c	SS	4	4	5	4380.7	6819.2	5600	10	2438.52	0.07	2337.85
10	c	SS	5	4	5	4381.1	6819.2	5600	10	2438.05	0.13	2336.71
11	d	SS	1	5	6	4515.9	6684.2	5600	10	2168.35	0.05	2067.8
12	d	SS	2	5	6	4522.3	6678.2	5600	10	2155.93	0.24	2053.56
13	d	SS	3	5	6	4549	6651.3	5600	10	2102.33	0.13	2001.06
14	d	SS	4	5	6	4522.6	6678	5600	10	2155.38	0.29	2052.52
15	d	SS	5	5	6	4532.6	6667.5	5600	10	2134.97	0.05	2034.42
16	n	SS	1	3	4	4037.6	7162.3	5600	10	3124.7	0	3124.68
17	n	SS	2	3	4	4037.6	7162.3	5600	10	3124.7	0	3124.68
18	n	SS	3	3	4	4037.6	7162.3	5600	10	3124.7	0.01	3124.58
19	n	SS	4	4	5	4377.7	6822.3	5600	10	2444.61	0.01	2444.56
20	n	SS	5	3	4	4037.7	7162.4	5600	10	3124.71	0	3124.66
21	b	CC	1	4	5	4433.8	6766.1	5600	10	2332.3	0.01	2232.2
22	b	CC	2	4	5	4434.5	6765.3	5600	10	2330.79	0.11	2229.73
23	b	CC	3	4	5	4436.5	6763.8	5600	10	2327.25	0.16	2225.62
24	b	CC	4	4	5	4436.9	6763.4	5600	10	2326.53	0.19	2224.68
25	b	CC	5	4	5	4434.4	6766.2	5600	10	2331.85	0.32	2228.67
26	c	CC	1	4	5	4434.8	6765.7	5600	10	2330.92	0.24	2228.5
27	c	CC	2	4	5	4434.3	6766.4	5600	10	2332.15	0.35	2228.7
28	c	CC	3	4	5	4436.5	6763.6	5600	10	2327.1	0	2227.06
29	c	CC	4	4	5	4435	6765.1	5600	10	2330.09	0.03	2229.81
30	c	CC	5	4	5	4435.3	6765.1	5600	10	2329.83	0.17	2228.14
31	d	CC	1	4	5	4524.6	6675.4	5600	10	2150.85	0.02	2050.63
32	d	CC	2	4	5	4531	6669.7	5600	10	2138.62	0.36	2035.04
33	d	CC	3	4	5	4523.5	6676.8	5600	10	2153.24	0.15	2051.75
34	d	CC	4	4	5	4530.2	6670.4	5600	10	2140.16	0.29	2037.3
35	d	CC	5	4	5	4526.3	6675.9	5600	10	2149.63	1.11	2038.53
36	n	CC	1	3	4	4226.3	6973.7	5600	10	2747.37	0	2747.35
37	n	CC	2	3	4	4226.3	6973.7	5600	10	2747.37	0	2747.34
38	n	CC	3	3	4	4226.3	6973.7	5600	10	2747.37	0.01	2747.31
39	n	CC	4	3	4	4226.3	6973.7	5600	10	2747.37	0	2747.37
40	n	CC	5	3	4	4226.3	6973.7	5600	10	2747.37	0.01	2747.32
41	b	CF	1	5	6	4454	6745.5	5600	10	2291.46	0.28	2188.7
42	b	CF	2	5	6	4457.4	6743.3	5600	10	2285.94	0.33	2182.67
43	b	CF	3	5	6	4454.7	6745.5	5600	10	2290.78	0.07	2190.12
44	b	CF	4	5	6	4455.5	6744.5	5600	10	2288.93	0.01	2188.81
45	b	CF	5	5	6	4454.4	6745.9	5600	10	2291.45	0.17	2189.76
46	c	CF	1	5	6	4456	6744	5600	10	2288.05	0.01	2187.99
47	c	CF	2	5	6	4454.5	6744.5	5600	10	2290.02	0.48	2185.24
48	c	CF	3	5	6	4454.5	6745.4	5600	10	2290.92	0.07	2190.19
49	c	CF	4	5	6	4456.2	6744	5600	10	2287.79	0.09	2186.84
50	c	CF	5	5	6	4454.8	6745.1	5600	10	2290.26	0.06	2189.62
51	d	CF	1	5	6	4545.8	6654.2	5600	10	2108.4	0.05	2007.93
52	d	CF	2	5	6	4533.9	6664.5	5600	10	2130.6	0.76	2022.97
53	d	CF	3	5	6	4536.7	6666.8	5600	10	2130.09	1.77	2012.43
54	d	CF	4	5	6	4542.9	6657.2	5600	10	2114.34	0.05	2013.82
55	d	CF	5	5	6	4545.2	6656.1	5600	10	2110.91	0.66	2004.34
56	n	CF	1	4	5	4229.5	6970.6	5600	10	2741.08	0.01	2740.93
57	n	CF	2	4	5	4229.5	6970.5	5600	10	2741.08	0.01	2740.99
58	n	CF	3	4	5	4229.4	6970.5	5600	10	2741.06	0.03	2740.78
59	n	CF	4	4	5	4229.5	6970.5	5600	10	2741.07	0.01	2741
60	n	CF	5	4	5	4229.5	6970.5	5600	10	2741.07	0	2741.02
61	b	FC	1	5	6	4422.4	6777.4	5600	10	2354.93	0.09	2254.03
62	b	FC	2	5	6	4444.4	6758.9	5600	10	2314.46	1.68	2197.68
63	b	FC	3	5	6	4421	6779.3	5600	10	2358.37	0.15	2256.82
64	b	FC	4	5	6	4421	6778	5600	10	2357.07	0.51	2251.98
65	b	FC	5	5	6	4421.7	6778.6	5600	10	2356.86	0.14	2255.5
66	c	FC	1	5	6	4426.7	6772.9	5600	10	2346.19	0.24	2243.77
67	c	FC	2	5	6	4427.3	6773	5600	10	2345.68	0.14	2244.33
68	c	FC	3	5	6	4427.3	6772.2	5600	10	2344.97	0.26	2242.39
69	c	FC	4	5	6	4423.4	6776.7	5600	10	2353.3	0.02	2253.13
70	c	FC	5	5	6	4428.6	6770.7	5600	10	2342.14	0.37	2238.49
71	d	FC	1	5	6	4497.1	6702.9	5600	10	2205.79	0.01	2105.65
72	d	FC	2	5	6	4497.1	6702.5	5600	10	2205.36	0.19	2103.48
73	d	FC	3	5	6	4498.7	6701.3	5600	10	2202.6	0	2102.6
74	d	FC	4	5	6	4495.9	6704.1	5600	10	2208.2	0.03	2107.94
75	d	FC	5	5	6	4498.3	6701.8	5600	10	2203.49	0.03	2103.23
76	n	FC	1	4	5	4229.4	6970.6	5600	10	2741.2	0	2741.16
77	n	FC	2	4	5	4229.4	6970.6	5600	10	2741.21	0.02	2741.01
78	n	FC	3	4	5	4229.4	6970.6	5600	10	2741.2	0.01	2741.13
79	n	FC	4	4	5	4229.4	6970.6	5600	10	2741.2	0	2741.19
80	n	FC	5	4	5	4229.4	6970.6	5600	10	2741.21	0	2741.16

Table B.6 - *Optimization results - result group 6*

ITEM	TC	BC	CURVE#	NWC1#	NWC2#	WC1(rd/s)	WC2(rd/s)	Wp(rd/s)	Fx(kN)	dw(rd/s)	wbe(rd/s)	FIT
1	b	SS	1	4	5	4343.7	6806.3	5600	0	2462.62	25.02	2112.47
2	b	SS	2	4	5	4343.7	6806.3	5600	0	2462.62	25.02	2112.47
3	b	SS	3	5	6	4589.1	6618.7	5600	0	2029.67	3.9	1890.69
4	b	SS	4	4	5	4343.7	6806.3	5600	0	2462.62	25.02	2112.47
5	b	SS	5	5	6	4589.1	6618.7	5600	0	2029.67	3.9	1890.69
6	c	SS	1	4	5	4367	6841	5600	0	2473.94	4.01	2333.82
7	c	SS	2	5	6	4587.4	6620.2	5600	0	2032.83	3.79	1894.96
8	c	SS	3	4	5	4367	6841	5600	0	2473.94	4.01	2333.82
9	c	SS	4	4	5	4367	6841	5600	0	2473.94	4.01	2333.82
10	c	SS	5	4	5	4367	6841	5600	0	2473.94	4.01	2333.82
11	d	SS	1	5	6	4515.6	6687.1	5600	0	2171.43	1.34	2058.06
12	d	SS	2	5	6	4515.6	6687.1	5600	0	2171.43	1.34	2058.06
13	d	SS	3	5	6	4515.6	6687.1	5600	0	2171.43	1.34	2058.06
14	d	SS	4	5	6	4515.6	6687.1	5600	0	2171.43	1.34	2058.06
15	d	SS	5	5	6	4515.6	6687.1	5600	0	2171.43	1.34	2058.06
16	n	SS	1	3	4	4043.2	7188.3	5600	0	3145.1	15.74	2987.65
17	n	SS	2	3	4	4043.2	7188.3	5600	0	3145.1	15.74	2987.65
18	n	SS	3	3	4	4043.2	7188.3	5600	0	3145.1	15.74	2987.65
19	n	SS	4	3	4	4043.2	7188.3	5600	0	3145.1	15.74	2987.65
20	n	SS	5	4	5	4366.4	6823.8	5600	0	2457.35	4.9	2408.37
21	b	CC	1	4	5	4492.6	6715	5600	0	2222.42	3.8	2084.4
22	b	CC	2	4	5	4412.5	6780	5600	0	2367.48	3.77	2229.8
23	b	CC	3	4	5	4481.4	6726.4	5600	0	2245.05	3.89	2106.13
24	b	CC	4	4	5	4492.6	6715	5600	0	2222.42	3.8	2084.4
25	b	CC	5	4	5	4492.6	6715	5600	0	2222.42	3.8	2084.4
26	c	CC	1	4	5	4418.1	6788.8	5600	0	2370.68	3.45	2236.21
27	c	CC	2	4	5	4449.1	6758.1	5600	0	2309.04	3.62	2172.82
28	c	CC	3	4	5	4449.1	6758.1	5600	0	2309.04	3.62	2172.82
29	c	CC	4	4	5	4449.1	6758.1	5600	0	2309.04	3.62	2172.82
30	c	CC	5	4	5	4418.1	6788.8	5600	0	2370.68	3.45	2236.21
31	d	CC	1	4	5	4512.9	6697.7	5600	0	2184.8	5.33	2031.54
32	d	CC	2	4	5	4512.9	6697.7	5600	0	2184.8	5.33	2031.54
33	d	CC	3	4	5	4514.2	6685.3	5600	0	2171.07	0.24	2068.63
34	d	CC	4	4	5	4523	6694.7	5600	0	2171.71	8.88	1982.9
35	d	CC	5	5	6	4579.4	6632.1	5600	0	2052.74	5.75	1895.29
36	n	CC	1	3	4	4224.7	6984.3	5600	0	2759.61	4.54	2714.25
37	n	CC	2	3	4	4224.7	6984.3	5600	0	2759.61	4.54	2714.25
38	n	CC	3	3	4	4224.7	6984.3	5600	0	2759.61	4.54	2714.25
39	n	CC	4	3	4	4224.7	6984.3	5600	0	2759.61	4.54	2714.25
40	n	CC	5	3	4	4224.7	6984.3	5600	0	2759.61	4.54	2714.25
41	b	CF	1	5	6	4459.5	6746	5600	0	2286.58	2.75	2159.07
42	b	CF	2	5	6	4459.5	6746	5600	0	2286.58	2.75	2159.07
43	b	CF	3	5	6	4410	6782.2	5600	0	2372.22	3.91	2233.13
44	b	CF	4	5	6	4463.4	6744.8	5600	0	2281.32	4.1	2140.34
45	b	CF	5	5	6	4463.4	6744.8	5600	0	2281.32	4.1	2140.34
46	c	CF	1	5	6	4444.1	6740.9	5600	0	2296.81	7.47	2122.11
47	c	CF	2	5	6	4444.1	6740.9	5600	0	2296.81	7.47	2122.11
48	c	CF	3	5	6	4461.8	6748.6	5600	0	2286.76	5.23	2134.48
49	c	CF	4	5	6	4409.4	6783	5600	0	2373.69	3.8	2235.65
50	c	CF	5	5	6	4444.1	6740.9	5600	0	2296.81	7.47	2122.11
51	d	CF	1	5	6	4517.8	6681.9	5600	0	2164.1	0.15	2062.62
52	d	CF	2	5	6	4517.8	6681.9	5600	0	2164.1	0.15	2062.62
53	d	CF	3	5	6	4517.8	6681.9	5600	0	2164.1	0.15	2062.62
54	d	CF	4	5	6	4517.8	6681.9	5600	0	2164.1	0.15	2062.62
55	d	CF	5	5	6	4522.8	6673.5	5600	0	2150.76	1.84	2032.39
56	n	CF	1	4	5	4221.5	6979.2	5600	0	2757.7	0.36	2754.06
57	n	CF	2	4	5	4221.5	6979.2	5600	0	2757.7	0.36	2754.06
58	n	CF	3	4	5	4221.5	6979.2	5600	0	2757.7	0.36	2754.06
59	n	CF	4	4	5	4221.5	6979.2	5600	0	2757.7	0.36	2754.06
60	n	CF	5	4	5	4221.5	6979.2	5600	0	2757.7	0.36	2754.06
61	b	FC	1	5	6	4388.3	6789.8	5600	0	2401.48	10.99	2191.62
62	b	FC	2	5	6	4467.7	6730.8	5600	0	2263.02	0.75	2155.48
63	b	FC	3	5	6	4388.3	6789.8	5600	0	2401.48	10.99	2191.62
64	b	FC	4	5	6	4467.7	6730.8	5600	0	2263.02	0.75	2155.48
65	b	FC	5	5	6	4479.9	6715.8	5600	0	2235.91	2.14	2114.52
66	c	FC	1	5	6	4392.6	6783.9	5600	0	2391.36	11.77	2173.69
67	c	FC	2	5	6	4392.6	6783.9	5600	0	2391.36	11.77	2173.69
68	c	FC	3	5	6	4436.4	6750	5600	0	2313.62	6.77	2145.95
69	c	FC	4	5	6	4392.6	6783.9	5600	0	2391.36	11.77	2173.69
70	c	FC	5	5	6	4392.6	6783.9	5600	0	2391.36	11.77	2173.69
71	d	FC	1	5	6	4491	6726.6	5600	0	2235.59	8.8	2047.57
72	d	FC	2	5	6	4514.5	6737.1	5600	0	2222.59	25.79	1864.73
73	d	FC	3	5	6	4498.3	6737.9	5600	0	2239.56	18.1	1958.56
74	d	FC	4	5	6	4466.1	6720.1	5600	0	2253.99	6.94	2084.55
75	d	FC	5	5	6	4475.4	6703.6	5600	0	2228.17	10.53	2022.91
76	n	FC	1	4	5	4218.6	6974.6	5600	0	2756	3.39	2722.05
77	n	FC	2	4	5	4218.6	6974.6	5600	0	2756	3.39	2722.05
78	n	FC	3	4	5	4227	6988.4	5600	0	2761.46	7.7	2684.48
79	n	FC	4	4	5	4218.6	6974.6	5600	0	2756	3.39	2722.05
80	n	FC	5	4	5	4215.2	6968.9	5600	0	2753.74	7.98	2673.94

Table B.7 - *Optimization results - result group 7*

ITEM	TC	BC	CURVE#	NWC1#	NWC2#	WC1(rd/s)	WC2(rd/s)	Wp(rd/s)	Fx(kN)	dw(rd/s)	wbe(rd/s)	FIT
1	b	SS	1	4	5	4384.1	6820.3	5600	10	2436.15	2.2	2314.19
2	b	SS	2	4	5	4384.1	6820.3	5600	10	2436.15	2.2	2314.19
3	b	SS	3	4	5	4384.1	6820.3	5600	10	2436.15	2.2	2314.19
4	b	SS	4	4	5	4384.1	6820.3	5600	10	2436.15	2.2	2314.19
5	b	SS	5	5	6	4582.6	6600	5600	10	2017.37	8.7	1830.33
6	c	SS	1	4	5	4379	6813.7	5600	10	2434.64	3.66	2298.06
7	c	SS	2	5	6	4626.1	6573.9	5600	10	1947.81	0.05	1847.35
8	c	SS	3	4	5	4381	6824.4	5600	10	2443.35	2.72	2316.16
9	c	SS	4	4	5	4379	6813.7	5600	10	2434.64	3.66	2298.06
10	c	SS	5	4	5	4379	6813.7	5600	10	2434.64	3.66	2298.06
11	d	SS	1	5	6	4540.3	6661.6	5600	10	2121.35	0.96	2011.75
12	d	SS	2	5	6	4540.3	6661.6	5600	10	2121.35	0.96	2011.75
13	d	SS	3	5	6	4540.3	6661.6	5600	10	2121.35	0.96	2011.75
14	d	SS	4	5	6	4540.3	6661.6	5600	10	2121.35	0.96	2011.75
15	d	SS	5	5	6	4540.3	6661.6	5600	10	2121.35	0.96	2011.75
16	n	SS	1	3	4	4043.1	7172.1	5600	10	3128.97	7.58	3053.13
17	n	SS	2	3	4	4043.1	7172.1	5600	10	3128.97	7.58	3053.13
18	n	SS	3	3	4	4043.1	7172.1	5600	10	3128.97	7.58	3053.13
19	n	SS	4	3	4	4043.1	7172.1	5600	10	3128.97	7.58	3053.13
20	n	SS	5	3	4	4043.1	7172.1	5600	10	3128.97	7.58	3053.13
21	b	CC	1	4	5	4436.2	6765.1	5600	10	2328.88	0.66	2222.28
22	b	CC	2	4	5	4436.2	6765.1	5600	10	2328.88	0.66	2222.28
23	b	CC	3	4	5	4436.2	6765.1	5600	10	2328.88	0.66	2222.28
24	b	CC	4	4	5	4463.2	6731.9	5600	10	2268.64	2.45	2144.1
25	b	CC	5	4	5	4436.2	6765.1	5600	10	2328.88	0.66	2222.28
26	c	CC	1	4	5	4441.1	6773.3	5600	10	2332.13	7.2	2160.12
27	c	CC	2	4	5	4441.1	6773.3	5600	10	2332.13	7.2	2160.12
28	c	CC	3	4	5	4441.1	6773.3	5600	10	2332.13	7.2	2160.12
29	c	CC	4	4	5	4441.5	6766.7	5600	10	2325.19	4.11	2184.08
30	c	CC	5	4	5	4441.1	6773.3	5600	10	2332.13	7.2	2160.12
31	d	CC	1	4	5	4527.5	6676.9	5600	10	2149.35	2.21	2027.23
32	d	CC	2	4	5	4527.5	6676.9	5600	10	2149.35	2.21	2027.23
33	d	CC	3	4	5	4527.5	6676.9	5600	10	2149.35	2.21	2027.23
34	d	CC	4	4	5	4527.5	6676.9	5600	10	2149.35	2.21	2027.23
35	d	CC	5	4	5	4527.5	6676.9	5600	10	2149.35	2.21	2027.23
36	n	CC	1	3	4	4225.7	6972.7	5600	10	2746.99	0.76	2739.36
37	n	CC	2	3	4	4225.7	6972.7	5600	10	2746.99	0.76	2739.36
38	n	CC	3	3	4	4225.7	6972.7	5600	10	2746.99	0.76	2739.36
39	n	CC	4	3	4	4225.7	6972.7	5600	10	2746.99	0.76	2739.36
40	n	CC	5	3	4	4225.7	6972.7	5600	10	2746.99	0.76	2739.36
41	b	CF	1	5	6	4517.8	6682	5600	10	2164.12	0.1	2063.11
42	b	CF	2	5	6	4470.4	6743.5	5600	10	2273.16	6.95	2103.63
43	b	CF	3	5	6	4517.8	6682	5600	10	2164.12	0.1	2063.11
44	b	CF	4	5	6	4470.4	6743.5	5600	10	2273.16	6.95	2103.63
45	b	CF	5	5	6	4516.6	6696.3	5600	10	2179.71	6.46	2015.15
46	c	CF	1	5	6	4466.8	6741.4	5600	10	2274.63	4.07	2133.92
47	c	CF	2	5	6	4516.4	6682.8	5600	10	2166.34	0.38	2062.52
48	c	CF	3	5	6	4516.4	6682.8	5600	10	2166.34	0.38	2062.52
49	c	CF	4	5	6	4516.4	6682.8	5600	10	2166.34	0.38	2062.52
50	c	CF	5	5	6	4516.4	6682.8	5600	10	2166.34	0.38	2062.52
51	d	CF	1	5	6	4558.8	6632.5	5600	10	2073.67	4.38	1929.85
52	d	CF	2	5	6	4558.8	6632.5	5600	10	2073.67	4.38	1929.85
53	d	CF	3	5	6	4558.8	6632.5	5600	10	2073.67	4.38	1929.85
54	d	CF	4	5	6	4558.8	6632.5	5600	10	2073.67	4.38	1929.85
55	d	CF	5	5	6	4558.8	6632.5	5600	10	2073.67	4.38	1929.85
56	n	CF	1	4	5	4210.9	6939.8	5600	10	2728.87	24.63	2482.6
57	n	CF	2	4	5	4231.2	6973.3	5600	10	2742.18	2.24	2719.73
58	n	CF	3	4	5	4231.2	6973.3	5600	10	2742.18	2.24	2719.73
59	n	CF	4	4	5	4231.2	6973.3	5600	10	2742.18	2.24	2719.73
60	n	CF	5	4	5	4231.2	6973.3	5600	10	2742.18	2.24	2719.73
61	b	FC	1	5	6	4419.9	6771.6	5600	10	2351.7	4.29	2208.8
62	b	FC	2	5	6	4460.9	6742.4	5600	10	2281.48	1.62	2165.27
63	b	FC	3	5	6	4460.9	6742.4	5600	10	2281.48	1.62	2165.27
64	b	FC	4	5	6	4419.9	6771.6	5600	10	2351.7	4.29	2208.8
65	b	FC	5	5	6	4419.9	6771.6	5600	10	2351.7	4.29	2208.8
66	c	FC	1	5	6	4434.7	6790	5600	10	2355.28	12.39	2131.39
67	c	FC	2	5	6	4434.7	6790	5600	10	2355.28	12.39	2131.39
68	c	FC	3	5	6	4423.4	6767.1	5600	10	2343.75	4.73	2196.46
69	c	FC	4	5	6	4454.8	6758.3	5600	10	2303.51	6.56	2137.93
70	c	FC	5	5	6	4434.7	6790	5600	10	2355.28	12.39	2131.39
71	d	FC	1	5	6	4476.7	6679.5	5600	10	2202.73	21.89	1883.83
72	d	FC	2	5	6	4476.7	6679.5	5600	10	2202.73	21.89	1883.83
73	d	FC	3	5	6	4502.9	6697	5600	10	2194.04	0.05	2093.54
74	d	FC	4	5	6	4476.7	6679.5	5600	10	2202.73	21.89	1883.83
75	d	FC	5	5	6	4502.9	6697	5600	10	2194.04	0.05	2093.54
76	n	FC	1	4	5	4229.4	6970.6	5600	10	2741.19	0.04	2740.82
77	n	FC	2	4	5	4229.4	6970.6	5600	10	2741.19	0.04	2740.82
78	n	FC	3	4	5	4225.9	6964.8	5600	10	2738.92	4.62	2692.73
79	n	FC	4	4	5	4229.4	6970.6	5600	10	2741.19	0.04	2740.82
80	n	FC	5	4	5	4229.4	6970.6	5600	10	2741.19	0.04	2740.82

Table B.8 - *Optimization results - result group 8*

Appendix C – Detailed D_{ij} formulation for tapered laminates

The detailed formulation of the bending stiffness coefficient D_{ij} is presented for tapered laminates for the three main taper configurations: B, C and D. The D_{ij} coefficient is evaluated for a tapered laminate, with non-symmetric geometry with the horizontal plane, as displayed at figures C.1, C.2 and C.3. For tapered laminates with symmetry to the horizontal plane, the D_{ij} value must be doubled.

In order to define the taper slope, the total height variation due to the taper is defined as ΔH_T following the equation:

$$\Delta H_T = (m - n)t \tag{C.1}$$

Where m is the number of plies in the higher thickness, n is the number of plies in the lower thickness, and t is the total height of each ply thickness. With this the taper slope M can be defined as,

$$M = \frac{-|\Delta H_T|}{L} \tag{C.2}$$

C.1. Detailed $D_{ij}(x)$ formulation for taper configuration B

For the taper configuration B, the formulation is presented.

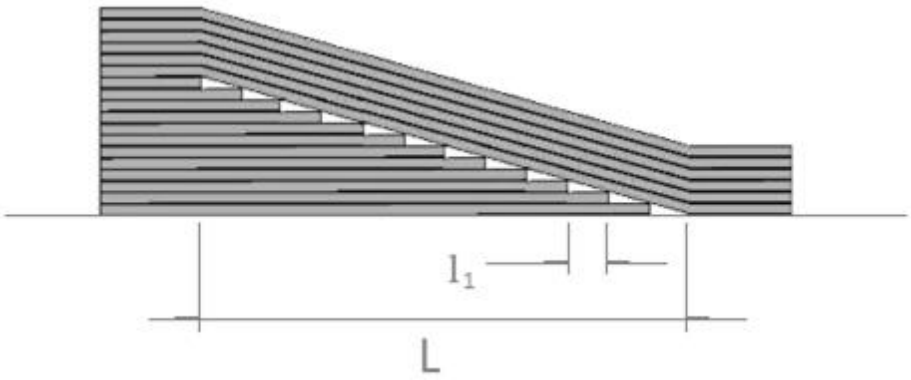

Figure C.1 – *Taper configuration B with dimensions*

The value L represents the total length of the tapered section of the laminate, to which the bending stiffness coefficient is calculated. The value l_1 defines the length of a single resin pocket in the taper configuration B and C. The coefficient $D_{ij}(x)$ for the tapered laminate with configuration B can be defined as the summation of three components, as given by equation C.3,

$$D_{ij}(x) = D_{m_{ij}}(x) + D_{u_{ij}}(x) + D_r\,(x) \tag{C.3}$$

Where $D_{m_{ij}}(x)$ stands for the component related to the external oblique plies, $D_{u_{ij}}(x)$ represents the contribution of the segmented horizontal plies and $D_r(x)$ defines the contribution of the resin pocked in the bending stiffness coefficient, along the x axis. The contribution of the external oblique plies is calculated by the equation C.4,

$$D_{m_{ij}}(x) = \sum_{k=n-m+1}^{n} [(Mx + kt)^3 - (Mx + (k-1)t)^3] \frac{\bar{Q}_{ij}}{3} \tag{C.4}$$

The contribution of internal segmented plies can be defined as equation C.5,

$$D_{u_{ij}}(x) = \sum_{s=1}^{n-m-1} f_1(x) * f_2(x) \tag{C.5}$$

Where f_1 and f_2 are calculated following the formulation,

$$f_1(x) = \begin{cases} 1, & if\ \{x \leq sl_1\ \ and\ \ x > (s-1)l_1\} \\ 0, & if\ \{x > sl_1\ \ or\ \ x \leq (s-1)l_1\} \end{cases} \tag{C.6}$$

$$f_2(x) = \sum_{i=1}^{n-m-s} [(it)^3 - \big((i-1)t\big)^3] \frac{\bar{Q}_{ij}}{3} \tag{C.7}$$

The contribution of the resin pockets to the bending stiffness is given by the equation (C.8),

$$D_r(x) = \sum_{s=1}^{n-m} f_1(x) * f_3(x) \tag{C.8}$$

Where the value of $f_3(x)$ is defined as,

$$f_3(x) = [(Mx + (n-m)t)^3 - \big((n-m-s)t\big)^3] \frac{Q_{r_{ij}}}{3} \tag{C.9}$$

With this, the D_{ij} coefficient is defined for the taper configuration B along the x axis.

C.2. Detailed $D_{ij}(x)$ formulation for taper configuration C

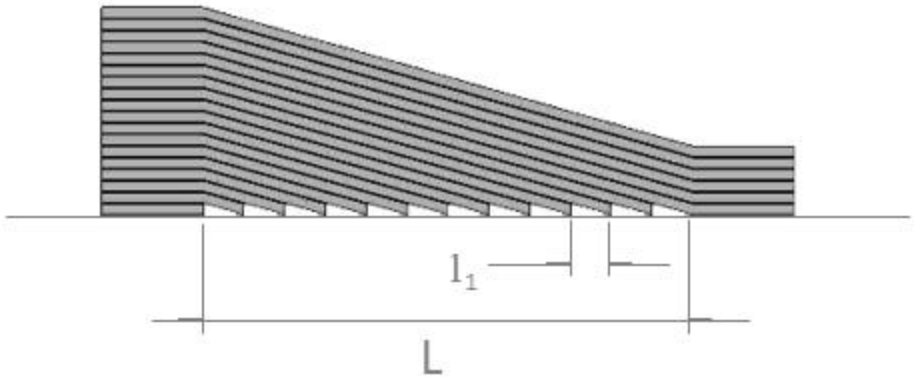

Figure C.2 – *Taper configuration C with dimensions*

The bending stiffness coefficient along the taper configuration C is defined by two components:

$$D_{ij}(x) = D_{m_{ij}}(x) + D_r\,(x) \tag{C.10}$$

Where $D_{m_{ij}}(x)$ represents the components related to the oblique plies, and $D_r(x)$ represents the contribution of the resin pockets. The oblique plies contribution can be calculated for each resin pocket section along the horizontal axis, following the equation (C.11),

$$D_{m_{ij}}(x) = \sum_{s=1}^{n-m} f_1(x) * f_4(x) \tag{C.11}$$

At figure C.2, l_1 represents the total length of a single resin pocket. The value of the $f_4(x)$ function is defined by equation (C.12),

$$f_4(x) = \sum_{k=s+1}^{n} [(Mx + kt)^3 - (Mx + (k-1)t)^3] \frac{\bar{Q}_{ij}}{3} \tag{C.12}$$

The contribution of the resin pocket in the bending stiffness coefficient of the taper configuration C can be calculated as by equation (C.13),

$$D_r(x) = \sum_{s=1}^{n-m} f_1(x) * f_5(x) \tag{C.13}$$

Where the coefficient f_5 is defined along the x axis as,

$$f_5(x) = (Mx + st)^3 \frac{Q_{r_{ij}}}{3} \tag{C.14}$$

C.3. Detailed $D_{ij}(x)$ formulation for taper configuration D

Due to the complexity of the formulation for taper configuration D, it will is given to the particular case of the taper with three resin pockets, where m assumes the value of 18 and n the value of 12 ply layers, and $l_2 = L/3$.

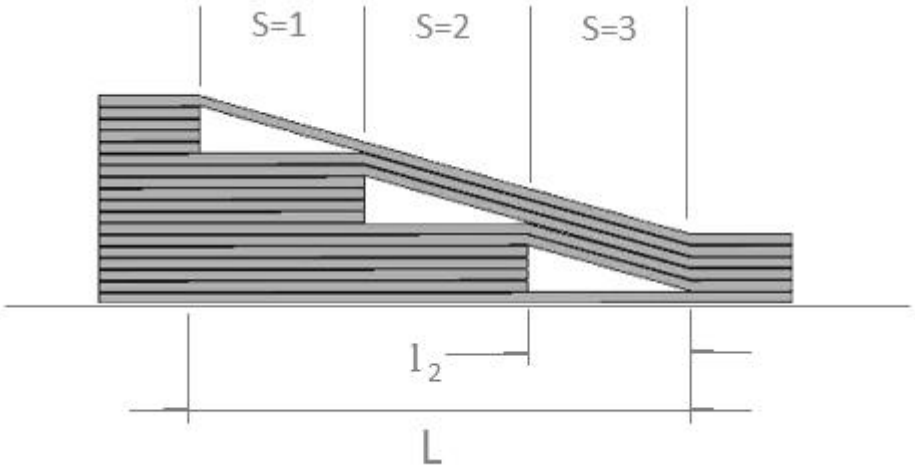

Figure C.3 – *Taper configuration D with dimensions*

The $D_{ij}(x)$ coefficient also is the result of three components, defined by:

$$D_{ij}(x) = D_{m_{ij}}(x) + D_{u_{ij}}(x) + D_r\,(x) \tag{C.15}$$

The contribution of the external oblique plies of the laminate $D_{m_{ij}}$ to the D_{ij} coefficient along the x axis is evaluated following the equation,

$$D_{m_{ij}}(x) = \sum_{s=1}^{3} f_6(x) * f_7(x) \tag{C.16}$$

Where the values of $f_6(x)$ and $f_7(x)$ are defined by,

$$f_6(x) = \begin{cases} 1, & if\ \{x \leq s(L/3)\ \ and\ \ x > (s-1)(L/3)\} \\ 0, & if\ \{x > s(L/3) \quad or\ \ x \leq (s-1)(L/3)\} \end{cases} \tag{C.17}$$

The function $f_7(x)$ can be defined as,

$$f_7(x) = \sum_{k=n-2(s-1)}^{n} [(Mx + kt)^3 - (Mx + (k-1)t)^3] \frac{\bar{Q}_{ij}}{3} \tag{C.18}$$

The contribution of the second component $D_{u_{ij}}(x)$, related to the segmented plies, is defined by the equation,

$$D_{u_{ij}}(x) = \sum_{s=1}^{3} f_6(x) * f_8(x) \tag{C.19}$$

Where the coefficient $f_8(x)$ can be calculated as,

$$f_8(x) = \sum_{i=1}^{n-6s+1} \left[(it)^3 - \left((i-1)t\right)^3\right] \frac{\bar{Q}_{ij}}{3} \tag{C.20}$$

The third component on the $D_{ij}(x)$ coefficient, related to the resin pocket, is defined by equation (C.21),

$$D_r(x) = \sum_{s=1}^{3} f_6(x) * f_9(x) \tag{C.21}$$

Where the value of $f_9(x)$ can be defined as,

$$f_9(x) = \sum_{z=n-2(s-1)-4}^{n-2(s-1)-1} [{R_1}^3 - {R_2}^3] \frac{Q_{r_{ij}}}{3} \tag{C.22}$$

Where the coefficients R_1 and R_2 can be calculated from P_0, P_1 and P_2, following,

$$\begin{cases} P_0 = (n - 6s + 1)t \\ P_1 = Mx + zt \\ P_2 = Mx + (z-1)t \end{cases} \tag{C.23}$$

From these equations, R_1 and R_2 are defined following equation (C.24),

$$\begin{cases} if\ P_1 - P_0 \leq 0, R_1 = P_0 \\ if\ P_1 - P_0 > 0, R_1 = P_1 \end{cases} \quad \text{(C.24)}$$

While the values of R_1 are given from,

$$\begin{cases} if\ P_1 - P_0 \leq 0, R_1 = P_0 \\ if\ P_1 - P_0 > 0, R_1 = P_1 \end{cases} \quad \text{(C.25)}$$

And the values of R_2 are defined as,

$$\begin{cases} if\ P_2 - P_0 \leq 0, R_2 = P_0 \\ if\ P_2 - P_0 > 0, R_2 = P_2 \end{cases} \quad \text{(C.26)}$$

C.4. Formulation for H_l and H_r, for taper configuration B and C

In the equation (2.23) from chapter 2, the equivalent height of resin and laminate is applied to evaluate the mass along the length of the taper. For this purpose, H_l and H_r are expressed as a function of x.

For taper configuration B and C, we can define l_1 as the total length of each resin pocket l_1 as,

$$l_1 = \frac{L}{n-m} \tag{C.27}$$

Where the coefficient n represents the number of plies in the higher thickness, and m represents the number of plies in the lower thickness. The resin local position x_r is given by,

$$x_r = mod(x, l_1) \tag{C.28}$$

In this equation, $mod(x, l_1)$ represents the residual part of the division of x by l_1. Along the x axis, the total height of the ply $H_P(x)$ and the resin $H_r(x)$ can be calculated following,

$$H_r(x) = t + Mx_R \tag{C.29}$$

$$H_P(x) = nt + Mx - H_r(x) \tag{C.30}$$

C.5. Formulation for H_l and H_r, for taper configuration D

For taper configuration D is defined the length of its related resin pocket l_2,

$$l_2 = \frac{4L}{n-m} \tag{C.31}$$

In the same form as for the taper configuration B and C, we have for the taper configuration D,

$$x_r = mod(x, l_2) \tag{C.32}$$

With this, the laminate equivalent height H_p and the resin equivalent height H_r can be defined by,

$$H_r(x) = 4t + Mx_R \tag{C.33}$$

$$H_p(x) = nt + Mx - H_r(x) \tag{C.34}$$

References

[1] F. X. Irisarri, D. M. J. Peeters, and M. M. Abdalla, “Optimisation of ply drop order in variable stiffness laminates,” *Compos. Struct.*, vol. 152, pp. 791–799, 2016.

[2] N. Zehnder and P. Ermanni, “A methodology for the global optimization of laminated composite structures,” *Compos. Struct.*, vol. 72, pp. 311–320, 2006.

[3] F. S. Almeida and A. M. Awruch, “Design optimization of composite laminated structures using genetic algorithms and finite element analysis,” *Compos. Struct.*, vol. 88, no. 3, pp. 443–454, 2009.

[4] D. Keller, “Optimization of ply angles in laminated composite structures by a hybrid, asynchronous, parallel evolutionary algorithm.,” *Compos Struct*, p. 92:2781–90, 2010.

[5] Kaufmann, Zenkert, and Mattei, “Cost optimization of composite aircraft structures including variable laminate qualities,” *Compos Sci Technol*, p. 68:2748–54, 2008.

[6] D. E. Koelle, “Specific Transportation Costs to GEO - Past, Present and Future,” *Acta Astronaut. 53*, no. 797, 2003.

[7] “Magazine Aeor Qtr 04-06,” *Boeing*, 2014. [Online]. Available: https://www.boeing.com/commercial/aeromagazine/articles/2014_q4/pdf/AERO_2014q4.pdf.

[8] M. A. Fazili, “Vibration Analysis of Thickness- and Width- Tapered Laminated Composite Beams using Hierarchical Finite Element Method,” no. September, 2013.

[9] L. Chen, “Free vibration analysis of tapered composite beams using hierarchical finite element method,” *Master’s thesis, Concordia Univ.*, 2004.

[10] K. He, S. V. Hoa, and R. Ganesan, “The study of tapered laminated composite structures: A review,” *Compos. Sci. Technol.*, vol. 60, no. 14, pp. 2643–2657, 2000.

[11] R. Ganesan and A. Zabihollah, “Vibration analysis of tapered composite beams using a higher-order finite element. Part I: Formulation,” *Compos. Struct.*, vol. 77, no. 3, pp. 306–318, 2007.

[12] R. Ganesan and A. Zabihollah, “Vibration analysis of tapered composite beams using a higher-order finite element. Part II: parametric study,” *Compos. Struct.*, vol. 77, no. 3, pp. 319–330, 2007.

[13] H. E. U. Ahmed, “Free and forced vibrations of tapered composite beams including the effects of axial force and damping,” *Masters thesis, Concordia Univ.*, 2008.

[14] K. B. Vijay, “Dynamic Response of Width- and Thickness-tapered Composite Beams Using Rayleigh-Ritz Method and Modal Testing,” *Masters thesis, Concordia Univ.*, 2012.

[15] P. Salajegheh, “Vibrations of Thickness-and-width Tapered Laminated Composite Beams with Rigid and Elastic Supports,” *Masters thesis, Concordia Univ.*, 2013.

[16] A. A. K. and J. N. Reddy, “Free Vibration of Cross-Ply Laminated Beams with Arbitrary Boundary Conditions,” *Int. J. Eng.*, vol. 32, 1994.

[17] R. Abarcar and Cunniff PF, “The Vibration of Cantilever Beams of Fiber Reinforced Material,” *J Compos Mater*, p. 6:504–17, 1972.

[18] P. E. S. and V. R. A Ananda Babu, “Dynamic characterization of thickness tapered laminated composite plates.”

[19] E. S. H Ghaffari, A Zabihollah, “Vibration based damage detection in smart nonuniform thickness laminated composite beams,” *Toronto Int. 2009 - ieeexplore.ieee.org*.

[20] “A technical note on the response of a tapered beam,” *Comput. Struct. Vol.45, No.1, 1992, pp.185-195*, 1992.

[21] S. S. Gupta, R.S. and Rao, “Finite element eigenvalue analysis of tapered and twisted Timoshenko beams. Journal of Sound and Vibration,” pp. 187–200, 1978.

[22] L. W. Hodges, Dewey H., Atilgan, Ali R., Fulton, Mark V., Rehfield, “Free Vibration Analysis of Composite Beams,” *J. Am. Helicopter Soc.*

[23] A. Houmat, “Vibrations of Timoshenko beams by variable order finite elements,” *J. sound Vib. – Elsevier*, 1995.

[24] F. F. Çalım, “Free and forced vibrations of non-uniform composite beams,” *Compos. Struct. – Elsevier*, 2009.

[25] F. Javidrad and M. Nazari, “A new hybrid particle swarm and simulated annealing stochastic optimization method,” vol. 60, pp. 634–654, 2017.

[26] F. Javidrad, M. Nazari, and H. R. Javidrad, “Optimum stacking sequence design of laminates using a hybrid PSO-SA method,” *Compos. Struct. 185 607–618*, vol. 185, no. September 2017, pp. 607–618, 2018.

[27] F. L. Niordson, “On the Optimal Design of a Vibrating Beam,” *Q. Appl. Math. Vol. 23, No. 1, 1965, pp. 47-53*.

[28] C. B. Rogers, H. H. Mabie, “Transverse vibration of tapered cantilever beams v&h end supports,” *I. Acoust. Sot. Am.*, no. 44, pp. 1739–1741, 1968.

[29] W. A. Thornton, “Optimality Criterion Techniques Applied to Mechanical Design,” no. 77, pp. 319–327, 1978.

[30] E. Carrera, P. Nali, and M. Petrolo, “Unified Formulation Applied to Free Vibrations Finite Element Analysis of Beams with Arbitrary Section,” *Shock Vib.*, vol. 18, no. 3, pp. 485–502, 2011.

[31] R. K. K. S. Raciti, “Recent Advances in Analysis of Laminated Beams and Plates, Part II: Vibrations and Wave Propagation,” 1989.

[32] M. W. Nixon, “Preliminary Structural Design of Composite Main Rotor Blades for Minimum Weight,” *TP 2730, NASA*, 1987.

[33] A. S. Bassiouni, R. M. Gad-Elrab, and T. H. Elmahdy, “Dynamic Analysis for Laminated Composite Beams,” *Compos. Struct.*, vol. 44, pp. 81–87, 1999.

[34] W. Q. Chen, C. F. Lv, and Z. G. Bian, “Elasticity solution for free vibration of laminated beams,” *Compos. Struct.*, no. 62, pp. 75–82, 2003.

[35] R. Grandhi, “Structural Optimization with Frequency Constraints - A Review,” *Wright State Univ. Dayton, Ohio 45435, AIAA JOURNAL, Vol. 31, No. 12*.

[36] Jun Li, H. Hongxing, and S. Rongying, “Dynamic finite element method for generally laminated composite beams,” *Int J Mech Sci*, vol. 50, pp. 466–80, 2008.

[37] M. Hajianmaleki and M. S. Qatu, “Vibrations of straight and curved composite beams: A review,” *Compos. Struct.*, vol. 100, pp. 218–232, 2013.

[38] E. F. Rached and N. Ghazouani, “Higher order composite beam theory built on Saint-Venant’s solution. Part-I: Theoretical developments,” *Compos Struct*, vol. 93, no. 2, pp. 557–66, 2011.

[39] S. P. Machado and V. H. Cortínez, “Free vibration of thin-walled composite beams with static initial stresses and deformations,” *Eng. Struct*, vol. 29, no. 3, pp. 372–382, 2007.

[40] O. Song and L. Librescu, “Free Vibration Of Anisotropic Composite Thin-Walled Beams Of Closed Cross-Section Contour,” *J. Sound Vib.*, no. 167, pp. 129–147, 1993.

[41] J. R. Banerjee, “Frequency equation and mode shape formulae for composite Timoshenko beams,” *Compos. Struct.*, no. 51, pp. 381–388, 2001.

[42] J. Kosmatka and P. P. Friedmann, “Vibration analysis of composite turbopropellers using a nonlinear beam-type finite-element approach,” *AIAA J.*, vol. 27, no. 11, pp. 1606--1614, 1989.

[43] R. D. Cook, “Concepts and applications of finite element analysis,” *John Wiley Sons*, 2007.

[44] K.J. Bathe, *Finite element procedures*. Prentice-Hall, Englewood, Springer, Springer, 1996.

[45] D. Goldberg, “Genetic Algorithms in Search, Optimization and Machine Learning,” *Addison-Wesley Prof.*, 1989.

[46] J. Koza, “Genetic Programming: On the Programming of Computers by Means of Natural Selection,” *Cambridge, MA MIT Press.*, 1992.

[47] M. Mitchell, *An Introduction to Genetic Algorithms (Complex Adaptive Systems)*. MIT Press, Cambridge, 1998.

[48] J. Kennedy and R. Eberhart, “Particle Swarm Optimization,” *Proc. IEEE Int. Conf. Neural Networks*, pp. 1942–1948, 1995.

[49] F. Marini and B. Walczak, “Particle swarm optimization (PSO). A tutorial,” *Chemom. Intell. Lab. Syst.*, vol. 149, pp. 153–165, 2015.

[50] P. D. Ghiasi H Lessard L., “Optimum stacking sequence design of composite materials Part I: Constant stiffness design.,” *Compos Struct*, p. 90:1-11, 2009.

[51] M. A. Nik, K. Fayazbakhsh, D. Pasini, and L. Lessard, “Surrogate-based multi-objective optimization of a composite laminate with curvilinear fibers,” *Compos. Struct.*, vol. 94, no. 8, pp. 2306–2313, 2012.

[52] J. Lee and P. Hajela, “Parallel genetic algorithm implementation in multidisciplinary rotor blade design,” *J. Aircr. - arc.aiaa.org*, vol. 33, no. 5, pp. 962–969, 1996.

[53] F. X. Irisarri, A. Lasseigne, F. H. Leroy, and R. Le Riche, “Optimal design of laminated composite structures with ply drops using stacking sequence tables,” *Compos. Struct.*, vol. 107, pp. 559–569, 2014.

[54] A. A. CAC Coello, AD Christiansen, “Using a new GA-based multiobjective optimization technique for the design of robot arms,” *Robot. -Cambridge Univ Press*, vol. 16, no. 4, pp. 401–414, 1998.

[55] B. F. W Hansel, A Treptow, W Becker, “A heuristic and a genetic topology optimization algorithm for weight-minimal laminate structures,” *Compos. Struct. 2002 - Elsevier*.

[56] L. L. Ghiasi H, Fayazbakhsh K, Pasini D, “Optimum stacking sequence design of composite materials. Part II: Variable stiffness design,” *Compos Struct, 2010;93(1)1–13.*

[57] H. Adeli and N.T. Cheng, “Integrated genetic algorithm for optimization of space structures,” *J. Aerosp. Eng., ASCE.*, vol. 6, no. 4, pp. 315–28, 1993.

[58] S. Nagendra, “Improved Genetic Algorithm for the Design of Stiffened Composite Panels,” *Comput Struct*, vol. 58, no. 3, p. 543, 1996.

[59] H. R. Todoroki A, “Stacking sequence optimization by a genetic algorithm with a new recessive gene like repair strategy,” *Compos B Eng*, vol. 29, no. 3, pp. 277–85, 1998.

[60] R. G. G. Narayana Naik, S. Gopalakrishnan, “Design optimization of composites using genetic algorithms and failure mechanism based failure criterion,” *Compos. Struct.*, vol. 83, no. 4, pp. 354–367, 2008.

[61] T. H. A. Scollen, “Simulated Annleaing, Introduction, Application and Theory,” *Nove Sci. Publ. Inc. New York*, 2018.

[62] Esfandiari, *Numerical Methods for Engineer and Scientists Using Matlab*. CRC Press, 2013.

[63] J. S. Arora, *Introduction to Optimum Design*, McGraw-Hil. 1989.

[64] X. Yang, *Introduction to Mathematical Optimization: From Linear Programming to Metaheuristics*, Cambridge. 2008.

[65] M. W. Hyer, *Stress Analysis of Fiber-Reinforced Composite Materials*, McGraw-Hi. 1998.

[66] V. K. Badagi, “Dynamic Response of Width- and Thickness-Tapered Composite Beams using Rayleigh- Ritz Method and Modal Testing,” 2012.

[67] “A commercial turbofan gas turbine,” 2018. [Online]. Available: https://www.rolls-royce.com/products-and-services/civil-aerospace/airlines/trent-1000.aspx#section-technology.

[68] W. electric C. Campbell, “Protection of steam turbine disk wheels from axial vibration,” *Trans.*

Am. Soc. Mech. Eng., vol. 46, pp. 31–160, 1924.

[69] S. Seraj, "Free vibration and dynamic instability analyses of doubly-tapered rotating laminated composite beams," Master's thesis, Concordia Univ., 2016.

[70] T. W. Athan and P. Y. Papalambros, "A note on weighted criteria methods for compromise solutions in multi-objective optimization," *Eng. Optim*, no. 27, pp. 155–176, 1996.

[71] D. Germund and A. Bjork, *Numerical Methods in Scientific Computing*, Vol. I SIA. 2008.

[72] S. Kirkpatrick, C. Gelatt, and M. Vecchi, "Optimization by simulated annealing," *Science*, vol. 220, no. 4598. pp. 671–680, 1983.

[73] J. H. Holland, "Adaptation in Natural and Artificial Systems: An Introductory Analysis with Applications to Biology, Control, and Artificial Intelligence.," *MIT Press*, 1992.

[74] R. V. Grandhi, "Structural optimization with frequency constraints-A Review," *AIAA J.*, vol. 31, no. 7, pp. 2296–2330, 1993.